

# ADVANCED STEEL CONSTRUCTION

*An International Journal*

Volume 2 Number 2

June 2006

CONTENTS

## Technical Papers

Recent Developments in Welded Hollow Section Joint Recommendations

*Jaap Wardenier and Yoo Sang Choo*

Reliability-Based Integrated Design Approach for Planar Steel Frames

*Yu-Shu Liu and Guo-Qiang Li*

Analytical and Experimental Investigations of Bolted Haunched

Beam-to-column Joints with a View of Seismic Design

*A. Lachal, J.M. Aribert and G. Loho*

The Cyclic Behaviours of Box-section Steel Beam-columns:

Experiment & Numerical Comparison

*Ming-zhou Su, Lin Shen and Qiang Gu*

Structural Performance of Composite Base Column Connections

*L. Di Sarno, G. Fabbrocino and M.R. Pecce*

ISSN 1816-112X

Copyright © 2006 by :

The Hong Kong Institute of Steel Construction

Website: <http://www.hkisc.org/>

ADVANCED STEEL CONSTRUCTION

VOL.2, NO.2 (2006)

# ADVANCED STEEL CONSTRUCTION

*an International Journal*

ISSN 1816-112X

Volume 2 Number 2

June 2006



## Editors-in-Chief

**S.L. Chan**, *The Hong Kong Polytechnic University, Hong Kong*

**W.F. Chen**, *University of Hawaii at Manoa, USA*

**R. Zandonini**, *Trento University, Italy*

## EDITORS-IN-CHIEF

### Asian Pacific, African and organizing Editor

S.L. Chan  
*The Hong Kong Poly. Univ.,  
Hong Kong*

### American Editor

W.F. Chen  
*Univ. of Hawaii at Manoa, USA*

### European Editor

R. Zandonini  
*Trento Univ., Italy*

## INTERNATIONAL EDITORIAL BOARD

F.G. Albermani  
The Univ. of Queensland, Australia

F.S.K. Bijlaard  
Delft Univ. of Technology, The Netherlands

R. Bjorhovde  
The Bjorhovde Group, USA

M.A. Bradford  
The Univ. of New South Wales, Australia

D. Camotim  
Technical Univ. of Lisbon, Portugal

C.M. Chan  
Hong Kong Univ. of Science & Technology,  
Hong Kong

S.P. Chiew  
Nanyang Technological Univ., Singapore

K.F. Chung  
The Hong Kong Polyt. Univ.  
Kowloon, Hong Kong

G.G. Deierlein  
Stanford Univ., California, USA

L. Dezi  
Univ. of Ancona, Italy

D. Dubina  
The "Politehnica" Univ. of Timisoara, Romania

R. Greiner  
Technical Univ. of Graz, Austria

G.W.M. Ho  
Ove Arup & Partners Hong Kong Ltd.,  
Hong Kong

J.P. Jaspart  
Univ. of Liege, Belgium

S. Kitipornchai  
City Univ. of Hong Kong, Hong Kong

D. Lam  
Univ. of Leeds, UK

G.Q. Li  
Tongji Univ., China

J.Y.R. Liew  
National Univ. of Singapore, Singapore

X. Liu  
Tsinghua Univ., China

E.M. Lui  
Syracuse Univ., USA

Y.L. Mo  
Univ. of Houston, USA

J.P. Muzeau  
CUST, Clermont Ferrand, France

D.A. Nethercot  
Imperial College of Science, Technology  
and Medicine, UK

D.J. Oehlers  
The Univ. of Adelaide, Australia

K. Rasmussen  
The Univ. of Sydney, Australia

T.M. Roberts  
Cardiff Univ., UK

J.M. Rotter  
The Univ. of Edinburgh, UK

C. Scawthorn  
Scawthorn Porter Associates, USA

P. Schaumann  
Univ. of Hannover, Germany

G.P. Shu  
Southeast Univ. China

J.G. Teng  
The Hong Kong Polyt. Univ., Hong Kong

G.S. Tong  
Zhejiang Univ., China

K.C. Tsai  
National Taiwan Univ., Taiwan

C.M. Uang  
Univ. of California, USA

B. Uy  
The Univ. of Wollongong, Australia

M. Veljkovic  
Univ. of Lulea, Sweden

F. Wald  
Czech Technical Univ. in Prague,  
Czech

Y.C. Wang  
The Univ. of Manchester, UK

D. White  
Georgia Institute of Technology,  
USA

E. Yamaguchi  
Kyushu Institute of Technology,  
Japan

Y.B. Yang  
National Taiwan Univ., Taiwan

B. Young  
The Univ. of Hong Kong, Hong Kong

X.L. Zhao  
Monash Univ., Australia



## General Information

### *Advanced Steel Construction, an international journal*

#### **Aims and scope**

The International Journal of Advanced Steel Construction provides a platform for the publication and rapid dissemination of original and up-to-date research and technological developments in steel construction, design and analysis. Scope of research papers published in this journal includes but is not limited to theoretical and experimental research on elements, assemblages, systems, material, design philosophy and codification, standards, fabrication, projects of innovative nature and computer techniques. The journal is specifically tailored to channel the exchange of technological know-how between researchers and practitioners. Contributions from all aspects related to the recent developments of advanced steel construction are welcome.

#### **Instructions to authors**

**Submission of the manuscript.** Authors may submit three double-spaced hard copies of manuscripts together with an electronic copy on a diskette or cd-rom in an editable format (MS Word is preferred). Manuscripts should be submitted to the regional editors as follows for arrangement of review.

Asian Pacific, African and organizing editor :	Professor S.L. Chan
American editor :	Professor W.F. Chen
European editor :	Professor R. Zandonini

All manuscripts submitted to the journal are highly recommended to accompany with a list of four potential reviewers suggested by the author(s). This list should include the complete name, address, telephone and fax numbers, email address, and at least five keywords that identify the expertise of each reviewer. This scheme will improve the process of review.

#### **Style of manuscript**

**General.** Author(s) should provide full postal and email addresses and fax number for correspondence. The manuscript including abstract, keywords, references, figures and tables should be in English with pages numbered and typed with double line spacing on single side of A4 or letter-sized paper. The front page of the article should contain:

- a) a short title (reflecting the content of the paper);
- b) all the name(s) and postal and email addresses of author(s) specifying the author to whom correspondence and proofs should be sent;
- c) an abstract of 100-200 words; and
- d) 5 to 8 keywords.

The paper must contain an introduction and a conclusion. The length of paper should not exceed 25 journal pages (approximately 15,000 words equivalents).

**Tables and figures.** Tables and figures including photographs should be typed, numbered consecutively in Arabic numerals and with short titles. They should be referred in the text as Figure 1, Table 2, etc. Originally drawn figures and photographs should be provided in a form suitable for photographic reproduction and reduction in the journal.

**Mathematical expressions and units.** The Systeme Internationale (SI) should be followed whenever possible. The numbers identifying the displayed mathematical expression should be referred to in the text as Eq. (1), Eq. (2).

**References.** References to published literature should be referred in the text, in the order of citation with Arabic numerals, by the last name(s) of the author(s) (e.g. Zandonini, R.). References should be in English with occasional allowance of 1-2 exceptional references in local languages and reflect the current state-of-technology. Journal titles should be abbreviated in the style of the Word List of Scientific Periodicals. References should be cited in the following style.

Journal: Chen, W.F. and Kishi, N., "Semi-rigid steel beam-to-column connections, data base and modeling", Journal of Structural Engineering, ASCE, 1989, 115(1), pp.105-119.

Book: Chan, S.L. and Chui, P.P.T., "Non-linear static and cyclic analysis of semi-rigid steel frames", Elsevier Science, 2000, pp.336.

Proceedings: Zandonini, R. and Zanon, P., "Experimental analysis of steel beams with semi-rigid joints", Proceedings of International Conference on Advances in Steel Structures, Hong Kong, 1996, vol. 1, pp.356-364.

**Proofs.** Proof will be sent to the corresponding author to correct any typesetting errors. Alternations to the original manuscript at this stage will not be accepted. Proofs should be returned within 48 hours of receipt by Express Mail, Fax or Email.

**Copyright.** Submission of an article to "Advanced Steel Construction" implies that it presents the original and unpublished work, and not under consideration for publication nor published elsewhere. On acceptance of a manuscript submitted, the copyright thereof is transferred to the publisher by the Transfer of Copyright Agreement and upon the acceptance of publication for the papers, the corresponding author must sign the form for Transfer of Copyright.

**Permission.** Quoting from this journal is granted provided that the customary acknowledgement is given to the source.

**Page charge and Reprints.** There will be no page charges if the length of paper is within the limit of 25 journal pages. A total of 30 free offprints will be supplied free of charge to the corresponding author. Purchasing orders for additional offprints can be made on order forms which will be sent to the authors. These instructions can be obtained at the Hong Kong Institute of Steel Construction, Journal website: <http://www.hkisc.org>

The International Journal of Advanced Steel Construction is published quarterly by non-profit making learnt society, The Hong Kong Institute of Steel Construction, c/o Department of Civil & Structural Engineering, The Hong Kong Polytechnic University, Hung Hom, Kowloon, Hong Kong.

**Disclaimer.** No responsibility is assumed for any injury and / or damage to persons or property as a matter of products liability, negligence or otherwise, or from any use or operation of any methods, products, instructions or ideas contained in the material herein.

**Subscription inquiries and change of address.** Address all subscription inquiries and correspondence to Member Records, IJASC. Notify an address change as soon as possible. All communications should include both old and new addresses with zip codes and be accompanied by a mailing label from a recent issue. Allow six weeks for all changes to become effective.

#### **The Hong Kong Institute of Steel Construction**

HKISC

c/o Department of Civil and Structural Engineering,

The Hong Kong Polytechnic University,

Hunghom, Kowloon, Hong Kong, China.

Tel: 852- 2766 6047 Fax: 852- 2334 6389

Email: [ceslchan@polyu.edu.hk](mailto:ceslchan@polyu.edu.hk) Website: <http://www.hkisc.org/>

ISSN 1816-112X

Copyright © 2006 by:

The Hong Kong Institute of Steel Construction.



ISSN 1816-112X

## EDITORS-IN-CHIEF

### Asian Pacific, African and organizing Editor

S.L. Chan

*The Hong Kong Polyt. Univ.,  
Hong Kong*

### American Editor

W.F. Chen

*Univ. of Hawaii at Manoa, USA*

### European Editor

R. Zandonini

*Trento Univ., Italy*

# Advanced Steel Construction

*an international journal*

---

VOLUME 2 NUMBER 2

JUNE 2006

---

## Technical Papers

Recent Developments in Welded Hollow Section Joint 109  
Recommendations

*Jaap Wardenier and Yoo Sang Choo*

Reliability-Based Integrated Design Approach for Planar Steel 128  
Frames

*Yu-Shu Liu and Guo-Qiang Li*

Analytical and Experimental Investigations of Bolted Haunched 137  
Beam-to-column Joints with a View of Seismic Design

*A. Lachal, J.M. Aribert and G. Loho*

The Cyclic Behaviours of Box-section Steel Beam-columns: 161  
Experiment & Numerical Comparison

*Ming-zhou Su, Lin Shen and Qiang Gu*

Structural Performance of Composite Base Column Connections 172

*L. Di Sarno, G. Fabbrocino and M.R. Pecce*



# RECENT DEVELOPMENTS IN WELDED HOLLOW SECTION JOINT RECOMMENDATIONS

Jaap Wardenier<sup>1,\*</sup> and Yoo Sang Choo<sup>2</sup>

<sup>1</sup> *Emeritus Professor, Faculty of Civil Engineering and Geosciences,  
Delft University of Technology, P.O. Box 5048, 2600 GA Delft, The Netherlands*

*\*(Corresponding author: E-mail: j.wardenier@citg.tudelft.nl)*

<sup>2</sup> *Director, Centre for Offshore Research & Engineering, Faculty of Engineering,  
National University of Singapore, Kent Ridge, 117576 Singapore  
cvecys@nus.edu.sg*

**ABSTRACT:** This paper considers recent research results on hollow section joints and the effect on the current design rules and is an extended version of the ICASS keynote lecture [1]. Main attention is paid to Rectangular Hollow Section (RHS) overlap joints, Circular Hollow Section (CHS) joints with thick-walled chords and the influence of the chord stress on the joint strength. Further, the effect of reinforcement plates on the strength of thin-walled joints is discussed. Also, some special aspects on elliptical hollow sections, stainless steel, high strength steel and delivery requirements for cold-formed hollow sections are considered. Finally, some developments regarding the fatigue design of hollow section joints are presented.

**Keywords:** Circular hollow section (CHS); Rectangular hollow section (RHS); Gap joints; Overlap joints; Static strength; Fatigue strength; High strength steel.

## NOMENCLATURE

CHS	Circular Hollow Section
RHS	Rectangular Hollow Section
$A_i$	cross section area of the overlapping brace member $i$
$A_s$	effective shear area of the joint
$F_{u,c}$	ultimate load capacity of the collar reinforced joint
$F_{u,u}$	ultimate load capacity of the of the unreinforced joint
$M_0$	in plane bending moment in the chord (general)
$M_{i,0}$	in plane bending moment in the chord in the plane $i=1$ or $2$
$M_{i,u,c}$	ultimate in plane bending moment capacity of the collar reinforced joint
$M_{i,u,u}$	ultimate in plane bending moment capacity of the unreinforced joint
$M_{o,u,c}$	ultimate out of plane bending moment capacity of the collar reinforced joint
$M_{o,u,u}$	ultimate out of plane bending moment capacity of the unreinforced joint
$M_{pl,0}$	plastic moment capacity of the chord
$N_i$	axial force in the overlapping brace member $i$
$N_j$	axial force in the overlapped brace member $j$
$N_{0p}$	maximum prestressing force in the chord
$N_0$	maximum chord axial force
$N_{1,0}$	axial ultimate load capacity of the joint based on the load in member 1 for chord load nearly zero
$N_{i,u}$	axial ultimate load capacity of the joint based on the load in member $i$
$N_{pl,0}$	plastic design capacity of the chord
$N_{i, effec\ width}$	ultimate load capacity of the overlapping brace based on the effective width criterion
Ov	Overlap in %
$R_{N0-M0}$	interaction factor of bending moment and axial loading
$V_u$	ultimate shear capacity ratio
$b_i$	external width of the overlapping brace $i$
$b_j$	external width of the overlapped brace $j$
$b_0$	external width of a chord
$b_{ei}$	effective width of the overlapping brace $i$ with the chord connection
$b_{ej}$	effective width of the overlapped brace $j$ with the chord connection

$b_{e(ov)}$	effective width of the overlapping brace i with the overlapped brace j connection
$c$	constant for external corner radius
$d_i$	external diameter of brace i ( $i=1$ or $2$ in a K joint)
$d_0$	external diameter of a chord
$f_{yi}$	design yield strength of the overlapping brace i
$f_{yj}$	design yield strength of the overlapped brace j
$f_{y0}$	design yield strength of a chord
$f_{ui}$	ultimate stress of the overlapping brace i
$f_{uj}$	ultimate stress of the overlapped brace j
$h_i$	external depth of the overlapping brace i
$h_j$	external depth of the overlapped brace j
$l_c$	length of the collar plate reinforcement
$n$	maximum chord stress divided by the chord yield stress
$t_c$	wall thickness of the collar plate reinforcement
$t_i$	wall thickness of the overlapping brace i
$t_j$	wall thickness of the overlapped brace j
$t_0$	wall thickness of a chord
$\beta$	diameter or width ratio between braces and chord: $\beta = d_i/d_0$ or $\beta = b_i/b_0$
$\gamma$	half diameter or half width to thickness ratio of the chord, $d_0/2t_0$ or $b_0/2t_0$
$\theta_i$	acute angle between the overlapping brace member i and the chord
$\theta_j$	acute angle between the overlapped brace member j and the chord
$\tau_c$	relative reinforcement plate-to-chord wall thickness ratio, $t_c/t_0$
$\phi$	angle in between the two planes in a multiplanar joints ( $\phi = 90^\circ$ )

## INTRODUCTION

The design rules in the second edition of the “Design Recommendations for Hollow Section Joints - Predominantly Statically Loaded” by the Sub-commission XV-E of the International Institute of Welding, (IIW-XV-E, 1989) [2] are the basis for many national and international design recommendations or standards, e.g. the Eurocode 3, (CEN, 2003) [3]. Based on these IIW-XV-E recommendations the Comité International pour le Développement et l’Etude de la Construction Tubulaire (CIDECT) has published several design guides for designers and fabricators, see for example [4].

Since the publication of the 2<sup>nd</sup> edition of the IIW-XV-E recommendations, considerable research has been carried out in various areas, during the last years, including joints of very thin-walled and very thick-walled hollow sections. Further, research has been carried out to fill gaps in knowledge, e.g. multiplanar joints or for strength upgrading of joints in existing structures. Currently, the IIW-XV-E recommendations are revised and extended for the third edition [5]. Some of the research on which these revised recommendations and extensions are based, will be dealt with in this paper, as well as some other work in which the authors are involved.

For the fatigue design of hollow section joints the IIW-XV-E sub-committee has published in 1999 the “Recommended fatigue design procedure for welded hollow section joints”, (IIW-XV-E, 1999) [6]. These recommendations are now the basis for drafting of an ISO standard. In these recommendations the fatigue design is based on the “hot spot stress” approach or also called the “geometrical stress” approach. Nowadays, such an approach becomes also usual for plated structures like ships and FPSO’s. During the last few years, many investigations have been, or are still being carried out to compare and synchronize the various methods for the determination of the hot spot stress in relation to the fatigue classification and the thickness effect.

This paper gives a brief review of some of the research recently carried out on hollow section joints, in particular those topics in which the authors are involved. Further, some other research is briefly discussed and references are given for more detailed information.

## STATIC DESIGN OF RECTANGULAR HOLLOW SECTION JOINTS

### *Uniplanar and multiplanar K-gap joints*

In the current CIDECT Design Guide for Rectangular Hollow Section Joints [7], it is recommended to assess multiplanar KK-gap joints with the uniplanar K-gap joint design formulae by applying a reduction factor of 0.9. In addition a chord shear check should be performed for the gap location of gap joints.

Since the experimental evidence was limited, CIDECT initiated programme 5BJ in which all influencing parameters have been investigated [8]. In this research, it was found that in case of chord face failures, multiplanar KK-joints behaved nearly similar to uniplanar K-joints if the chords of the uniplanar joints were additionally loaded by a chord (pre)stressing force equal to  $N_{op} = -2N_i \cdot \cos\theta_i$  which represents the difference in the chord reaction force (see Figure 1).

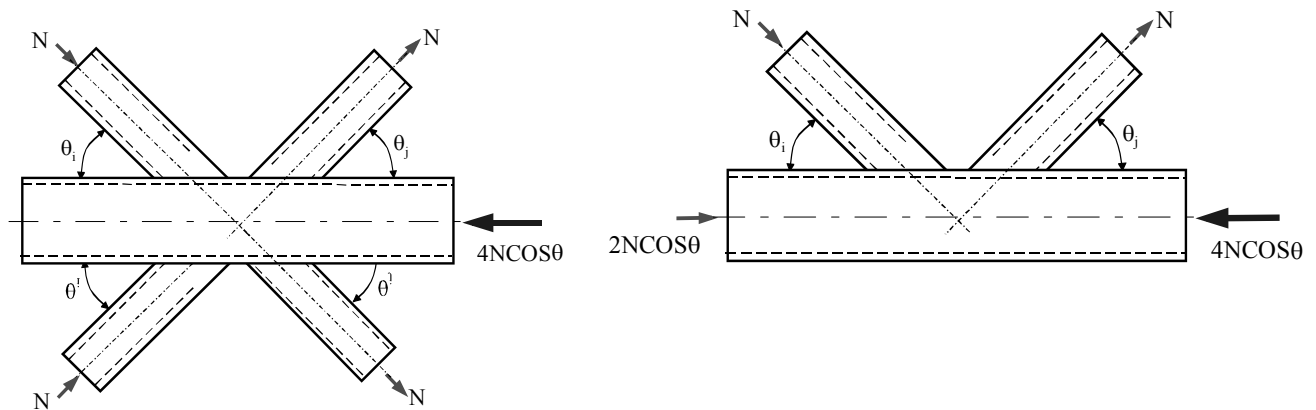


**Figure 1.** Uniplanar and multiplanar joints with equivalent behaviour

Consequently, it can be concluded that if for multiplanar KK-joints the larger chord load is taken into account in the chord stress function for chord face failure, the same formula can be used as for uniplanar K-joints and no further reduction factors have to be applied. However, due to the possible larger shear in the gap for particular loadings, the chord has always to be checked for the interaction of shear and axial load. The interaction is based on the well known Von Mises Huber-Hencky criterion. For example for a symmetrically loaded RHS multiplanar KK-joint with an included angle  $\phi=90^\circ$  and no eccentricity, all sides of the RHS chord are loaded by axial load and shear and for each plane the following interaction Eq. (1) is valid:

$$\left( \frac{\sum N_i \cdot \cos\theta_i}{0.5A_0 \cdot f_y} \right)^2 + \left( \frac{\sum N_i \cdot \sin\theta_i}{0.5A_0 \cdot f_y / \sqrt{3}} \right)^2 \leq 1.0 \quad (1)$$

For the multiplanar joint the chord axial load  $N_0$  is the sum of the horizontal components of the brace forces in both planes or two times the value in one plane. The resulting shear force  $V_0$  in the multiplanar joint is the vectorial resultant of the vertical components of the brace forces in both planes being  $\sqrt{2}$  times the shear force in one plane. Thus the Eq. (1) can also be written as Eq. (1a):



$$\left( \frac{0.5N_0}{0.5A_0 \cdot f_y} \right)^2 + \left( \frac{V_0 \cdot \cos\phi_j/2}{0.5A_0 \cdot f_y/\sqrt{3}} \right)^2 \leq 1.0 \quad (1a)$$

or with  $N_{0,pl}^* = A_0 f_{y0}$  and  $V_{0,pl}^{**} = A_0 f_{y0} / \sqrt{3}$  and  $\phi=90^\circ$ :

$$\left( \frac{N_0}{N_{0,pl}^*} \right)^2 + \left( \frac{1.4V_0}{V_{0,pl}^{**}} \right)^2 \leq 1.0 \quad (1b)$$

In case of asymmetric loading or for  $\phi \neq 90^\circ$  it is easier to consider the interaction for each plane.

In the framework of a new CIDECT programme a numerical programme is being carried out to investigate the chord load functions for K-joints with gap. Based on the results, new chord load functions are being developed based on the maximum chord load [9]. The new proposed functions will have a format, which is similar for all types of circular and rectangular hollow section joints, as given below in Eq. (2):

$$f(n) = \left[ 1 - n^{c_1} \right]^{(c_2 + c_3\beta + c_4\gamma)} \quad (2)$$

Some of the results are shown in Figure 2 in comparison to the current chord stress function [7,10].

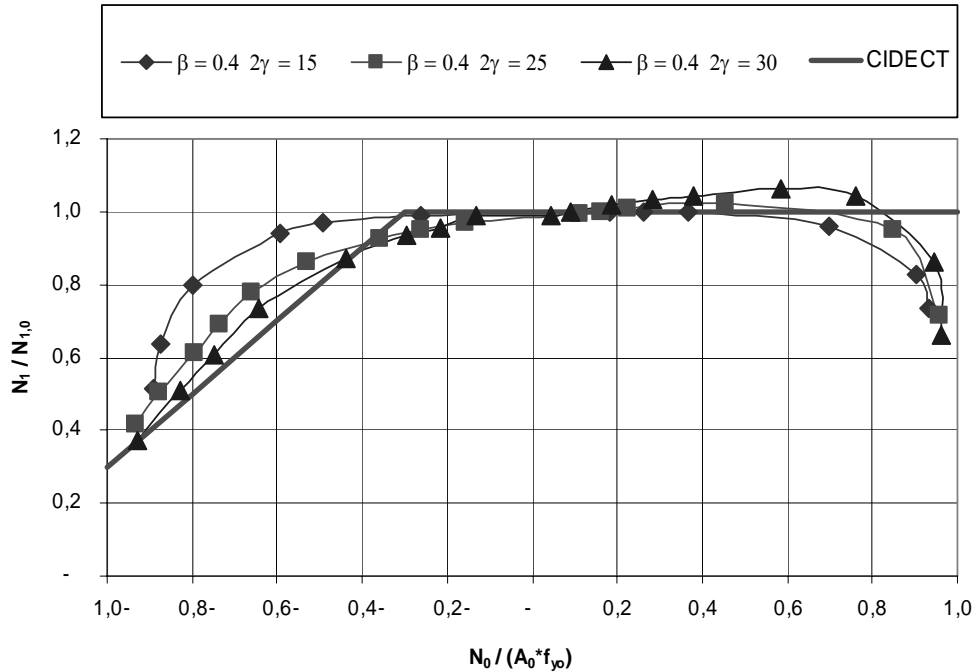


**Figure 2.** Chord stress reduction for RHS-K joints with gap ( $\beta = 0.4$ )

In this study, as in other studies, it was shown that for  $n \gg 0$ , with chords loaded in tension a reduction factor also has to be applied, although the reduction is much smaller than for compression loading.

#### **Uniplanar and multiplanar K-overlap joints**

In the above-mentioned investigation it was also observed that, especially for multiplanar KK-overlap joints with medium to slender chord width to thickness ratios, chord face failure could occur which is not covered by the current codes and recommendations. Therefore, a detailed numerical study was carried out to study 50% and 100% uniplanar K- and multiplanar KK-overlap joints in more detail.

Based on this study it was found that three failure modes have to be checked [11,12], i.e.:

- overlapping brace failure (brace effective width criterion)
- brace shear failure at the connection with the chord
- local chord failure

The brace effective width criterion, e.g. shown in Figure 3 for a 100% overlap joint, was already given in the current recommendations but the other two criteria are added, although the chord member has always to be checked for member failure. This investigation showed that at the joint location a linear interaction between axial load and bending moment is better than the member interaction formula. Besides these failure modes, it was found that the shear in the cross section of the braces just above the connection with the chord face has to be limited to avoid chord face failure. The first author indicated already in 1976 that brace shear failure at the connection with the chord face should be considered as a possible failure mode. However, brace shear failure was not observed in the experiments, which may be due to the small shear deformations. As a result this failure mode is not included in the current IIW and CIDECT recommendations and only a the brace effective width criterion was proposed to cover the strength of RHS overlap joints.

As indicated in Figure 4, the brace walls parallel to the chord axis are fully effective for shear and the brace cross wall at the heel is theoretically not effective or only effective for a part  $b_e$ . The toe part of the overlapped brace of an overlap joints with an overlap  $O_v < 100\%$  is generally not fully welded to the chord (hidden location) and therefore not effective; it is only fully effective in case of 100% overlap joints. The results for 100% overlap joints showed that in those cases where the joint capacity is not limited by other criteria, the ultimate shear capacity can be reached, i.e.  $A_s \cdot \frac{f_u}{\sqrt{3}}$ .

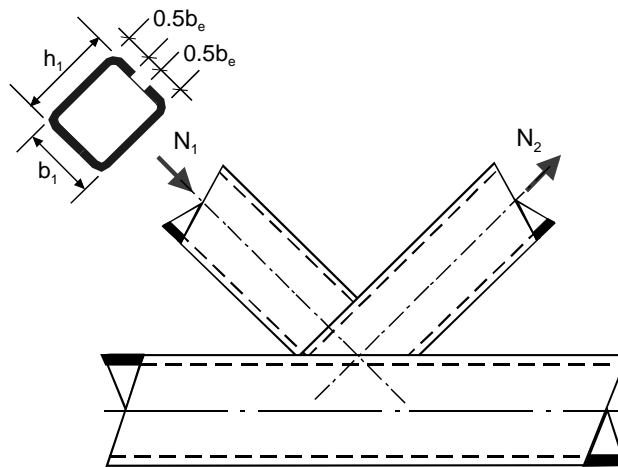


**Figure 3.** Brace effective width criterion for 100% overlap joints

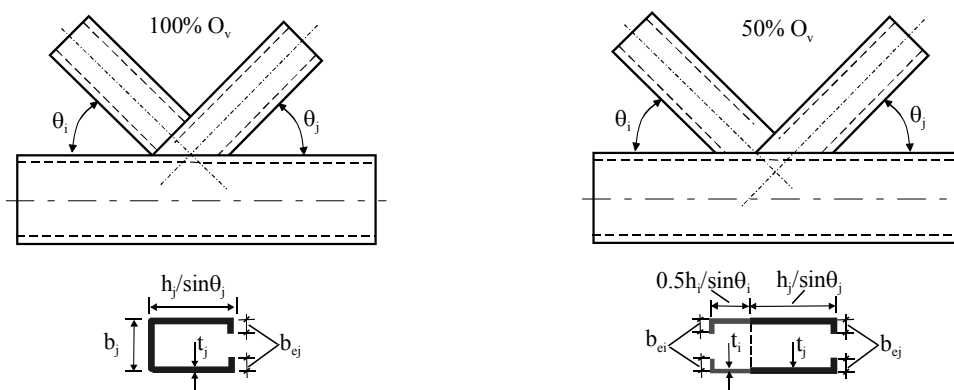


**Figure 4.** Joint configuration and definition of the shear area for 100% and 50% overlap joints

Adopting this ultimate brace shear capacity limit to avoid chord face failures still gives an additional reserve in joint capacity of 1.1 to 1.15.

Nowadays, higher strength steels are more frequently used, therefore, also the validity ranges for the width to thickness ratios have been reconsidered and are now related to the section class. In this case the section classes for the compression parts in hollow sections of Eurocode 3 are used.

Based on these studies the design recommendations are formulated as given in Table 1. The formulae are presented in a general format even allowing different steel grades for the overlapping and overlapped brace.

### ***Joints of thin-walled rectangular hollow sections***

Research on X, T and Y-joints of thin-walled hollow sections [13], indicated that the validity range of the width to thickness ratios in the design recommendations could, in particular cases, be more liberal. However, in actual structures always secondary effects like secondary moments exist and in case of thin-walled members these may cause premature failure because of lack of deformation and rotation capacity. Thus, using thin-walled sections outside the validity ranges of the current recommendations requires a more detailed elastic analysis. Further, it should be noted that in case of tests on joints of thin-walled sections all moments should be carefully measured because these may influence the axial load capacity due to the lower rotation/deformation capacity. Neglecting these moments may give test rig dependent test results.

### ***Joints of stainless steel rectangular hollow sections***

Rectangular hollow section joints of stainless steel, type 304 L, have been investigated at the University of Sydney [14]. In these investigations, X and K-gap joints made of cold formed austenitic stainless steel hollow sections have been used. The ultimate strengths were compared with the IIW-CIDECT design equations and the joint deformation at service-ability (ultimate strength divided by 1.5) was compared with the 1% chord width criterion. It was concluded that if the 0.2% proof stress based on the cold formed finished product is used, the joint strength can be evaluated using the IIW-CIDECT design rules for hollow section joints made of carbon steel.

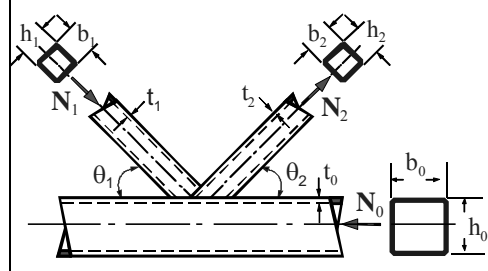
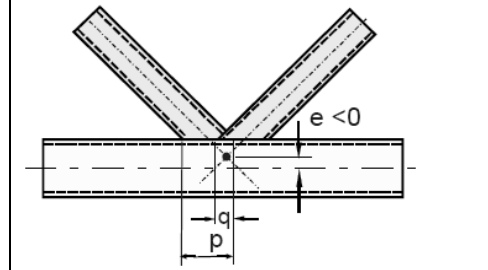
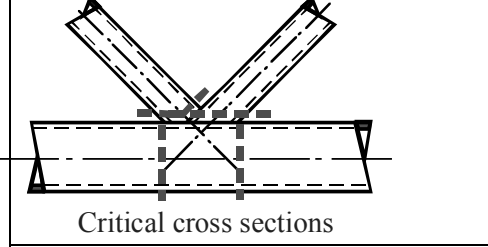
The joints loaded in tension fractured mainly through the weld in the heat affected zones. Thus, using electrodes of a stronger metal could even enhance the strength, allowing the 0.5% proof stress to be used in the formulae. In the analysis it was already shown that using the 0.5% proof stress, the service-ability limit was satisfied. However, the strength did not meet that according to the current IIW-CIDECT design equations for high chord loads. It is noted that the newly developed chord stress functions for rectangular hollow section joints (see before) are more conservative for high chord loads.

### ***Other investigated areas***

Other connections recently investigated more in detail and/or those still being investigated are e.g. plate-to-RHS connections at the University of Toronto by Koteski & Packer [15], corner connections, by Karcher & Puthli [16], bird beak connections by Davies *et al.* [17] and bolted connections by Willibald *et al.* [18]. For detailed information, reference is given to the various proceedings of the International Symposia on Tubular Structures, for example, Jaurietta *et al.* [19].



**Table 1.** Proposed design recommendations for RHS overlap joints

 <p><math>O_v = \text{overlap} = \frac{q}{p} \times 100\%</math></p>  <p>definition overlap</p>  <p>Critical cross sections</p>	<p style="text-align: center;"><b><math>O_v = 25</math> to <math>100\%</math></b></p> <p><b>Overlapping brace effective width criterion<sup>*)</sup></b>  <b>for <math>25\% \leq O_v &lt; 50\%</math> overlap:</b>  <math>N_i^* = f_{yi} t_i \{ (O_v / 50)(2h_i - 4t_i) + b_{ei} + b_{e(ov)} \}</math>  <b>for <math>50\% \leq O_v &lt; 100\%</math> overlap:</b>  <math>N_i^* = f_{yi} t_i [2h_i - 4t_i + b_{ei} + b_{e(ov)}]</math>  <b>for <math>O_v = 100\%</math> overlap:</b>  <math>N_i^* = f_{yi} t_i [2h_i - 4t_i + b_i + b_{e(ov)}]</math></p> <p><b>Brace chord connection shear criterion<sup>**) (**)</sup></b>  <b>for <math>50\% &lt; O_v &lt; 100\%</math> overlap:</b>  <math display="block">N_i \cos \theta_i + N_j \cos \theta_j \leq \frac{f_{ui}}{\sqrt{3}} \left[ \left( \frac{100 - O_v}{100} \right) \cdot 2h_i + b_{ei} \right] \cdot t_i + \frac{f_{uj}}{\sqrt{3}} \frac{(2h_j + b_{ej}) \cdot t_j}{\sin \theta_j}</math>  <b>for <math>O_v = 100\%</math> overlap:</b>  <math display="block">N_i \cos \theta_i + N_j \cos \theta_j \leq \frac{f_{uj}}{\sqrt{3}} \left[ \frac{(2h_j + b_j + b_{ej}) t_j}{\sin \theta_j} \right]</math></p> <p><b>Local chord yield criterion for uniplanar joints</b>  <math display="block">\frac{N_0}{N_{pl,0}} + \frac{M_0}{M_{pl,0}} \leq 1.0</math>  <b>Local chord yield criterion for multiplanar joints<sup>***) (***)</sup></b>  <math display="block">\frac{N_0}{N_{pl,0}} + \frac{M_{1,0}}{M_{pl,0}} + \frac{M_{2,0}}{M_{pl,0}} \leq 1.0</math></p>
<p style="text-align: center;"><b>Functions</b></p> $b_{ei} = \frac{10}{b_0/t_0} \cdot \frac{f_{y0} \cdot t_0}{f_{yi} \cdot t_i} \cdot b_i \leq b_i, \quad b_{ej} = \frac{10}{b_0/t_0} \cdot \frac{f_{y0} \cdot t_0}{f_{yj} \cdot t_j} \cdot b_j \leq b_j, \quad b_{e(ov)} = \frac{10}{b_j/t_j} \cdot \frac{f_{yj} \cdot t_j}{f_{yi} \cdot t_i} \cdot b_i \leq b_i$	
<p style="text-align: center;"><b>Range of validity <math>O_v \geq 25\%</math></b></p> $\frac{b_i}{b_0}, \frac{h_i}{b_0}, \frac{b_j}{b_0}, \frac{h_j}{b_0} \geq 0.25, \quad \frac{t_i}{t_j} \leq 1.0 \quad \text{and} \quad \frac{b_i}{b_j} \geq 0.75$	<p>Compression brace : class 1 <span style="float: right;">****)</span>  Tension brace : class 1 or 2  Chord : class 1 or 2</p>

\*) Efficiency capacity of the overlapped brace should not exceed that of the overlapping brace

\*\*) This shear failure criterion is generally not critical for overlap joints with  $O_v \leq 50\%$ . In this criterion with  $O_v < 100\%$ , it is assumed that the hidden location at the overlapped brace with the chord is not welded.

\*\*\*) The moments  $M_{1,0}$  and  $M_{2,0}$  are the in-plane moments in the two planes, respectively and  $M_{pl,0}$  and  $M_{pl,0}$  refers to the belonging in-plane plastic moment capacity of the chord.

\*\*\*\*)

Limit (b-ct)/t	S 235	S 275	S 355	S 460
<b>Class 1</b>	33	30	27	23
<b>Class 2</b>	38	35	31	27

Note: c=3 for hot formed hollow sections and c=5 for cold formed hollow sections (rounded off figures).

## STATIC DESIGN OF CIRCULAR HOLLOW SECTION JOINTS

### *Uniplanar and multiplanar joints*

The recommendations for circular hollow section joints in the offshore codes, e.g. the API [20] and the draft ISO, ISO TC67/SC7/WG3/P3 [21], differ from the IIW-XV-E and CIDECT recommendations. This is one of the reasons that the IIW-XV-E Sub-committee has decided to reanalyse the behaviour of circular hollow section joints as a basis to derive international consensus for the current revision of the IIW-XV-E recommendations. In the evaluation also other proposals, for example, Dexter & Lee [22], Dier & Lalani [23], Yamada et al. [24] and Choo & Qian [25] are considered. Another aspect to be reviewed is the different behaviour of gap and overlap K-joints which in the current IIW recommendations are covered by only a single strength formula. It is the opinion of the authors of this paper that these joints should be dealt with separately. Overlap joints may be approached in a similar way as done for rectangular hollow sections.

Further, the influence of the chord stress on the joint strength of circular hollow sections is currently based on the so-called chord pre-load, i.e. the chord load minus the load, which reacts the brace load components. This is in contradiction with rectangular hollow section joints for which the chord load function is based on the maximum chord load. Therefore, in the framework of the CIDECT programme 5BK the existing formulae have been analysed and a numerical programme was carried out [26,27]. Based on this, new chord load functions were developed based on the maximum chord load. The new proposed functions have the general format of Eq. (2).

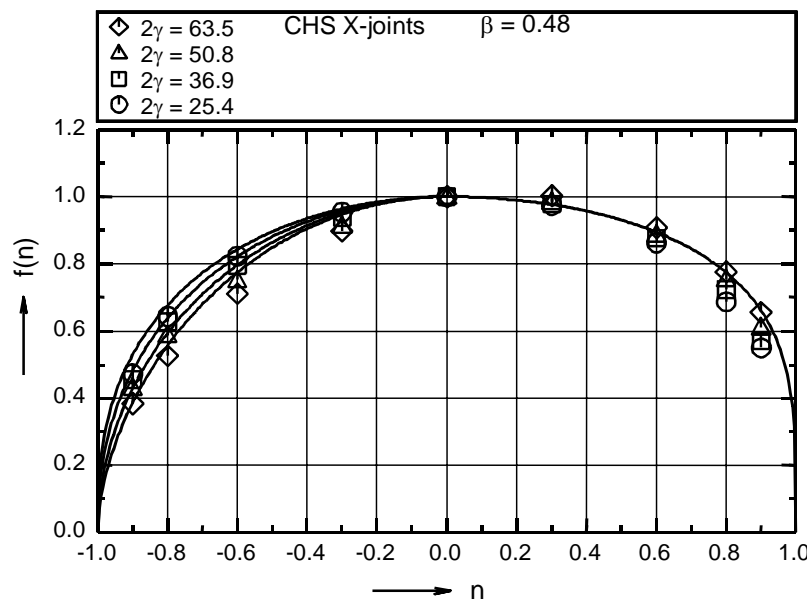


**Figure 5.** Chord stress reduction for CHS-X joints ( $\beta = 0.48$ )

Also here, for chords loaded in tension ( $n > 0$ ), a reduction factor has to be applied. Figure 5 shows a typical example for a X-joint with a diameter ratio  $\beta = 0.48$ . The results have also been compared with recent work carried out by Pecknold *et al.* [28-29].

In the revised recommendations for T joints the chord stress to be used also includes the bending stress which always occurs due to brace loading. In the previous IIW-XV E recommendations and all other recommendations due to the experimental evidence this was indirectly also included in the joint capacity equations. With the current numerical methods it is easier to separate the influence of brace and chord loading [30] and to incorporate this in an easy way in the recommendations.

Especially in the analyses of K gap joints the effect of the relatively large welds in small size experiments has to be excluded, that is why Yura [31] did not include in his analysis the test results of specimens with small chord members. In the past all recommendations have been based on experiments but the calculations with the current calibrated numerical models showed that the existing experimental data base has to be even more carefully screened. Furthermore, like for rectangular hollow section joints, a check may need to be carried out to ensure that the chord shear criterion in the gap is not critical. At present numerical calculations have been carried out for the whole parameter range and new strength equations have been developed. These new equations still need to be checked with the more refined experimental data base.

Currently various strength functions exist for overlap joints; some based on shear between the braces and punching shear, others relating the strength to that of gap joints. It is the authors opinion that the strength can be approached in a similar way as done for overlap joints of rectangular hollow sections with the effective parts related to the  $d/t$  ratios of the relevant members, however, such a reanalysis has still to be done.

In the current CIDECT design guide 1 [32] based on the work of the Kumamoto team, it is recommended to assess multiplanar joints in each plane with the uniplanar joint strength formulae but applying a reduction factor of 0.9. Additionally the chord has to be checked for shear in the gap. For rectangular hollow section joints it is shown above that the lower strength can be attributed to the larger chord force. By considering the maximum chord stress for the chord stress effect instead of the pre-stress due to additional chord loading, the reduction is in the same range but gives a consistent approach. This means that multiplanar K joints with gap of CHS (similar as RHS joints) can also be dealt with as uniplanar joints but taking account of the larger chord force and the additional shear check in the gap of the chord.

### ***Joints of thick-walled circular hollow sections***

In modern bridges and jack-up platform designs more and more use is made of very thick-walled hollow sections, sometimes in combination with cast steel nodes. As a consequence several investigations regarding the static behaviour of welded thick-walled joints have been carried out. The various investigations in this field are summarized by Choo & Qian [25] and Choo [33].

The strength of circular hollow section joints with chord diameter to thickness ratios  $2\gamma \geq 15$  can generally be based on the simplified ring model and the punching shear model. However, for larger diameter ratios  $\beta$  the strength deviation is more significant. This can readily be explained as follows: In the simplified ring model, as shown in Figure 6, the brace axial load is simplified to two line loads over an effective chord length  $B_e$  and the joint strength is based on the plastic capacity of the chord with length  $B_e$  (the ring) while neglecting the effect of the axial and shear forces on the plastic moment capacity.

This means that the joint strength is a function of  $t_0^2$ . However, for larger diameter ratios  $\beta$  the load transfer is mainly by membrane action at the saddle location which means that the joint strength is a function of  $t_0$ . For thick-walled chords this membrane load transfer becomes already more important for medium diameter ratios  $\beta$ . As a consequence the current design recommendations have to be modified to cover also joints with thick-walled chords and thus the different failure modes.



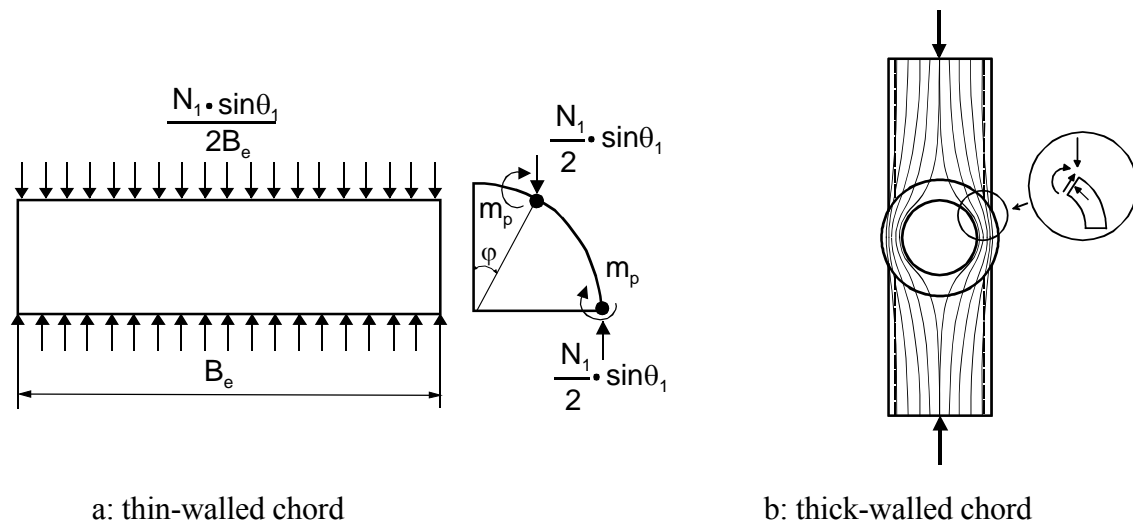


**Figure 6.** Ring model for thin- and thick-walled chords

In the investigations as summarised by Choo & Qian [25], the joint strength is defined based on a plastic limit load definition which agrees with Lu's 3% chord diameter limit for the joints with thinner chord sections. However, for joints with thick-walled chords the plastic limit load definition seems to give more consistent results. It was further observed that for X joints with a low inclined angle  $\theta$  in combination with a larger brace to chord diameter ratio  $\beta$ , chord shear, as shown in Figure 7 can reduce the load capacity, which is not covered in the current design recommendations.

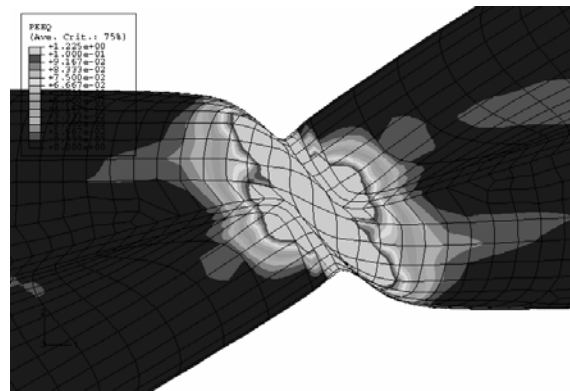


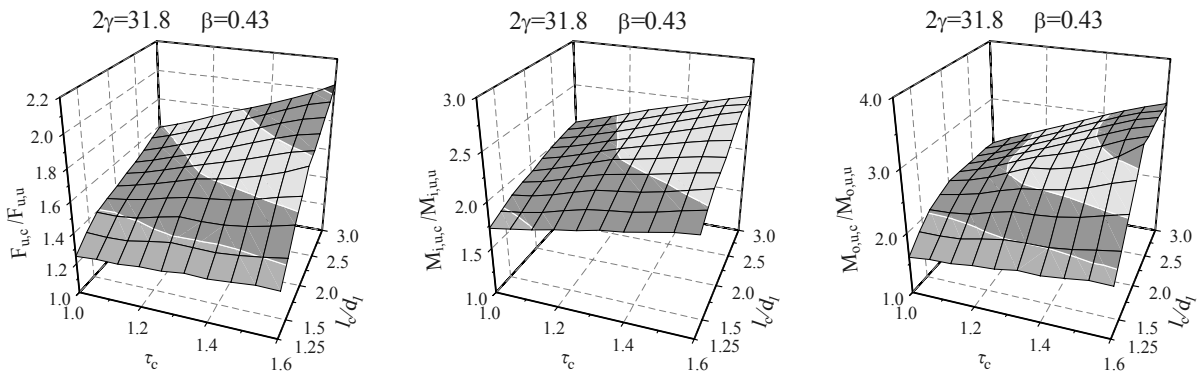
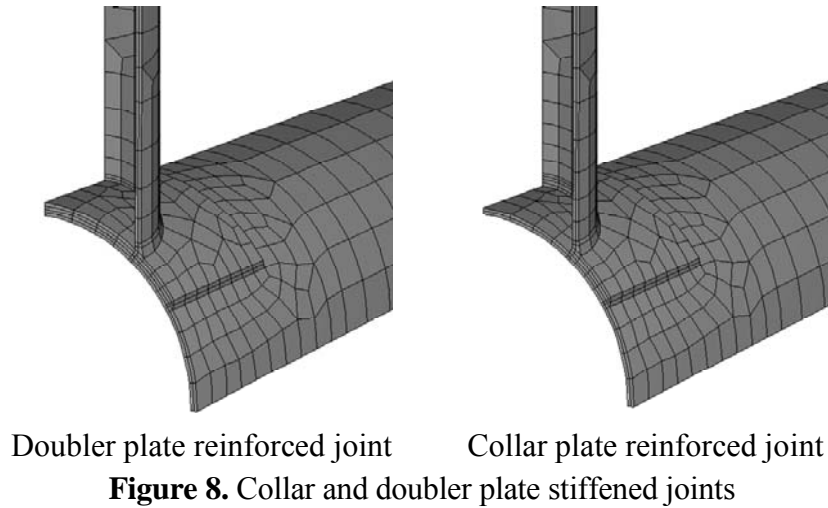
**Figure 7.** Interaction between chord plastification and chord shear in an X joint  
( $\theta = 30^\circ$ ,  $\beta = 1.0$  and  $2\gamma = 18$ )

### ***Collar and doubler plate joints***

For the enhancement of the strength of joints with thin-walled chords, reinforcement by collar and doubler plates may be used, as highlighted by Choo *et al.* [34]. In case of collar plates, the brace is welded to the chord and the collar consisting of two or four parts is welded to the chord and the brace around the brace to chord connection, as shown in Figure 8. In case of doubler plates the doubler plate is welded to the chord and the brace is welded to the doubler plate.

These reinforced joints have been extensively investigated at the National University of Singapore under axial brace loading and under bending-in-plane moments, for example, as presented in [34-37]. In all the investigations it was shown that for collar and doubler plates with a thickness equal or larger than that of the chord, the strength could be enhanced by 30% upwards, depending on the

dimensions of the collar and doubler plates and geometrical parameters and the loading. As an example for joints with  $2\gamma=31.8$  and  $\beta=0.43$ , Figure 9 shows the ratio of the strength of the collar plate reinforced joint with respect to that of referenced un-reinforced joints, as a function of the relative plate-to-chord wall thickness ratio  $\tau_c (=t_c/t_0)$  and the relative plate length to brace diameter ratio  $l_c/d_1$ . The strengthening effect is further depending on the loading, i.e. compression, tension, bending in-plane or bending out-of-plane.



### ***Ring-stiffened joints***

Although in the past several experimental and numerical investigations have been carried out, more evidence is becoming available for the design of these joints with the recent and improved numerical methods [38,39].

## **STATIC DESIGN OF JOINTS WITH HOLLOW SECTION BRACES AND AN I-SECTION CHORD**

The design equations for overlap joints with an I-section chord will be modified in a similar way as for rectangular hollow section joints, see Table 1. This has not been investigated in tests but the behaviour is rather similar.

## MISCELLANEOUS

### *Static design of elliptical hollow section joints*

Nowadays elliptical hollow sections are used in various architectural projects because of their special appearance. However, limited evidence is available on the joint behaviour.

Currently, research is underway at the University of Liege [40] and the National University of Singapore [41]. These initial investigations, show that the ring model can be used for explaining the numerically determined strengths. Further, research is being carried out at Toronto University to define the class limitations for the sections.

### *Hollow section joints in high strength steel*

The revised IIW recommendations for hollow section joints will cover joints made of steels with design yield stresses up to 460 N/mm<sup>2</sup>. Previously the validity was limited to steels with design yield stresses up to 355 N/mm<sup>2</sup>. However, joints with higher yield stresses will have a lower ductility for redistribution (e.g. effective width and punching shear), a lower deformation capacity (e.g. thin-walled joints with a high  $\beta$  ratio) or in other cases a larger deformation under service load (thin walled joints with a low  $\beta$  ratio). Further, it was found by Kurobane [42], that the strength for circular hollow section K-joints is a function of the yield to ultimate stress ratio. The effect was found to be most pronounced for K-joints for which the following relation was given:

$$\left( \frac{f_y}{f_u} \right)^{-0.757} \quad (3)$$

Figure 10 shows the relative effect related to the yield stress ratio for S235. It is shown that compared to K-joints of steel S 235 the non-dimensional strength of circular hollow section K-joints of S 460 would drop by 17%.

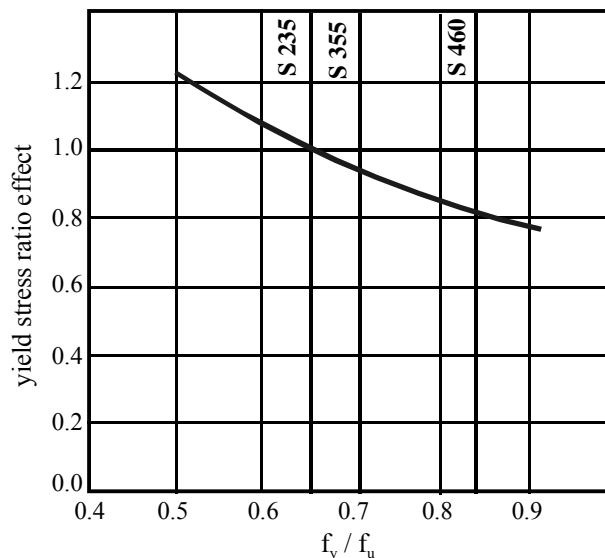


**Figure 10.** Influence yield to ultimate stress ratio for steel grades S 235, S 355 and S 460

Based on the ultimate strength only, without considering the ductility aspects and the larger deformation in Ref [43], it is proposed to limit the design yield stress to 0.8 times the ultimate stress, but even this does not fully compensate the lower non-dimensional strength.



Additional numerical calculations at Delft University of Technology [44] using the 3% of the chord width as ultimate deformation limit [45], showed that RHS K-joints made of S 460 had a 10 to 15% lower non-dimensional strength than comparable joints made from steel S 235, see Table 2.

**Table 2.** Non dimensional joint capacity related to the capacity for S 235

$2\gamma$	$\beta$					
	0.4		0.6		0.8	
	S 355	S 460	S 355	<b>S 460</b>	S 355	S 460
15	0.95	<b>0.90</b>	0.92	<b>0.84</b>	0.96*	**
25	0.95	<b>0.89</b>	0.95	<b>0.90</b>	0.96*	<b>0.92</b>
30	0.95	<b>0.90</b>	---	---	---	---
35	---	---	0.92	<b>0.85</b>	0.82*	<b>0.77*</b>

\* : Maximum capacity; others based on the 3% chord face indentation.

\*\* : Brace Buckling in compression.

The evaluation of the influence for the different steel grades on the static capacity of the joints is based on a factor  $R$ , which can be calculated by:

$$R = \frac{N_{ultimate, S...}}{N_{ultimate, S235}} \times \frac{f_y(S235)}{f_y(S...)} \quad (4)$$

Considering the larger deformations in joints of S460 in case the failure modes corresponding to chord face failure (RHS) or chord plastification (CHS) are governing, and the lower ductility in case of punching shear failure and brace effective width failure, it is proposed to adopt a general reduction factor of 0.9 and to limit the yield stress  $f_y$  to  $0.8f_u$  [44].

This avoids different corrections depending on the failure mode and this has been agreed by sub-commission IIW-XV-E for joints in steels with design yield stresses exceeding  $355 \text{ N/mm}^2$  up to  $460 \text{ N/mm}^2$ . This will result in a total joint capacity reduction of about 15%.

Furthermore, the  $b/t$  limitations given in the recommendations for the compression braces will be related to either class 1 or class 2 sections.

In Mang [46], it was shown that the strength of some tested K-joints made of S690 was only about 2/3 of the predicted joint strength using the joint strength equations developed for S235, thus care has to be taken to extrapolate the recommendations directly to joints of higher strength steel.

### ***Quality requirements for cold formed sections***

Since the available cold finished hollow sections on the market have different corner radii and different qualities, several investigations have been carried out during the last few years regarding checks for delivery requirements for cold-finished hollow sections [47]. Based on European research, e.g. recently at the University of Karlsruhe [48], it can be concluded that if welding is performed in or close to the corners, the corner radii have to meet the requirements given in Eurocode 3 [3], and in the IIW recommendations and recorded in Table 3. Furthermore, it is recommended to use fine-grained Al-killed steels. The modern steels are clean and have a low Carbon content. Si-killed steels may result in cracking after galvanizing.

In Europe the cold finished sections are delivered according to EN 10219-Part 2 (1998) [49] and up to 12 mm the average corner radii agree with those of table 3. However, a certain tolerance is allowed, which means that according to EN 10219 sections can be delivered with actual inner corner radii smaller than those in Table 3. In the research programme sections were also tested with small corner radii which satisfy the tolerances of EN 10219 but with actual corner radii smaller than those in Table 3. These sections are only allowed to be welded in the corners if these satisfy EN 10219 with the following additional material requirements:

- The maximum nominal wall- thickness is not exceeding 12.5 mm
- Aluminium killed steels with the quality grades J2H, K2H, MH, MLH, NH or NLH are used and
- the following maximum values are kept:  $C \leq 0.18\%$ ,  $P \leq 0.020\%$  and  $S \leq 0.012\%$

In other cases welding is only permitted at a distance of 5t from the corner or additional tests have to be performed to show that welding in the corners is permitted for that particular application. The requirements for steel S 460 are currently under discussion.

**Table 3.** Minimum inner corner radii for full aluminium ( $\geq 0.02\%$ ) killed cold finished hollow sections to allow welding in the corners

Steel grade	Wall thickness t (mm)	Minimum r/t (r = inner corner radius)	Remarks
<b>S235, S275, S355</b> (indicated by yield stresses in N/mm <sup>2</sup> )	<b>24</b> <b>12</b> <b>10</b> <b>6</b>	<b>3.0</b> <b>2.0</b> <b>1.5</b> <b>1.0</b>	The steels are indicated by yield stresses in N/mm <sup>2</sup>

No recommendation exists at present internationally for the determination of the required quality in relation to the service temperature, the welding condition, the loading, the static system, the thickness, the cold forming and the consequence of failure. According to the Dutch recommendations, NEN 6774 (2000) [50], the required quality for cold formed sections is generally one or two qualities higher than that required for hot-formed hollow sections. For example, if for a structural application in hot-formed hollow sections a Charpy value of 27 J at 20° is required, then for equivalent cold finished hollow sections this Charpy value is required at a temperature of 0° or -20°. Further work on this topic is being carried out at the University of Lappeenranta [51], where RHS K joints are tested at various temperatures between +20°C and -60°C. Based on this work it might be that proper selection criteria can be established.

## FATIGUE DESIGN OF HOLLOW SECTION JOINTS

### General

Based on the IIW-XV-E fatigue design recommendations for welded hollow section joints (IIW-XV-E, 1999) [6], CIDECT has published a design guide [52]. Since the publication, additional research is going on for thin-walled hollow section joints at the Monash University of Melbourne, and at the University of Karlsruhe. Further, stress concentration factors for bird beak connections are determined at the Delft University of Technology [53]. The connections with cast-steel nodes are under investigation at the Universities of Lausanne and Karlsruhe. During the last years, progress is also made in the development of 3D fracture mechanics models, for example at Nanyang Technological University in Singapore, the National University of Singapore and Delft University of Technology [54-56]. Currently, the hot spot stress method is reviewed to derive at a common procedure for hollow section joints and plate connections [57,58].

## GENERAL

At present still many investigations are going on and not all areas could be covered within the scope of this article. For example, many investigations just started in China, especially at the Tongji University, and it is expected that the coming years further improvements of the design rules may be expected.

In all areas the available information increases and many codes and recommendations become increasingly more voluminous and complicated with the probability of more errors. To the opinion of the authors, the information in codes should be limited to basic items and other relevant information should be given in background documents or design guides, for example, the CIDECT Design Guides and Packer & Henderson [59]. Furthermore, the recommendations should be consistent and as simple as possible. In the education, emphasis should be given to understanding by using simple models [60,61].

## ACKNOWLEDGEMENT

The authors wish to thank their colleagues in the IIW-XV-E committee and the CIDECT technical commission for their friendship and collaboration. Further, appreciation is extended to Dr.D.K.Liu, Dr.G.J.van der Vegte and Dr.X.D.Qian for providing the figures and doing final layout checks.

## REFERENCES

- [1] Wardenier, J. and Choo, Y.S., "Some developments in tubular joint research", Proceedings of the 4<sup>th</sup> International Conference on Advances in Steel Structures, Shanghai, China, Elsevier, 2005, Vol. 1, pp.31-40.
- [2] IIW-XV-E, International Institute of Welding Subcommittee XV-E, "Design recommendations for hollow section joints – Predominantly statically loaded", 2<sup>nd</sup> Edition, IIW. Doc. XV-701-89, International Institute of Welding, Paris, France, 1989.
- [3] CEN, Eurocode 3, "Design of steel structures, Part 1.8, Design of joints", Stage 49 Draft, Brussels, Belgium, November, 2003.
- [4] Kurobane, Y., Packer, J.A., Wardenier, J. and Yeomans, N., "Design guide for structural hollow section column connections", TUV-Verlag GmbH, Cologne, Germany, 2004.
- [5] Zhao, X-L., "Status of IIW static design recommendations for welded tubular joints", Proceedings of the 15<sup>th</sup> International Offshore and Polar Engineering Conference, Seoul, Korea, 2005, Vol. IV, pp.264-271.
- [6] IIW-XV-E, International Institute of Welding Subcommittee XV-E, "Recommended fatigue design procedure for welded hollow section joints, Part 1: Recommendations and Part 2: Commentary", IIW. Docs. XV-1035-99/XIII-1804-99, International Institute of Welding, Paris, France, 1999.
- [7] Packer, J.A., Wardenier, J., Kurobane, Y., Dutta, D. and Yeomans, N., "Design guide for rectangular hollow section (RHS) joints under predominantly static loading", TUV-Verlag GmbH, Cologne, Germany, 1992.
- [8] Liu, D.K. and Wardenier, J., "Multiplanar influence on the strength of RHS multiplanar gap KK-joints", Proceedings of the 9<sup>th</sup> International Symposium on Tubular Structures, Düsseldorf, Germany, Tubular Structures IX, A.A.Balkema Publishers, Lisse, The Netherlands, 2001, pp.203-212.

- [9] Liu, D.K. and Wardenier, J., "New chord stress functions for RHS gap K-joints", To be presented at the 11<sup>th</sup> International Symposium on Tubular Structures, Quebec City, Canada, 2006.
- [10] Wardenier, J., "Hollow section joints", Delft University Press, Delft, The Netherlands, 1982.
- [11] Chen, Y.Q., Liu, D.K. and Wardenier, J., "Design recommendations for RHS K-joints with 100% overlap", Proceedings of the 15<sup>th</sup> International Offshore and Polar Engineering Conference, Seoul, Korea, 2005, Vol. IV, pp.300-307.
- [12] Liu, D.K., Chen, Y.Q. and Wardenier, J., "Design recommendations for RHS K-joints with 50% overlap", Proceedings of the 15<sup>th</sup> International Offshore and Polar Engineering Conference, Seoul, Korea, 2005, Vol. IV, pp.308-315.
- [13] Veselcic, M., Herion, S. and Puthli, R.S., "Static behaviour of X, T and Y joints made of thin-walled RHS under brace axial load", Proceedings of the 9<sup>th</sup> International Symposium on Tubular Structures, Düsseldorf, Germany, Tubular Structures IX, A.A.Balkema Publishers, Lisse, The Netherlands, 2001, pp.155-164.
- [14] Rasmussen, J.R. and Young, B., "Tests on X- and K-joints in SHS stainless steel tubes", Journal of Structural Engineering, ASCE, 2001, 127(10), pp.1173-1182.
- [15] Kostas, N. and Packer, J.A., "Experimental examination of branch plate-to-RHS member connections", Proceedings of the 9<sup>th</sup> International Symposium on Tubular Structures, Düsseldorf, Germany, Tubular Structures IX, A.A.Balkema Publishers, Lisse, The Netherlands, 2001, pp. 135-144.
- [16] Karcher, D. and Puthli, R.S., "The static design of stiffened and unstiffened CHS L joints", Proceedings of the 9<sup>th</sup> International Symposium on Tubular Structures, Düsseldorf, Germany, Tubular Structures IX, A.A.Balkema Publishers, Lisse, The Netherlands, 2001, pp. 221-228.
- [17] Davies, G., Owen, J.S. and Kelly, R.B., "The effect of purlin loads on the capacity of overlapped bird beak K joints", Proceedings of the 9<sup>th</sup> International Symposium on Tubular Structures, Düsseldorf, Germany, Tubular Structures IX, A.A.Balkema Publishers, Lisse, The Netherlands, 2001, pp.229-238.
- [18] Willibald, S., Packer, J.A. and Puthli, R.S., "Experimental evaluation of bolted RHS flange-plate connection design models", Proceedings of the 9<sup>th</sup> International Symposium on Tubular Structures, Düsseldorf, Germany, Tubular Structures IX, A.A.Balkema Publishers, Lisse, The Netherlands, 2001, pp.127-134.
- [19] Jaurrieta, M.A., Alonso, A. and Chica, J.A., Eds., Proceedings of the 10<sup>th</sup> International Symposium on Tubular Structures, Madrid, Spain, Tubular Structures X, A.A.Balkema Publishers, Lisse, The Netherlands, 2003.
- [20] API, "Recommended practice for planning, designing and constructing offshore platforms RP-2A", American Petroleum Institute, USA, 1997.
- [21] ISO TC67/SC7/WG3/P3, "Draft code provisions for section E", Revision R6, International Organization for Standardization, 1997.
- [22] Dexter, E.M. and Lee, M.M.K., "Ultimate capacity of axially loaded K-joints in CHS", Proceedings of the 8<sup>th</sup> International Symposium on Tubular Structures, Singapore, Tubular Structures VIII, A.A.Balkema Publishers, Lisse, The Netherlands, 1998, pp.259-268.
- [23] Dier, A.F. and Lalani, M., "New code formulations for tubular joint static strength", Proceedings of the 8<sup>th</sup> International Symposium on Tubular Structures, Singapore, Tubular Structures VIII, A.A.Balkema Publishers, Lisse, The Netherlands, 1998, pp.107-116.
- [24] Yamada, Y., Morita, M., Makino, Y. and Wilmshurst, S.R., "A new ultimate capacity formula for unstiffened CHS T, TT, X, K and KK-joints under axial brace loads", Proceedings of the 8<sup>th</sup> International Symposium on Tubular Structures, Singapore, Tubular Structures XIII, A.A.Balkema Publishers, Lisse, The Netherlands, 1998, pp.213-222.

- [25] Choo, Y.S. and Qian, X.D., "Recent research on tubular joints with very thick-walled chords", Proceedings of the 15<sup>th</sup> International Offshore and Polar Engineering Conference, Seoul, Korea, 2005, Vol. IV, pp.272-278.
- [26] Van der Vegte, G.J., Makino, Y. and Wardenier, J., "The effect of chord pre-load on the static strength of uniplanar tubular K-joints", Proceedings of the 12<sup>th</sup> International Offshore and Polar Engineering Conference, Kitakyushu, Japan, 2002, Vol. IV, pp.1-10.
- [27] Van der Vegte, G.J., Liu, D.K., Makino, Y. and Wardenier, J., "New chord load functions for circular hollow section joints", Cidect report 5BK-4/03, Stevin report 6.03.1 (revised), Cidect, UK, 2003.
- [28] Pecknold, D.A., Ha, C.C. and Mohr, W.C., "Ultimate strength of DT tubular joints with chord preloads", Proceedings of the 19<sup>th</sup> International Conference on Offshore Mechanics and Arctic Engineering, New Orleans, USA, 2000.
- [29] Pecknold, D.A., Park, J.B. and Koppenhoefer, K.C., "Ultimate strength of gap K tubular joints with chord preloads", Proceedings of the 20<sup>th</sup> International Conference on Offshore Mechanics and Arctic Engineering, Rio de Janeiro, Brazil, 2001.
- [30] Van der Vegte, G.J., and Makino, Y., "Ultimate strength formulation for axially loaded CHS uniplanar T-joints", Proceedings of the 15<sup>th</sup> International Offshore and Polar Engineering Conference, Seoul, Korea, 2005, Vol. IV, pp.279-286.
- [31] Yura, J.A., "Ultimate capacity equations for tubular joints", OTC 3690, Houston, USA, 1980.
- [32] Wardenier, J., Kurobane, Y., Packer, J.A., Dutta, D. and Yeomans, N., "Design guide for circular hollow section (CHS) joints under predominantly static loading", TUV-Verlag GmbH, Cologne, Germany, 1991.
- [33] Choo, Y.S., "Recent development and innovation in tubular structures", Advances in Structural Engineering, 2005, 8(3), pp.217-230.
- [34] Choo, Y.S., Liang, J.X. and Van der Vegte, G.J., "An effective external reinforcement scheme for circular hollow section joints", Connections in Steel Structures V – Amsterdam, 2004, pp.423-432.
- [35] Choo, Y.S., Liang, J.X., Van der Vegte, G.J., and Liew, J.Y.R., "Static strength of doubler plate reinforced CHS X-joints loaded by in-plane moment", Journal of Constructional Steel Research, 2004, 60, pp.1725-1744.
- [36] Choo, Y.S., Liang, J.X., Van der Vegte, G.J., and Liew, J.Y.R., "Static strength of collar plate reinforced CHS X-joints loaded by in-plane moment", Journal of Constructional Steel Research, 2004, 60, pp.1745-1760.
- [37] Van der Vegte, G.J., Choo, Y.S., Liang, J.X., Zettlemoyer, N. and Liew, J.Y.R., "Static strength of T-joints reinforced with doubler or collar plates. Part II: Numerical simulations", Journal of Structural Engineering, ASCE, 2005, 131(1), pp.129-138.
- [38] Lee, M.M.K. and Llewelyn-Parry, A., "Strength estimation of offshore ring-stiffened DT joints", Proceedings of the 10<sup>th</sup> International Symposium on Tubular Structures, Madrid, Spain, Tubular Structures X, A.A.Balkema Publishers, Lisse, The Netherlands, 2003, pp.245-252.
- [39] Willibald, S., "The static design of ring-stiffened tubular T- and Y-joints", Proceedings of the 9<sup>th</sup> International Symposium on Tubular Structures, Düsseldorf, Germany, Tubular Structures IX, A.A.Balkema Publishers, Lisse, The Netherlands, 2001, pp.581-588.
- [40] Pietrapertosa, C. and Jaspart, J-P., "Study of the behaviour of welded joints composed of elliptical hollow sections", Proceedings of the 10<sup>th</sup> International Symposium on Tubular Structures, Madrid, Spain, Tubular Structures X, A.A.Balkema Publishers, Lisse, The Netherlands, 2003, pp.601-608.
- [41] Choo, Y.S., Liang, J.X. and Lim, L.V., "Static strength of elliptical hollow section X-joint under brace compression", Proceedings of the 10<sup>th</sup> International Symposium on Tubular

- Structures, Madrid, Spain, Tubular Structures X, A.A.Balkema Publishers, Lisse, The Netherlands, 2003, pp.253-258.
- [42] Kurobane, Y., “New developments and practices in tubular joint design”, IIW Doc. XV-488-81 and XIII-1004-81, International Institute of Welding, Paris, France, 1981.
  - [43] Noordhoek, C. and Verheul, A., “Static strength of high strength steel tubular joints”, ECSC Agreement 7210-MC/602-(F5.05d/93), 1996.
  - [44] Liu, D.K. and Wardenier, J., “Effect of the yield strength on the static strength of uniplanar K-joints in RHS”, Doc. IIW-XVE-04-293, Delft University, Delft, The Netherlands, 2005.
  - [45] Lu, L.H., de Winkel, G.D., Yu, Y. and Wardenier, J., “Ultimate deformation limit for tubular joints”, Proceedings of the 6<sup>th</sup> International Symposium on Tubular Structures, Melbourne, Australia, Tubular Structures VI, A.A.Balkema Publishers, Lisse, The Netherlands, 1994, pp.341-348.
  - [46] Mang, F., “Untersuchungen an Verbindungen von geschlossenen und offenen Profilen aus hochfesten Stählen“, AIF – Nr. 3347, Universität Karlsruhe, Germany, 1978.
  - [47] Packer, J.A. and Henderson, J.E., “Hollow structural section connections and trusses – A design guide”, Canadian Institute of Steel Construction, Toronto, Canada, 1997. (also available in Chinese)
  - [48] Puthli, R.S., Herion, S., Boellinghaus, Th. and Florian, W., “Welding in cold-formed areas of rectangular hollow sections”, Cidect final report and addendum 1A-6/05, Cidect, UK, 2005.
  - [49] EN 10219-Part 2, “Cold formed structural hollow sections of non-alloy and fine grain structural steels – Part 2: Tolerances, dimensions and sectional properties”, CEN, Brussels, Belgium, 1998.
  - [50] NEN 6774, “Eisen aan de staalkwaliteit voor constructiestaalsoorten in relatie tot het brosse breukgedrag voor overwegend statisch belaste constructies”, NEN, Delft, The Netherlands, 2000.
  - [51] Björk, T., Marquis, G., Kemppainen, R. and Ilvonen, R., “The capacity of cold-formed rectangular hollow section K-gap joints”, Proceedings of the 10<sup>th</sup> International Symposium on Tubular Structures, Madrid, Spain, Tubular Structures X, A.A.Balkema Publishers, Lisse, The Netherlands, 2003, pp.227-234.
  - [52] Zhao, X-L., Herion, S., Packer, J.A., Puthli, R.S., Sedlacek, G., Wardenier, J., Weynand, K., Van Wingerde, A.M., and Yeomans, N.F., “Design guide for circular and rectangular hollow section welded joints under fatigue loading”, Cidect design guide Nr. 8, TUV-Verlag GmbH, Cologne, Germany, 2000.
  - [53] Keizer, R., Romeijn, A., Wardenier, J. and Glijnis, P.C., “The fatigue behaviour of diamond bird beak T-joints”, Proceedings of the 10<sup>th</sup> International Symposium on Tubular Structures, Madrid, Spain, Tubular Structures X, A.A.Balkema Publishers, Lisse, The Netherlands, 2003, pp. 303-310.
  - [54] Lie, S.T., Chiew, S.P., Lee, C.K. and Huang, Z.W., “Modelling through-thickness and surface cracks in tubular joints”, Proceedings of the 9<sup>th</sup> International Symposium on Tubular Structures, Düsseldorf, Germany, Tubular Structures IX, A.A.Balkema Publishers, Lisse, The Netherlands, 2001, pp.285-290.
  - [55] Qian, X., Dodds, R.H. and Choo, Y.S., “Elastic-plastic crack driving force for tubular X-joints with mismatched welds”, Engineering Structures, 2005, Vol. 27, Issue 9, pp.1419-1434.
  - [56] Oomens, M., Romeijn, A., Wardenier, J. and Dijkstra, O.D., “Development and validation of a 3D fracture mechanics model for thick-walled CHS T-joints”, Proceedings of the 15<sup>th</sup> International Offshore and Polar Engineering Conference, Seoul, Korea, 2005, Vol. IV, pp.333-340.

- [57] Doerk, O., Fricke, W. and Weissenborn, C., “Comparison of different calculation methods for structural stresses at welded joints”, *International Journal of Fatigue*, 2003, 25(5), pp.359-369.
- [58] Marshall, P.W. and Wardenier, J., “Tubular vs non-tubular hot spot methods”, *Proceedings of the 15<sup>th</sup> International Offshore and Polar Engineering Conference*, Seoul, Korea, 2005 Vol. IV, pp.254-263.
- [59] Packer, J.A., “Whither tubular structures research?”, *Proceedings of the 10<sup>th</sup> International Symposium on Tubular Structures*, Madrid, Spain, *Tubular Structures X*, A.A.Balkema Publishers, Lisse, The Netherlands, 2003, pp.3-11.
- [60] Wardenier, J., “From a tubular morning mist to the tubular morning glow”, *Proceedings of the 9<sup>th</sup> International Symposium on Tubular Structures*, Düsseldorf, Germany, *Tubular Structures IX*, A.A.Balkema Publishers, Lisse, The Netherlands, 2001, pp.3-12.
- [61] Wardenier, J., “Hollow sections in structural applications”, *Bouwen met Staal*, Rotterdam, The Netherlands, 2002. (also available in Chinese and Spanish)



# RELIABILITY-BASED INTEGRATED DESIGN APPROACH FOR PLANAR STEEL FRAMES

Yu-Shu Liu\* and Guo-Qiang Li

*School of Civil Engineering, Tongji University, Shanghai, China*

*\*(Corresponding author: E-mail: yslu@mail.tongji.edu.cn)*

---

**ABSTRACT:** The current design method of steel structures is based on the member reliability and cannot assure the structural system reliability. To overcome the shortcoming of the current method, the integrated structural design approach, with consideration of system reliability for planar steel frames, is studied in this paper. The reliability-based integrated design approach (RID) directly checks the structural system limit states, based on structural nonlinear analysis, and the corresponding system reliability. In this paper, the reliability-based integrated design approach for planar steel frames is established on the basis of evaluating the ultimate load-carrying capacity and system reliability of planar steel frames. In the process of constructing the design formula, the target reliability index and importance factor are determined according to the current specification and the two common load combinations are considered. Design examples and comparisons demonstrate that RID provides a feasible way for structural engineers to improve the design quality of steel frame structures with certain and consistent system reliability levels.

**Keywords:** Reliability-based integrated design; Planar steel frames; Member reliability; System reliability; Target reliability index.

---

## 1. INTRODUCTION

As we all know, the system reliability of a structure is not only related to structural member reliability, but also influenced by the correlation between the members, the correlation between resistance and load, the configuration of the structure, the structural redundancy and ductility [1]. Actually, a building structure fulfills its function as an integrity, and a designer should aim at ensuring the reliability level of the structural system rather than the individual members. Therefore a structural design should be implemented based on integral structural analysis and reliability assessment [2]. However, the current limit state design for steel frames, e.g. AISC LRFD [3], is based on individual member checks, comprising the elastic integrated structural analysis for determining internal forces in the structural members and the capacity check of individual members. This approach leads to an ambiguous system reliability of the structure designed with only implementing member safety checks. The load and resistance factors design approach (LRFD), a probability-based limit state design approach, is just such a method. As an improvement, a structural design approach called preliminary integrated design (PID) [4] is constructed based on the frame analysis-frame check instead of the frame analysis-member check. Although it is a design approach oriented to system capacity limit states, PID cannot provide a check of the structural system reliability since the load and resistance factors in this approach are not obtained on the basis of the structural system reliability evaluation. However, the reliability-based integrated design approach (RID) proposed in this paper makes up the insufficiency of PID, which can ensure the structures designed to have the reliability index as close as possible to the target values.

## 2. APPROACH

### 2.1. Target Reliability Index

The target reliability index is the expected reliability index of structural design, it is an important factor in the reliability-based structural design. Theoretically, the value of target reliability index

should be established through optimal method according to the importance of structures, failure consequences, causes and modes of structures, and economic ability. Because of the deficiency of statistical information and considering the succession of the specifications, the target reliability index used in current codes is adopted by calibrating to the safety level implied by existing codes. Similar to AISC LRFD [3], GB50068-2001 [5] is also a probabilistic design code based on the limit states of structural components, and its target safety level, as shown in Table 1 ( $\beta$  denotes reliability index,  $P_f$  denotes failure probability), is taken to be the probabilities of structural failure implied by given codes which are judged to be acceptable in China. For the sake of simplification and conservative consideration, it is reasonable that the target reliability index used in RID can has a increase of 0.5 compared to the target reliability index employed in the limit state design approach based on individual members with ductile failure mode, because although the integrated failure of steel frames is ductile, its importance level is comparative to that of component failure of structures with brittle mode, so the target reliability index of the former is the same as the latter.

**Table 1.** Target reliability index employed in current specification and RID

Design method	Failure mode	Importance class of structures					
		Class 1		Class 2		Class 3	
		$\beta$	$P_f$	$\beta$	$P_f$	$\beta$	$P_f$
Current specification	Brittle failure	4.2	$1.3 \times 10^{-5}$	3.7	$1.1 \times 10^{-4}$	3.2	$6.9 \times 10^{-4}$
	Ductile failure	3.7	$1.1 \times 10^{-4}$	3.2	$6.9 \times 10^{-4}$	2.7	$3.5 \times 10^{-3}$
RID	Ductile failure	4.2	$1.3 \times 10^{-5}$	3.7	$1.1 \times 10^{-4}$	3.2	$6.9 \times 10^{-4}$

## 2.2. Load and Load Combination

Three types of loads need to be considered in the reliability-based integrated design of steel frames. They are dead load, live load and wind load. The statistic data of these loads are tabulated in Table 2. Two loading cases are investigated. One is vertical dead load with vertical live load and the other is vertical dead load with simultaneously vertical live load and horizontal wind load. In assessment of system reliability, dead load and live load are treated as random load in loading case 1 while only wind load is treated as random load in loading case 2.

**Table 2.** Statistic data of various loads

	Ratio of mean to normal value (K)	Coefficient of variance(COV)	Distribution type
Dead load	1.06	0.07	Normal
Live load	1.00	0.25	Gumbel
Wind load	0.999	0.193	Gumbel

## 2.3. Statistics of Structural Resistance

The randomness of structural resistance of steel frames is mainly relevant to the randomness of the sectional geometry, the randomness of material yielding strength and the randomness of calculation mode for determining structural resistance, the statistics of which are listed in Table 3 [6].

It is observed that the PDF curves of structural resistance of steel frames under the two loading cases fit lognormal distribution quite well [7]. Therefore, the structural integrated resistance of steel frames will be assumed to follow a lognormal distribution in the following calculation of load and resistance factors.

**Table 3.** Statistics of principal random variables influencing structural resistance

		Ratio of mean to normal value	Coefficient of variance
Geometrical parameters	Length or width thickness	1.000	0.0135
		1.000	0.0350
Yielding strength of steel	Q235	$t \leq 16\text{mm}$	1.070
		$16\text{mm} < t \leq 40\text{mm}$	1.074
		$40\text{mm} < t \leq 60\text{mm}$	1.118
		$60\text{mm} < t \leq 100\text{mm}$	1.087
	Q345	$t \leq 16\text{mm}$	1.040
		$16\text{mm} < t \leq 35\text{mm}$	1.025
		$35\text{mm} < t \leq 50\text{mm}$	1.125
		$50\text{mm} < t \leq 100\text{mm}$	1.184
Calculation mode for determining structural resistance	Vertical load	1.000	0.075
	Horizontal and vertical load	1.000	0.075

## 2.4. Practical Design Formula

Reliability-based integrated design method for steel portal frames is first introduced in [4]. The practical design formula of this method can be written as

$$R_n / \phi \geq \gamma_0 \cdot \sum \gamma_i \cdot S_{ni} \quad (1)$$

where  $R_n$  is the nominal value of structural resistance determined by nonlinear structural analysis,  $S_{ni}$  is a load effect,  $\phi$  and  $\gamma_i$  are the factors of structural resistance and load effect, which can be obtained by reliability analysis of structures,  $i$  stands for the number of load effects, and  $\gamma_0$  is the importance factor of structures. Though Eq.(1) is similar to that of traditional LRFD, they factually differ from each other because the factors of resistance and load in RID are based on ensuring reliability of structural system, rather than reliability of individual members as in LRFD.

### 2.4.1. Importance Factor

The value of importance factor  $\gamma_0$  used in conventional member-checked approach is taken as

1. for structure components whose importance class is class one or serviceable life is more than 100 years,  $\gamma_0$  should not be less than 1.1;
2. for structure components whose importance class is class two or serviceable life is 50 years,  $\gamma_0$  should not be less than 1.0;
3. for structure components whose importance class is class three or serviceable life is 5 years,  $\gamma_0$  should not be less than 0.9.

Since  $\gamma_0$  is only relevant to the importance of structures, the importance factor of structures employed in RID can take the same value as in LRFD, stated as above.

### 2.4.2. Load and Resistance Factors

The process of determining the load and resistance factors in the formula for RID is similar to that for traditional limit-state design, except that the factors of the former come from assessment of system reliability of structures whereas those of the latter from reliability calibration of individual members [2]. The flow chart for determining load and resistance factors for RID is given in

Figure 1 and the data used for this purpose are listed in Table 4, the values of resistance statistics in Table 4 are taken from the sampling of the structural resistance which is calculated by finite element program.

**Table 4.** Data used in calculation of load and resistance factors

(a) Q235						
Load case	Resistance factor	Load factor		Load ratio	Resistance statistics	
1	1.20	Dead load	Live load	Live load/ dead load	COV	$K_R^{(3)}$
		1.00-1.60 <sup>1)</sup>	1.40-3.00 <sup>1)</sup>	0.50-1.10 <sup>2)</sup>	0.110	1.035
2	1.20	Dead load + live load <sup>4)</sup>	Wind load	none	COV	$K_R^{(3)}$
		1.0	1.10-2.65 <sup>1)</sup>	none	0.108	1.065

(b) Q345						
Load case	Resistance factor	Load factor		Load ratio	Resistance statistics	
1	1.20	Dead load	Live load	Live load/ dead load	COV	$K_R^{(3)}$
		1.00-1.60 <sup>1)</sup>	1.40-3.00 <sup>1)</sup>	0.50-1.10 <sup>2)</sup>	0.110	1.046
2	1.20	Dead load + live load <sup>4)</sup>	Wind load	none	COV	$K_R^{(3)}$
		1.0	1.10-2.65 <sup>1)</sup>	none	0.121	1.103

1) Interval is equal to 0.05;

2) Interval is equal to 0.15;

3)  $K_R$  is the ratio of mean to normal value of structure resistance;

4) The summation of dead load and live load is treated as a constant load in load case 2.

For the convenience of practical application, the resistance factor,  $\phi$ , can be taken as a constant being equal to 1.2, and the optimal load factors can then be determined according to the target reliability with this strategy. Following the process of calculation shown in Figure 1, the load and resistance factors with a certain system reliability for reliability-based integrated design of steel frames can be determined. The relative errors between  $R_{Kij}$  and  $R_{Kj}^*$  indicated in Figure 1 under different load factors and different target reliability index is shown in Figure 2. The optimal load and resistance factors for RID aiming at definite target reliability levels are listed in Table 5.

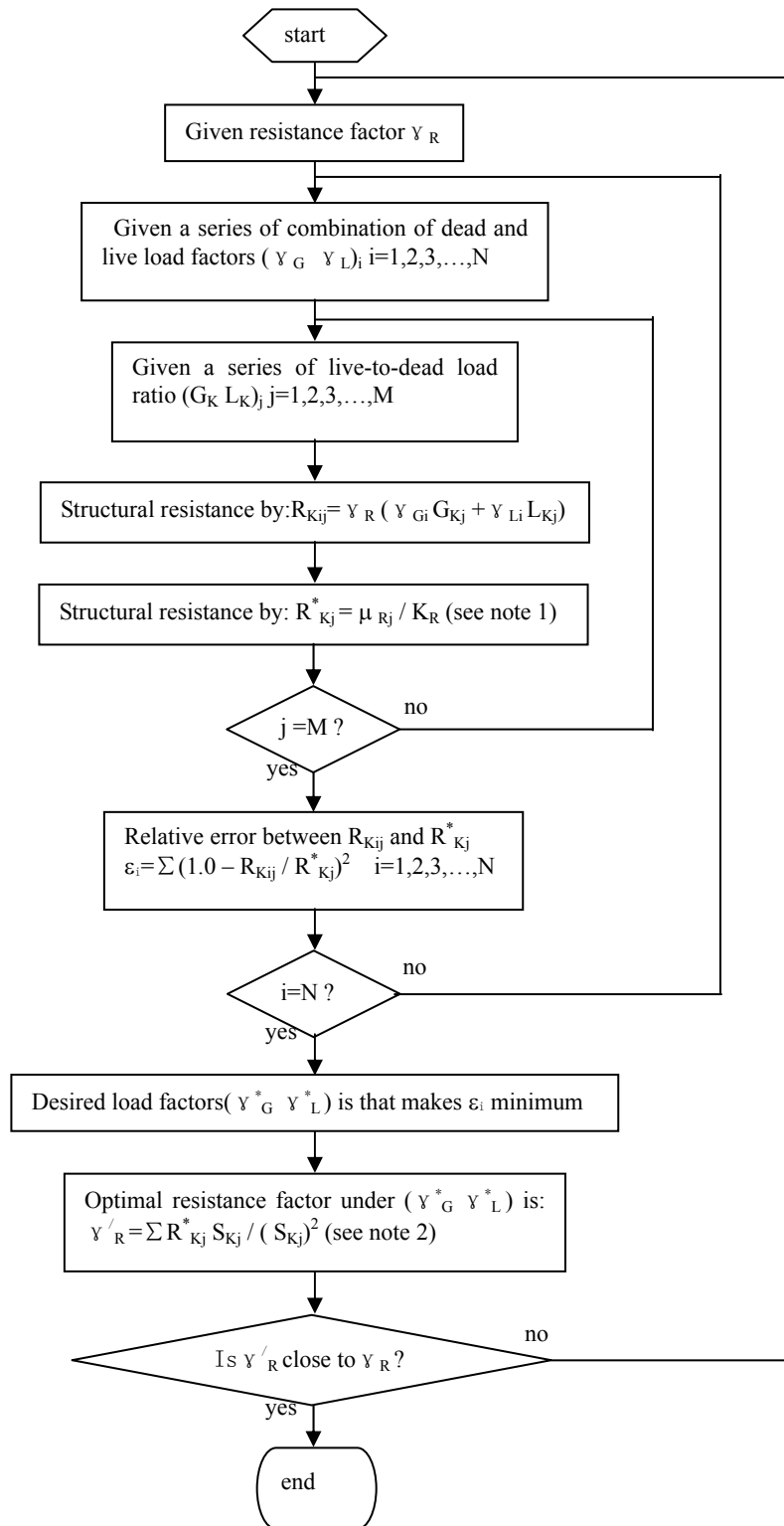
Since the final values of resistance factors are very close to the initial value 1.2, it is acceptable that uniform resistance factor for RID,  $\phi=1.2$ , can be employed in the practical application.

**Table 5.** Optimal load and resistance factors and their errors

(a) Q235						
$\beta_t$	Load case 1				Load case 2	
	$\gamma_G$	$\gamma_L$	$\gamma_R$	$\epsilon$	$\gamma_W$ ( $\gamma_G + \gamma_L = 1.0$ )	$\epsilon$
2.7	1.10	1.60	1.1898	5.08398e-004	1.45	2.53647e-004
3.2	1.10	1.90	1.1969	7.09022e-005	1.70	1.46003e-005
3.7	1.10	2.25	1.2023	2.55264e-005	1.95	1.61455e-007
4.2	1.10	2.70	1.1927	2.21763e-004	2.25	9.66120e-006

(b) Q345						
$\beta_t$	Load case 1				Load case 2	
	$\gamma_G$	$\gamma_L$	$\gamma_R$	$\epsilon$	$\gamma_W$ ( $\gamma_G + \gamma_L = 1.0$ )	$\epsilon$
2.7	1.10	1.55	1.1972	2.80723e-004	1.45	1.07029e-005
3.2	1.10	1.85	1.2025	1.02353e-004	1.65	8.15408e-005
3.7	1.10	2.20	1.2061	1.40213e-004	1.90	1.22249e-004
4.2	1.10	2.65	1.1948	1.13074e-004	2.20	5.76273e-005



note1.  $\mu_{Rj}$  is determined by First Order Second Moment(FOSM) method with the statistics listed in table 4;

note2.  $R_{Kj}$  is obtained by  $R_{Kj} = \gamma_G^* G_{Kj} + \gamma_L^* L_{Kj}$

**Figure 1.** Flow chart for calculation of load and resistance factors.

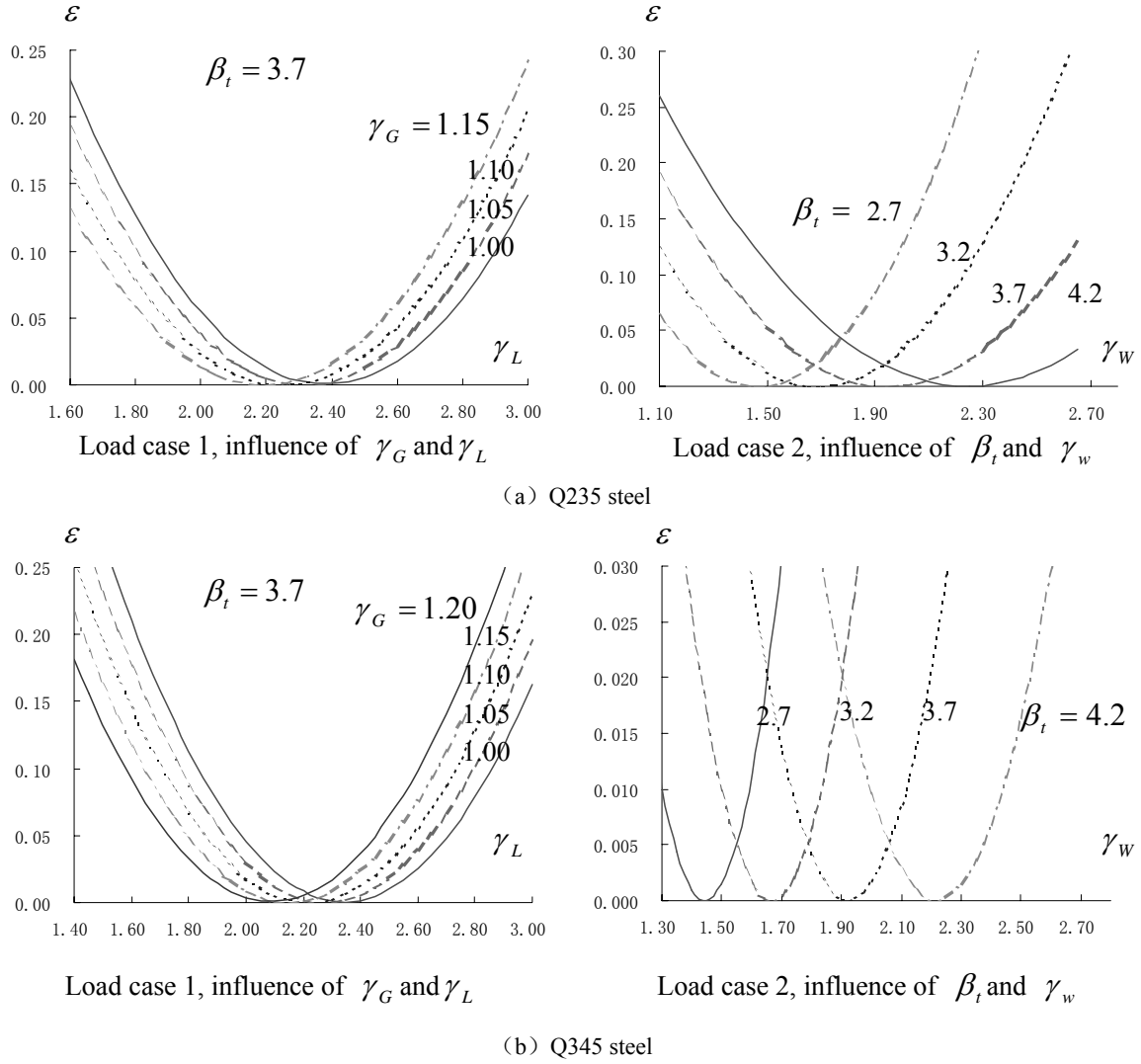


**Figure 2.** Relative error comparisons when calculating load and resistance factors

Then the expressions for design of steel frames under loading cases 1 and 2 with the target system reliability index being equals 3.7 can be obtained as

For Loading case 1, Q235 steel

$$R_n / 1.2 \geq 1.10 \cdot G_n + 2.25 \cdot L_n \quad (2a)$$

Q345 steel

$$R_n / 1.2 \geq 1.10 \cdot G_n + 2.20 \cdot L_n \quad (2b)$$

where  $R_n$  is the normal value of structure resistance under loading case 1, determined by nonlinear structural analysis;  $G_n$  and  $L_n$  represent the normal values of dead and live load effects.

For Loading case 2, Q235 steel

$$R_n / 1.2((G + L) = 1.00 \cdot (G_n + L_n)) \geq 1.95 \cdot W_n \quad (3a)$$

Q345 steel

$$R_n / 1.2((G + L) = 1.00 \cdot (G_n + L_n)) \geq 1.90 \cdot W_n \quad (3b)$$

where  $R_n$  is the normal value of structure resistance under loading case 2, determined by nonlinear structural analysis(in the process of calculation, the value of  $R_n$  is determined under constant dead load and live load);  $W_n$  represents the normal value of wind load.

## 2.5. Design steps

The design steps using RID are

1. determine the structural size, material type, and the values of nominal loads of the steel frame design for;
2. select a group of sectional dimensions for the frame and perform the integrated nonlinear frame analysis, by which the nominal resistances of the trial frame ( $R_n$  in the design formula) under two loading cases are obtained;
3. check the design formula with the nominal frame resistances and the nominal loads;
4. repeat steps 2 and 3 till the design equations are satisfactorily met.

## 3. APPLICATION

### 3.1. An Example

An asymmetric two-storey two-bay steel frame is shown in Figure 3 [8]. Using this example, we can compare different design methods such as RID, PID and LRFD. The loads in Figure 3 is the summation of normal values of dead load and live load and the ratio of dead to live load is 1.0. The statistics used for reliability analysis is listed in Table 6. The normal value of yielding strength of steel is 248MPa and the elastic modulus is 206GPa.

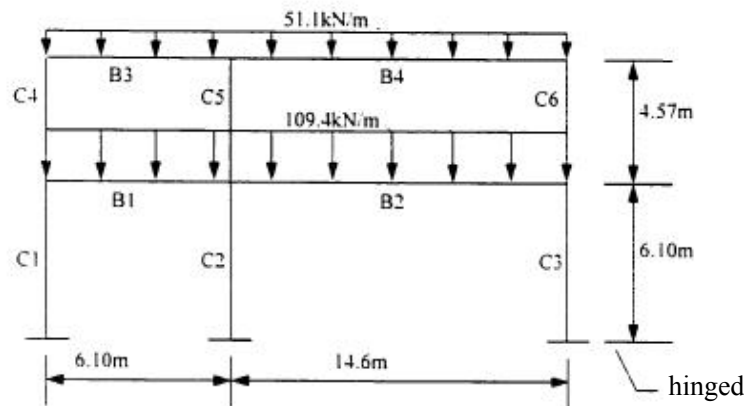


**Figure 3.** Dimensions and loads of a two-storey two-bay steel frame

**Table 6.** Statistics of loads and yielding strength of example frame [8]

Statistics	Ratio of mean to normal value	Coefficient of variance	distribution
Dead load	1.00	0.08	Normal
Live load	1.00	0.25	gumbel
Yielding strength	1.05	0.10	gumbel

The design steps of PID are similar with those of RID. However, the load and resistance factors employed in PID are taken from LRFD, as

for loading case 1

$$0.90 \cdot R_n \geq 1.20 \cdot G_n + 1.60 \cdot L_n \quad (4)$$



where  $R_n$  is the nominal value of the structural resistance against vertical loads determined by nonlinear integrated structural analysis, and  $G_n$  and  $L_n$  are respectively the nominal value of dead and live load effects, and

for loading case 2

$$0.90 \cdot R_n ((G + L) = 1.20 \cdot (G_n + L_n)) \geq 1.30 \cdot W_n \quad (5)$$

where  $R_n$  is the nominal value of the structural resistance against horizontal loads determined by nonlinear integrated structural analysis when the summation of dead load and live load is equal to 1.20 times of its nominal values, and  $W_n$  is the nominal value of wind load.

### 3.2. Design Results

The steel frame shown in Figure 3 is designed by various methods, including traditional LRFD, PID and RID. The sections of components and the steel consumption of the frame obtained by different design methods are given in Table 7. Since for this steel frame, the loading case 1 is the control loading case, then the reliability of loading case 2 is not considered.

The results of system reliability for the frame designed by various methods are listed in Table 8, where  $\beta$  and  $p_f$  are respectively the reliability index and failure probability.

The design results show that the system reliability index of the frame designed by LRFD is larger than the target reliability index, which is 3.7, but the system reliability of PID is lower than that level. While the reliability index of frame designed by RID is close to the expected reliability level and meets the requirement of structural integrated design. The steel consumption of the frame designed by RID is also reasonable, which is between the values obtained respectively by LRFD and PID.

**Table 7.** Comparison of component sections and steel consumption obtained by various methods

	Design method	LRFD	PID	RID
Components	C1	W12×19	W12×14	W12×16
	C2	W14×132	W14×99	W14×109
	C3	W14×109	W14×82	W14×99
	C4	W10×12	W10×12	W10×12
	C5	W14×109	W14×99	W14×109
	C6	W14×109	W14×99	W14×109
	B1	W27×84	W27×84	W27×84
	B2	W36×135	W30×108	W30×108
	B3	W18×40	W18×40	W18×40
	B4	W27×94	W27×84	W27×94
	Steel consumption (10 <sup>3</sup> kg)	9.59	8.51	9.12

**Table 8.** System reliability of the frame designed by LRFD, PID and RID

Design method	$\beta$	$P_f$
LRFD	4.4591	4.1148e-006
PID	3.2033	6.7923e-004
RID	3.8427	6.0856e-005

#### 4. CONCLUSIONS

The Reliability-based Integrated Design (RID) of planar steel frames is studied in this paper. The following conclusions can be drawn from above studies:

- 1). The system reliability index of steel frames designed by RID is larger than that designed by PID and lower than that designed by LRFD, while it is close to the expected reliability level and meets the requirement of structural integrated design.
- 2). Although it is also an integrated design method, PID cannot provide a check of the system reliability level since the load and resistance factors in its design expressions are coming directly from LRFD without consideration of system reliability. So the system reliability of a structure designed by PID cannot be guaranteed.
- 3). From the example concerning design of a steel frame, it can be seen that RID consumes less steel than LRFD. This novel design method can make up the insufficiency of conventional design method and facilitate the design procedure without requirement of member checks, while ensuring system reliability.

#### REFERENCES

- [1] Ellingwood, B.R., "Probability-based codified design: past accomplishments and future challenges", Structural Safety, 1994, 13, pp.159-176.
- [2] Li, J-H., "Probabilistic limit-state design for building structures", Beijing, Press of Chinese Construction Industry, 1990 (in Chinese).
- [3] AISC LRFD, "Manual of steel construction, load and resistance factor design", 2nd edition, Chicago (IL): American Institute of Steel Construction, 1994.
- [4] Li, J-J. and Li, G-Q, "Reliability-based integrated design of steel portal frames with tapered members", Structural Safety, 2004, 26, pp.221-239
- [5] GB 50068-2001, "The reliability design uniform standard for building structures", 2001 (in Chinese).
- [6] Zhang, X-P., "Reliability analysis and design for building structures", Beijing, Science Press, 2001 (in Chinese).
- [7] Liu, Y-S, "Research on theory of nonlinear analysis and integrated reliability design for planar steel frames", PhD dissertation, Tongji University, Shanghai, PR China, 2004 (in Chinese).
- [8] Zhou, W-X, "Reliability evaluations of reinforced concrete columns and steel frames", Ph.D dissertation, University of Western Ontario, 2000.

# ANALYTICAL AND EXPERIMENTAL INVESTIGATIONS OF BOLTED HAUNCHED BEAM-TO-COLUMN JOINTS WITH A VIEW OF SEISMIC DESIGN

A. Lachal\*, J.M. Aribert and G. Loho

*Institut National des Sciences Appliquées, Rennes, France*

*\*(Corresponding author: E-mail: Alain.Lachal@insa-rennes.fr)*

---

**ABSTRACT:** A possible solution to strengthen end-plate bolted composite joints is to extend the end-plate below the beam and to add a haunch in the corner with the column. This strengthening arrangement is studied in this paper from both theoretical and experimental approaches. Experimental results are analysed and compared with theoretical ones issued from analytical models essentially based on Eurocodes 3, 4 and 8 [1-6]. Results are interpreted in terms of rotational stiffness, moment resistance and rotation capacity. The contribution of haunches to strengthen a beam-to-column joint and to dissipate energy under cyclic loadings is quantified.

**Keywords:** Composite construction; Beam-to-column joint; End-plate bolted joint; Haunch; Seismic action.

---

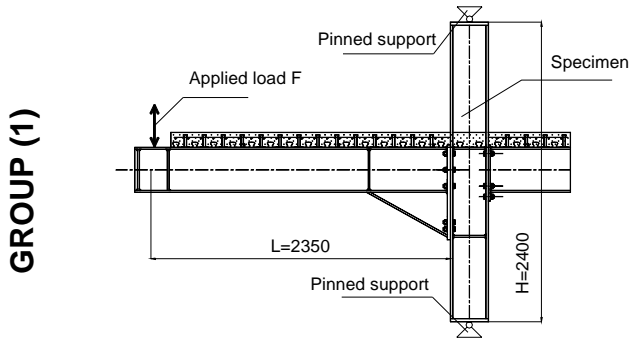
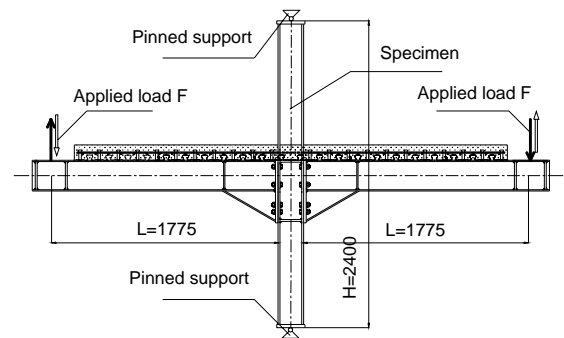
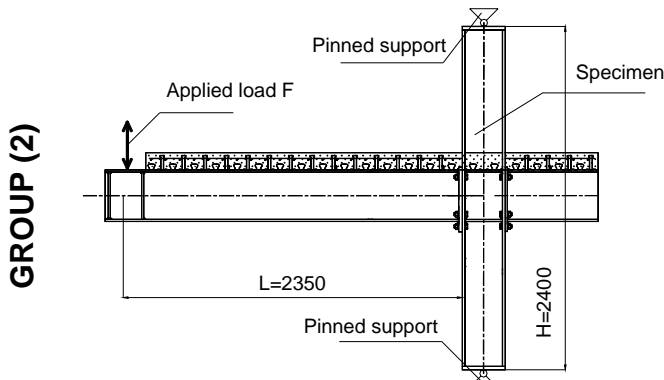
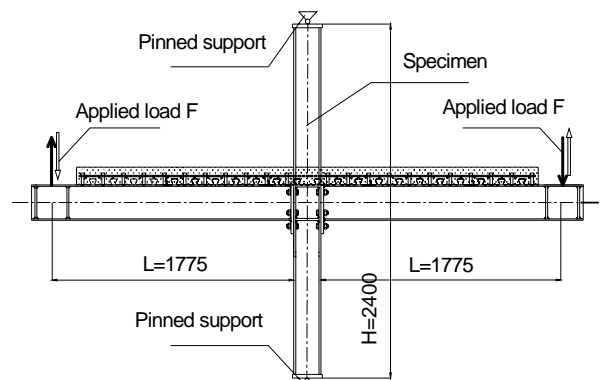
## 1. INTRODUCTION

End-plate bolted beam-to-column joints are currently used in Europe in steel and composite constructions. In composite constructions, generally these joints appear semi-rigid and partial strength. The use of such joints in anti-seismic moment resisting frames is allowed now by the seismic code Eurocode 8 - Part 1 [5]. Nevertheless, recent studies have shown that such design should be limited to areas of low and medium seismicity; but in zone of high seismicity, the joints should be strengthened to become rigid and full-strength.

After Northridge earthquake, researches carried out on steel welded beam-to-column joints have shown that adding haunches provided a good solution to strengthen a joint and to obtain good seismic performances, SAC [7], Lee and Uang [8], NIST [9], Gross *et al.* [10], Yu *et al.* [11]. Main results of these researches were grouped in a State of the Art Report published by the Federal Emergency Management Agency, FEMA-355D [12], as well as recommendations, FEMA-351 [13], including a design procedure for welded haunch connections. More recently, a draft of Eurocode 8 - Part 3 [6] has proposed recommendations to strengthen beam-to-column steel and composite connections by adding haunches.

In the case of end-plate bolted composite connections, haunches located at the bottom side of the beam flanges seem more convenient for fabrication. Also it is suggested by Gross *et al.* [10] to adopt an haunch depth  $b \approx 0.33$  times the beam depth  $d_b$ , with an angle of the haunch  $\theta \approx 30^\circ$  to limit the haunch web slenderness. In the present study, we have opted for a simple predesign method adopting the haunch depth  $b$  equal to the steel beam depth  $d_b$  and the haunch length  $a$  equal to  $2b$ . These dimensions make easier the haunch fabrication cut out directly from the steel beam. In addition, such a predesign method allows to ensure a better balance between hogging and sagging moment resistances in a composite connection (Table 2).

Adopting such a strengthening strategy, 5 tests dealing with steel and composite joints equipped with haunched bolted end-plates, with two arrangements (T and cruciform as shown in Figures 1 and 2 respectively) has been fabricated and tested (group 1 in Table 1). A companion series of 5 similar tests, simply end-plate connected without haunch strengthening (Figures 3 and 4), has been fabricated simultaneously and then tested in order to clearly evaluate the haunch contribution (group 2 in Table 1).

**Figure 1. T with an haunch****Figure 2. Haunched joint****Figure 3. T without haunch****Figure 4. Joint without haunch  
Cruciform arrangement  
(unsymmetrically loaded)****T arrangement**

An analytical approach mainly based on the works of Lee and Uang [8] and adopted recently in Eurocode 8 – Part 3 is firstly adapted to the static design of haunches in composite beam to steel column joints. In a second step the main characteristics of rotational stiffness and moment resistance of haunched end-plate bolted connections have been determined from Eurocodes 4 and 3 concepts (using measured material properties). Analytical results are compared to experimental ones in order to evaluate the good performances of these analytical models. The influence of the haunch on the joint design has been taken into account (with regard to shear connection, reinforcement, column web panel...). In addition the plastic energy dissipation mainly located outside the joint in the case of full-strength beam-to-column joints is evaluated experimentally and compared to the energy dissipation obtained in the case of partial-strength beam-to-column joints.

## 2. ANALYTICAL STATIC DESIGN MODELS

### 2.1. Haunch Static Design

#### 2.1.1. Determination of the bending moment and the vertical shear at the haunch tip

Previous studies, Yu *et al.* [11], have shown that the contribution of the haunch web to the stiffness in the haunch flange direction was minor (equal or less than 5%). So, a simplified model idealizing the haunch flange as an elastic strut has been developed. Considering the beam vertical shear,  $V_{Ed}^{\pm}$ , at the haunch tip, a parameter  $\beta^{\pm}$  is introduced to define the vertical reaction force  $\beta^{\pm} V_{Ed}^{\pm}$  transmitted to the steel beam at the haunch tip. This parameter  $\beta^{\pm}$  quantifies the force distribution within the haunch region.

The model was developed only for steel joints; in this study it is adapted to composite solutions of haunched joints, introducing composite beam characteristics and distinguishing moment values and neutral axis positions in sagging and hogging bending.

The static design of the haunch is based on the moment and vertical shear that develop at the tip of the haunch when a plastic hinge occurs in the beam. Following the step-by-step design procedure proposed by Yu *et al.* [11], a first step consists in the determination of maximum sagging and hogging bending moments  $M_{Ed}^{\pm}$  exerted by the composite beam, namely:

$$M_{Ed}^{\pm} = \alpha M_{pl,R}^{\pm} \quad (1)$$

$\alpha$  is a moment overstrength factor for which the adopted value of 1.1 seems reasonable in comparison with current codes (see 6.5.5 (3) in Eurocode 8 – Part 1).

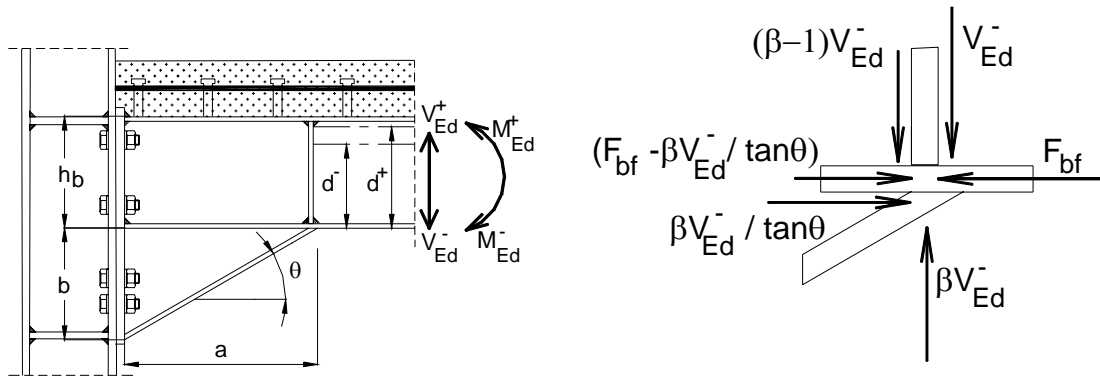


**Figure 5.** Simplified Model of Haunch Connection

In the experimental context of the present paper  $M_{pl,R}^{\pm}$  is determined using the mean measured values of the yield strength of structural steel  $f_y$ , of the concrete strength  $f_c$  and of reinforcement strength  $f_s$ . It should be noted that in actual design where the properties of the materials are defined generally by the nominal or characteristics values  $f_{yk}$ ,  $f_{ck}$  and  $f_{sk}$ , the strengths used to determine the design moment resistance  $M_{pl,Rd}^{\pm}$  would be obtained introducing material overstrength factors, in particular for the structural steel:  $f_{ye} = \gamma_{ov} f_y$  with  $\gamma_{ov} \approx 1.25$ . Also partial safety factors would be used for the materials taking into account the accidental nature of the seismic action (for instance:  $\gamma_a = 1.0$  for the structural steel;  $\gamma_s = 1.0$  for the reinforcing steel; and  $\gamma_c = 1.30$  for the concrete).

Considering the testing arrangement, the design vertical shear  $V_{Ed}^{\pm}$  is evaluated simply as follows:

$$V_{Ed}^{\pm} = M_{Ed}^{\pm} / L' \quad (2)$$

where :  $L' = L - a$  (see Figures 1 to 5)

In actual design,  $V_{Ed}^{\pm}$  would be given by:

$$|V_{Ed}^{\pm}| = \alpha \frac{M_{pl,Rd}^{+} + M_{pl,Rd}^{-}}{L''} + |V_{Ed,G}|$$

where

$L''$  would be the distance between the two plastic hinges occurring near the ends of the concerned beam span, and

$V_{Ed,G}$  would be the vertical shear at the plastic hinge location due to uniform and concentrated vertical loads acting within  $L''$ .

From the idealized model presented in Figure 5 of an elastic composite beam bearing on an elastic support represented by the haunch flange, the non-dimensional parameter  $\beta^\pm$  (in sagging (+) and hogging (-) bending respectively) may be evaluated considering the force equilibrium and the deformation compatibility at the haunch tip between the beam flange and the haunch flange.

So, in both sagging (+) and hogging (-) bendings,  $\beta^\pm$  is given by:

$$\beta^\pm = \frac{b}{a} \left( \frac{6L'd^\pm + 3ad^\pm + 3bL' + 2ab}{6(d^\pm)^2 + 6bd^\pm + 2b^2 + \frac{6I_{1,2}}{A_b^\pm} + \frac{6I_{1,2}}{A_{hf} \cos^3 \theta}} \right) \quad (3)$$

where:

$I_1$  and  $A_b^+$  are respectively the second moment of area under sagging bending and the associated cross-sectional area of the composite beam;

$I_2$  and  $A_b^-$  are respectively the second moment of area and the cross-sectional area of the composite beam, neglecting the concrete in tension but including reinforcement;

$A_{hf}$  is the area of the haunch flange;

$a$ ,  $b$  and  $\theta$  are the length, the depth and the angle of the haunch, defined in Figure 5;

$d^+$  ( $d^-$ ) is the distance from the plastic neutral axis under sagging bending (hogging bending) to the external face of the lower flange of the beam.

### 2.1.2. Design checking

Firstly, a global check should be satisfied which consists in having the sum of the moment resistances of the two columns above and below the joint greater than the sum of the moments transmitted by the two beams through the haunch that frame into the column. This condition has led to extend the supplementary web plates of the column sufficiently beyond the web panel (over 20 cm).

The strength and the stability of the haunch flange have to be checked using the following conditions:

$$\text{Strength: } A_{hf} \geq \frac{\beta^\pm V_{Ed}^\pm}{f_{y,hf} \sin \theta}; \quad (4)$$

$$\text{Stability: } \frac{c_{hf}}{t_{hf}} \leq 10 \sqrt{\frac{235}{f_{y,hf}}}, \text{ according to class 2 of Eurocode 3 - Part 1.1 [1]} \quad (5)$$

Likewise for the haunch web:

$$\text{Strength: } \tau_{hw}^\pm = \frac{aV_{Ed}^\pm}{2(1+\nu)I_{1,2}} \left[ \frac{L'}{2} - \frac{\beta^\pm}{\tan \theta} \left( \frac{d^\pm}{2} \right) + \frac{(1-\beta^\pm)a}{3} \right] \leq \frac{f_{y,hw}}{\sqrt{3}} \quad (6)$$

$$\text{Stability: } \frac{2a \sin \theta}{t_{hw}} \leq 38 \sqrt{\frac{235}{f_{y,hw}}} \quad (7)$$

(class 2 of Eurocode 3 for a web depth  $2a \sin \theta$  in compression)

$f_{y,hf}$  and  $f_{y,hw}$  are the mean yield strengths of the haunch flange and the haunch web respectively;

$c_{hf}$  and  $t_{hf}$  are the flange outstanding and the flange thickness of the haunch respectively;

$t_{hw}$  is the haunch web thickness.

Yielding and shear buckling of the web of the steel beam part above the haunch should be checked on the basis of the hereafter vertical shear:

$$V_{Ed,b}^{\pm} = (1 - \beta^{\pm}) V_{Ed}^{\pm} \quad (8)$$

noting that  $V_{Ed,b}^{\pm}$  is, in general, significantly less than  $V_{Ed}^{\pm}$ . It may be observed from (8) that the direction of the beam vertical shear  $V_{Ed,b}^{\pm}$  is opposite to that developed outside the haunch region when  $\beta^{\pm} > 1.0$  (which occurs most of the time)

The local resistance due to the concentrated load  $\beta^{\pm} V_{Ed}^{\pm} / \tan \theta$  where the haunch flange intersects the column flange should be checked and the column web should be stiffened if necessary; likewise the steel beam web at the haunch tip should possess sufficient strength to resist the concentrated load  $\beta^{\pm} V_{Ed}^{\pm}$ ; generally, it needs to be stiffened transversally.

Yielding in tension of the top flange of the steel beam part above the haunch and of the slab reinforcement under hogging bending should be checked appropriately. For instance, the tension stress in the steel flange is given by:

$$\sigma_{bft,Ed} = \frac{M_{Ed}^{-} + V_{Ed}^{-} (1 - \beta^{-}) a}{I_2} (h_b - d^{-}) - \frac{\beta^{-} V_{Ed}^{-} / \tan \theta}{I_2} \left[ (h_b - d^{-}) d^{-} - \frac{I_2}{A_b^{-}} \right] \quad (9)$$

A similar expression of (9) may be obtained for  $\sigma_{s,Ed}$  in the reinforcement. Conditions  $\sigma_{bft,Ed} = f_y$  and  $\sigma_{s,Ed} = f_{ys}$  lead to a minimum value  $\beta_{min}^{-}$  of  $\beta$ . If  $\beta$  is less than minimum value  $\beta_{min}^{-}$  the area of the haunch flange or the haunch geometry should be modified.

Also yielding of the lower flange of the steel beam and concrete strength in compression of the slab under sagging bending should be checked leading to satisfy other minimum value  $\beta_{min}^{+}$ .

Recommendations are made to use full penetration butt welds to connect the end of the beam and the haunch to the end-plate, the haunch to the lower flange of the beam and transverse stiffeners to the flanges of the beam and the column. According to Eurocode 8, full penetration butt welds are deemed to satisfy the overstrength criterion with regard to the adjacent structural steel.

Nevertheless if two-sides fillet welds were considered to connect webs of the beam and the haunch to the end-plate, also to connect the haunch web to the beam flange and the transverse stiffeners to the beam, the following requirement of Eurocode 8 should be met:

$$R_d \geq \alpha R_{ye};$$

where:

$R_d$  is the resistance of the two fillet welds;

$R_{ye}$  is the plastic resistance of the connected dissipative member based on the mean measured value of yield stress of material (adopting a value  $\gamma_{ov} R_{fy}$ , where  $\gamma_{ov}$  is the overstrength factor, in a design context).

## 2.2. Joint Static Design

The joint static design was based on the component method of Eurocode 3 – Part 1-8 [3] considering the joint as an assembly of simple components whose mechanical properties are clearly identified and able to characterize the whole behaviour of the joint generally expressed in terms of moment-rotation curve. A refined model for the general case of haunched composite beam-to-

column joint is shown in figure 6. All components are modelled physically by translational springs and are able to simulate the transmission of internal forces in the joint as tension, compression, bending or shear.

The particular case of haunched steel joints is very partially covered in clause 6.1.1 (2) of Eurocode3 Part 1-8.

It can be seen in Figure 6 that groups of springs may act in parallel or in series. The springs presented in this figure deal with the following components:

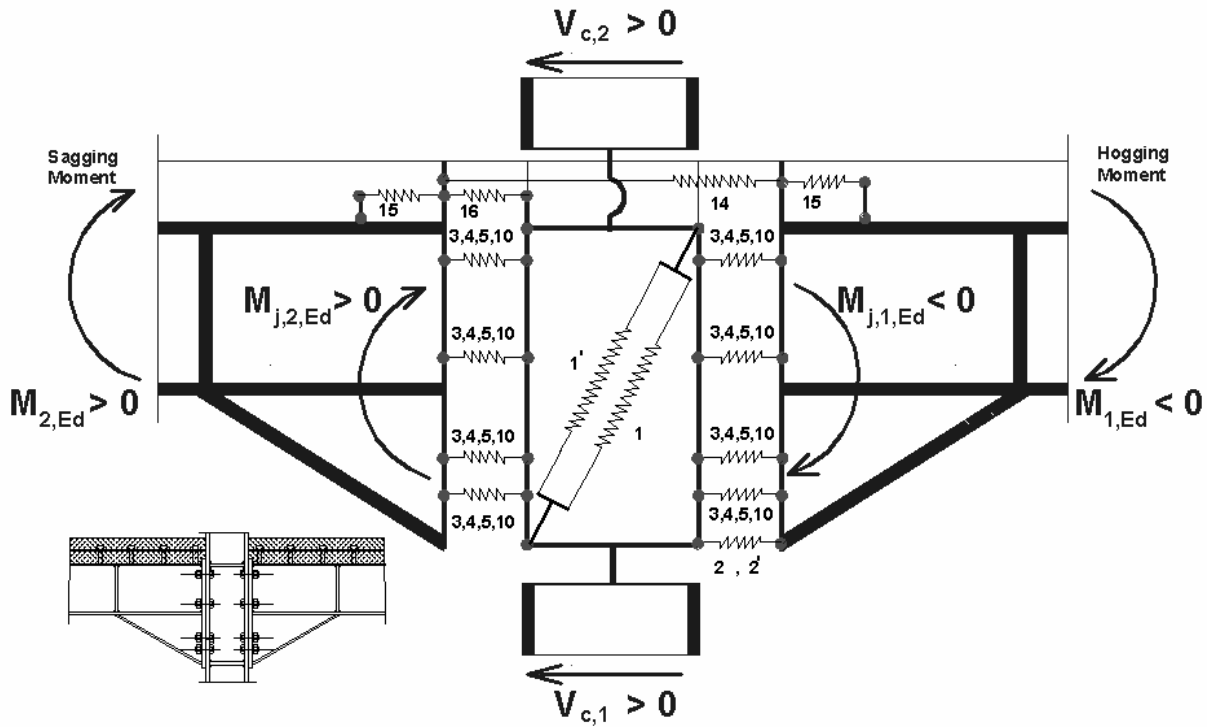


**Figure 6.** Component model for a composite beam-to-column haunched joint

Column web panel in shear (1); effect of concrete encasement on the stiffness and strength of the web panel (1');

Column web in transverse compression (2); effect of concrete encasement on the stiffness and strength of the column web (2');

Column web in tension (3);

Column flange in bending (4);

End-plate in bending (5);

Bolts in tension (10);

Longitudinal steel reinforcement in tension (14);

Shear connection (15);

Slab in compression facing the column (16).

In hogging bending, taking into account the position of a transverse stiffener just in front of the haunch flange, the centre of compression is assumed to be located at mid-thickness of the haunch flange. According to Eurocode 3 – Part 1-8 [3], the resistance moment in hogging bending  $M_{j,R}^{-(th)}$  may be determined from:

$$M_{j,R}^{-(th)} = F_{tr,s,R} \cdot h_{sr}^- + \sum_r F_{tr,R} \cdot h_r^- \quad (10)$$



where:

$F_{tr,R}$  is the effective design tension resistance of bolt-row  $r$ ;

$F_{tr,s,R}$  is the design tension resistance of a row  $r$  of the reinforcing bars included within the effective width of the concrete flange (adopting an effective width  $b_{eff}^- = (\ell_0 / 4) / (0.25 / 0.15)$  where  $\ell_0$  is the cantilever span and where 0.25/0.15 is an amplification factor for hogging bending zone in accordance with clause 5.4.1.2 in Eurocode 4.1.1 [4];

$h_{sr}^-$  and  $h_r^-$  are the distances from row  $r$  of reinforcing bars or bolts to the centre of compression,  $r$  is the number of a particular row.

The tension resistance  $F_{tr,R}$  of bolt-row  $r$  as an individual bolt-row should be taken as the smallest value of the tension resistance for an individual bolt-row of the following basic components: the column web in tension  $F_{t,wc,R}$ , the column flange in bending  $F_{t,fc,R}$ , the end-plate in bending  $F_{t,ep,R}$  and the beam web or the haunch web in tension  $F_{t,wb,R}$ .

Dealing with the bolt-rows closest to the centre of compression, a reduction of their tension resistances may be applied in such a way that:

$$F_{tr,s,R} + \sum_r F_{t,R} \leq \min( F_{c,wc,R}, F_{c,fh,R}, \frac{V_{wp,R}}{\beta} ) \quad (11)$$

where:

$F_{c,wc,R}$  and  $F_{c,fh,R}$  are the resistance of the column web in compression and the resistance of the haunch flange in compression (and partially the web), respectively.

$V_{wp,Rd}$  is the plastic shear resistance of the column web panel (of appropriate slenderness) and

$\beta$  is a transformation parameter defined in clause 7.3.3 of Eurocode 3 Part 1-8:

$$\begin{aligned} \beta_1 &= \left| 1 - M_{j,2,Ed} / M_{j,1,Ed} \right| \leq 2 \\ \beta_2 &= \left| 1 - M_{j,1,Ed} / M_{j,2,Ed} \right| \leq 2 \end{aligned} \quad (12)$$

where:

$\beta_1$  is the value of the transformation parameter  $\beta$  for the right-hand side joint ;

$\beta_2$  is the value of the transformation parameter  $\beta$  for the left-hand side joint;

$M_{j,1,Ed}$  is the moment applied to the right joint at the load introduction cross section (figure 6);

$M_{j,2,Ed}$  is the moment applied to the left joint at the load introduction cross section (figure 6);

In the present study,  $\beta = 1$  for the T joint configuration and  $1.5 \leq \beta \leq 2.0$  for the cruciform one.

Provided that the axial force  $N_{Sd}$  in the connected member does not exceed 10% of the axial cross-sectional resistance  $N_{pl,Rd}$  of its cross-section, the initial rotational stiffness  $S_{i,ini}$  of a joint, for a moment  $M_{j,Sd}$  less than the moment resistance  $M_{j,Sd}$  of the joint, may be obtained from:

$$S_{j,ini}^{-(th)} = E_a (z_{eq}^-)^2 \left[ \frac{1}{k_1} + \frac{1}{k_2} + \frac{1}{k_{eq}^-} \right]^{-1} \quad (13)$$

$$k_{eq}^- = \frac{\sum_r k_{eff,r} h_r^-}{z_{eq}^-} \quad ; \quad z_{eq}^- = \frac{\sum_r k_{eff,r} (h_r^-)^2}{\sum_r k_{eff,r} h_r^-} \quad ; \quad k_{eff,r} = \left[ \sum_i \frac{1}{k_{i,r}} \right]^{-1} \quad (14)$$

where:

$E_a$  is the modulus of elasticity of steel;

$z_{eq}^-$  is the equivalent lever arm,

$k_1$  is the stiffness coefficient for the column web panel in shear,

$k_2$  is the stiffness coefficient for the column web in compression,

$k_{eq}^-$  is the equivalent stiffness coefficient related to the group of bolt-rows and longitudinal reinforcement in tension (the latter modified by the reduction factor  $k_{slip}$  due to the slip effect of the shear connection as given by clause (A5) in Eurocode 4 Part 1-1 [4];

$k_{eff,r}$  is the effective stiffness coefficient for layer  $r$ ; and

$k_{i,r}$  is the stiffness coefficient representing component  $i$  relative to layer  $r$ ;

$h_r^-$  is the distance between layer  $r$  and the centre of compression.

In sagging bending, assuming a centre of compression located at the mid-thickness of the concrete slab (only considering the thickness above the sheeting ribs), expressions similar to the above ones may be adopted, replacing  $F_{c,wc,R}$  and  $F_{c,fb,R}$  by the bearing resistance  $F_{c,R}$  between the slab and the column and introducing a specific stiffness coefficient  $k_c$  for the slab in compression. More details may be found in Ciutina [14].

$$M_{j,R}^{+(th)} = \sum_r F_{tr,R} \cdot h_r^+ \quad (15)$$

$$S_{j,ini}^{+(th)} = E(Z_{eq}^+)^2 \left[ \frac{1}{k_1} + \frac{1}{k_c} + \frac{1}{k_{eq}^+} \right]^{-1} \quad (16)$$

Under reversal bending moment, the total force due to the compression of the slab on one side plus the tension of the reinforcement on the other side should be transferred to the column using the resistances of two mechanisms Eurocode 8 - Part 1 (Annex C) [5]:

- a direct compression on the column flange:

$$F_{R1} = b_c d_{eff} (0.85 f_c) \quad (17)$$

where:

$b_c$  is the column flange width,

$d_{eff}$  is the thickness of the slab above the ribs of the profiled sheeting for composite slabs (and overall depth of the slab in case of solid slab);

- a compressed concrete struts inclined to  $45^\circ$  on the column sides:

$$F_{R2} = 0.7 h_c d_{eff} (0.85 f_c) \quad (18)$$

where  $h_c$  is the depth of the column steel section.

In addition the tension strut model requires a tension-tie cross-sectional area:

$$A_T \geq 0.5 \frac{F_{R2}}{f_{sk}} \quad (19)$$

over a width  $h_c$  and fully anchored. This area  $A_T$  is introduced on both sides of the column to account for reversal of bending moments

The resistance offered by the two mechanisms is given by:

$$F_{c,R} = F_{R1} + F_{R2} \quad (20)$$

It is to point out that the presence of haunch in a beam to column connection creates an enlarged panel zone. The distribution of internal forces in a such enlarged panel zone is different from that of

the single panel zone (without haunch). Lee and Uang [8] for welded beam-to-column joint and on the basis of results of finite element analysis and available full-scale test results have developed an analytical procedure to model the stiffness and strength of an enlarged panel zone. In the case of haunched end-plate bolted composite joints the problem is more complex and has not been investigated yet. In the next future one of the objectives of the authors of this paper is to develop a scientific background about this topic. For want of something better, a simplified checking may be used evaluating the panel shear as follows:

$$V_{wp,Ed} = \frac{M_{j2,Ed}}{Z_{eq}^+} - \frac{M_{j1,Ed}}{Z_{eq}^-} - \frac{V_{C2} - V_{C1}}{2} \leq 0.9 A_{vc} \frac{f_{y,cw}}{\sqrt{3}} \quad (21)$$

where

$V_{C1}$  and  $V_{C2}$  are the horizontal forces exerted by the column ends (Figure 6) and  $A_{vc}$  is the shear area of the column.

### 3. PRESENTATION OF THE EXPERIMENTAL INVESTIGATION

#### 3.1. Program of tests

Completing Figures 1 to 4, Table 1 presents the main characteristics of ten full-scale beam-to-column joints (major axis connections) tested at INSA of Rennes-France. All the specimens include bolted end plate connections, with upper and lower external rows of bolts in the case of steel joints and only lower external bolt row in the case of composite joints.

In Table 1, two main Groups of tests may be distinguished:

- Group 1 with full-strength joints with haunches;
- Group 2 with partial strength joints without haunches.

Each group comprises steel and composite joints with T and cruciform arrangements, monotonically or cyclically loaded.

For all the tests, as shown in Figures 1 to 4, transverse stiffeners have been welded to the column flanges in the web-panel. Except for test G13, all the bolts were tightened at their nominal preload. All the welds were made by the semi-automatic inert-gas arc method with full penetration butt welds, using E MAG 136 procedure and T46 4 MM2 H5 consumables, according to European norms (EN 287 and EN 288).

For all the composite specimens (except G18), common characteristics are a full shear connection with welded headed studs  $\Phi = 19$  mm ( $h = 80$  mm or  $100$  mm) and , a composite slab (cast on a steel sheeting COFRASTRA 40) whose cross-section of dimensions  $120 \times 1000$  mm is reinforced by 10 longitudinal rebars  $\Phi 10$  mm and by transverse rebars  $\Phi 10$  mm spaced each 10 cm, with 2 additional transverse rebars near the column flanges to ensure a strut-tie action according to (19).

Although the main objective of the present research is the effect of joint strengthening on the joint seismic performances by introducing haunches, other parameters are considered as the performance of the composite solution in comparison with the steel one (for that, steel reference tests have been performed prior each series of composite tests; i.e. G13, G16 and G19 in comparison with G15, G18 and G20 respectively. The contribution of the column web panel to the global performance of the joint is also analysed.

**Table 1.** Description of Specimens

Group	Test N°	Arrangement	<u>SPECIMEN</u> -Column -Column web stiffener -Beam	Type of loading	Supplementary web plates (thickness mm) (S235)	End plate Bolt
GROUP (1) FULL – STRENGTH JOINTS WITH HAUNCHES	G16 (steel)	<b>T</b>  (external joint)	HEB300 (S355) ( $f_y = 454 \text{ N/mm}^2$ )  web stiffeners IPE 360 (S235) ( $f_y = 278 \text{ N/mm}^2$ )	cyclic (ECCS)	NO	430×220×25 (S235) ( $f_y = 242 \text{ N/mm}^2$ ) HS10.9 $\Phi$ 22mm
	G17			monotonic (hogging bending)		745×250×25 (S235) ( $f_y = 242 \text{ N/mm}^2$ ) HS10.9 $\Phi$ 22mm
	G18			cyclic (ECCS)		
	G22	<b>Cruciform</b> (internal joint)	HEB200 (S355) ( $f_y = 350 \text{ N/mm}^2$ )  web stiffeners IPE 240 (S235) ( $f_y = 347 \text{ N/mm}^2$ )	cyclic (ECCS)	NO	510×160×20 (S235) ( $f_y = 320 \text{ N/mm}^2$ ) HS10.9 $\Phi$ 20mm
	G23				YES (2×12)	
GROUP (2) PARTIAL – STRENGTH JOINTS	G13 (steel)	<b>T</b>  (external joint)	HEB300 (S355) ( $f_y = 454 \text{ N/mm}^2$ )  web stiffeners IPE 360 (S235) ( $f_y = 278 \text{ N/mm}^2$ )	cyclic (ECCS)	NO	500×200×15 (S235) HS10.9 $\Phi$ 22mm
	G15					430×220×15 (S235) ( $f_y = 280 \text{ N/mm}^2$ ) HS10.9 $\Phi$ 22mm
	G19 (steel)	<b>Cruciform</b>  (internal joint)	HEB200 (S355) ( $f_y = 413 \text{ N/mm}^2$ )  web stiffeners IPE 240 (S235) ( $f_y = 340 \text{ N/mm}^2$ )		NO	390×160×15 (S235) ( $f_y = 296 \text{ N/mm}^2$ ) HS10.9 $\Phi$ 20mm
	G20				YES (2×6)	330×160×15 (S235) ( $f_y = 296 \text{ N/mm}^2$ ) HS10.9 $\Phi$ 20mm
	G21				YES (2×10)	330×160×20 (S235) ( $f_y = 320 \text{ N/mm}^2$ ) HS10.9 $\Phi$ 20mm

### 3.2. Test Setups

As presented in Figure 7 in the case of joints with a T arrangement the vertical load was applied at the end cross-section of the beam by means of an hydraulic servo controlled actuator.

In the case of joints with a cruciform arrangement two vertical loads were applied at each cantilever beam end on each side of the column (Figure 8) by two hydraulic servo controlled actuators acting out-of- phase for creating opposite directional loads. For all the tests the column was connected at its lower end to the platform by a fixed pinned support and at its upper end to a rigid braced frame by a moveable pinned support.

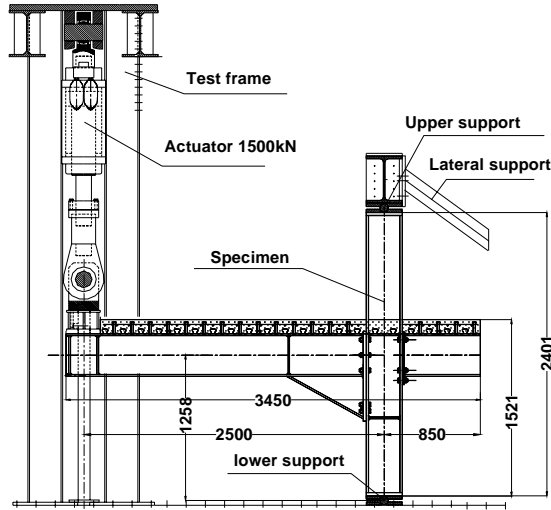


Figure 7. Test setup (T arrangement)

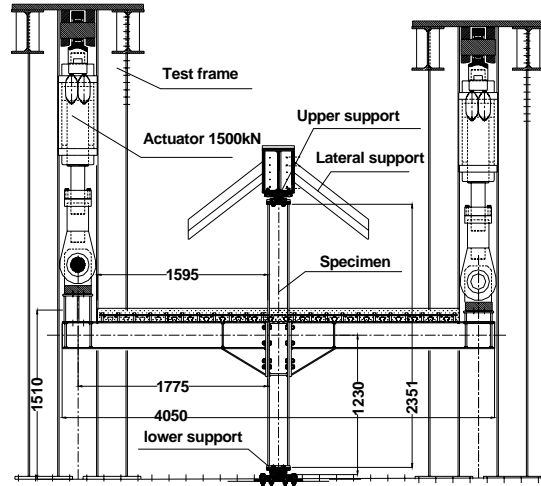


Figure 8. Test setup (Cruciform arrangement)

### 3.3. Loading Procedures

In the case of monotonic tests, increases in joint rotation were applied continuously up to failure of the joint. For cyclic tests, the ECCS procedure was followed [15] in order to simulate the seismic action. The implementation of this procedure requires the first determination of two conventional elastic limit rotations  $\Phi_y^-$  and  $\Phi_y^+$  associated with the corresponding elastic limit moments in hogging bending  $M_{j,y}^-$  and sagging bending  $M_{j,y}^+$  respectively.

As shown in Figure 9 the determination of such conventional elastic limit moments is obtained from the intersection between the initial tangent of slope  $S_{j,ini}$  to the monotonic curve and the particular tangent having a slope equal to  $S_{j,ini}/10$ . Due to the difficulty to determine practically the initial tangent to the monotonic curve, the authors propose to adopt a similar definition to the one given in Eurocode 3 [1-3]; then, the initial stiffness is defined as the slope of the secant line joining the origin and the point on the monotonic curve located at ordinate  $\frac{2}{3}M_{j,y}$ ; this construction requiring a short iterative procedure. Having no monotonic moment-rotation curves of reference for most of the tests presented in table 1, the skeleton curve enveloping the peaks of the first cyclic M- $\Phi$  curves have been used to determine the conventional characteristics  $\Phi_y^{+/-}$  useful to apply the ECCS procedure to the cyclic tests. So, the following simplified values have been adopted:

$$\Phi_y^- = \Phi_y^+ = \Phi_y = 2 \text{ mrad for external joints with a T configuration and;}$$

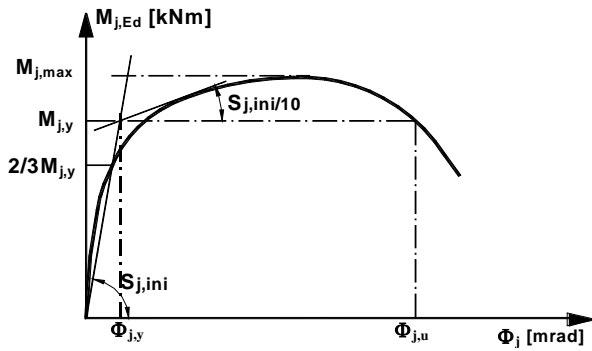
$$\Phi_y^- = \Phi_y^+ = \Phi_y = 4 \text{ mrad for internal joint with a cruciform configuration.}$$

Figure 10 shows the successive increases of rotation corresponding to the ECCS cyclic loading procedure:

$$4 \text{ cycles successively for the ranges } \pm \frac{\Phi_y}{4}, \pm \frac{\Phi_y}{2}, \pm \frac{3}{4}\Phi_y, \pm \Phi_y;$$

followed up to failure by series of 3 cycles each with a range  $\pm 2n\Phi_y$  where  $n = 1, 2, 3, \dots$

Figures 11 to 14 show the experimental arrangements used for the tests.



**Figure 9.**  $M-\Phi$  characteristic definitions

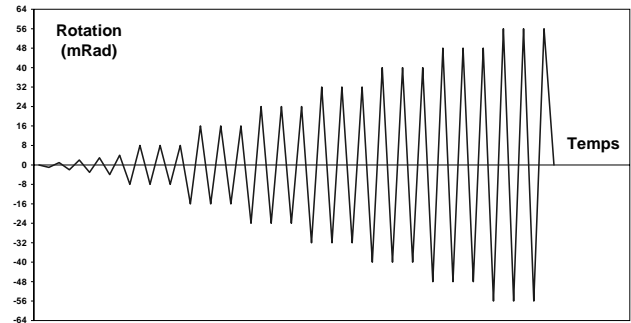


**Figure 10.** Load History

GROUP (1)

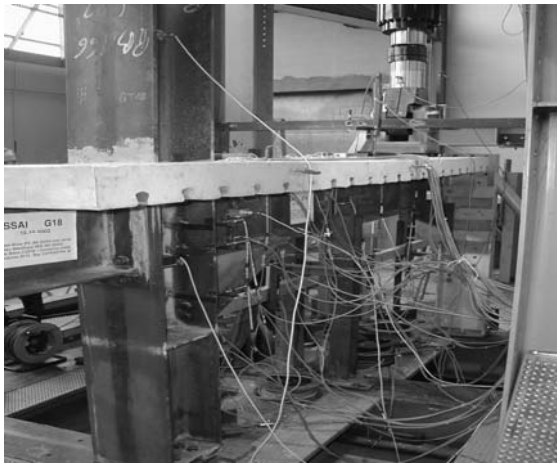


**Figure 11.** T with an haunch

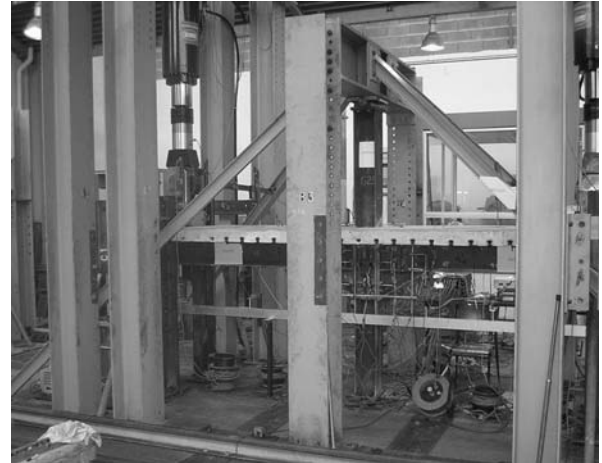


**Figure 12.** haunched joint

GROUP (2)

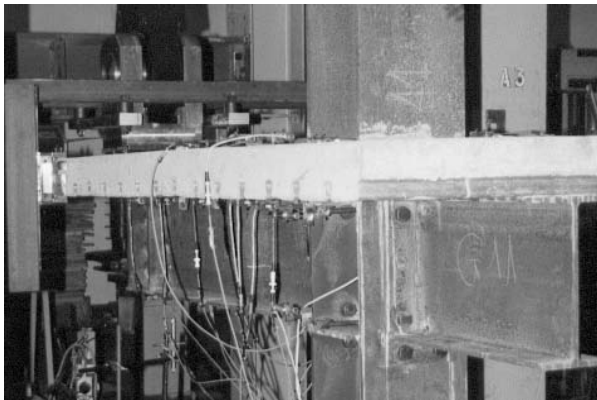


**Figure 13.** T without haunch



**Figure 14.** joint without haunch

**T arrangement**

**Cruciform arrangement  
(unsymmetrically loaded)**

### 3.4. Measuring Arrangement and Data Processing

The measurement system is shown in Figure 15 (Test G18) for a T arrangement and in Figure 16 (Test G23) for a cruciform arrangement. It comprises inclinometers for rotation measurements and transducers to measure deflection of the beams, slip between the composite slab and the steel flange in several locations along the beams, and displacements in significant zones of the joint:

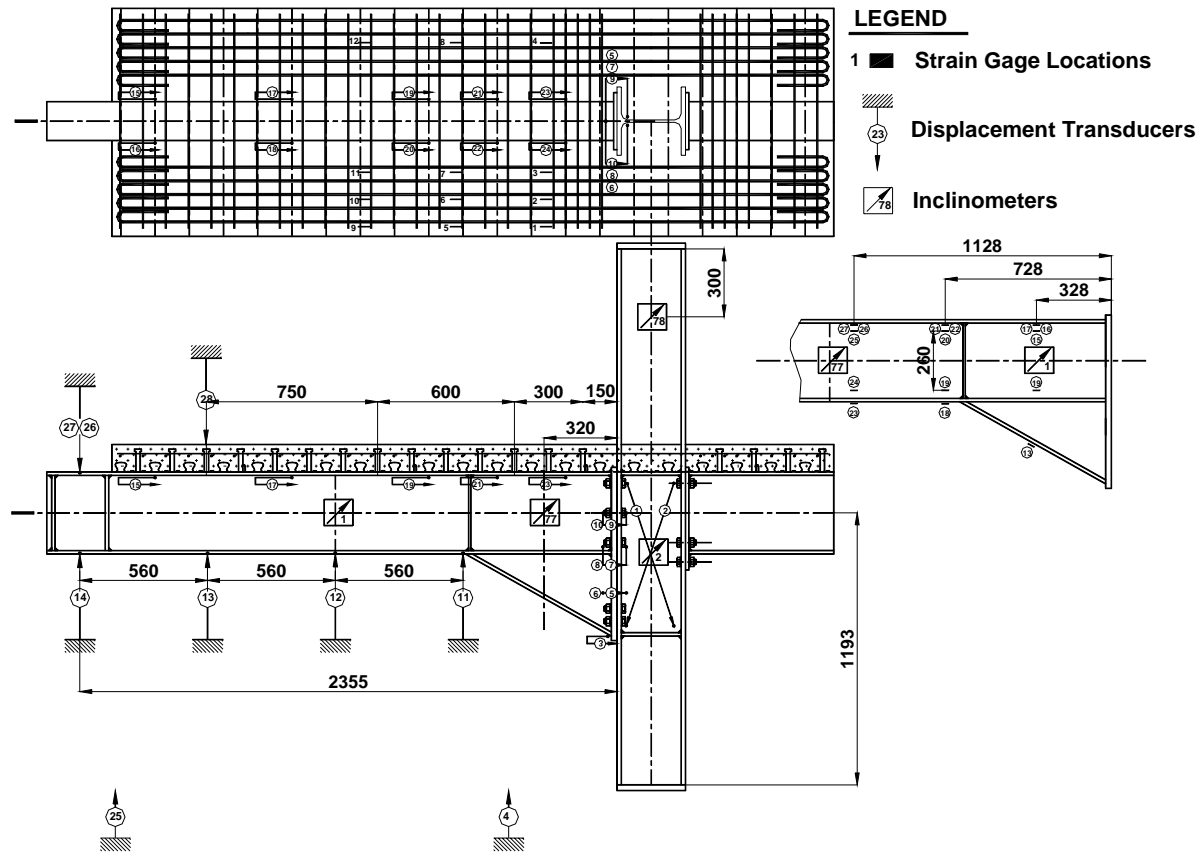


Figure 15. Measurement system used for T arrangement

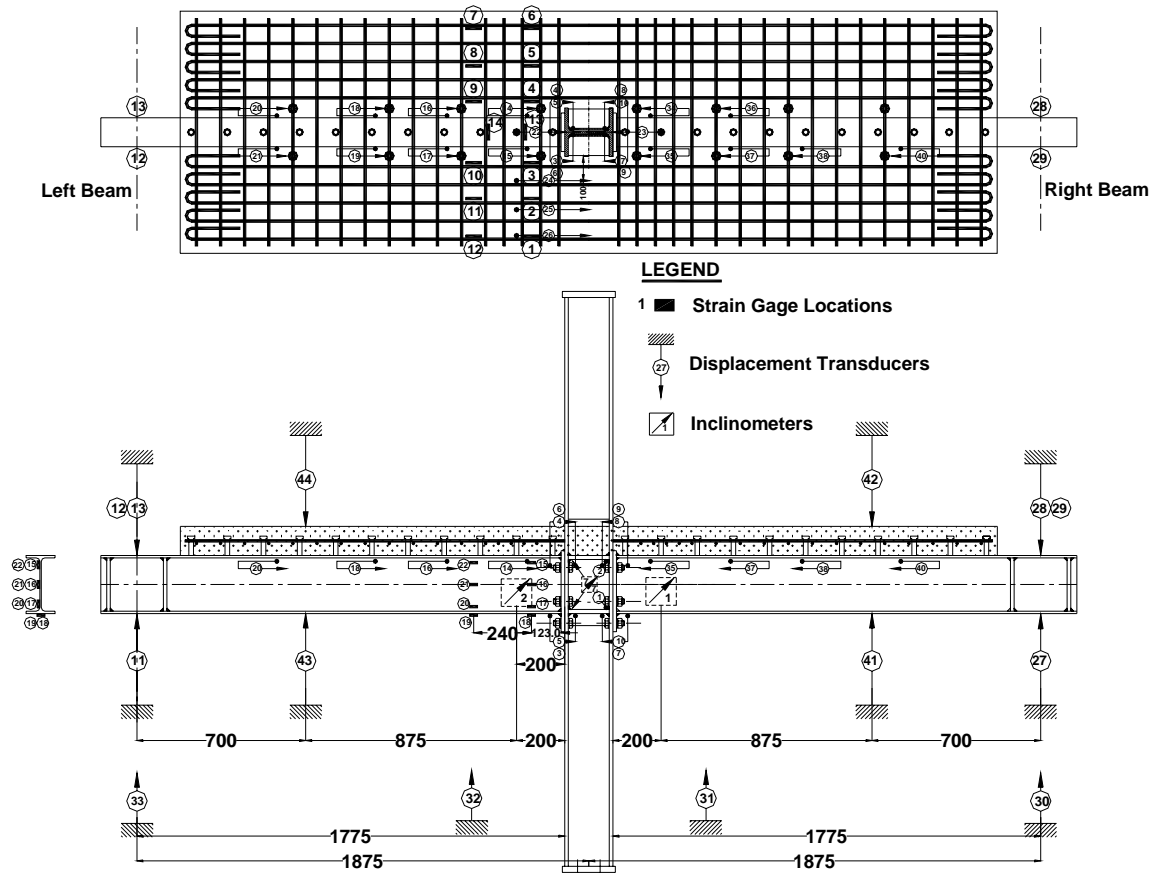


Figure 16. Measurement system used for Cruciform arrangement

elongation of bolts, flexural bending of end-plates and column flanges, shear deformation of the column web panel. Strain measurements are made for some tests by means of electric gauges bonded on longitudinal and transversal rebars near the column, in several beam cross-sections near the joint or inside the haunch.

To determine the moment-rotation curves presented later on the following definitions have been considered:

- the bending moment  $M_j$  applied to the joint is located at the column face, hence given by the product:

$$M_j = FL \text{ (kN.m)} \quad (21)$$

where  $L$  is the appropriate lever arm defined in Figures 1 to 4.

- the total joint rotation  $\Phi_j$ , including the connection rotation and the column web panel distortion, is deduced from the difference between the two inclinometers  $I_2$  (distinguishing  $I_{2L}$  on the left side and  $I_{2R}$  on the right side in the case of a cruciform joint) and  $I_1$ :

$$\Phi_j = I_2 - I_1 \text{ (mrad)} \quad (22)$$

For end-plate connections (without haunches) where the beam contribution to the joint rotation is low, inclinometer  $I_2$  has been located at a short distance from the column flange, equal to about the half depth of the steel beam. On the contrary, for end-plate connections with haunches, where the joint rotation is due essentially to the beam rotation with the formation of a plastic hinge near the end of the haunch, inclinometer  $I_2$  has been located at a distance from the end of the haunch, generally greater or at least equal to the depth of the steel beam. Inclinometer  $I_1$  gives the rotation due to the flexural bending of the column.

For joints with haunches, a supplementary inclinometer  $I_3$  is placed on the beam at mid-length of the haunch; allowing to distinguish the rotation due to the connection  $\Phi_{\text{connection}} = (I_3 - I_1)$  and the beam rotation  $\Phi_{\text{beam}} = (I_2 - I_3)$ .

A global evaluation of the column web panel distortion can be deduced from the algebraic elongations  $\Delta_1$  and  $\Delta_2$  of the two diagonal transducers 1 and 2 as follows:

$$\gamma = \sqrt{a^2 + b^2} (\Delta_1 - \Delta_2) / (2ab) \quad (23)$$

where  $a$  and  $b$  are the horizontal and vertical sizes of the web panel.

Other rotations of the connection part have been deduced from elongation measurements of bolt rows, in the longitudinal direction, located on the width of end-plates. These values have been compared to the ones directly measured.

## 4. EXPERIMENTAL RESULTS AND INTERPRETATION

### 4.1. Global Results For Rotational Stiffness, Moment Resistance And Rotational Capacity

All the experimental values collected in table 2 are defined at the load-introduction cross-section of the connection, i.e. the interface between end-plate and column flange. Elastic limit moments  $M_{j,y}^{(exp)+}$  in sagging bending and  $M_{j,y}^{(exp)-}$  in hogging bending, maximum bending moments  $M_{max}^{(exp)+/-}$ , initial rotational stiffnesses  $S_{j,ini}^{(exp)+/-}$  and global ultimate rotations  $\Phi_u^{(exp)+/-}$  (adding the joint and beam contributions) have been deduced from monotonic (test G17) or skeleton curves enveloping the peaks of cyclic  $M - \Phi$  curves; as a reminder the exact definitions adopted for these



characteristics were defined before (figure 9). Theoretical values of rotational stiffnesses  $S_{j,ini}^{(th)+/-}$  and moment resistances  $M_{j,R}^{(th)+/-}$  have been calculated from the above-mentioned formulae, using mean values of the material properties and geometrical characteristics measured on each specimen (safety factors for materials being considered equal to one).

**Table 2.** Theoretical (TH) and Experimental (EXP) Results

TEST N°	$\frac{S_{j,ini}^{(th)+}}{S_{j,ini}^{(th)-}}$ (kN.m/rad)	$\frac{S_{j,ini}^{(exp)+}}{S_{j,ini}^{(exp)-}}$ (kN.m/rad)	$\frac{M_{j,R}^{(th)+}}{M_{j,R}^{(th)-}}$ (kN.m)	$\frac{M_{j,y}^{(exp)+}}{M_{j,y}^{(exp)-}}$ (kN.m)	$\frac{M_{max}^{(exp)+}}{M_{max}^{(exp)-}}$ (kN.m)	$\frac{\Phi_u^{(exp)+}}{\Phi_u^{(exp)-}}$ (mrad)	failure mode
<b>GROUP (1)</b>							
<b>FULL – STRENGTH JOINTS WITH HAUNCHES</b>							
(cyclic) <b>G16</b> (steel)	179200/177300	120000/93500	598/608	483/484	620/560	60/51	yielding of the steel beam
(monotonic) <b>G17</b> (composite)	--/183700	--/126500	--/728	--/512	--/640	--/88	yielding of the composite beam
(cyclic) <b>G18</b> (composite)	207500/183700	132100/115900	696/728	541/494	740/670	40/35	yielding of the beam (limited by stud rupture)
(cyclic) <b>G22</b> (steel)	49900/53500	24900/22500	197/209	194/183	198/191	50/58	yielding of the steel beam
(cyclic) <b>G23</b> (composite)	87300/65900	150800/72300	306/308	290/245	345/255	54/45	yielding of the steel beam
<b>GROUP (2)</b>							
<b>PARTIAL – STRENGTH JOINTS WITHOUT HAUNCHES</b>							
(cyclic) <b>G13</b> (steel)	53600/53600	32400/32400	224/224	260/260	300/326	30/33	beam flange to end-plate weld rupture
(cyclic) <b>G15</b> (composite)	74600/38800	41100/53600	282/299	237/300	326/340	25/28	weld rupture under hogging bending
(cyclic) <b>G19</b> (steel)	16000/16000	8500/8500	74/74	94/72	125/105	70/70	beam flange to end-plate weld rupture
(cyclic) <b>G20</b> (composite)	35890/15830	50517/22837	150/150	162/101	237/150	48/58	beam flange to end-plate weld rupture
(cyclic) <b>G21</b> (composite)	44810/18940	55182/21983	172/157	194/126	235/159	25/31	beam flange to end-plate weld rupture

In general, for joints equipped with haunches, it is observed that theoretical values of stiffness and moment resistance are greater than the experimental ones (except the stiffness for test G23). The overstrength ratio between the theoretical moment resistance and the elastic limit moment (exerted by the haunched beam) ranges from 1.1 in sagging bending to 1.3 in hogging bending. These values appear sufficient compared to factor  $\alpha = 1.1$  already mentioned in relationship (1) to satisfy the principle of capacity design (leading to a main dissipation outside the joint). Consequently for tests of Group 1, the flexural yielding occurs systematically in the beam at the end of the haunch providing a rotation capacity generally greater than 35 mrad. As a reminder, this rotation capacity is required by Eurocode 8-1 (clause 6.6.4 (3)) in dissipative zones to consider frames in high ductility class (DCH) for which the behaviour factor  $q$  is equal to 6 at least.

A reduction in rotation capacity often appears for tests of group 2 (for T as well as cruciform joint arrangements) due to the premature rupture in low-cycle fatigue of welds connecting end-plate to the beams. It should be pointed out that some details of the joint may lead to a premature rupture of welds (for example, an increase of the thickness of end-plate and supplementary web plates between test G20 and test G21 produced a premature rupture of the weld connecting beam flanges to the end-plate, possibly explained by some lack of flexibility of the end-plates. Contrary to the

haunched joints, only the medium ductility class (DCM) seems acceptable for the partial-strength composite joints since the rotation capacity may be limited to 25 mrad (particularly in sagging bending).



**Figure 17.** Yielding rupture in the beam at the haunch toe



**Figure 18.** Yielding rupture in the beam at the haunch toe

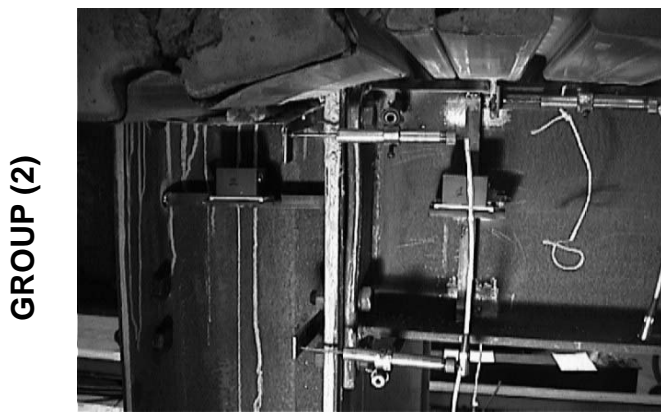


**Figure 19.** End-plate deflection



**Figure 20.** Rupture of welds and fracture of beam web in heat affected zone (HAZ)

#### **T arrangement**

#### **Cruciform arrangement (unsymmetrical loaded)**

Whereas all failures of group 2 occurred by rupture of welds connecting beams to end-plates (Figures 19 and 20), failures of group 1 resulted from excessive flexural yielding of the steel section at the haunch tip (Figures 17 and 18). It is to underline that the haunch stiffening effect leads to a strong reduction of the deformations in the joint, these latter ones being transferred in the beam, and consequently to a limitation of risks of low-cycle fatigue in such components as welds, bolts and end-plates.

#### **4.2. Comments on the Moment-Rotation curves**

For test G20 of group 2 (without haunch) moment-rotation curves in Figures 21-1, 21-2 and 21-3 on the left side of the figure are related to the left side of the joint and show the respective contribution of the load introduction cross-section (connection) rotation  $\Phi_{li}$  (Figure 21-1) and the column web panel rotation  $\Phi_{wp}$  (Figure 21-2) to the global joint rotation  $\Phi_j$  (Figure 21-3). A similar comparison is made in Figures 22-1, 22-2 and 22-3 on the right side of the same test G20.

Considering the rotation ranges, the contribution of the connection rotation  $\Phi_{li}$  to the global joint rotation  $\Phi_j$  increases from 20% at the beginning of the test to 50% at the end before rupture of welds connecting beams to end-plates. The unsymmetrical behaviour observed in Figures 21 and 22 between left side and right sides of the joint is not only a consequence of the composite behaviour of the beams but also the plastic state initiated during the first cycles according to the sense of rotation.

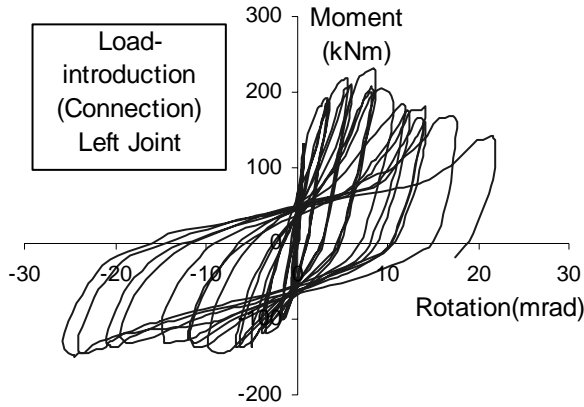


**Figure 21-1.**  $M_{j,2,Ed} - \Phi_{li}$  (Test G20)

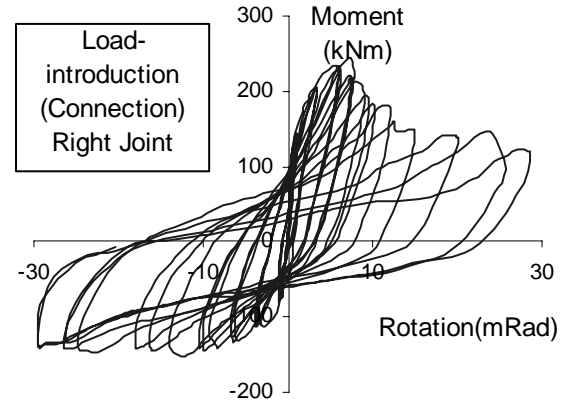


**Figure 22-1.**  $M_{j,1,Ed} - \Phi_{li}$  (Test G20)

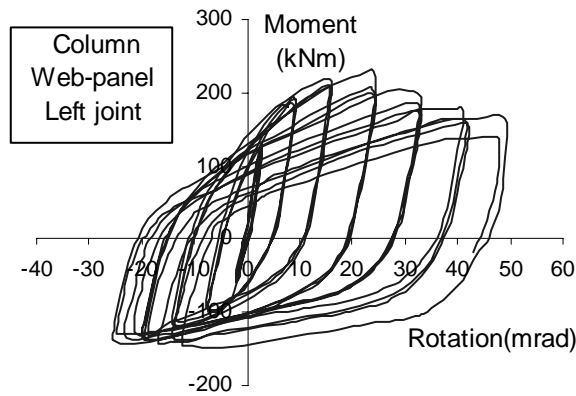


**Figure 21-2.**  $M_{j,2,Ed} - \Phi_{wp}$  (Test G20)

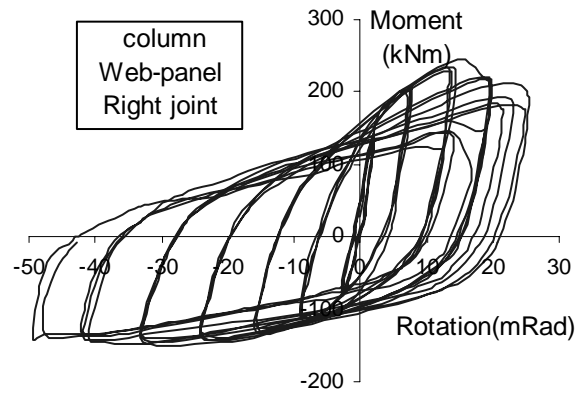


**Figure 22-2.**  $M_{j,1,Ed} - \Phi_{wp}$  (Test G20)

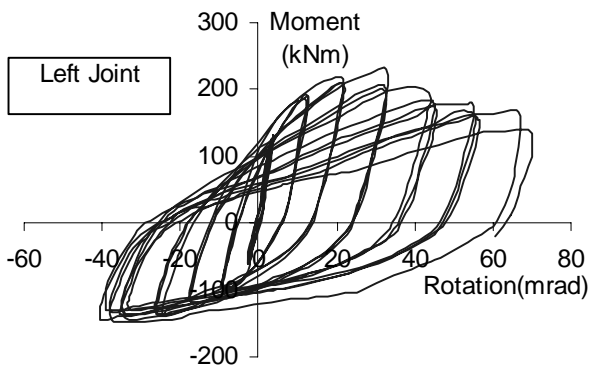


**Figure 21-3.**  $M_{j,2,Ed} - \Phi_j$  (Test G20)

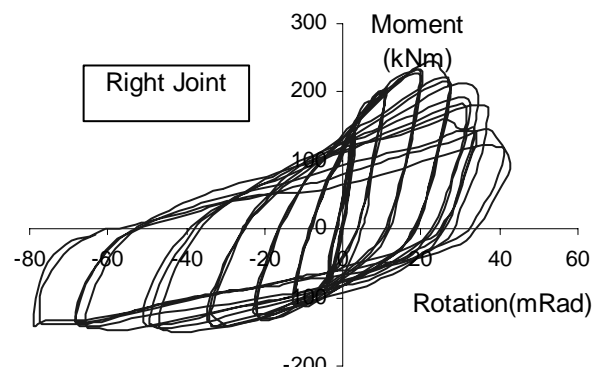


**Figure 22-3.**  $M_{j,1,Ed} - \Phi_j$  (Test G20)

For test G23 of group 1 (with haunch) moment-rotation curves of the connection, the column web panel, the joint and the beam (at the haunch tip) to the right side of the joint are presented in Figures 23-1, 23-2, 23-3 and 23-4 respectively. Considering the rotation ranges, the contribution of the connection rotation  $\Phi_{li}$  to the global joint rotation  $\Phi_j$  remains rather limited at the beginning of

the test in comparison to  $\Phi_{wp}$  and greater at the end of the test before beam failure to reach 45 % of the global joint rotation  $\Phi_j$ ; this latter remaining clearly lower (only 20%) than the beam rotation outside the haunch tip (as shown in Figure 23-4).

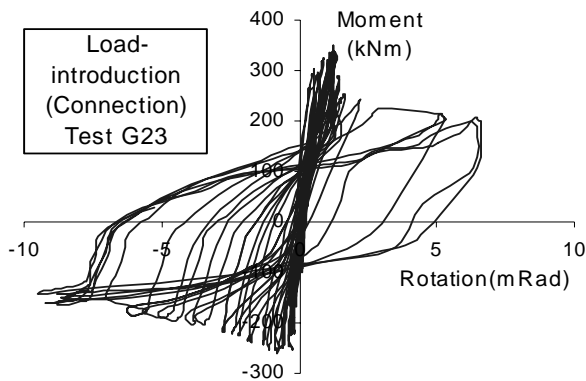


**Figure 23-1.**  $M_{j,2,Ed} - \Phi_{li}$  ( Right Joint)

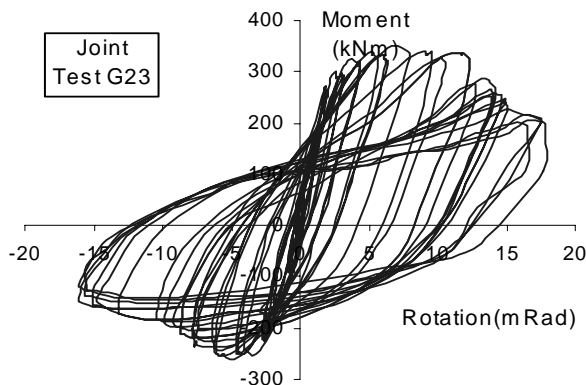


**Figure 23-2.**  $M_{j,2,Ed} - \Phi_{wp}$  ( Right Joint)

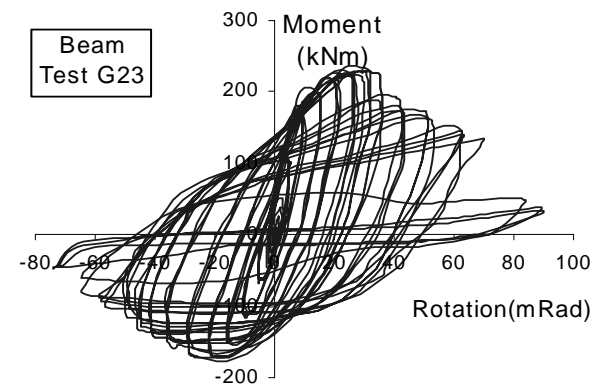


**Figure 23-3.**  $M_{j,2,Ed} - \Phi_j$  ( Right Joint)

**Figure 23-4.**  $M_{b,2,Ed} - \Phi_b$  ( Right Beam)

In figures 24-1 to 24-4 a comparison is made between the moment-rotation curves of the connection (Figure 24-1), the column web panel (Figure 24-2), the joint (Figure 24-3) and the beam (Figure 24-4) obtained for the monotonic test G17 and the corresponding cyclic test G18. For these tests, with a T arrangement, the same observations than the previous ones for tests G20 and G23 dealing with the relative contribution of the connection, the column web panel, the joint and the beam to the global rotation can be made.

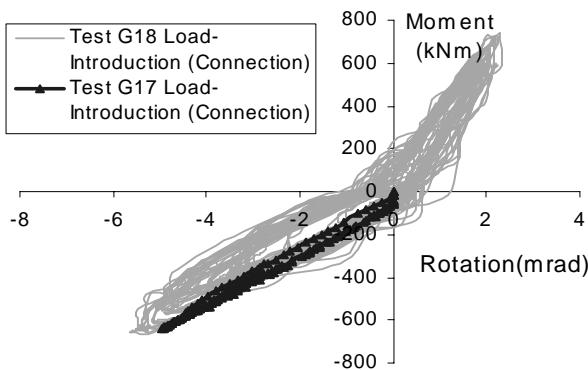


**Figure 24-1.**  $M_{j,Ed} - \Phi_{li}$

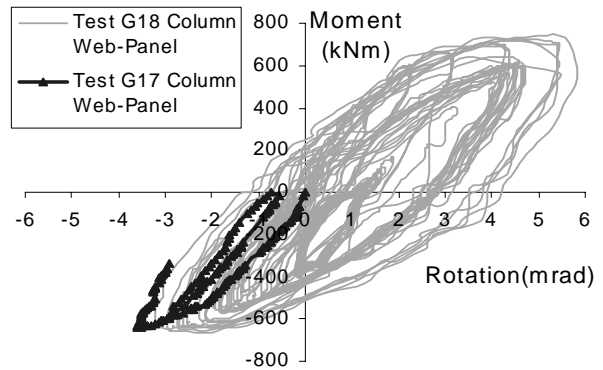


**Figure 24-2.**  $M_{j,Ed} - \Phi_{wp}$

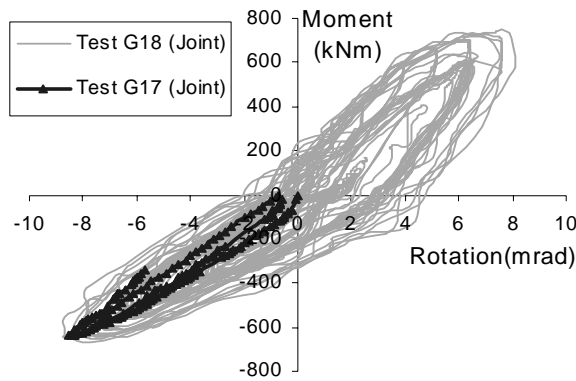


Figure 24-3.  $M_{j,Ed} - \Phi_j$

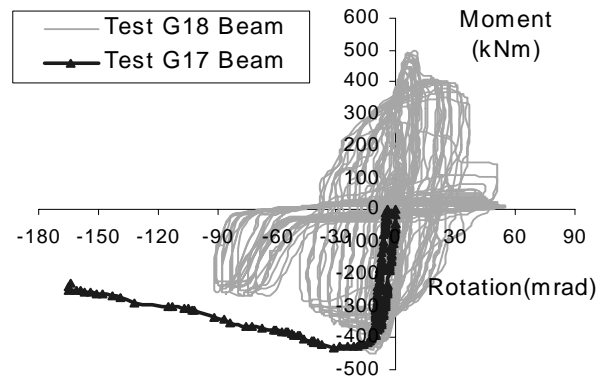


Figure 24-4.  $M_{b,Ed} - \Phi_b$

In addition, except for the beam rotation, it can be observed that the monotonic curves in hogging bending of the test G17 are enveloped by the cyclic curves of the test G18. The decrease of the beam cross-section moment resistance in hogging bending is mainly due to the yielding and the flange-web buckling of the beam cross-section near the haunch tip (Figure 25-1) which appears more pronounced in cyclic loading with the low-cycle fatigue effect than in monotonic loading. In sagging bending risks of flange buckling are excluded by the stiffening effect of the composite slab.

The stiffening effect of the composite slab is confirmed again in Figure 25-2 where skeleton curves enveloping the peaks of the cycles are compared between the two tests G23 and G22. In sagging bending the maximum moment of the composite test G23 appears 64% greater than the maximum moment of the steel companion test G22 ; in hogging bending the maximum moment of the composite test is only 32% greater than the corresponding steel one.



Figure 25-1. Buckling of beam web and beam bottom flange: haunch specimens

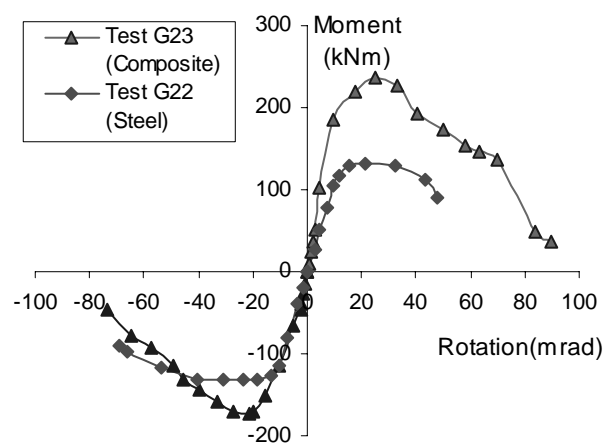
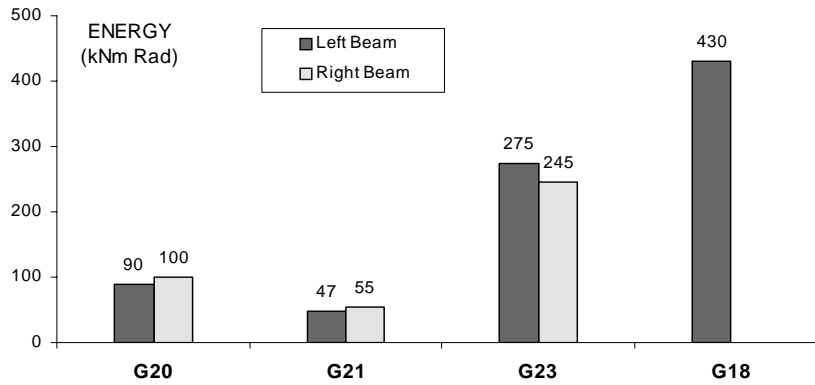


Figure 25-2. Moment- rotation envelopes: haunch specimens (right beam )

#### 4.3. Comparisons of Plastic Energy Dissipation Capacities

These results may be also interpreted in terms of cumulative plastic energy dissipation for all the cycles. As example, energy dissipation of bolted end plate joints (G20 and G21) is compared in Figure 26 to the dissipation of haunched bolted end-plate joints (G23 and G18); which appears 2.8 times greater for joints with haunches than for simple end-plate bolted joints.



**Figure 26.** Comparison of Energy dissipation capacities

In Figure 27, for haunched joints, the joint contribution is only 20% to 30% of the plastic beam energy dissipation (contrary to joints without haunches where the joint contribution is close to 100%). Contribution of the joint components to the plastic energy dissipation is illustrated in Figure 28 for test G20 (without haunch) where the contribution of the connection is about 20% for a web panel contribution of 80% to the total joint rotation.

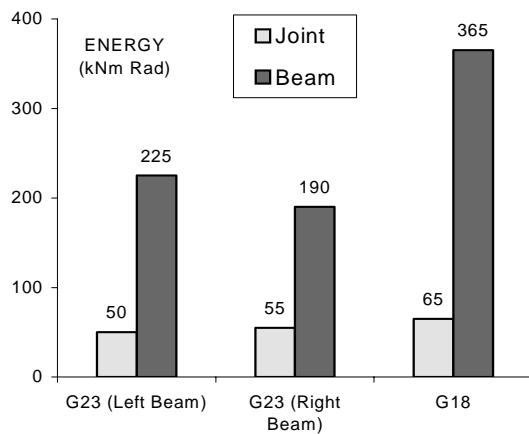


**Figure 27.** Comparison of plastic energy dissipation in beam and joint (haunch specimens)

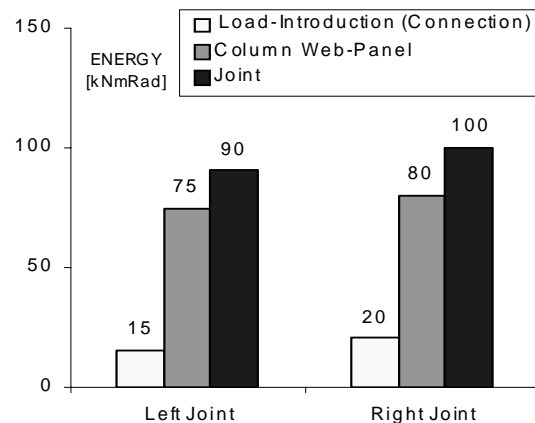


**Figure 28.** Comparison of plastic energy dissipation in the components of joint test (G20)

#### 4.4. Flexural Stress and Strain Distribution over the Depth of the Beams

Figure 29-1 for the test G23 in hogging bending and Figure 29-2 for the same test in sagging bending show the flexural strain distribution within the steelwork part of the depth of two beam cross sections located near the haunch tip, one in the haunch region at 328 mm from the flange column face and the other outside the haunch region at 528 mm from the flange column face.

In both cases, in hogging as well as in sagging bending a clear decrease of flexural strains appears in the lower part of the beam where the stiffening effect of the haunch acts. On the other end, in the upper part of the beam the strain reduction effect of the haunch remains negligible. For test G18 with a T joint configuration similar observations are made in Figures 30-1 and 30-2 in both hogging and sagging bending.

From tri-axial strain gauge measurements, load - shear strain curves from the mid-depth of the web of two beam cross sections located on each side of the stiffener above the haunch tip (Figure 31-1) may be compared in Figures 31-2 and 31-3. For a same load exerted by the actuator, it can be

observed that the shear strain in the haunch region is in opposite direction as compared with the corresponding shear strain outside the haunch region, the range of shear strain variation being more reduced in the haunch region than outside the haunch region.

This experimental result is a direct consequence of the effect of the vertical shear reaction transmitted by the haunch flange to the beam at the haunch tip. It confirms the hypotheses adopted previously in the haunch static design.

Flexural stress distributions within the depth of the steel beam in the haunch region at 328 mm from the flange column face are presented in Figures 32-1, 32-2, 32-3 and 32-4 for both tests G23 (cruciform internal joint) and G18 (T external joint). Test results are compared with two theoretical ones issued from the above proposed haunch design model on the one hand and from the simple beam theory on the other hand assuming the haunch region as a length of beam of variable cross-section. A better accordance appears between experimental results and the proposed model than the beam theory one, more particularly for test G18 where the depth beam (IPE360) is higher than for test G23 (IPE 240).

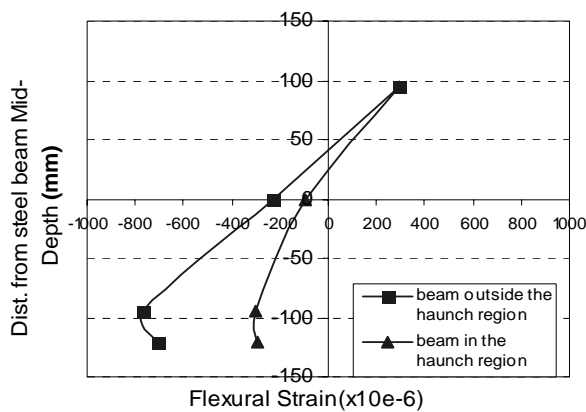


**Figure 29-1.** Hogging bending (Test G23)

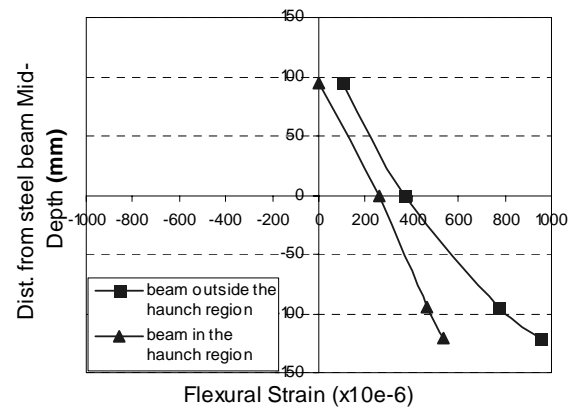


**Figure 29-2.** Sagging bending (Test G23)

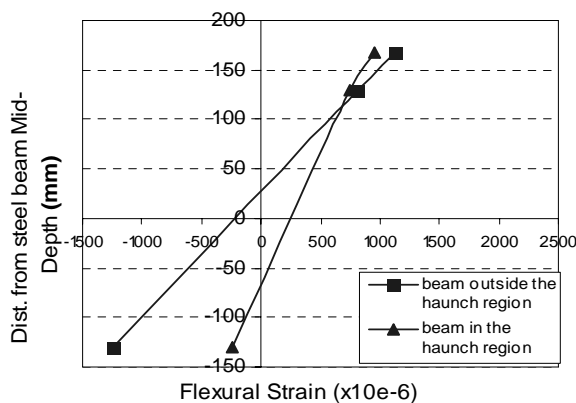


**Figure 30-1.** Hogging bending (Test G18)

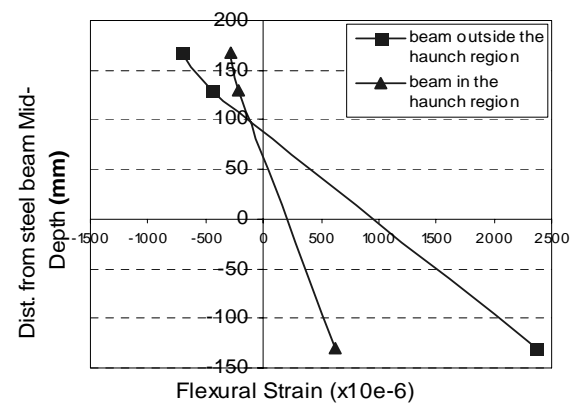


**Figure 30-2.** Sagging bending (Test G18)

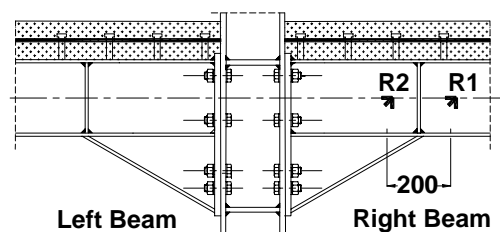


**Figure 31-1.** Location of rosette strain gauges

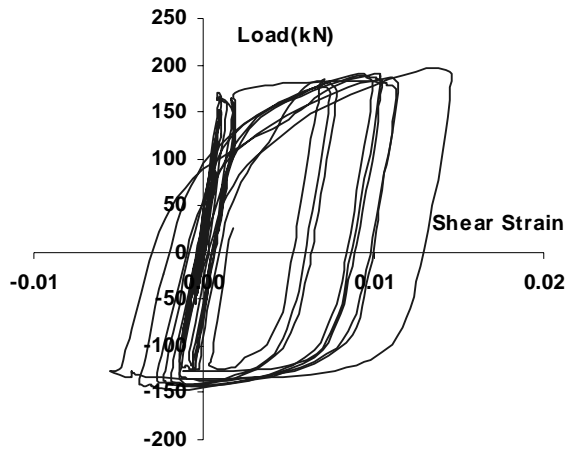


**Figure 31-2.** Shear strains of the beam web outside the haunch region R1

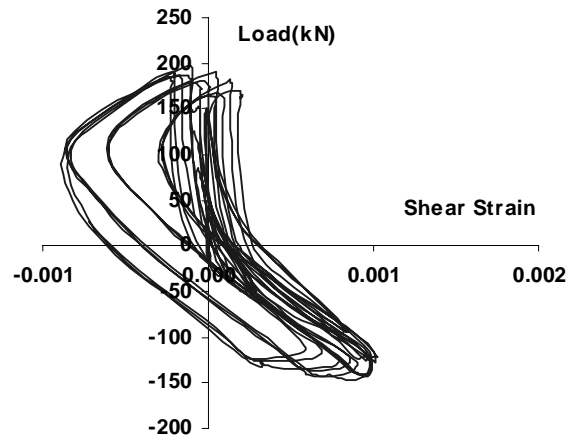


**Figure 31-3.** Shear strains of the beam web in the haunch region R2

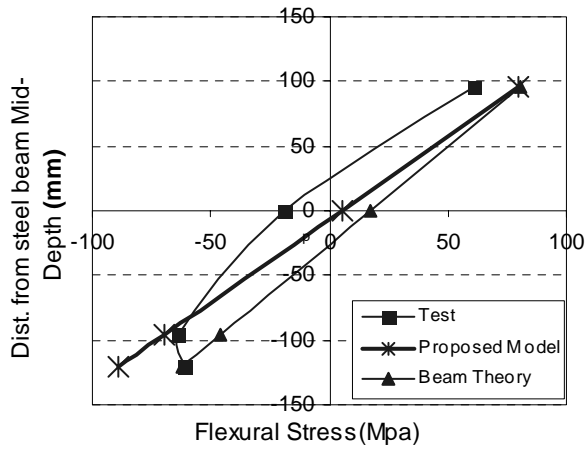


**Figure 32-1.** Hogging bending (Test G23)

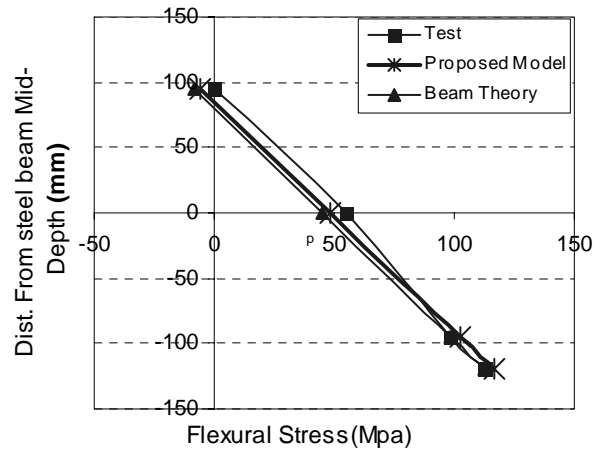


**Figure 32-2.** Sagging bending (Test G23)

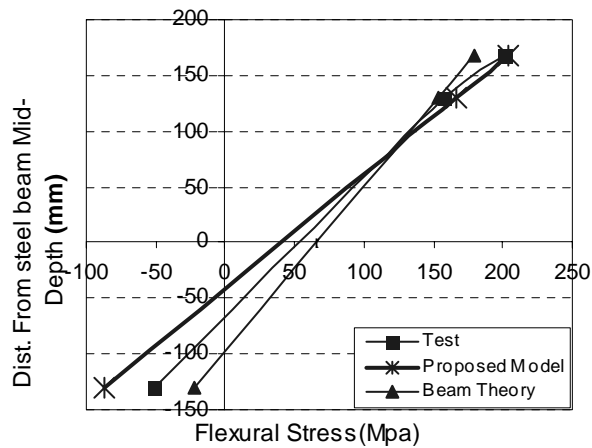


**Figure 32-3.** Hogging bending (Test G18)

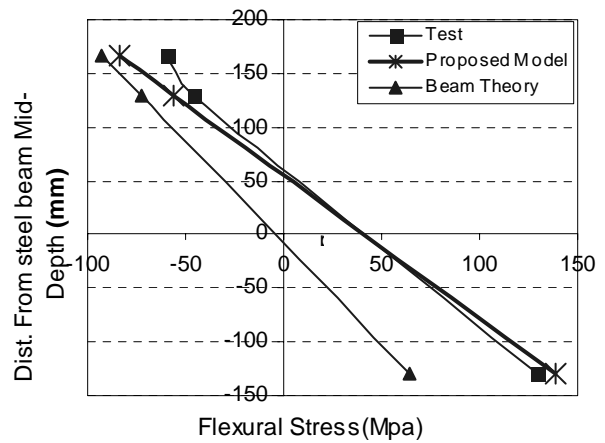


**Figure 32-4.** Sagging bending (Test G18)

## 5. CONCLUSIONS

Though haunched joints may be an expensive solution and their use limited to constructions with heavy loads in zones of high seismicity, the following conclusions may be drawn:



- ❑ Above results confirm, as well as for joints with a T arrangement than joints with a cruciform arrangement, that the use of haunch with a triangular shape cut out directly from a steel beam appears as a good solution to strengthen beam-to-column joints.
- ❑ Haunch solution improved significantly joint cyclic performances. Plastic energy dissipation may be twice greater at least and the rotation capacity can exceed 35mrad without risk of low-cycle fatigue rupture in the welds connecting beam flanges on the end-plates. A significant increase of rotational stiffness, moment resistance and rotation capacity was observed in comparison with similar beam-to-column composite joints without haunches.
- ❑ The stiffening effect of the composite slab prevents any risk of buckling in the upper beam flange leading under sagging cyclic bending to an increase of 60% of the maximum moment compared with a same steel joint. On the other hand, in hogging bending, the composite slab does not bring reinforcing effect on the lower beam flange and the increase of the maximal moment is only 30%.
- ❑ Experimental results are rather in good agreement with the simplified model developed by the authors which appears well adapted for the haunch static design in composite beam-to-column joints.
- ❑ It has been shown that Eurocodes 3 and 4 which do not give specific provisions about haunch strengthening, may offer a basic design guidance to suitably predict initial stiffnesses and moment resistances.

## ACKNOWLEDGEMENTS

The authors would like to thank the “French Ministry for Infrastructure, Transport, Spatial planning, Tourisme and the sea” through the DRAST (Research management) managed by Prof. André Colson for the financial support to the experimental part of this research.

## REFERENCES

- [1] Eurocode 3: Design of Steel Structures Part 1-1: General rules for buildings, European Committee for Standardization, CEN, 2003.
- [2] Eurocode 3: Design of Steel Structures Part 1-3: General rules – supplementary rules for cold-formed thin gauge members and sheeting, European Committee for Standardization, CEN, 2003.
- [3] Eurocode 3: Design of Steel Structures Part 1-8: Design of joints, European Committee for Standardization, CEN, 2003.
- [4] Eurocode 4: Design of composite steel and concrete structures Part 1-1: General rules and rules for buildings, European Committee for Standardization, CEN, 2003.
- [5] Eurocode 8: Design of structures for earthquake resistance Part 1: General rules, seismic actions and rules for buildings, European Committee for Standardization, CEN, 2003.
- [6] Eurocode 8: Design of structures for earthquake resistance Part 3: Strengthening and repair of buildings, European Committee for Standardization, CEN, 2003.
- [7] Rep. No. SAC-96-01, SAC Joint Venture, Sacramento, Calif., 1996.
- [8] Lee, C.H. and Uang, C.-M., “Analytical modeling of dual panel zone in haunch repaired SAC, “Technical report: Experimental investigations of beam-column subassemblies.” steel MRFs”, Journal of Structural Engineering, ASCE, 1997, 123(1), pp.20-29.

- [9] NIST, Modification of existing Welded Steel Moment Frame Connections for Seismic Resistance, Draft Report, National Institute for Standards and Testing, Gaithersburg, MD, 1998.
- [10] Gross, J.L., Engelhardt, M.D., Uang, C.M., Kasai, K. and Iwankiw, N.R., "Modification of Existing Welded Steel Moment Frame Connections for Seismic Resistance", AISC Design Guide Series 12, American Institute of Steel Construction, Chicago, Illinois, 1999.
- [11] Yu, Q.-S., Uang, C.-M. and Gross, J., "Seismic rehabilitation design of steel moment connection with welded haunch", Journal of Structural Engineering, ASCE, 2000, 126(1), pp.69-78.
- [12] FEMA- 355D, "State of the Art Report on Connection Performance". Ch 3, 2000.
- [13] FEMA- 351, "Recommended Seismic Evaluation and Upgrade Criteria for Existing Welded Moment-Frame Buildings", Ch 6, 2000.
- [14] Ciutina, A., Aribert, J.M. and Lachal, A., "Testing and numerical modelling of steel and composite bolted joints under seismic cyclic loads", French Journal of Steel Construction, 2004, n 1, pp.3-33.
- [15] ECCS, "Recommended Testing Procedures for Assessing the Behaviour of Structural Elements under Cyclic Loads", TC 1, TWG 1.3 – Seismic Design, 1986, n 45.

# THE CYCLIC BEHAVIORS OF BOX-SECTION STEEL BEAM-COLUMNS: EXPERIMENT AND NUMERICAL COMPARISON

Ming-zhou Su<sup>1,\*</sup>, Lin Shen<sup>2</sup>, Qiang Gu<sup>3</sup>

<sup>1</sup>*School of Civil Engineering, Xi'an University of Architecture & Technology, Xian, 710055, China*

*\*(Corresponding author: E-mail: sumingzhou@163.com)*

<sup>2</sup>*China Institute of Building Standard Design and Research, Beijing, 100044, China*

<sup>3</sup>*University of Science and Technology of Suzhou, Suzhou, 215011, China*

---

**ABSTRACT:** A series of tests were performed to evaluate the cyclic behaviors of box-section steel beam-columns under cyclic bending. The test was set up as a cantilever beam-column, loaded with cyclic transverse shear force at its free end, while the axial compression kept unchanged. Three sets of tests with various axial compression ratios were tested to find out their influencing on cyclic behaviors, which were 0.0, 0.4 and 0.6, respectively. In each set, there were five members with various width-to-thickness ratios of plates to consider their effects. The hysteretic curves and failure mechanisms of each member were given according the test results, and the main influencing factors, such as axial compression ratio of the member, width-to-thickness ratio of its plates, were analyzed. Then, the test results were compared with that of numerical analysis by the author. In general, there was a good agreement between two results, it revealed that the numerical analysis was reasonable and could be used in practice.

**Keywords:** Beam-column; Cyclic bending; Experiment; Numerical analysis; Hysteretic behavior; Box-section.

---

## 1. INTRODUCTION

High-rise building will not only undergo the gravity static loads, but also the dynamic horizontal actions, such as earthquake and wind action. In general, the latter becomes more important with the increase of building's height. In this case, the columns are subjected to large unchanged axial compression and varied bending moment. As the inflection point of columns generally lies near its mid-height, the problem can be simplified as a cantilever subjected to cyclic transverse shear at its free end, while the axial compression kept unchanged. For the facility of analysis, most researchers simplified the various action as a quasi-static manner, i.e., cyclic loading.

In the early 1960s, Kato [1] established the cyclic curve of beam-columns under cyclic bending. In his model, the relationship of moment-curvature was built based on monotonic loading, and the material was assumed to follow rigid plastic hardening, so the model was inaccurate and overestimated the bearing capacity of the member.

Toma and Chen [2] and Han and Chen [3] discussed the response of beam-columns under cyclic bending. Many simplifications were introduced in the analysis to get a closed-form solution, so only one or less cycle could be performed, the behavior of members could not be predict after several cycles.

Billio and Calado [4] carried out an experiment on beams under cyclic bending. The phenomenon of capacity deterioration of beams was found in case of local buckling occurred in their study. Furthermore, a simplified numerical model was established to consider the effect of local buckling and fracture on the capacity deterioration.

Macrae [5] performed an experiment on beam-columns under cyclic bending with constant or various axial compressions. The aim of the test was to investigate the influence of axial force on the behavior of beam-columns. It noted that the results on few tests were not reliable, and the limitation of axial force would not be relaxed before thorough analysis.

Watanabe [6] put forward a simplified model to study the cyclic behavior of beam-columns with square hollow section. In that model, the section was divided into many fibers, each fiber was assumed to follow uniaxial stress state, perfect elastic-to-plastic material was assumed, and the residual stress and initial geometric imperfection were not considered.

Hao [7] studied the cyclic behavior of beam-columns with H-shaped sections. The simplified plastic zone model was adopted in his numerical analysis, and the plastic damage accumulation was considered. But the critical factors in the model were based on experimental results and varied with each member, so it could not be used to predict the behavior of members untested.

Yamazaki and Minami [8] performed experiment and numerical analysis on box-section beam-columns under various axial force and cyclic bending. In their analysis, the plane section hypothesis was used, and the one-dimensional hysteretic model of Ohi *et al.* [9] was adopted. As a result, they found the transverse resistance of the member decreased dramatically with large axial compression, and the strength was between that of cyclic bending with constant maximum axial compression and that with minimum axial compression.

Miki and Nethercot [10] built up a multi-failure mechanism numerical model of beam-columns with varied cross-section. It found that two failure mechanisms would appear alternatively in one cycle, and the member would then lose its stability.

Gao *et al.* [11] performed a finite element analysis on the ultimate strength and ductility capacity correlation between centrally loaded and eccentrically loaded columns subjected to cyclic transverse load. Both geometrical and material nonlinearity was considered in the analysis, and a modified two-surface plasticity model is employed to model material nonlinearity. As a result, equations were proposed to evaluate the ultimate strength and ductility capacity of the eccentrically loaded columns from those of the centrally loaded columns.

To analysis the behavior of steel beam-columns under cyclic bending, the author [12,13] suggested a numerical method based on degenerated shell element, together with the updated Lagrange formulation and the mixed hardening material. As a result, the author gave suggestions about the limit of width-to-thickness ratio of plates and the bearing capacity of members.

In order to evaluate the hysteretic behavior of box-section steel beam-columns under cyclic bending, a series of tests was carried by the author. This paper contains a description of test specimens, set-up and instrumentation, procedure, and results. A comparison of the experimental and analytical results is also provided.

## 2. TEST SPECIMENS

A series of three group tests was conducted, corresponding with various axial compression ratios, which were 0.0, 0.4 and 0.6, respectively. Each of the three groups contained five members with various width-to-thickness ratios of their plates. These specimens were welded by hand-arc welds with E43 electrode rod, and the material of their plates is Q235B. The test was set up as a cantilever beam-column, loaded with cyclic transverse shear force at its free end, while the axial compression kept unchanged. The test was controlled by the transverse displacement at the free end. The configuration of specimens and loading scheme were described in Figure 1 and Table 1.

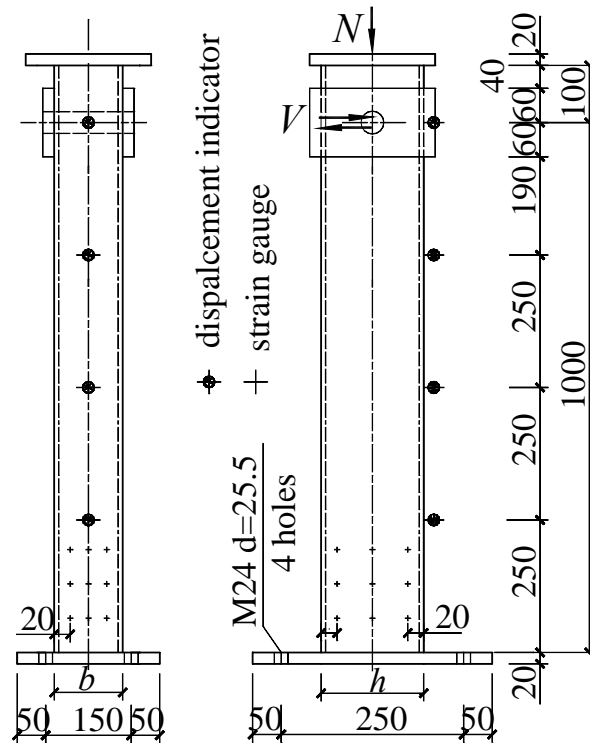
**Table 1.** Configuration of Specimens

Item	$h/t_w$	$b/t_f$	$h$ (mm)	$b$ (mm)	$t_f, t_w$ (mm)	$N/Af_y$	$\delta_y$ (mm)	Displacements (mm)		
								$\delta_1$	$\delta_2$	$\Delta$
S-1-0	23.0	19.0	92	76	4	0.0	9.81	10	20	10
S-2-0	33.3	23.5	133	94	4	0.0	6.79	7	10	10
S-3-0	33.5	29.0	134	116	4	0.0	6.74	7	10	10
S-4-0	43.3	29.0	173	116	4	0.0	5.22	5	10	10
S-5-0	43.5	36.0	174	144	4	0.0	5.19	5	10	5
S-1-4	23.8	19.0	95	76	4	0.4	5.70	6	10	10
S-2-4	33.3	23.5	133	94	4	0.4	4.07	4	5	5
S-3-4	33.5	29.0	134	116	4	0.4	4.04	4	5	5
S-4-4	43.3	29.0	173	116	4	0.4	3.15	3	5	5
S-5-4	43.5	36.0	174	144	4	0.4	3.14	3	5	5
S-1-6	23.0	19.0	92	76	4	0.6	3.96	4	5	2.5
S-2-6	33.5	23.5	134	94	4	0.6	2.72	3	5	2.5
S-3-6	33.5	29.0	134	116	4	0.6	2.72	3	5	2.5
S-4-6	44.0	29.0	176	116	4	0.6	2.08	2	5	2.5
S-5-6	43.5	36.0	174	144	4	0.6	2.11	2	5	2.5

Note: i.  $h$  and  $b$  are the height and the width of the cross-section, and  $t_w$  and  $t_f$  are the thickness of its web and flange, respectively.

ii.  $N/Af_y$  is the axial compression ratio.

iii.  $\delta_y$  is the transverse displacement when the extreme fiber at the fix end of the member yields.

**Figure 1.** Configuration of Specimens

### 3. TEST SET-UP AND TEST PROCEDURE

Test set-up was shown in Figure 2. The specimen (1) was fixed on the floor girder (2) through 4 high-strength bolts (3), the diameter of which are 24mm, with the material grade of 10.9S (the tensile ultimate strength of the material is  $1040\text{N/mm}^2$ , and the yield strength is  $940\text{N/mm}^2$ ). The tested member was subjected to transverse cyclic load applied through horizontal actuator (4), while a constant compressive load applied by vertical jack (5), which was free to move laterally in-plane on greased roller bearings (6). The jacks were fastened in the test rig (7). To prevent lateral-torsional buckling of the tested member, a lateral support (8) was provided.

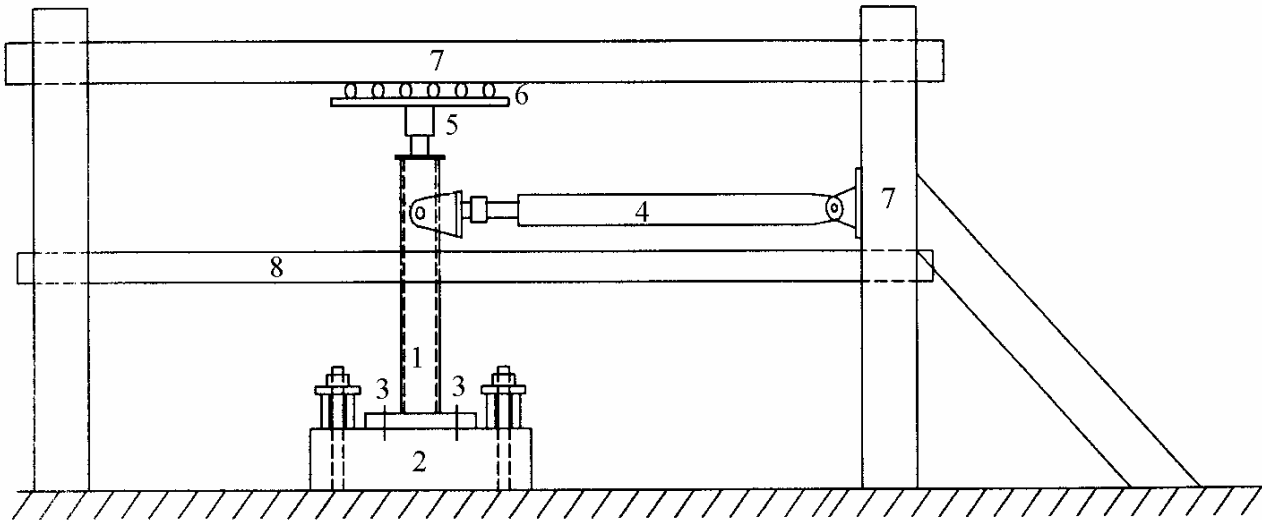


Figure 2. Test set-up

The following procedure was used to obtain accurate and reliable results of each specimen:

1. The specimen was set into position and connected to the floor girder.
2. Jacks were mounted, connected, and aligned in order to prevent eccentricity.
3. The axial compression was applied to the beam-column by vertical jack according to design.
4. The cyclic transverse displacements were applied according ECCS loading scheme. The displacement of first step was about  $\delta_1/2$  for one cycle as the member stayed in elastic state, and then displacement of  $\delta_1$  and  $\delta_2$  were applied for three cycles for some fibers of member yielded, after that an incremental displacement of  $\Delta$  was added to the former step for three cycles ( $\delta_1$ ,  $\delta_2$  and  $\Delta$  were shown in Table 1).
5. Test stopped when the specimen fractured or its bearing capacity dropped below 80% of the maximum.

### 4. TEST RESULTS AND DISCUSSION

#### 4.1. Results of Coupon Test

The coupon was designed according to the demand of Chinese National Standard *Metallic materials - Tensile testing at ambient temperature* (GB228-2002). Based on the testing results, the material Q235B used in the experiment had the following characteristic values: Yong's modulus  $E=2.05 \times 10^5 \text{MPa}$ , yield stress  $f_y=279 \text{MPa}$ , hardening modulus  $E_{st}=1.84\%E$ , hardening strain  $\varepsilon_{st}=1.1\%$ .

## 4.2. Test Results of Beam-Columns

### 4.2.1. Members without Axial Force ( $N/Af_y=0.0$ )

For members without axial force, the hysteretic curves were quite smooth and plump, the ductility factor was over 7.5, which revealed that the energy dissipation was very excellent. Figure 3 to Figure 7 gave the hysteretic curves of S-1-0 to S-5-0 respectively. In these figures, the vertical axis denotes the transverse shear at the free end of the member, while the horizontal one denotes the corresponding transverse displacement at the same point and the ductility factor of the member. Except that members S-2-0 and S-3-0 failed with welds fractured at the fix end due to lack of enough weld throat, all the others failed with plastic cracks of flanges near half of the section width away from the fix end, owing to low cycle fatigue. The cracks firstly developed in the intersect lines of flanges and webs, and then expanded with the increase of cyclic load, finally the section fractured. Before failure, the slop of hysteretic curve increased with the increase of displacement due to cracks closed, obviously in the member with large width-to-thickness ratios of plates, as shown in Figures 6 and 7. Fracture of S-5-0 was shown in Figure 8. The local buckling of all the five members just occurred before fracture and the buckling deformation was very small. The hysteretic behaviors of members without axial compression were listed in Table 2.

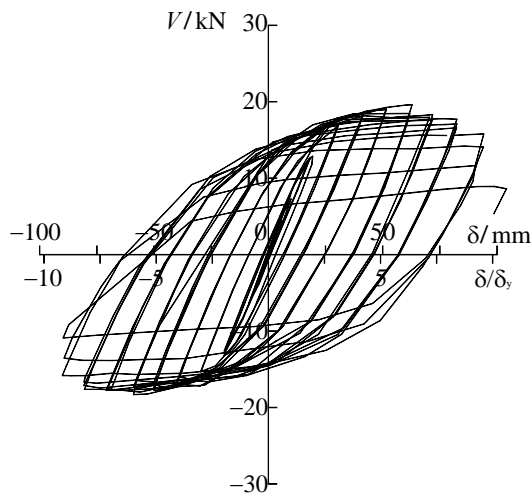


Figure 3. Hysteretic curve of S-1-0

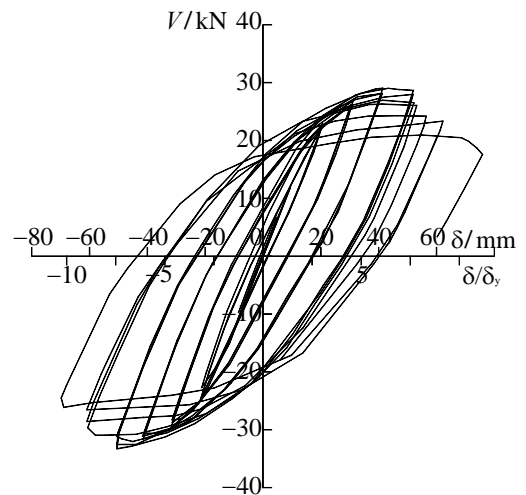


Figure 4. Hysteretic curve of S-2-0

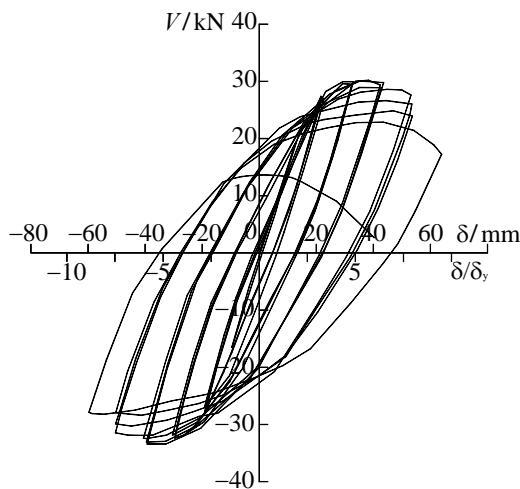


Figure 5. Hysteretic curve of S-3-0

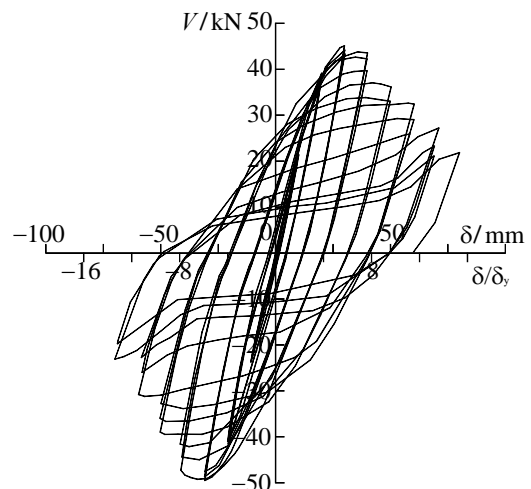
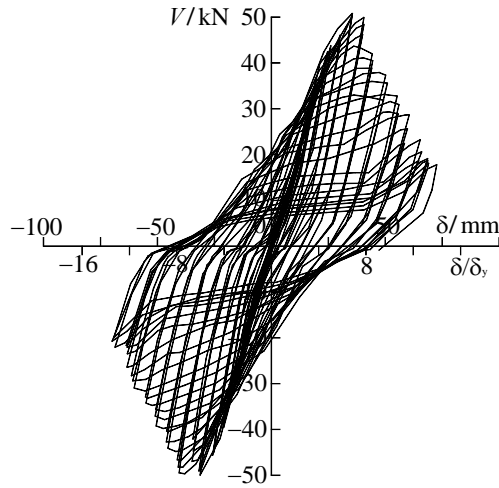


Figure 6. Hysteretic curve of S-4-0



**Figure 7.** Hysteretic curve of S-5-0



**Figure 8.** Fracture of member S-5-0

**Table 2.** The Hysteretic Behaviors of Members without Axial Force

Item	S-1-0	S-2-0	S-3-0	S-4-0	S-5-0
Rotation angle (%) <sup>a</sup>	9.0	6.0	5.0	5.0	5.0
Ductility factor <sup>b</sup>	9.5	9.0	7.5	8.0	8.3
Location of plastic hinge	0.53b	0.53b	0.47b	0.52b	0.38b
Failure mode	Section fractured	Section cracked, but failure due to welds fractured at the fix end	Similar to S-2-0	Similar to S-1-0	Similar to S-1-0

Note: <sup>a</sup> Rotation angle is defined as total transverse displacement ( $\delta$ ) over the length of the member ( $l$ ).

<sup>b</sup> Ductility factor is termed as  $\delta$  over  $\delta_y$ .

#### 4.2.2. Members with axial compression ratio $N/Af_y=0.4$

The hysteretic curves of members S-1-4 to S-5-4 were shown in Figure 9 to Figure 13, respectively. It was shown in the figure that plates of members were susceptible to buckle locally as the existence of large axial compression, and the capacities of ductility and energy dissipation were seriously deteriorated owing to the local buckling. Even for the member S-1-4 with smallest plate width-to-thickness ratios, the ductility factor was only about 5. Local buckling developed in the section near the fix end with the increase of transverse shear, members failed owing to the cyclic local buckling, and no cracks were found in the section or in the welds of fix end. The members with small width-to-thickness ratios of plates failed due to dramatic decrease of bearing capacity, while ones with large width-to-thickness ratios failed due to severe local buckling. Local buckling of S-4-4 was shown in Figure 14, and hysteretic behaviors of these five members were described in Table 3. The failure mode in this Table referred to the dominant deformation of the member, Plastic referred to the failure mainly caused by plastic deformation; Local Buckling referred to the failure mainly caused by local buckling.

**Table 3.** The Hysteretic Behaviors of Members with Axial Compression Ratio  $N/Af_y = 0.4$

Item	S-1-4	S-2-4	S-3-4	S-4-4	S-5-4
Rotation angle (%)	3.0	2.0	2.0	1.3	1.0
Ductility factor	5.0	4.8	4.5	4.0	3.0
Location of local buckling	0.71b	0.85b	0.56b	0.93 b	0.79b
Failure mode	Plastic	Plastic, local Buckling	Plastic, local Buckling	Local buckling	Local buckling



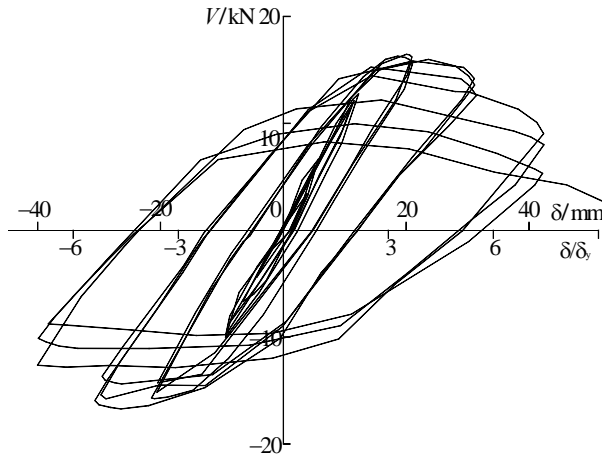


Figure 9. Hysteretic curve of S-1-4

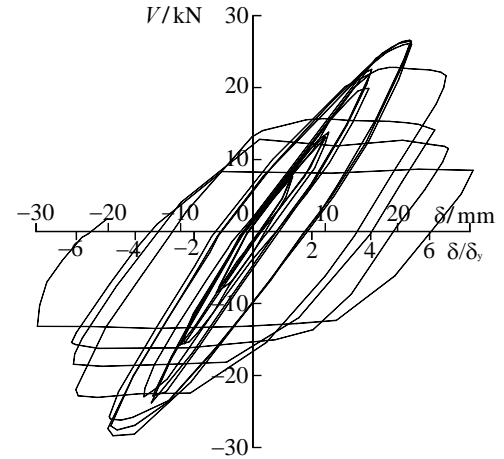


Figure 10. Hysteretic curve of S-2-4

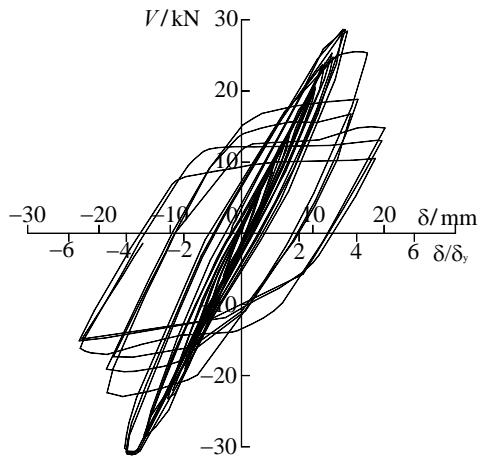


Figure 11. Hysteretic curve of S-3-4

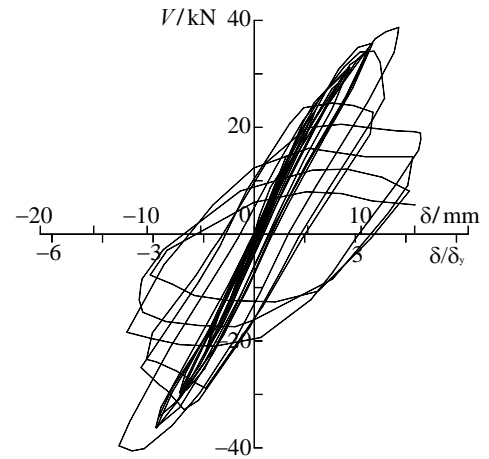


Figure 12. Hysteretic curve of S-4-4

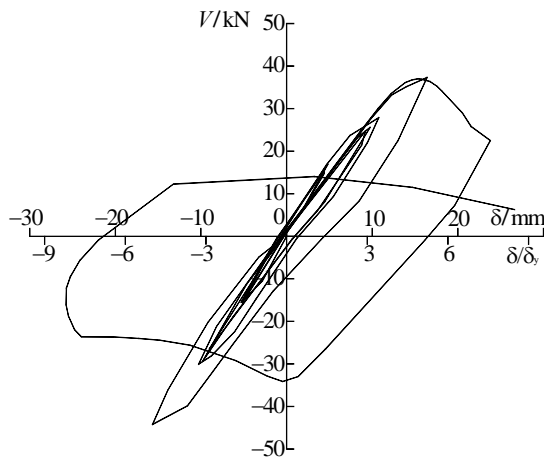


Figure 13. Hysteretic curve of S-5-4

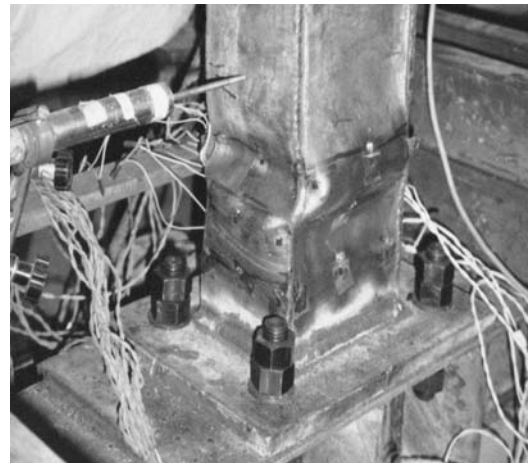
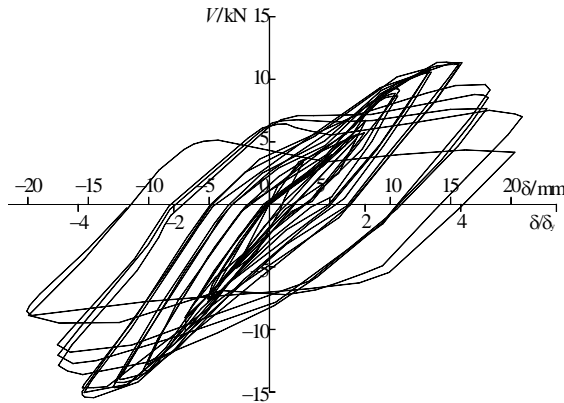


Figure 14. Local buckling of S-4-4

#### 4.2.3. Members with Axial Compression Ratio $N/Af_y=0.6$

The ductility and bearing capacity of members with  $N/Af_y=0.6$  deteriorated more seriously than those with  $N/Af_y=0.4$ . This phenomenon is mainly caused by severe local buckling of their plates due to the large axial compression ratio. These members failed mainly due to the local buckling.

As soon as the bearing capacity reached, the maximum load decreased quickly with the increase of transverse displacement, brittle failure might occur in the member with large plate width-to-thickness ratio, such as S-4-6 and S-5-6. The hysteretic curves of members with axial compression ratio  $N/Af_y = 0.6$  were shown in Figures 15 to 19. Except that S-1-6 underwent large plastic deformation, the other 4 members failed mainly due to local buckling. Figure 20 showed the local buckling of S-4-6 when failure occurred, which was similar to Figure 14. The hysteretic behaviors were listed in Table 4.



**Figure 15.** Hysteretic curve of S-1-6

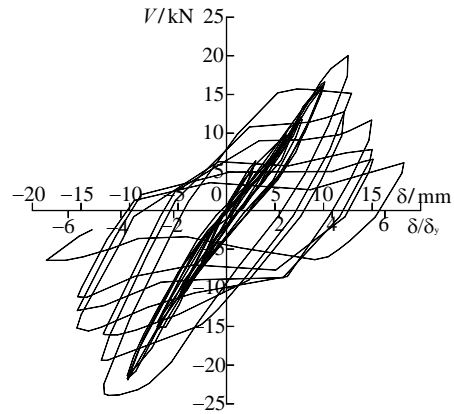


**Figure 16.** Hysteretic curve of S-2-6

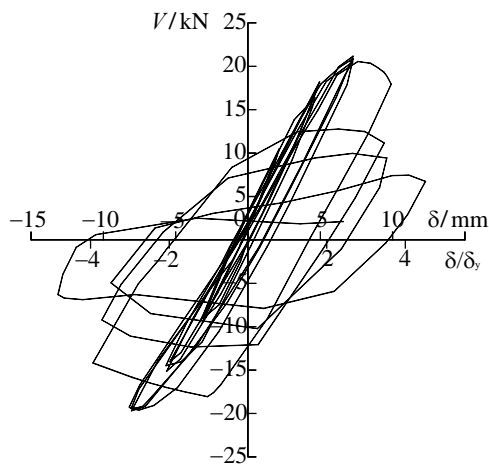


**Figure 17.** Hysteretic curve of S-3-6

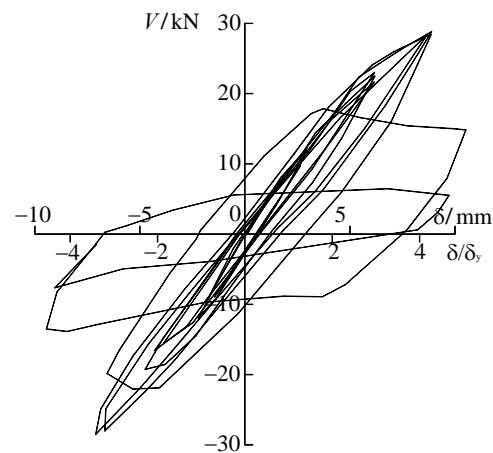


**Figure 18.** Hysteretic curve of S-4-6

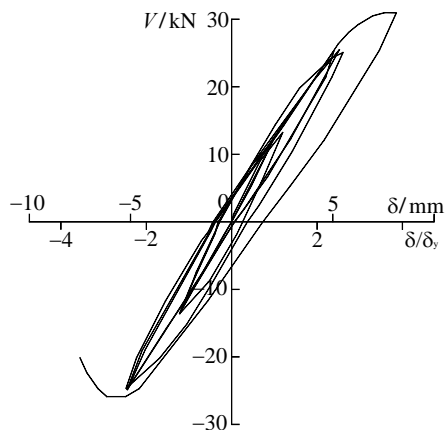


**Figure 19.** Hysteretic curve of S-5-6

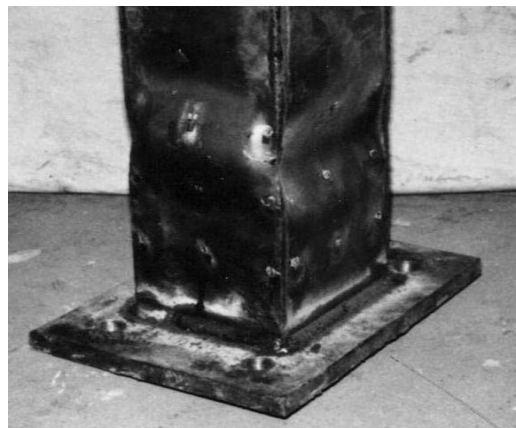


**Figure 20.** Local buckling of S-4-6

**Table 4.** The Hysteretic Behaviors of Specimens with Axial Compression Ratio  $N/Af_y = 0.6$ 

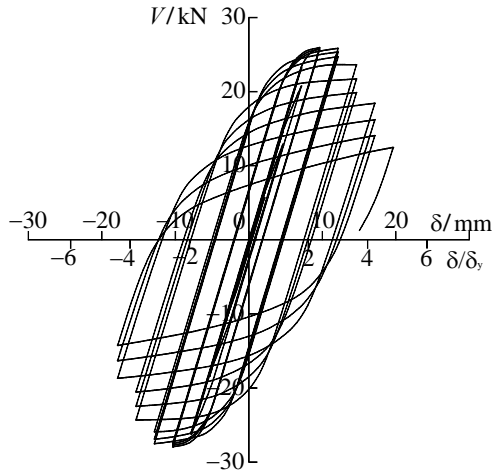
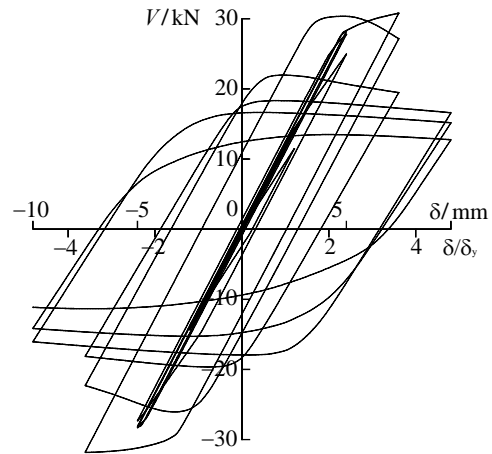
Item	S-1-6	S-2-6	S-3-6	S-4-6	S-5-6
Rotation angle (%)	1.8	1.3	0.75	0.75	0.5
Ductility factor	4.5	4.2	2.8	3.8	2.5
Location of local buckling	$0.98b$	$0.53b$	$0.56b$	$0.78b$	$1.30b$
Failure mode	Plastic	Plastic, local Buckling	Local buckling	Local buckling	Local buckling

## 5. THE COMPARISON OF EXPERIMENTAL AND NUMERICAL RESULTS

### 5.1. Comparisons of Hysteretic curves

A degenerated shell element with eight nodal points was used for implementing the formulation. Both material and geometric non-linearity were taken into account. The program had the following characteristics: 1) Degenerated shell element assumption is adopted, i.e., the normal of the mid-surface of shell keeps straight after deflection, but no longer keeps normal. 2) The virtual work equation is expressed in terms of updated Lagrange formulation. 3) The plastic flow theory is applied considering the Mises' yield function as a plastic potential. 4) The material is assumed to follow the mixed hardening law, which linearly combines isotropic and kinematic hardening. Details can be found in the reference [13].

Based on the numerical analysis, the calculated curves of S-3-4 and S-4-6 were shown in Figure 21 and Figure 22 respectively. By comparing of Figure 21 with Figure 11 and Figure 22 with Figure 18, it was shown that the bearing capacity, deterioration rate of maximum load and ductility

**Figure 21.** Numerical curve of S-3-4**Figure 22.** Numerical curve of S-4-6

factor of both curves were very close, so there was a good agreement between two results. However, there was an obvious deference in stiffness that the experimental one was lower than that of calculating, and the experimental curve was not as plumb as that of calculating. This was mainly due to the following reasons:

1. Only the welded residual stress along the longitudinal axial was considered in numerical analysis. As the thick end-plate was welded to the member, the distribution of residual stress in the end was very complex, it might have large influencing on the stiffness of the member, but it was very difficult to simulate and was not considered in the numerical analysis.

2. As the member was anchored to the floor beam by four high-strength bolts, the rotation of fix end could not be avoid, the bolts would loosen when many cycles repeated, this would decrease the stiffness of the member, and it was not considered in calculation.
3. Only initial deflection was considered in numerical analysis, the eccentricity of axial load was no to be taken into account, and this was unavoidable in experiment.

## 5.2. Verification of Interrelation of Bending Moment and Axial Compression

Eq. 1 gave the interrelation of non-dimensional bending moment and axial compression ( $M/M_P-N/N_P$ ), which was put forward by the author through numerical analysis [12]. The parameter  $a$  in Eq.1 could be taken as 1.10 for box-section steel beam-columns. The comparison of test data with Eq. 1 was given in Figure 23. The test data fully lay above the curve, so it was safety to use this equation. Eq. 2 could be used in practice according to Chinese Code for Design of Steel Structures GB50017-2003, in which plastic adoption  $\gamma_x$  (only part of plastic deformation considered) equal to  $1.05 \times a = 1.16$  might be adopted (1.05 is the original plastic adoption in this Code).

$$N/N_P + M/(a M_P) = 1 \quad (1)$$

$$\frac{N}{\varphi_x A} + \frac{\beta_{mx} M}{\gamma_x W_x (1 - 0.8 N/N'_{Ex})} \leq f \quad (2)$$

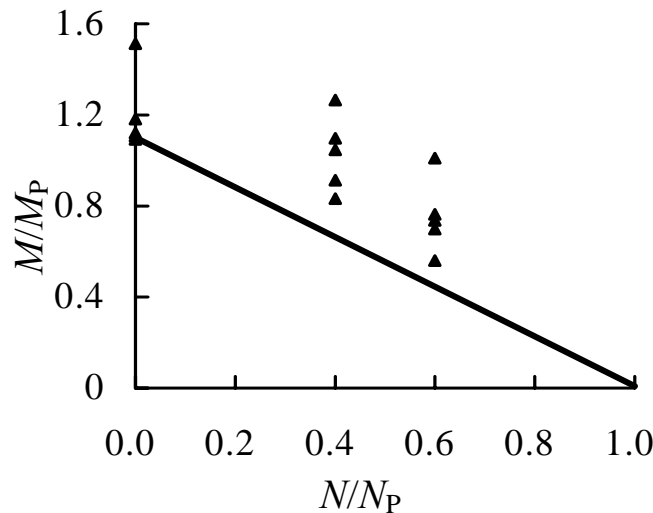


Figure 23. Interrelation of  $M/M_P-N/N_P$

## 6. CONCLUSIONS

This paper has described a series of tests of steel beam-columns with box-section under cyclic bending. Three axial compression ratios were taken into account to investigate its influence, which was 0.0, 0.3, and 0.6 respectively, and five width-to-thickness ratios of plates were considered. Then the test results were present and analyzed. At the last part of this paper, the experimental results were compared with the numerical ones. The following conclusions could be made from this paper:

1. Beam-columns under cyclic bending might fail in fatigue fracture when no axial force presented, otherwise they might fail in cyclic plastic deformation and/or local buckling based on their width-to-thickness ratios of their plates and on the axial compression carried.

2. The largest deformations generally located in the height of  $b/2 \sim b$  near the fix end according to test results.
3. By comparing the experimental and numerical results, the design formula was verified, and proved to be reasonable and could be used in practice.

## REFERENCES

- [1] Kato, B., "Inelastic bar subjected to thrust and cyclic bending", Journal of Structure Division, 1969, 95(1), pp.562-590.
- [2] Toma, S. and Chen, W.F., "Cyclic analysis of fix-ended steel beam-columns", Journal of Structure Division, ASCE, 1982, 108(6), pp.1385-1399.
- [3] Han, D.J. and Chen, W.F., "Buckling and cyclic inelastic analysis of steel tubular beam-columns", Engineering Structures, 1982, 5, pp.119-132.
- [4] Ballio, G. and Calado, L., "Steel bent sections under cyclic loads: experiments and numerical approaches", Costruzioni Metalliche, 1986, 1, pp.2-24.
- [5] Macrae, G.A., "Cyclic bending of steel I-shaped beam-columns", Proceeding of Pacific Structural Steel Conference, Brisbane, 1989.
- [6] Watanabe, E., "Modeling of hysteric behavior of thin-walled box members", Stability and Ductility of Steel Structures under Cyclic Loading. CRC press, 1992, pp.225-235.
- [7] Hao, J.P., "Test and theoretical study on the local buckling and low cycles fatigue of steel structures under cyclic loading", PhD. thesis, School of Civil Engineering, Xi'an University of Architecture & Technology, Xi'an, China, 1995 (in Chinese).
- [8] Yamazaki, S. and Minami, S., "Inelastic behavior of steel beam-columns subject to varying axial force and cyclic bending moment", Proceeding of the 5th International Colloquium on Stability and Ductility of Steel Structures, Nagoya, Japan, 1997, pp.561-568
- [9] Ohi, K., Chen, Y. and Takanashi, K., "An experimental study on inelastic behavior of H-shaped steel beam columns subject to varying axial and lateral load", Journal of Structure Engineering, Architecture Institute of Japan, 1996, 42B, pp.421-430.
- [10] Miki, T. and Nethercot, D.A., "Cyclic instability of beam-columns with variable cross-section due to combination of collapse mechanisms", Proceeding of the 5th International Colloquium on Stability and Ductility of Steel Structures, Nagoya, Japan, 1997, pp.569-576.
- [11] Gao, S.B., Usami, T. and Ge, H.B., "Eccentrically Loaded Steel Columns under Cyclic In-Plane Loading", Journal of Structural Engineering, ASCE, 2000, 126(8), pp.964-973.
- [12] Su, M.Z. and Gu, Q., "Study on Hysteretic Behavior of Box-section Steel Beam-columns under Cyclic Bending and on Limiting Ratio of Width-to-thickness of its Plates", Journal of Building Structures (in Chinese), 2000, 21(5), pp.41-47.
- [13] Su, M.Z., Gu, Q. and Guo, B., "Finite Element Analysis of Steel Members under Cyclic Loading", Finite Elements in Analysis and Design, 2002, 39(4), pp.43-54.

# STRUCTURAL PERFORMANCE OF COMPOSITE BASE COLUMN CONNECTIONS

L. Di Sarno<sup>1,\*</sup>, G. Fabbrocino<sup>2</sup> and M.R. Pecce<sup>1</sup>

<sup>1</sup> *Department of Engineering, University of Sannio, 82100, Benevento, Italy*

*\*(Corresponding author: E-mail: disarno@unina.it)*

<sup>2</sup> *Department S.A.V.A., University of Molise, 86100, Campobasso, Italy*

---

**ABSTRACT:** The present paper provides the results of a comprehensive experimental research program carried out on partially encased composite steel-concrete columns connected to the foundation block through traditional (bolted steel end plate) and an innovative system employing a socket type system. Experimental tests under monotonic loads show that the structural behaviour of the traditional connection is significantly influenced by the response of the anchorage bolts. The latter cause large fixed end rotations and exhibit limited energy dissipation. Conversely, innovative composite base column connections with socket systems possess adequate inelastic deformations and energy absorption. Furthermore, the use of socket-type connections is beneficial for the spreading of inelasticity at the base of the composite columns without damage localization on concrete and interface components. It can thus be argued that the innovative connection assessed in this study is a viable solution for applications in framed structures fulfilling capacity design requirements, e.g. structural systems in earthquake prone regions.

**Keywords:** Composite columns; Partially encased columns; Base column joint; Socket-type connection.

---

## INTRODUCTION

The composite lateral-resisting system has the desired characteristics of conventional structures, such as stiffness, strength and ductility, and fire resistance, and has been found to be very cost-effective for buildings [1-3]. Steel-composite columns are used extensively in modern medium-to-high rise buildings. Composite structural systems for buildings often include a steel moment resisting, consisting of steel beams (acting compositely with a metal deck reinforced slab) and encased composite columns, or braced frame with steel-concrete composite columns. Consequently, the lateral drifts under horizontal forces (wind and/or earthquakes) are lowered. Under severe earthquake loading concrete encasement cracks and reduces the flexural stiffness of composite beam-columns but the steel core acts as a back-up system in providing the shear strength and the ductility to prevent brittle collapse. Partial encased beam-columns with local buckling inhibitors have been found very efficient to prevent local buckling and enhance the global stability of the frame, thus reducing sensitivity to P- $\Delta$  effects [4]. Moreover, to achieve effective composite action, shear stresses should be transferred between the encased steel and reinforced concrete; hence, shear connectors may be placed along the column [5].

The assessment of structural response of composite steel and concrete columns is thus of paramount importance, especially in the earthquake design of framed systems [6,7]. The inelastic response of composite columns can be significantly affected by the beam-column, brace-to-beam, brace-to-column connections and column bases. A comprehensive review of the experimental tests carried on steel-concrete composite beam-columns (both encased and concrete-filled) can be found, for instance, in Cosenza and Pecce [8] and Shanmugam and Lakshmi [9]. It is noteworthy that, to date, analytical and experimental research focusing on the effects of the base connection layout on the performance of beam-columns, either partially or fully encased, is lacking [10]. Few results are available and were derived chiefly from steel structures; their applicability within the capacity-design framework should be further investigated [11,12]. The composite action, may, however, affect the failure modes thus endangering the inelastic performance of the member.

The present paper analyzes the inelastic response of composite joints at column-foundation joints. An innovative base column connection, employing a socket-type system, is discussed and its

response is compared to that of a traditional steel base plate connection. The latter was designed in compliance with the rules utilized for the composite frame tested at JRC Ispra laboratory [13,14]. Several tests under either monotonic or cyclic lateral loads and different levels of axial loads were performed. This work focuses on the response of composite columns under monotonic regime. In the following, the results of the tests on specimens with welded base steel plate (traditional) and socket-type joints are discussed. It is found that for the traditional connections, concentrations of inelastic demand occur in the anchorage bolts and relies chiefly on bond type mechanisms. Conversely, the socket-type system leads to large energy dissipation; plastic hinges form at column base and the strength capacity does not drop even at large lateral drifts (greater than 5-6%). As a consequence, socket-type foundations may be reliably utilized for steel and composite steel-concrete framed structures, especially in regions with moderate-to-high seismicity.

## EXPERIMENTAL PROGRAM AND TEST SET-UP

Recently, several research programs have prompted in Europe to investigate the inelastic response of steel and concrete composite buildings. The experimental projects were funded by the European Community, e.g. ECSC-7210-PR-250 (*Applicability of composite structures to sway frames*), ECOLEADER (*Cyclic and PsD testing of a 3D steel-concrete composite frame*) and/or National Ministry of Research, e.g. by MIUR in Italy, COFIN 2002 (*Advanced design and control of global performance of composite steel and concrete frames for earthquake resistant building*) and COFIN 2004 (*Composite steel and concrete earthquake-resistant frames: advanced dissipative joint systems, methods for damage assessment and seismic design guidelines*). The latter have involved eight Italian Universities. In particular, the working group of University of Sannio is assessing the inelastic static and dynamic (seismic) response of base column connections. In so doing, a number of partial encased column specimens, with different base joints, were tested in the laboratory of the Department of Structural Analysis & Design (DAPS, University of Naples, Italy). The sample specimens included monotonic and cyclic tests; different levels of axial loads were considered during the tests. In addition, pull-out tests were carried out to define the force-slip relationships of the hooked anchorage bolts. In this work the results of the monotonic tests are discussed in details. The experiments were carried out on two types of partially encased composite columns: HEB260 and HEB280. The specimens tested employed two types of layouts for the base column joints as per Figure 1: traditional (*bolted steel base plate*) and innovative (*socket-type*) joints. The former consist of tapered steel plates welded onto base plates and anchored to the foundation block through steel bolted bars (*see also [14]*). The latter is an alternative and innovative socket type joint in which the column is fixed to the foundation block utilizing a special concrete filler; such joint was developed and designed to benefit of composite action.

The first set of specimens (traditional base column connections) replicate the columns and base joints designed in compliance with the guidelines of European standards [5] and used for the full-scale composite frame tested in ISPRA [13]. Similarly, the socket-type foundation was designed in compliance with Eurocode 2 [15].

The lateral loads were applied at two different locations along the height of the column, namely 1.6 m (*traditional joint*) and 1.7 m (*socket type*) above the foundation block to account for the different location of the restraint. Traditional base plates are generally placed at floor level, conversely socket type solution enables to use pavings that cover the foundation block. The horizontal load (T), simulating the earthquake loading, was applied via a 500 kN-hydraulic jack; the test was under displacement control. As a consequence, the maximum flexural moments (M), located at the base connection, was increased until failure. The displacement controlled loading regime allowed the softening branch of the response (*capacity*) curve to be investigated. The

connection of the jack to the column is ensured by two steel plates 30mm thick bolted on two opposite faces of the column. The reaction wall for the horizontal load is a stiff tapered cantilever element bolted to a steel system; its layout is shown in Figure 2 along with the test set-up. The cantilever system is connected to the laboratory floor slab (strong floor) by means of large steel rebars crossing the slab and the steel elements. These rebars are loaded in tension to prestress the connection. The vertical load ( $N$ ) is applied by two hydraulic jacks connected with two bars at the hinges placed at the foundation level. The axial load  $N$  acts along the column centroid axis. The reaction system for  $N$  consists of a steel plate located under the foundation block and connected to the hinges. This layout ensures that the load remains along the member axis during the column deformation. The transversal beam, at the column top, employs large stiffeners where is connected to the jack. An adequate lateral restraint along four prestressing bars at the corners were used to prevent slip and rocking of the foundation block and to guarantee the transfer of the shear forces to the strong floor level. Further details of the reaction wall and the set-up of the tests can be found elsewhere [14].

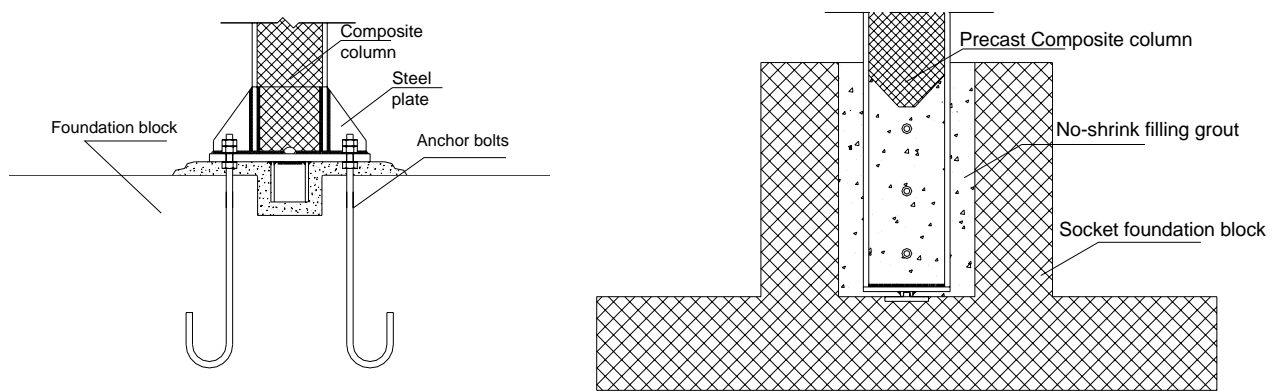


**Figure 1.** Layout of the sample base column connection: traditional (*left*) and socket-type (*right*).

## TEST SPECIMENS

The experimental program carried out at the laboratory of DAPS, in Naples, focuses on two sample partially encased composite steel and concrete columns: HEB260 and HEB280. The sample specimens tested were cantilever systems summarised as below (Table 1): partially encased columns with a steel HEB 260 member and traditional connection to foundation (stiffening plates and anchoring devices) and innovative socket-type system; HEB280 with socket-type foundation. The specimens were heavily instrumented to characterize reliably the concentration of inelastic demand at the base column. Figure 3 provides a close-up of the electrical displacement transducers (LVDTs) located at the base of the partially encased columns with either traditional or innovative joints.

The values of axial load ( $N$ ) used in the tests were equal to 170 kN and 330 kN. These values correspond to the minimum and maximum axial loads relative to the design load combinations of the full-scale composite framed building tested in the ELSA laboratory of JRC in Ispra [13]. The grade of the structural steel of the specimens was S235; the reinforcing bars grade was B450-C and the concrete was class C25/30. Actual values of the mechanical properties of steel and concrete were estimated from tensile (steel) and compression (concrete) tests. The values computed for the steel members and components are summarised in Table 2. Further details on the results of such tests can be found elsewhere [13]. The values of material overstrength ( $f_u/f_y$ ) relative to the element flange are on average higher than those in the webs. This result is in agreement with similar experimental data for steel members produced in Europe [16].



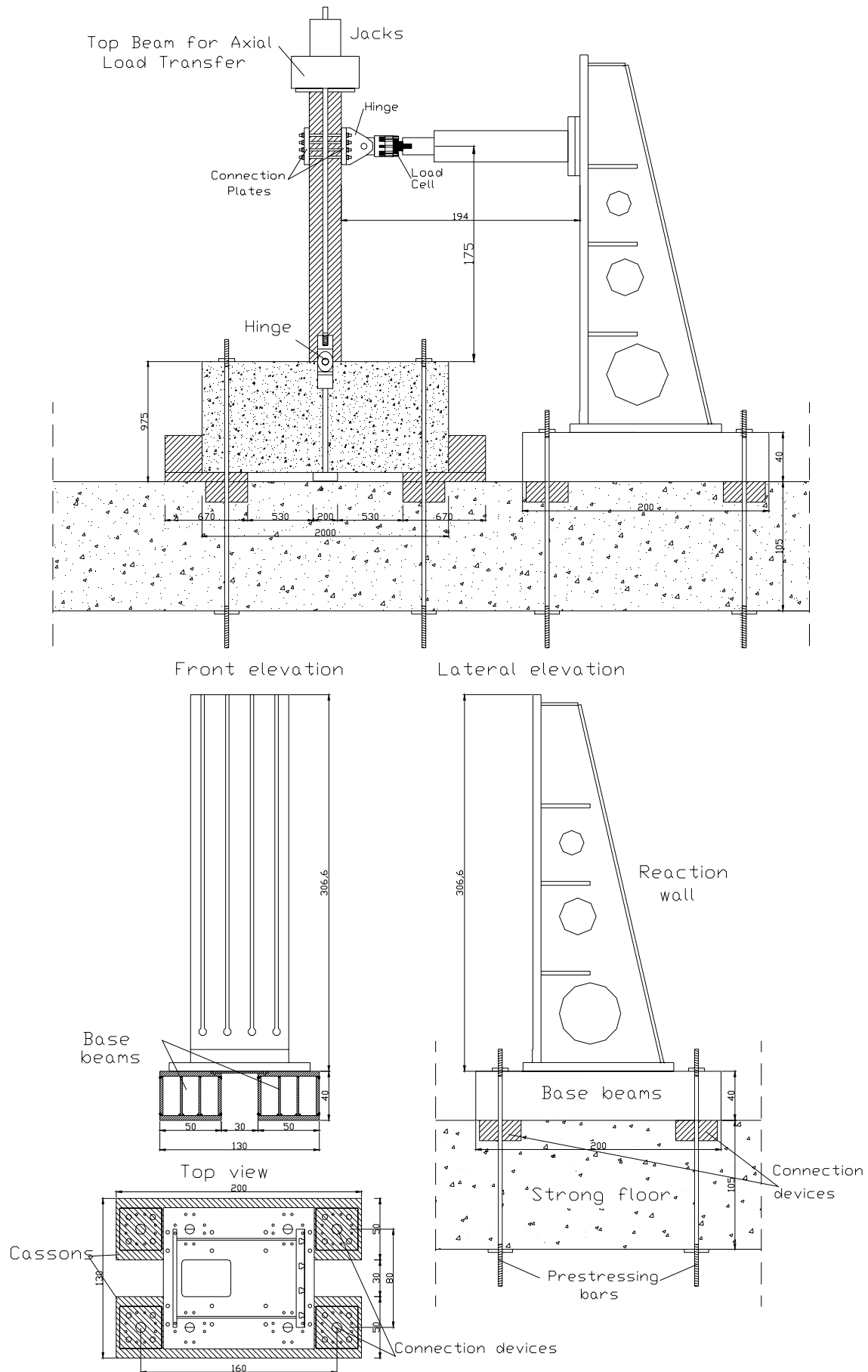


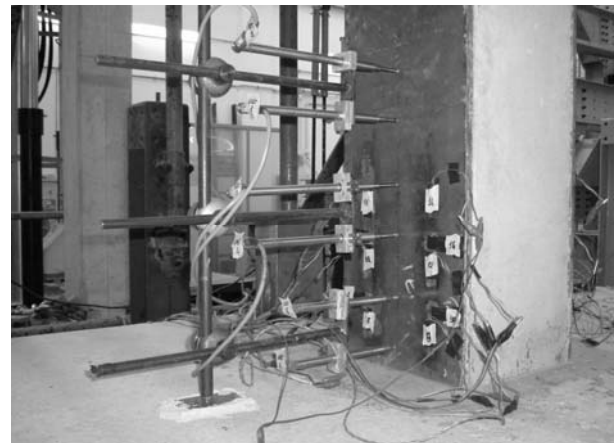
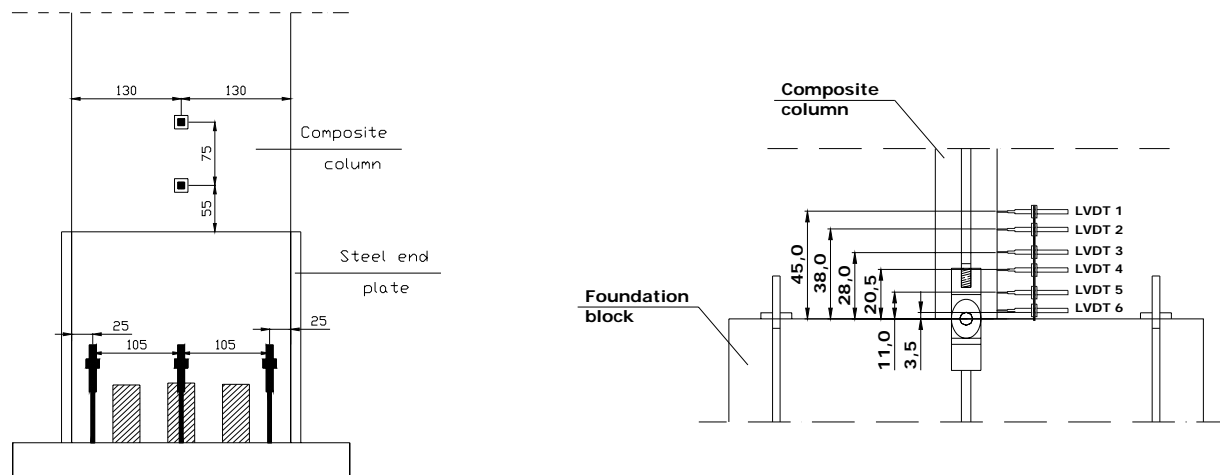
**Figure 2.** Layout of the test set-up (*top*) and reaction wall (*bottom*).

**Table 1.** Sample column specimens

Specimen	Axial load (kN)	Loading Type	Connection
HEB260	330	Monotonic	Traditional
HEB260	170	Monotonic	Traditional
HEB260	330	Monotonic	Socket

**Table 2.** Mechanical properties of the sample column specimens

Property	Beams				Columns			
	IPE240		IPE300		HEB260		HEB280	
	Web	Flange	Web	Flange	Web	Flange	Web	Flange
$f_y$ (MPa)	347	315	370	314	406	341	341	300
$f_u$ (MPa)	454	448	489	480	480	449	450	430
$f_u/f_y$	1.31	1.42	1.32	1.53	1.18	1.32	1.32	1.43
$\epsilon_u$ (%)	32.6	31.0	35.6	30.7	31.8	35.7	34.5	37.1

**Figure 3.** Close-up of the electrical displacement transducers (LVDTs): traditional (*left*) and innovative (*right*) joint.

The details of the foundation system is displayed in Figure 1. The design of such foundation block was based on the ultimate limit state corresponding to the stress values and distribution at the column failure. The layout of the composite column specimen employing HEB 260 steel section and traditional base joint is displayed in Figure 4, while the specimen HEB260 with socket type connection is provided in Figure 5. The thicknesses of the base of the socket is equal to 300 mm, while the walls of the socket are 250 mm thick. The total height of the foundation is 1050 mm.

The values of the internal actions, i.e. axial load ( $N_{Sd,j}$ ), flexural moment ( $M_{Sd,j}$ ) and shear ( $V_{Sd,j}$ ) used for the design are  $N_{Sd,j}=308\text{kN}$ ,  $M_{Sd,j}=906\text{ kNm}$  and  $V_{Sd,j}=444\text{ kN}$ . These values were derived conservatively from the ultimate flexural capacity of the HEB 280. In fact, for such section, the ultimate bending moment, computed according to Eurocode 4 [17], is  $M_{Rd,col}=755\text{kNm}$ ; note that the design value  $M_{Sd,j}$  accounts for the overstrength ( $f_u/f_y=1.20$ ) at the base column connection.

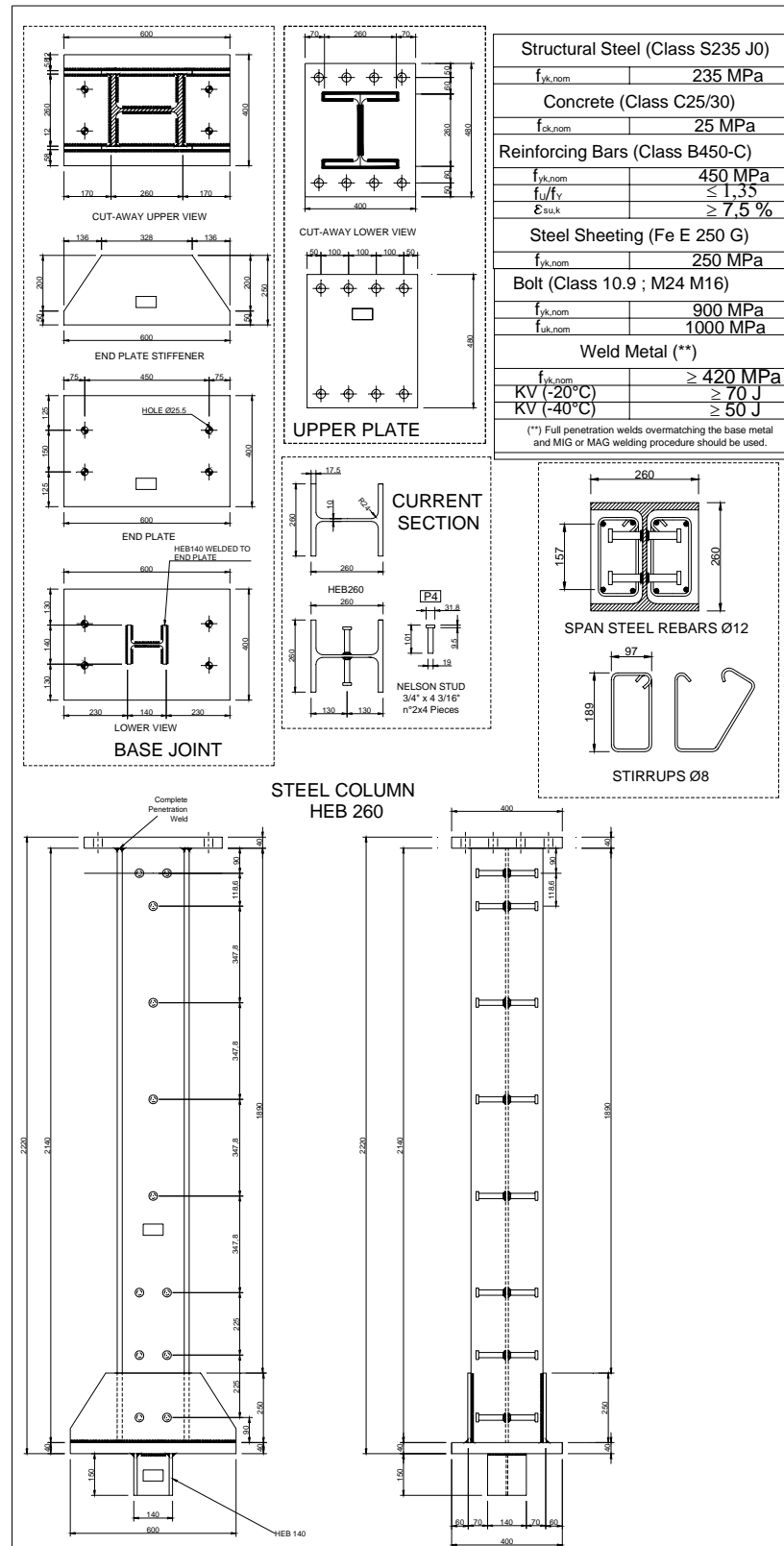


**Figure 4.** Traditional base column joint.

The value of the overstrength was derived by the provisions in Eurocode 3 [18]. The steel reinforcement used for the RC block of the traditional and socket type connections are displayed in Figures 6 and 7, respectively. It is worth mentioning that a solid foundation block is used to prevent an inelastic mechanism of the concrete component.

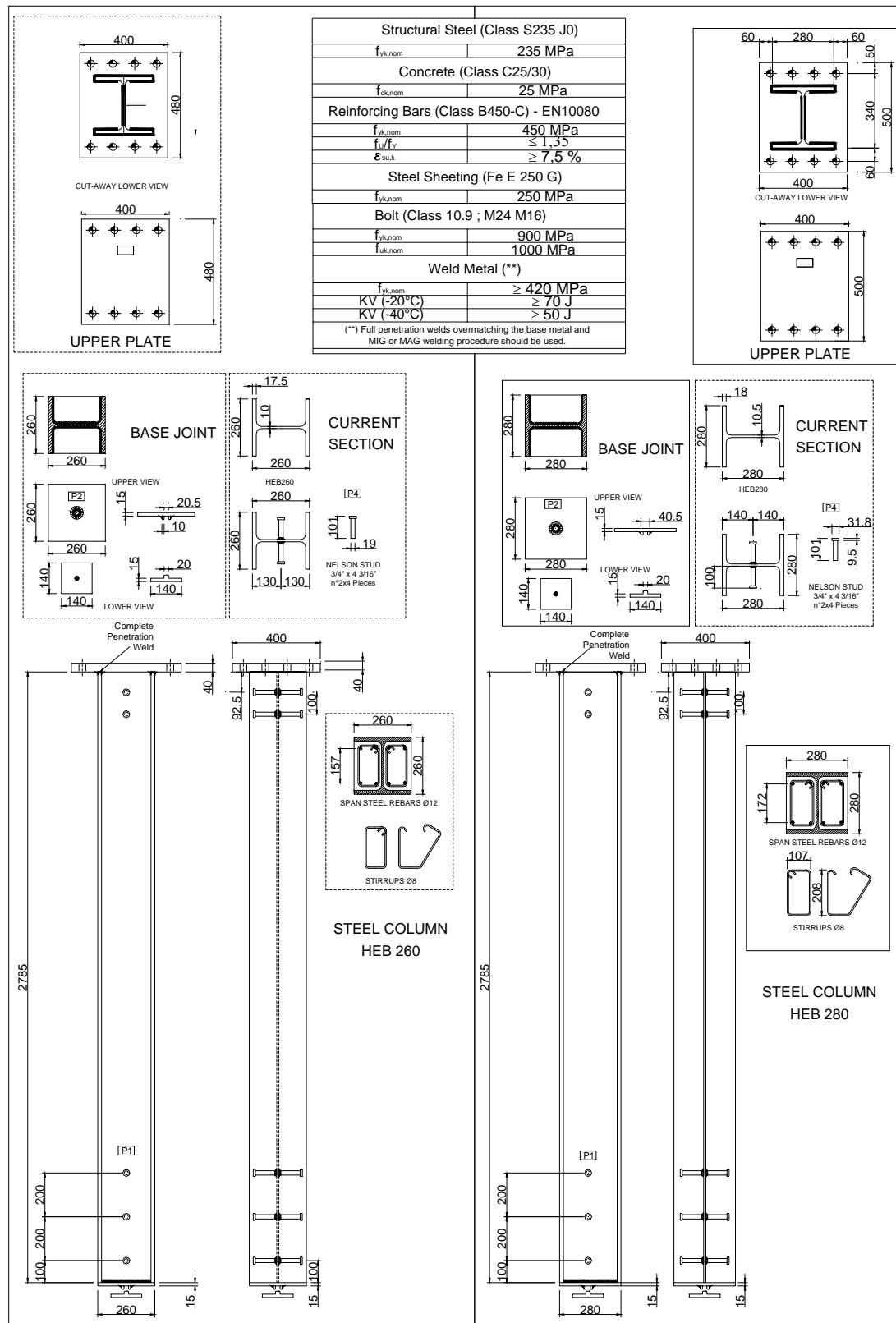
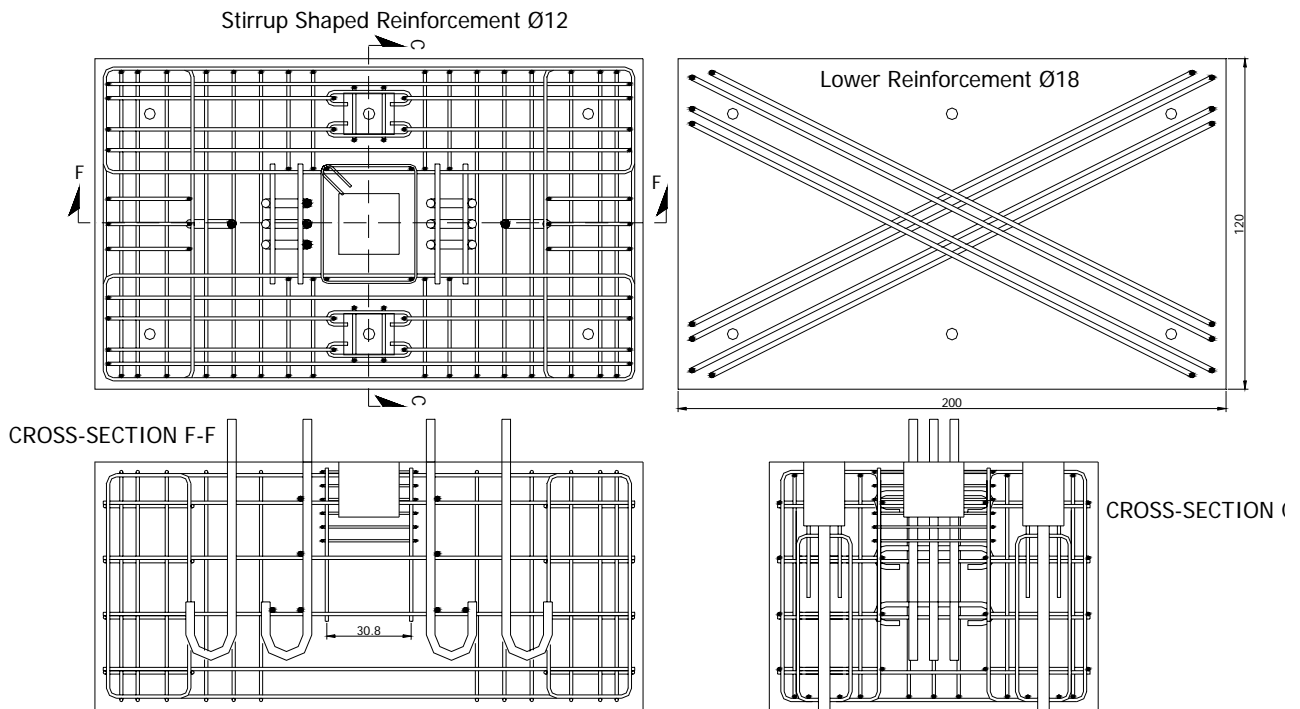
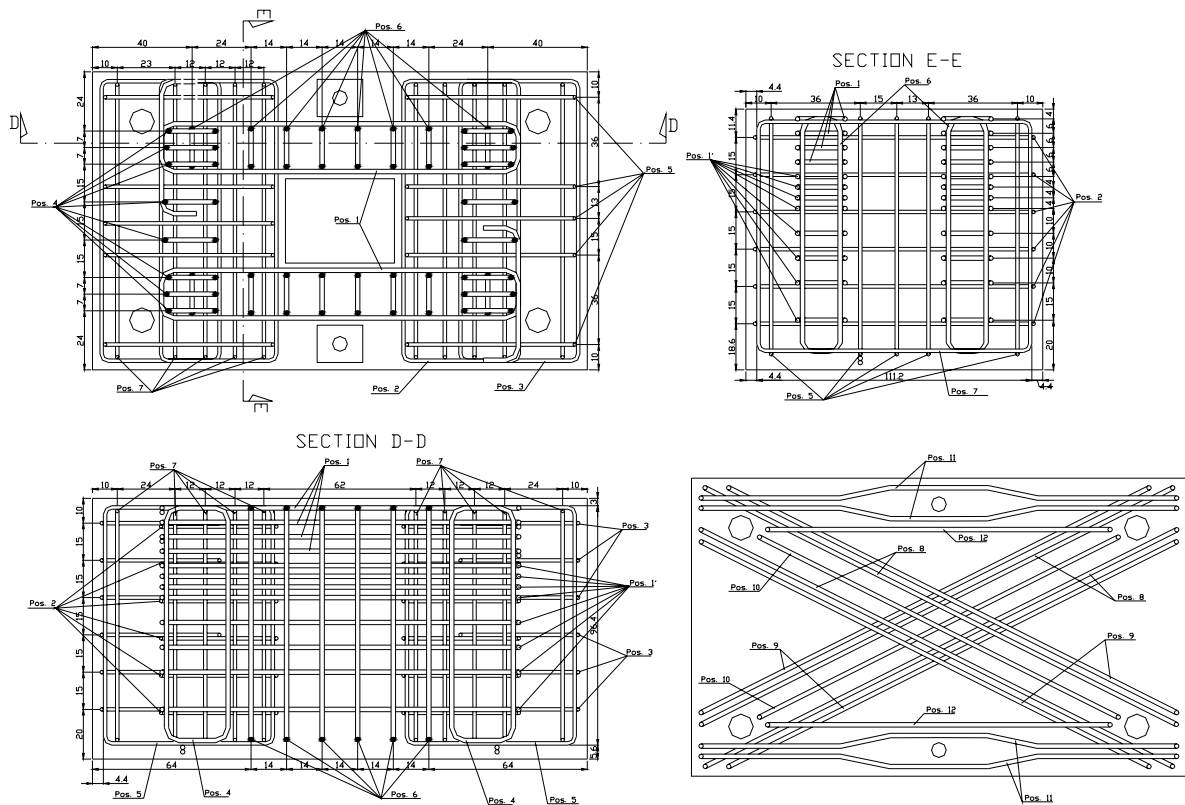


Figure 5. Socket-type base column joint.



**Figure 6.** Steel reinforcement used for the traditional base column joint.



**Figure 7.** Steel reinforcement used for the socket-type base column joint.

The results of the experimental tests carried out on composite columns employing innovative (socket-type) joints are discussed hereafter.

## TEST RESULTS

The test results of the partially encased composite columns were computed in terms of both local (moment-curvature  $M-\chi$  and moment-rotation  $M-\theta$ ) and global (lateral load-top displacement,  $F-\Delta$ ) response parameters. The capacity curves of the specimens HEB260 with axial load  $N=330\text{kN}$ , both traditional and innovative base connections, are provided in Figure 8. Such curves are expressed in terms of lateral force ( $F$ )-drift ( $d/H$ ), where  $H$  is the distance of the centreline of the hydraulic jack from the foundation and  $d$  the total horizontal displacement at the jack height. The forces corresponding to the onset of the plastic moment at the column base are also included in Figure 8. It is observed that the traditional connection layout exhibits higher lateral strength (600 kNm vs. 510 kNm) due to the steel stiffeners used at the base of the column and to overstrength for seismic design (*see* also Fabbrocino *et al.*, 2004). Conversely, the ultimate deformation capacity of the socket type connection is about 50% higher than the counterpart traditional (about 0,0583 rad vs. 0,0875 rad); in both cases the requirement of 35 mrad given by Eurocode 8 [5] is fulfilled. This requirement is more stringent than the 3% drift, which is assumed as the onset of the ultimate limit state in steel and composite frames in the US practice, FEMA 356 [19].

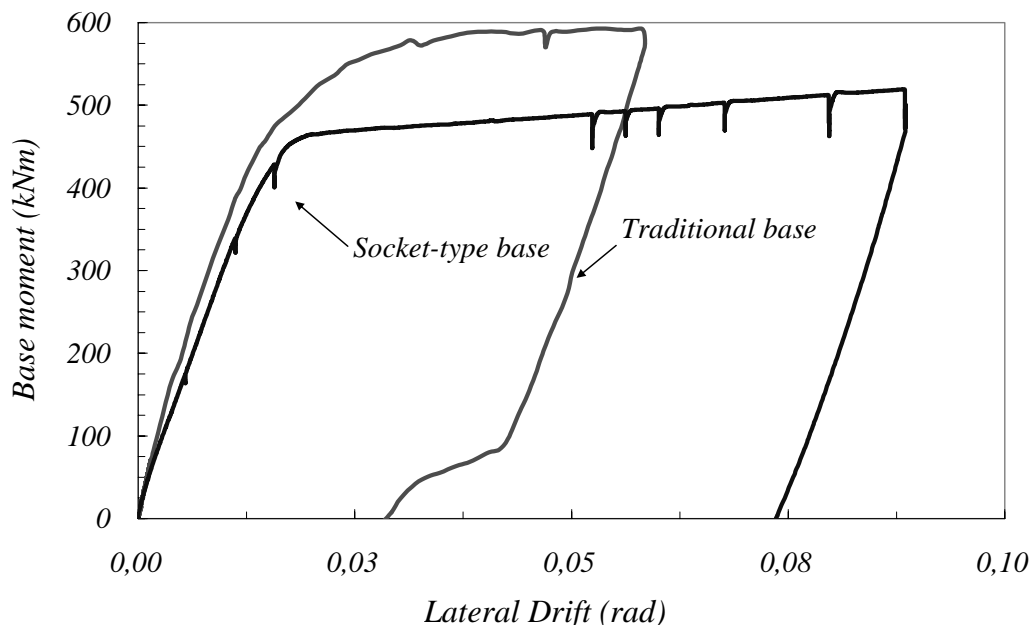


**Figure 8.** Capacity curves for the traditional and socket-type connections.

Furthermore the failure mode of the specimen with steel end plate is related to anchorage bolt fracture, while in the case of the socket type a very ductile mechanism is shown. At serviceability, the stiffness of the traditional connection is slightly higher than that of the socket connection. It can thus be argued that the experimental tests carried out both on traditional bolted steel end plate and innovative socket-type connections demonstrate that the former experience brittle failure modes. Rupture of anchorage bolts as per Figure 9 were observed under monotonic loads. The composite partially encased columns with traditional joint yield at about 310kN, which corresponds to a lateral drift of 26mm ( $d/h \sim 1.65\%$ ). The maximum force is equal, respectively, to 375kN for HEB260 with axial loads  $N=330\text{kN}$  and 340 kN for  $N=170\text{kN}$ . The lower value found in the second specimen (340kN) is related to the premature rupture of the base joint, probably caused by technological defects of the threaded bars [14]. In both specimens, i.e. with  $N=170\text{kN}$  and  $N=330\text{kN}$ , under monotonic regime, the column strength and energy dissipation do not exhibit significant loss for drift  $d/h \sim 5-6\%$ . The thick steel plate and the stiffeners used at the column base ensure that the end section of the column remains plane (rigid rotation). Under load reversal, the crushed concrete and the inelastic deformations in the steel components (anchorage), both at the

column base, endanger the global lateral stiffness of the composite column. Bond-related phenomena give rise to degrading effects, especially at large drifts, thus reducing significantly the energy dissipation capacity of the member. These results point out that traditional connections are not fully satisfactory, especially when relevance of reinforced concrete component increases, i.e. due to cross section dimensions. Conversely, innovative socket-type connections possess adequate ductility. Under monotonic load conditions, the test results show strain hardening of the base column equal to 1.32. This is due chiefly to the material over-strength of structural steel (see values of  $f_u/f_y$  of the member flange in Table 2). The contribution of the hardening of the longitudinal reinforcement bars is in fact very small (1.13 vs. 1.32). The tests carried out on the specimens employing the socket joint do not exhibit strength deterioration even at large lateral drifts, e.g.  $d/h > 0.04$ -0.05 radians. The formation of the plastic hinge occurs at the base column, as observed during the tests.



**Figure 9.** Close-up of the deformations of the specimen HEB260 with  $N=330\text{kN}$ .

Figure 9 shows the occurrence of inelastic deformations at the base column during the test on the HEB 260 with  $N=330\text{kN}$ ; the spreading of such inelasticity is also evident. At very large drifts, the flange plate of the column tends to bend outwards and the bond between the inner concrete and the exterior steel plate is broken as demonstrated by the close-up of the Figure 9, without any relevant effect on the global response. The tensile resistance of the concrete is exceeded and inclined (flexural) cracks initiate and propagate above the foundation block.

To shed light on the structural performance of the sample columns with either traditional or innovative socket-type member-to-foundation joint, the bending-axial load (M-N) interaction curves were computed for the specimens HEB 260 and HEB 280. These curves were estimated at two performance levels, namely yield and collapse, according to the provisions in Eurocode 4 [17]. The values of bending moments and axial loads at the ultimate stage of the monotonic tests are outlined in Tables 3 and 4 along with the values at yield and collapse. The computed values demonstrate that the failure mechanism is controlled in the case of traditional joint by the base column component. By contrast, for socket-type connections, the failure mode is controlled by the formation of the plastic hinges in the columns.

**Table 3.** Values of interaction curves for the test with HEB260 (N=170kN and N=330kN) and traditional joint at different performance state.

	Yield		Collapse		Test	
	M (kNm)	N (kN)	M (kNm)	N (kN)	M (kNm)	N (kN)
Section above stiffening plate	343	330	633	330	488	330
	339	170	628	170	433	170
Column base connection	440	330	550	330	596	330
	395	170	510	170	530	170

**Table 4.** Values of interaction curves for the test with HEB280 (N=330kN and N=520kN) and socket-type joint at different performance state (at column base connection).

Yield		Collapse		Test	
M (kNm)	N (kN)	M (kNm)	N (kN)	M (kNm)	N (kN)
390	330	740	330	608	330
420	520	750	520	762	520

The inelastic response of the critical region of the specimens with socket-type joints was monitored carefully through six electrical displacement transducers (LVDTs) located at the column base as displayed in Figure 3. These LVDTs record the lateral displacement of several points of the column flanges in order to define reliably the various inelastic phenomena, e.g. yielding, local buckling, fracture initiation, occurring at those locations during the tests. It is found that the section closer to the foundation block (LVDT #6) exhibits the typical response of reinforced concrete members. Conversely, the measurements derived from LVDT #5 and #6 show a typical structural steel nonlinear behaviour. Comparison between total cord rotation and the base column one derived from LVDT #6 measures enable to recognise that the higher is the drift, the higher is the contribution to the total drift given by the deformation of the socket type connection. Furthermore, due to the location of LVDT #1, 45.0cm far from the foundation, the socket type shows a yielding spreading that is nearly twice the width of the section (45.0cm vs. 52.0cm). As far as seismic design is concerned, the longer the spreading of inelasticity the higher the energy dissipation. By contrast, traditional connection systems, employing bolted steel end-plates [14] generate high concentrated inelastic demand on the anchorage bolts.

## CONCLUSIONS

Experimental tests carried out on composite steel and concrete columns were presented in this paper. Two layouts for the base column connections were assessed: the traditional system employing the bolted steel end plate and the innovative socket-type. The experimental results demonstrate that the socket system is beneficial for the spreading of inelasticity at the base of the composite columns. To assess the inelastic structural performance, the composite specimens were



subjected to monotonic loads at increasing lateral drifts (pushover experimental tests). It was found that the maximum drift of the socket type connection is nearly 50% higher than the traditional bolted steel end plate. Traditional base connections fail in a less ductile fashion because of the fracture of the anchorage bolts. Conversely, socket connections exhibit a ductile response due the formation of the plastic hinge at the base of the column, which extends over a length much higher than the cross section depth. As a result, socket-type joints can be reliably used for design of structures which may experience significant inelastic excursions. Further experimental tests and analytical simulations are being developed in order to assess the reliability and performance of the socket type connections under both monotonic, cyclic and earthquake loads.

## ACKNOWLEDGEMENTS

The present work was funded by the Italian Ministry of Research, through the grant PRIN02 (*Advanced design and control of global performance of composite steel and concrete frames for earthquake resistant building*); the financial support is gratefully acknowledged.

## REFERENCES

- [1] Ricles, J.M. and Paboojian, S.D., "Seismic performance of steel-encased composite columns", *Journal of Structural Engineering*, ASCE, 1994, 120(8), pp.2474-2494.
- [2] Broderick, B.M. and Elnashai, A.S., "Seismic response of composite frames-I. Response criteria and input motion", *Engineering Structures*, 1996, 18(9), pp.696-706.
- [3] Lee, T.K.L. and Pan, A.D.E., "Analysis of composite beam-columns under lateral cyclic loading", *Journal of Structural Engineering*, ASCE, 2001, 127(2), pp.186-193.
- [4] Elnashai, A.S. and Elghazouli, Y., "Performance of Composite Steel-Concrete Members Under Earthquake Loading, Part 2: Parametric Studies and Design Considerations", *Earthquake Engineering and Structural Dynamics*, 1993, 22(4), pp.347-368.
- [5] Eurocode 8, Design provisions for earthquake resistance of structures. Part 1.3: General rules. Specific rules for various materials and elements. European Committee for Standardization, Brussels, Belgium, 2004.
- [6] Fabbrocino, G., Manfredi, G., Cosenza, E. and Pecce, M.R., "Some remarks on deformation capacity of composite frames in seismic areas", *Proceeding of the 1<sup>st</sup> International Conference on Steel and Composite Structures*, ICSCS '01, Pusan, Korea, 2001.
- [7] Thermou, G.E., Elnashai, A.S., Plumier, A. and Doneux, C., "Seismic design and performance of composite frames", *Journal of Constructional Steel Research*, 2004, 60(1), pp.31-57.
- [8] Cosenza, E. and Pecce, M.R., "Le colonne composte acciaio-calcestruzzo: Analisi sperimentali, modelli di calcolo, indicazioni normative", *Costruzioni Metalliche*, 2001, 10(2), pp.49-60 (in *Italian*).
- [9] Shanmugam, N.E. and Lakshmi, B., "State of Art Report on Steel-Concrete Composite Columns", *Journal of Constructional Steel Research*, 2001, 57(10), pp.1041-1080.
- [10] Spacone, E. and El-Tawil, S., "Nonlinear analysis of steel-concrete composite structures: State of the art", *Journal of Structural Engineering*, ASCE, 2004, 130(2), pp.159-168.
- [11] Hajjar, J.F., "Composite Steel and Concrete Structural Systems for Seismic Engineering", *Journal of Constructional Steel Research*, 2002, 58(5-8), pp.702-723.
- [12] Mazzolani, F.M., "Steel and composite structures in European seismic areas: research, codification, design and applications", *Earthquake Spectra*, 2003, 19(2), pp.415-452.
- [13] Bursi, O.S., Caramelli, S., Fabbrocino, G., Molina, J., Salvatore, W. and Taucer, F., "3D Full-scale seismic testing of a steel-concrete composite building at ELSA", *Contr. No.*

- HPR-CT-1999-00059, European Community, 2004.
- [14] Fabbrocino, G., Pecce, M.R. and Di Sarno, L., “Inelastic Response of Steel and Concrete Columns”, Proceeding of The Fourth International Conference on Steel and Composite Structures, ICSCS '04, Seoul, Korea, 2004.
  - [15] Eurocode 2, Design of concrete structures. Part 1.1: General rules and rules for buildings. European Committee for Standardization, Brussels, Belgium, 2002.
  - [16] Byfield, M.P. and Nethercot, D.A., “Material and geometric properties of structural steel for use in design”, *The Structural Engineer, Journal of the Institution of Structural Engineers*, 1997, 75(21), pp.363-367.
  - [17] Eurocode 4. Design of composite steel and concrete structures. Part 1.1: General rules and rules for buildings. European Committee for Standardization, Brussels, Belgium, 2004.
  - [18] Eurocode 3. Design of steel structures. Part 1.1: General rules and rules for buildings. European Committee for Standardization, Brussels, Belgium, 2004.
  - [19] Federal Emergency Management Agency, “Prestandard and commentary for the seismic rehabilitation of buildings”, FEMA Report No.356., Washington D.C., USA, 2000.

# ADVANCED STEEL CONSTRUCTION

## *An International Journal*

Volume 2 Number 2

June 2006

CONTENTS

### Technical Papers

Recent Developments in Welded Hollow Section Joint Recommendations

*Jaap Wardenier and Yoo Sang Choo*

Reliability-Based Integrated Design Approach for Planar Steel Frames

*Yu-Shu Liu and Guo-Qiang Li*

Analytical and Experimental Investigations of Bolted Haunched Beam-to-column Joints with a View of Seismic Design

*A. Lachal, J.M. Aribert and G. Lohot*

The Cyclic Behaviours of Box-section Steel Beam-columns: Experiment & Numerical Comparison

*Ming-zhou Su, Lin Shen and Qiang Gu*

Structural Performance of Composite Base Column Connections

*L. Di Sarno, G. Fabbrocino and M.R. Pecce*

ISSN 1816-112X

Copyright © 2006 by :

The Hong Kong Institute of Steel Construction

Website: <http://www.hkisc.org/>

# ADVANCED STEEL CONSTRUCTION

*an International Journal*

ISSN 1816-112X

Volume 2 Number 2

June 2006



### Editors-in-Chief

**S.L. Chan**, *The Hong Kong Polytechnic University, Hong Kong*

**W.F. Chen**, *University of Hawaii at Manoa, USA*

**R. Zandonini**, *Trento University, Italy*

ADVANCED STEEL CONSTRUCTION

VOL.2, NO.2 (2006)

## EDITORS-IN-CHIEF

### Asian Pacific, African and organizing Editor

S.L. Chan  
*The Hong Kong Poly. Univ.,  
Hong Kong*

### American Editor

W.F. Chen  
*Univ. of Hawaii at Manoa, USA*

### European Editor

R. Zandonini  
*Trento Univ., Italy*

## INTERNATIONAL EDITORIAL BOARD

F.G. Albermani  
*The Univ. of Queensland, Australia*

F.S.K. Bijlaard  
*Delft Univ. of Technology, The Netherlands*

R. Bjorhovde  
*The Bjorhovde Group, USA*

M.A. Bradford  
*The Univ. of New South Wales, Australia*

D. Camotim  
*Technical Univ. of Lisbon, Portugal*

C.M. Chan  
*Hong Kong Univ. of Science & Technology,  
Hong Kong*

S.P. Chiew  
*Nanyang Technological Univ., Singapore*

K.F. Chung  
*The Hong Kong Polyt. Univ.  
Kowloon, Hong Kong*

G.G. Deierlein  
*Standford Univ., California, USA*

L. Dezi  
*Univ. of Ancona, Italy*

D. Dubina  
*The "Politehnica" Univ. of Timisoara, Romania*

R. Greiner  
*Technical Univ. of Graz, Austria*

G.W.M. Ho  
*Ove Arup & Partners Hong Kong Ltd.,  
Hong Kong*

J.P. Jaspart  
*Univ. of Liege, Belgium*

S. Kitipornchai  
*City Univ. of Hong Kong, Hong Kong*

D. Lam  
*Univ. of Leeds, UK*

G.Q. Li  
*Tongji Univ., China*

J.Y.R. Liew  
*National Univ. of Singapore, Singapore*

X. Liu  
*Tsinghua Univ., China*

E.M. Lui  
*Syracuse Univ., USA*

Y.L. Mo  
*Univ. of Houston, USA*

J.P. Muzeau  
*CUST, Clermont Ferrand, France*

D.A. Nethercot  
*Imperial College of Science, Technology  
and Medicine, UK*

D.J. Oehlers  
*The Univ. of Adelaide, Australia*

K. Rasmussen  
*The Univ. of Sydney, Australia*

T.M. Roberts  
*Cardiff Univ., UK*

J.M. Rotter  
*The Univ. of Edinburgh, UK*

C. Scawthorn  
*Scawthorn Porter Associates, USA*

P. Schaumann  
*Univ. of Hannover, Germany*

G.P. Shu  
*Southeast Univ. China*

J.G. Teng  
*The Hong Kong Polyt. Univ., Hong Kong*

G.S. Tong  
*Zhejiang Univ., China*

K.C. Tsai  
*National Taiwan Univ., Taiwan*

C.M. Uang  
*Univ. of California, USA*

B. Uy  
*The Univ. of Wollongong, Australia*

M. Veljkovic  
*Univ. of Lulea, Sweden*

F. Wald  
*Czech Technical Univ. in Prague,  
Czech*

Y.C. Wang  
*The Univ. of Manchester, UK*

D. White  
*Georgia Institute of Technology,  
USA*

E. Yamaguchi  
*Kyushu Institute of Technology,  
Japan*

Y.B. Yang  
*National Taiwan Univ., Taiwan*

B. Young  
*The Univ. of Hong Kong, Hong Kong*

X.L. Zhao  
*Monash Univ., Australia*

## General Information

### *Advanced Steel Construction, an international journal*

#### **Aims and scope**

The International Journal of Advanced Steel Construction provides a platform for the publication and rapid dissemination of original and up-to-date research and technological developments in steel construction, design and analysis. Scope of research papers published in this journal includes but is not limited to theoretical and experimental research on elements, assemblages, systems, material, design philosophy and codification, standards, fabrication, projects of innovative nature and computer techniques. The journal is specifically tailored to channel the exchange of technological know-how between researchers and practitioners. Contributions from all aspects related to the recent developments of advanced steel construction are welcome.

#### **Instructions to authors**

**Submission of the manuscript.** Authors may submit three double-spaced hard copies of manuscripts together with an electronic copy on a diskette or cd-rom in an editable format (MS Word is preferred). Manuscripts should be submitted to the regional editors as follows for arrangement of review.

Asian Pacific , African and organizing editor :	Professor S.L. Chan
American editor :	Professor W.F. Chen
European editor :	Professor R. Zandonini

All manuscripts submitted to the journal are highly recommended to accompany with a list of four potential reviewers suggested by the author(s). This list should include the complete name, address, telephone and fax numbers, email address, and at least five keywords that identify the expertise of each reviewer. This scheme will improve the process of review.

#### **Style of manuscript**

**General.** Author(s) should provide full postal and email addresses and fax number for correspondence. The manuscript including abstract, keywords, references, figures and tables should be in English with pages numbered and typed with double line spacing on single side of A4 or letter-sized paper. The front page of the article should contain:

- a) a short title (reflecting the content of the paper);
- b) all the name(s) and postal and email addresses of author(s) specifying the author to whom correspondence and proofs should be sent;
- c) an abstract of 100-200 words; and
- d) 5 to 8 keywords.

The paper must contain an introduction and a conclusion. The length of paper should not exceed 25 journal pages (approximately 15,000 words equivalents).

**Tables and figures.** Tables and figures including photographs should be typed, numbered consecutively in Arabic numerals and with short titles. They should be referred in the text as Figure 1, Table 2, etc. Originally drawn figures and photographs should be provided in a form suitable for photographic reproduction and reduction in the journal.

**Mathematical expressions and units.** The Systeme Internationale (SI) should be followed whenever possible. The numbers identifying the displayed mathematical expression should be referred to in the text as Eq. (1), Eq. (2).

**References.** References to published literature should be referred in the text, in the order of citation with Arabic numerals, by the last name(s) of the author(s) (e.g. Zandonini, R.). References should be in English with occasional allowance of 1-2 exceptional references in local languages and reflect the current state-of-technology. Journal titles should be abbreviated in the style of the Word List of Scientific Periodicals. References should be cited in the following style.

Journal: Chen, W.F. and Kishi, N., "Semi-rigid steel beam-to-column connections, data base and modeling", Journal of Structural Engineering, ASCE, 1989, 115(1), pp.105-119.

Book: Chan, S.L. and Chui, P.P.T., "Non-linear static and cyclic analysis of semi-rigid steel frames", Elsevier Science, 2000, pp.336.

Proceedings: Zandonini, R. and Zanon, P., "Experimental analysis of steel beams with semi-rigid joints", Proceedings of International Conference on Advances in Steel Structures, Hong Kong, 1996, vol. 1, pp.356-364.

**Proofs.** Proof will be sent to the corresponding author to correct any typesetting errors. Alternations to the original manuscript at this stage will not be accepted. Proofs should be returned within 48 hours of receipt by Express Mail, Fax or Email.

**Copyright.** Submission of an article to "Advanced Steel Construction" implies that it presents the original and unpublished work, and not under consideration for publication nor published elsewhere. On acceptance of a manuscript submitted, the copyright thereof is transferred to the publisher by the Transfer of Copyright Agreement and upon the acceptance of publication for the papers, the corresponding author must sign the form for Transfer of Copyright.

**Permission.** Quoting from this journal is granted provided that the customary acknowledgement is given to the source.

**Page charge and Reprints.** There will be no page charges if the length of paper is within the limit of 25 journal pages. A total of 30 free offprints will be supplied free of charge to the corresponding author. Purchasing orders for additional offprints can be made on order forms which will be sent to the authors. These instructions can be obtained at the Hong Kong Institute of Steel Construction, Journal website: <http://www.hkisc.org>

The International Journal of Advanced Steel Construction is published quarterly by non-profit making learnt society, The Hong Kong Institute of Steel Construction, c/o Department of Civil & Structural Engineering, The Hong Kong Polytechnic University, Hung Hom, Kowloon, Hong Kong.

**Disclaimer.** No responsibility is assumed for any injury and / or damage to persons or property as a matter of products liability, negligence or otherwise, or from any use or operation of any methods, products, instructions or ideas contained in the material herein.

**Subscription inquiries and change of address.** Address all subscription inquiries and correspondence to Member Records, IJASC. Notify an address change as soon as possible. All communications should include both old and new addresses with zip codes and be accompanied by a mailing label from a recent issue. Allow six weeks for all changes to become effective.

#### **The Hong Kong Institute of Steel Construction**

HKISC

c/o Department of Civil and Structural Engineering,

The Hong Kong Polytechnic University,

Hunghom, Kowloon, Hong Kong, China.

Tel: 852- 2766 6047 Fax: 852- 2334 6389

Email: [ceslchan@polyu.edu.hk](mailto:ceslchan@polyu.edu.hk) Website: <http://www.hkisc.org/>

ISSN 1816-112X

Copyright © 2006 by:

The Hong Kong Institute of Steel Construction.



ISSN 1816-112X

## EDITORS-IN-CHIEF

### Asian Pacific, African and organizing Editor

S.L. Chan

*The Hong Kong Polyt. Univ.,  
Hong Kong*

### American Editor

W.F. Chen

*Univ. of Hawaii at Manoa, USA*

### European Editor

R. Zandonini

*Trento Univ., Italy*

# Advanced Steel Construction

*an international journal*

VOLUME 2 NUMBER 2

JUNE 2006

## Technical Papers

Recent Developments in Welded Hollow Section Joint 109  
Recommendations

*Jaap Wardenier and Yoo Sang Choo*

Reliability-Based Integrated Design Approach for Planar Steel 128  
Frames

*Yu-Shu Liu and Guo-Qiang Li*

Analytical and Experimental Investigations of Bolted Haunched 137  
Beam-to-column Joints with a View of Seismic Design

*A. Lachal, J.M. Aribert and G. Loho*

The Cyclic Behaviours of Box-section Steel Beam-columns: 161  
Experiment & Numerical Comparison

*Ming-zhou Su, Lin Shen and Qiang Gu*

Structural Performance of Composite Base Column Connections 172

*L. Di Sarno, G. Fabbrocino and M.R. Pecce*

# RECENT DEVELOPMENTS IN WELDED HOLLOW SECTION JOINT RECOMMENDATIONS

Jaap Wardenier<sup>1,\*</sup> and Yoo Sang Choo<sup>2</sup>

<sup>1</sup> Emeritus Professor, Faculty of Civil Engineering and Geosciences,  
Delft University of Technology, P.O. Box 5048, 2600 GA Delft, The Netherlands

\*(Corresponding author: E-mail: j.wardenier@citg.tudelft.nl)

<sup>2</sup> Director, Centre for Offshore Research & Engineering, Faculty of Engineering,  
National University of Singapore, Kent Ridge, 117576 Singapore  
cvecys@nus.edu.sg

**ABSTRACT:** This paper considers recent research results on hollow section joints and the effect on the current design rules and is an extended version of the ICASS keynote lecture [1]. Main attention is paid to Rectangular Hollow Section (RHS) overlap joints, Circular Hollow Section (CHS) joints with thick-walled chords and the influence of the chord stress on the joint strength. Further, the effect of reinforcement plates on the strength of thin-walled joints is discussed. Also, some special aspects on elliptical hollow sections, stainless steel, high strength steel and delivery requirements for cold-formed hollow sections are considered. Finally, some developments regarding the fatigue design of hollow section joints are presented.

**Keywords:** Circular hollow section (CHS); Rectangular hollow section (RHS); Gap joints; Overlap joints; Static strength; Fatigue strength; High strength steel.

## NOMENCLATURE

CHS	Circular Hollow Section
RHS	Rectangular Hollow Section
$A_i$	cross section area of the overlapping brace member $i$
$A_s$	effective shear area of the joint
$F_{u,c}$	ultimate load capacity of the collar reinforced joint
$F_{u,u}$	ultimate load capacity of the of the unreinforced joint
$M_0$	in plane bending moment in the chord (general)
$M_{i,0}$	in plane bending moment in the chord in the plane $i=1$ or $2$
$M_{i,u,c}$	ultimate in plane bending moment capacity of the collar reinforced joint
$M_{i,u,u}$	ultimate in plane bending moment capacity of the unreinforced joint
$M_{o,u,c}$	ultimate out of plane bending moment capacity of the collar reinforced joint
$M_{o,u,u}$	ultimate out of plane bending moment capacity of the unreinforced joint
$M_{pl,0}$	plastic moment capacity of the chord
$N_i$	axial force in the overlapping brace member $i$
$N_j$	axial force in the overlapped brace member $j$
$N_{0p}$	maximum prestressing force in the chord
$N_0$	maximum chord axial force
$N_{1,0}$	axial ultimate load capacity of the joint based on the load in member 1 for chord load nearly zero
$N_{i,u}$	axial ultimate load capacity of the joint based on the load in member $i$
$N_{pl,0}$	plastic design capacity of the chord
$N_{i, effec\ width}$	ultimate load capacity of the overlapping brace based on the effective width criterion
Ov	Overlap in %
$R_{N0-M0}$	interaction factor of bending moment and axial loading
$V_u$	ultimate shear capacity ratio
$b_i$	external width of the overlapping brace $i$
$b_j$	external width of the overlapped brace $j$
$b_0$	external width of a chord
$b_{ei}$	effective width of the overlapping brace $i$ with the chord connection
$b_{ej}$	effective width of the overlapped brace $j$ with the chord connection



$b_{e(ov)}$	effective width of the overlapping brace i with the overlapped brace j connection
$c$	constant for external corner radius
$d_i$	external diameter of brace i ( $i=1$ or $2$ in a K joint)
$d_0$	external diameter of a chord
$f_{yi}$	design yield strength of the overlapping brace i
$f_{yj}$	design yield strength of the overlapped brace j
$f_{y0}$	design yield strength of a chord
$f_{ui}$	ultimate stress of the overlapping brace i
$f_{uj}$	ultimate stress of the overlapped brace j
$h_i$	external depth of the overlapping brace i
$h_j$	external depth of the overlapped brace j
$l_c$	length of the collar plate reinforcement
$n$	maximum chord stress divided by the chord yield stress
$t_c$	wall thickness of the collar plate reinforcement
$t_i$	wall thickness of the overlapping brace i
$t_j$	wall thickness of the overlapped brace j
$t_0$	wall thickness of a chord
$\beta$	diameter or width ratio between braces and chord: $\beta = d_i/d_0$ or $\beta = b_i/b_0$
$\gamma$	half diameter or half width to thickness ratio of the chord, $d_0/2t_0$ or $b_0/2t_0$
$\theta_i$	acute angle between the overlapping brace member i and the chord
$\theta_j$	acute angle between the overlapped brace member j and the chord
$\tau_c$	relative reinforcement plate-to-chord wall thickness ratio, $t_c/t_0$
$\phi$	angle in between the two planes in a multiplanar joints ( $\phi = 90^\circ$ )

## INTRODUCTION

The design rules in the second edition of the “Design Recommendations for Hollow Section Joints - Predominantly Statically Loaded” by the Sub-commission XV-E of the International Institute of Welding, (IIW-XV-E, 1989) [2] are the basis for many national and international design recommendations or standards, e.g. the Eurocode 3, (CEN, 2003) [3]. Based on these IIW-XV-E recommendations the Comité International pour le Développement et l’Etude de la Construction Tubulaire (CIDECT) has published several design guides for designers and fabricators, see for example [4].

Since the publication of the 2<sup>nd</sup> edition of the IIW-XV-E recommendations, considerable research has been carried out in various areas, during the last years, including joints of very thin-walled and very thick-walled hollow sections. Further, research has been carried out to fill gaps in knowledge, e.g. multiplanar joints or for strength upgrading of joints in existing structures. Currently, the IIW-XV-E recommendations are revised and extended for the third edition [5]. Some of the research on which these revised recommendations and extensions are based, will be dealt with in this paper, as well as some other work in which the authors are involved.

For the fatigue design of hollow section joints the IIW-XV-E sub-committee has published in 1999 the “Recommended fatigue design procedure for welded hollow section joints”, (IIW-XV-E, 1999) [6]. These recommendations are now the basis for drafting of an ISO standard. In these recommendations the fatigue design is based on the “hot spot stress” approach or also called the “geometrical stress” approach. Nowadays, such an approach becomes also usual for plated structures like ships and FPSO’s. During the last few years, many investigations have been, or are still being carried out to compare and synchronize the various methods for the determination of the hot spot stress in relation to the fatigue classification and the thickness effect.



This paper gives a brief review of some of the research recently carried out on hollow section joints, in particular those topics in which the authors are involved. Further, some other research is briefly discussed and references are given for more detailed information.

## STATIC DESIGN OF RECTANGULAR HOLLOW SECTION JOINTS

### *Uniplanar and multiplanar K-gap joints*

In the current CIDECT Design Guide for Rectangular Hollow Section Joints [7], it is recommended to assess multiplanar KK-gap joints with the uniplanar K-gap joint design formulae by applying a reduction factor of 0.9. In addition a chord shear check should be performed for the gap location of gap joints.

Since the experimental evidence was limited, CIDECT initiated programme 5BJ in which all influencing parameters have been investigated [8]. In this research, it was found that in case of chord face failures, multiplanar KK-joints behaved nearly similar to uniplanar K-joints if the chords of the uniplanar joints were additionally loaded by a chord (pre)stressing force equal to  $N_{op} = -2N_i \cdot \cos\theta_i$  which represents the difference in the chord reaction force (see Figure 1).

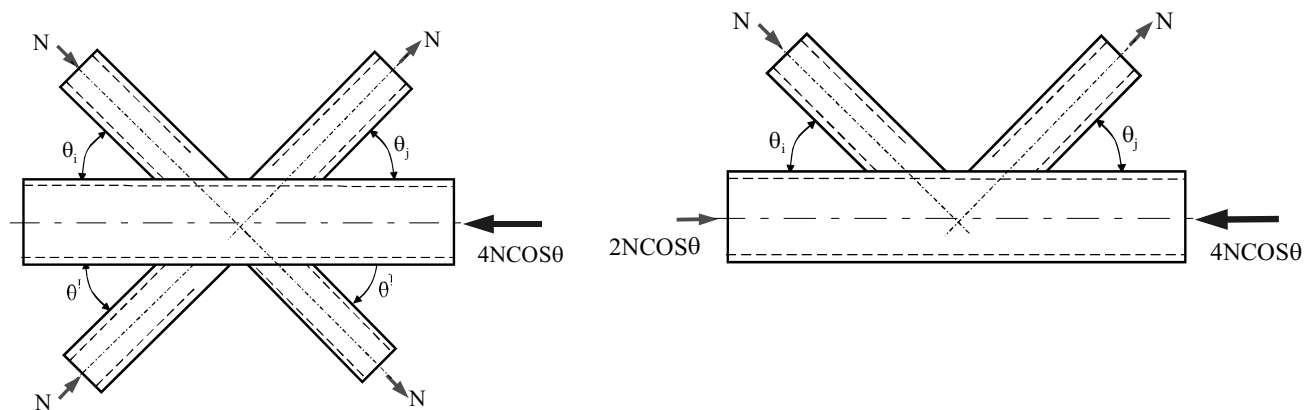


**Figure 1.** Uniplanar and multiplanar joints with equivalent behaviour

Consequently, it can be concluded that if for multiplanar KK-joints the larger chord load is taken into account in the chord stress function for chord face failure, the same formula can be used as for uniplanar K-joints and no further reduction factors have to be applied. However, due to the possible larger shear in the gap for particular loadings, the chord has always to be checked for the interaction of shear and axial load. The interaction is based on the well known Von Mises Huber-Hencky criterion. For example for a symmetrically loaded RHS multiplanar KK-joint with an included angle  $\phi=90^\circ$  and no eccentricity, all sides of the RHS chord are loaded by axial load and shear and for each plane the following interaction Eq. (1) is valid:

$$\left( \frac{\sum N_i \cdot \cos\theta_i}{0.5A_0 \cdot f_y} \right)^2 + \left( \frac{\sum N_i \cdot \sin\theta_i}{0.5A_0 \cdot f_y / \sqrt{3}} \right)^2 \leq 1.0 \quad (1)$$

For the multiplanar joint the chord axial load  $N_0$  is the sum of the horizontal components of the brace forces in both planes or two times the value in one plane. The resulting shear force  $V_0$  in the multiplanar joint is the vectorial resultant of the vertical components of the brace forces in both planes being  $\sqrt{2}$  times the shear force in one plane. Thus the Eq. (1) can also be written as Eq. (1a):

$$\left( \frac{0.5N_0}{0.5A_0 \cdot f_y} \right)^2 + \left( \frac{V_0 \cdot \cos\phi_j/2}{0.5A_0 \cdot f_y/\sqrt{3}} \right)^2 \leq 1.0 \quad (1a)$$

or with  $N_{0,pl}^* = A_0 f_{y0}$  and  $V_{0,pl}^{**} = A_0 f_{y0} / \sqrt{3}$  and  $\phi=90^\circ$ :

$$\left( \frac{N_0}{N_{0,pl}^*} \right)^2 + \left( \frac{1.4V_0}{V_{0,pl}^{**}} \right)^2 \leq 1.0 \quad (1b)$$

In case of asymmetric loading or for  $\phi \neq 90^\circ$  it is easier to consider the interaction for each plane.

In the framework of a new CIDECT programme a numerical programme is being carried out to investigate the chord load functions for K-joints with gap. Based on the results, new chord load functions are being developed based on the maximum chord load [9]. The new proposed functions will have a format, which is similar for all types of circular and rectangular hollow section joints, as given below in Eq. (2):

$$f(n) = \left[ 1 - n^{c_1} \right]^{(c_2 + c_3\beta + c_4\gamma)} \quad (2)$$

Some of the results are shown in Figure 2 in comparison to the current chord stress function [7,10].

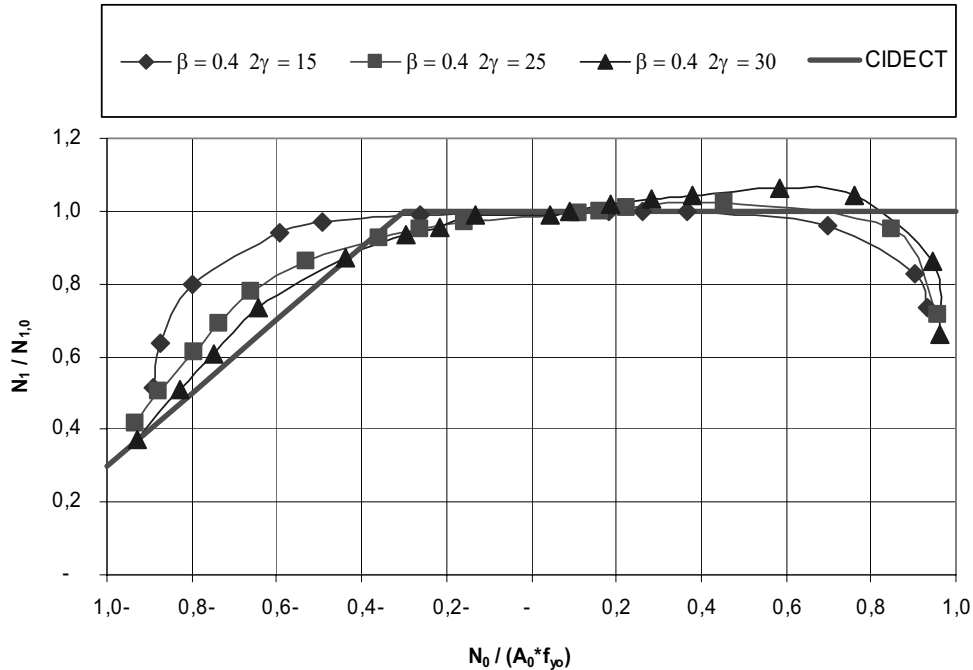


**Figure 2.** Chord stress reduction for RHS-K joints with gap ( $\beta = 0.4$ )

In this study, as in other studies, it was shown that for  $n \gg 0$ , with chords loaded in tension a reduction factor also has to be applied, although the reduction is much smaller than for compression loading.

### **Uniplanar and multiplanar K-overlap joints**

In the above-mentioned investigation it was also observed that, especially for multiplanar KK-overlap joints with medium to slender chord width to thickness ratios, chord face failure could occur which is not covered by the current codes and recommendations. Therefore, a detailed numerical study was carried out to study 50% and 100% uniplanar K- and multiplanar KK-overlap joints in more detail.

Based on this study it was found that three failure modes have to be checked [11,12], i.e.:

- overlapping brace failure (brace effective width criterion)
- brace shear failure at the connection with the chord
- local chord failure

The brace effective width criterion, e.g. shown in Figure 3 for a 100% overlap joint, was already given in the current recommendations but the other two criteria are added, although the chord member has always to be checked for member failure. This investigation showed that at the joint location a linear interaction between axial load and bending moment is better than the member interaction formula. Besides these failure modes, it was found that the shear in the cross section of the braces just above the connection with the chord face has to be limited to avoid chord face failure. The first author indicated already in 1976 that brace shear failure at the connection with the chord face should be considered as a possible failure mode. However, brace shear failure was not observed in the experiments, which may be due to the small shear deformations. As a result this failure mode is not included in the current IIW and CIDECT recommendations and only a the brace effective width criterion was proposed to cover the strength of RHS overlap joints.

As indicated in Figure 4, the brace walls parallel to the chord axis are fully effective for shear and the brace cross wall at the heel is theoretically not effective or only effective for a part  $b_e$ . The toe part of the overlapped brace of an overlap joints with an overlap  $O_v < 100\%$  is generally not fully welded to the chord (hidden location) and therefore not effective; it is only fully effective in case of 100% overlap joints. The results for 100% overlap joints showed that in those cases where the joint capacity is not limited by other criteria, the ultimate shear capacity can be reached, i.e.  $A_s \cdot \frac{f_u}{\sqrt{3}}$ .

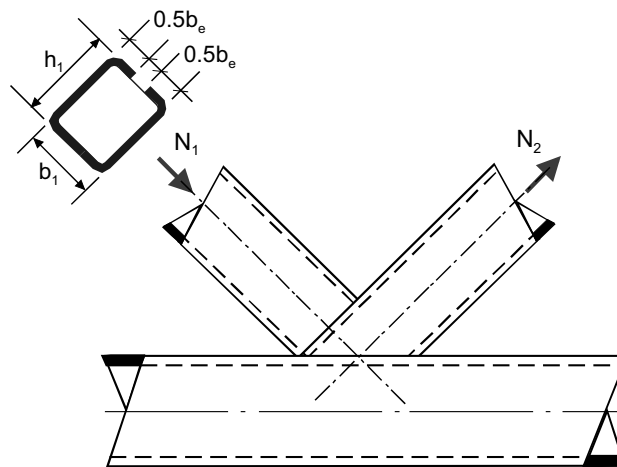


**Figure 3.** Brace effective width criterion for 100% overlap joints

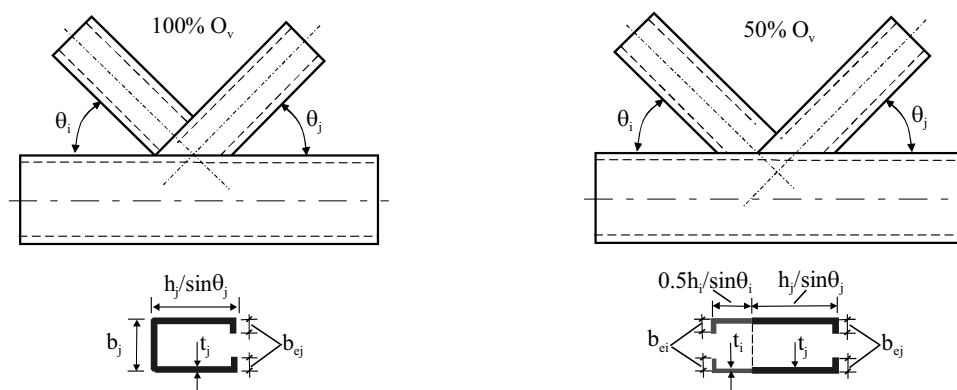


**Figure 4.** Joint configuration and definition of the shear area for 100% and 50% overlap joints

Adopting this ultimate brace shear capacity limit to avoid chord face failures still gives an additional reserve in joint capacity of 1.1 to 1.15.

Nowadays, higher strength steels are more frequently used, therefore, also the validity ranges for the width to thickness ratios have been reconsidered and are now related to the section class. In this case the section classes for the compression parts in hollow sections of Eurocode 3 are used.

Based on these studies the design recommendations are formulated as given in Table 1. The formulae are presented in a general format even allowing different steel grades for the overlapping and overlapped brace.

### ***Joints of thin-walled rectangular hollow sections***

Research on X, T and Y-joints of thin-walled hollow sections [13], indicated that the validity range of the width to thickness ratios in the design recommendations could, in particular cases, be more liberal. However, in actual structures always secondary effects like secondary moments exist and in case of thin-walled members these may cause premature failure because of lack of deformation and rotation capacity. Thus, using thin-walled sections outside the validity ranges of the current recommendations requires a more detailed elastic analysis. Further, it should be noted that in case of tests on joints of thin-walled sections all moments should be carefully measured because these may influence the axial load capacity due to the lower rotation/deformation capacity. Neglecting these moments may give test rig dependent test results.

### ***Joints of stainless steel rectangular hollow sections***

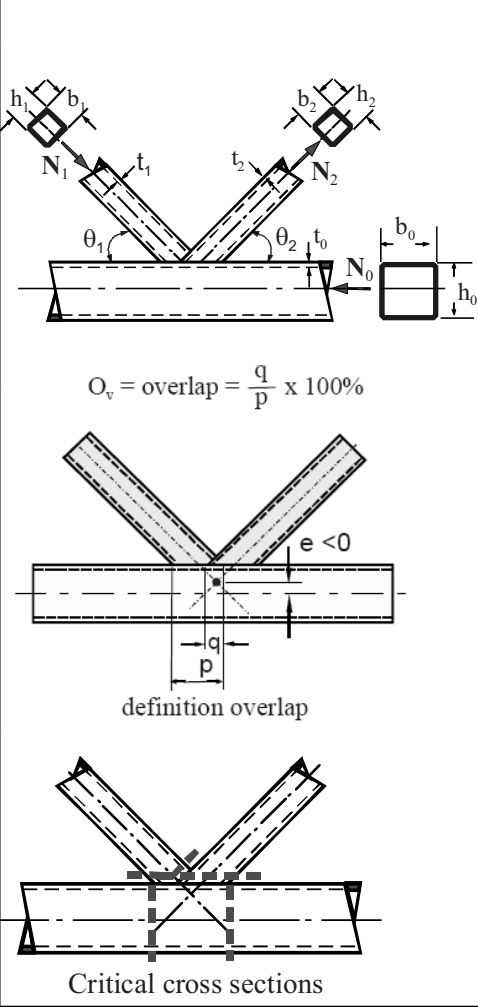
Rectangular hollow section joints of stainless steel, type 304 L, have been investigated at the University of Sydney [14]. In these investigations, X and K-gap joints made of cold formed austenitic stainless steel hollow sections have been used. The ultimate strengths were compared with the IIW-CIDECT design equations and the joint deformation at service-ability (ultimate strength divided by 1.5) was compared with the 1% chord width criterion. It was concluded that if the 0.2% proof stress based on the cold formed finished product is used, the joint strength can be evaluated using the IIW-CIDECT design rules for hollow section joints made of carbon steel.

The joints loaded in tension fractured mainly through the weld in the heat affected zones. Thus, using electrodes of a stronger metal could even enhance the strength, allowing the 0.5% proof stress to be used in the formulae. In the analysis it was already shown that using the 0.5% proof stress, the service-ability limit was satisfied. However, the strength did not meet that according to the current IIW-CIDECT design equations for high chord loads. It is noted that the newly developed chord stress functions for rectangular hollow section joints (see before) are more conservative for high chord loads.

### ***Other investigated areas***

Other connections recently investigated more in detail and/or those still being investigated are e.g. plate-to-RHS connections at the University of Toronto by Koteski & Packer [15], corner connections, by Karcher & Puthli [16], bird beak connections by Davies *et al.* [17] and bolted connections by Willibald *et al.* [18]. For detailed information, reference is given to the various proceedings of the International Symposia on Tubular Structures, for example, Jaurrieta *et al.* [19].

**Table 1.** Proposed design recommendations for RHS overlap joints

 <p><math>O_v = \text{overlap} = \frac{q}{p} \times 100\%</math></p> <p>definition overlap</p> <p>Critical cross sections</p>	<b><math>O_v = 25</math> to <math>100\%</math></b>
	<p><b>Overlapping brace effective width criterion<sup>*)</sup></b></p> <p><b>for <math>25\% \leq O_v &lt; 50\%</math> overlap:</b></p> $N_i^* = f_{yi} t_i \{ (O_v / 50)(2h_i - 4t_i) + b_{ei} + b_{e(ov)} \}$ <p><b>for <math>50\% \leq O_v &lt; 100\%</math> overlap:</b></p> $N_i^* = f_{yi} t_i [2h_i - 4t_i + b_{ei} + b_{e(ov)}]$ <p><b>for <math>O_v = 100\%</math> overlap:</b></p> $N_i^* = f_{yi} t_i [2h_i - 4t_i + b_i + b_{e(ov)}]$
	<p><b>Brace chord connection shear criterion<sup>**) (***))</sup></b></p> <p><b>for <math>50\% &lt; O_v &lt; 100\%</math> overlap:</b></p> $N_i \cos \theta_i + N_j \cos \theta_j \leq \frac{f_{ui}}{\sqrt{3}} \left[ \left( \frac{100 - O_v}{100} \right) \cdot 2h_i + b_{ei} \right] \cdot t_i + \frac{f_{uj}}{\sqrt{3}} \frac{(2h_j + b_{ej}) \cdot t_j}{\sin \theta_j}$ <p><b>for <math>O_v = 100\%</math> overlap:</b></p> $N_i \cos \theta_i + N_j \cos \theta_j \leq \frac{f_{uj}}{\sqrt{3}} \left[ \frac{(2h_j + b_j + b_{ej}) t_j}{\sin \theta_j} \right]$
	<p><b>Local chord yield criterion for uniplanar joints</b></p> $\frac{N_0}{N_{pl,0}} + \frac{M_0}{M_{pl,0}} \leq 1.0$ <p><b>Local chord yield criterion for multiplanar joints<sup>***))</sup></b></p> $\frac{N_0}{N_{pl,0}} + \frac{M_{1,0}}{M_{pl,0}} + \frac{M_{2,0}}{M_{pl,0}} \leq 1.0$
<p><b>Functions</b></p> $b_{ei} = \frac{10}{b_0/t_0} \cdot \frac{f_{y0} \cdot t_0}{f_{yi} \cdot t_i} \cdot b_i \leq b_i, \quad b_{ej} = \frac{10}{b_0/t_0} \cdot \frac{f_{y0} \cdot t_0}{f_{yj} \cdot t_j} \cdot b_j \leq b_j, \quad b_{e(ov)} = \frac{10}{b_j/t_j} \cdot \frac{f_{yj} \cdot t_j}{f_{yi} \cdot t_i} \cdot b_i \leq b_i$	
<p><b>Range of validity <math>O_v \geq 25\%</math></b></p> $\frac{b_i}{b_0}, \frac{h_i}{b_0}, \frac{b_j}{b_0}, \frac{h_j}{b_0} \geq 0.25, \quad \frac{t_i}{t_j} \leq 1.0 \quad \text{and} \quad \frac{b_i}{b_j} \geq 0.75$	<p>Compression brace : class 1 ****)</p> <p>Tension brace : class 1 or 2</p> <p>Chord : class 1 or 2</p>

\*) Efficiency capacity of the overlapped brace should not exceed that of the overlapping brace

\*\*) This shear failure criterion is generally not critical for overlap joints with  $O_v \leq 50\%$ . In this criterion with  $O_v < 100\%$ , it is assumed that the hidden location at the overlapped brace with the chord is not welded.

\*\*\*)) The moments  $M_{1,0}$  and  $M_{2,0}$  are the in-plane moments in the two planes, respectively and  $M_{pl,0}$  and  $M_{pl,0}$  refers to the belonging in-plane plastic moment capacity of the chord.

\*\*\*\*))

Limit (b-ct)/t	S 235	S 275	S 355	S 460
<b>Class 1</b>	33	30	27	23
<b>Class 2</b>	38	35	31	27

Note: c=3 for hot formed hollow sections and c=5 for cold formed hollow sections (rounded off figures).

## STATIC DESIGN OF CIRCULAR HOLLOW SECTION JOINTS

### *Uniplanar and multiplanar joints*

The recommendations for circular hollow section joints in the offshore codes, e.g. the API [20] and the draft ISO, ISO TC67/SC7/WG3/P3 [21], differ from the IIW-XV-E and CIDECT recommendations. This is one of the reasons that the IIW-XV-E Sub-committee has decided to reanalyse the behaviour of circular hollow section joints as a basis to derive international consensus for the current revision of the IIW-XV-E recommendations. In the evaluation also other proposals, for example, Dexter & Lee [22], Dier & Lalani [23], Yamada et al. [24] and Choo & Qian [25] are considered. Another aspect to be reviewed is the different behaviour of gap and overlap K-joints which in the current IIW recommendations are covered by only a single strength formula. It is the opinion of the authors of this paper that these joints should be dealt with separately. Overlap joints may be approached in a similar way as done for rectangular hollow sections.

Further, the influence of the chord stress on the joint strength of circular hollow sections is currently based on the so-called chord pre-load, i.e. the chord load minus the load, which reacts the brace load components. This is in contradiction with rectangular hollow section joints for which the chord load function is based on the maximum chord load. Therefore, in the framework of the CIDECT programme 5BK the existing formulae have been analysed and a numerical programme was carried out [26,27]. Based on this, new chord load functions were developed based on the maximum chord load. The new proposed functions have the general format of Eq. (2).

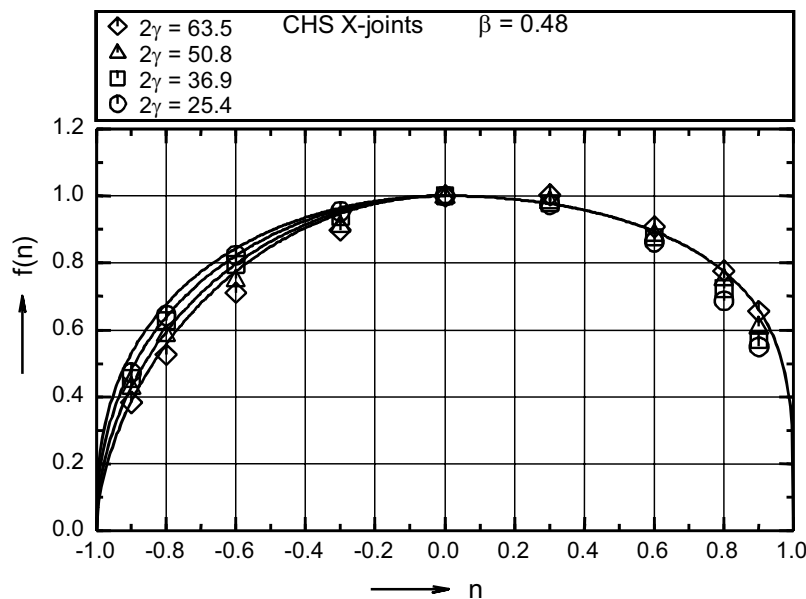


**Figure 5.** Chord stress reduction for CHS-X joints ( $\beta = 0.48$ )

Also here, for chords loaded in tension ( $n > 0$ ), a reduction factor has to be applied. Figure 5 shows a typical example for a X-joint with a diameter ratio  $\beta = 0.48$ . The results have also been compared with recent work carried out by Pecknold *et al.* [28-29].

In the revised recommendations for T joints the chord stress to be used also includes the bending stress which always occurs due to brace loading. In the previous IIW-XV E recommendations and all other recommendations due to the experimental evidence this was indirectly also included in the joint capacity equations. With the current numerical methods it is easier to separate the influence of brace and chord loading [30] and to incorporate this in an easy way in the recommendations.

Especially in the analyses of K gap joints the effect of the relatively large welds in small size experiments has to be excluded, that is why Yura [31] did not include in his analysis the test results of specimens with small chord members. In the past all recommendations have been based on experiments but the calculations with the current calibrated numerical models showed that the existing experimental data base has to be even more carefully screened. Furthermore, like for rectangular hollow section joints, a check may need to be carried out to ensure that the chord shear criterion in the gap is not critical. At present numerical calculations have been carried out for the whole parameter range and new strength equations have been developed. These new equations still need to be checked with the more refined experimental data base.

Currently various strength functions exist for overlap joints; some based on shear between the braces and punching shear, others relating the strength to that of gap joints. It is the authors opinion that the strength can be approached in a similar way as done for overlap joints of rectangular hollow sections with the effective parts related to the  $d/t$  ratios of the relevant members, however, such a reanalysis has still to be done.

In the current CIDECT design guide 1 [32] based on the work of the Kumamoto team, it is recommended to assess multiplanar joints in each plane with the uniplanar joint strength formulae but applying a reduction factor of 0.9. Additionally the chord has to be checked for shear in the gap. For rectangular hollow section joints it is shown above that the lower strength can be attributed to the larger chord force. By considering the maximum chord stress for the chord stress effect instead of the pre-stress due to additional chord loading, the reduction is in the same range but gives a consistent approach. This means that multiplanar K joints with gap of CHS (similar as RHS joints) can also be dealt with as uniplanar joints but taking account of the larger chord force and the additional shear check in the gap of the chord.

### ***Joints of thick-walled circular hollow sections***

In modern bridges and jack-up platform designs more and more use is made of very thick-walled hollow sections, sometimes in combination with cast steel nodes. As a consequence several investigations regarding the static behaviour of welded thick-walled joints have been carried out. The various investigations in this field are summarized by Choo & Qian [25] and Choo [33].

The strength of circular hollow section joints with chord diameter to thickness ratios  $2\gamma \geq 15$  can generally be based on the simplified ring model and the punching shear model. However, for larger diameter ratios  $\beta$  the strength deviation is more significant. This can readily be explained as follows: In the simplified ring model, as shown in Figure 6, the brace axial load is simplified to two line loads over an effective chord length  $B_e$  and the joint strength is based on the plastic capacity of the chord with length  $B_e$  (the ring) while neglecting the effect of the axial and shear forces on the plastic moment capacity.

This means that the joint strength is a function of  $t_0^2$ . However, for larger diameter ratios  $\beta$  the load transfer is mainly by membrane action at the saddle location which means that the joint strength is a function of  $t_0$ . For thick-walled chords this membrane load transfer becomes already more important for medium diameter ratios  $\beta$ . As a consequence the current design recommendations have to be modified to cover also joints with thick-walled chords and thus the different failure modes.

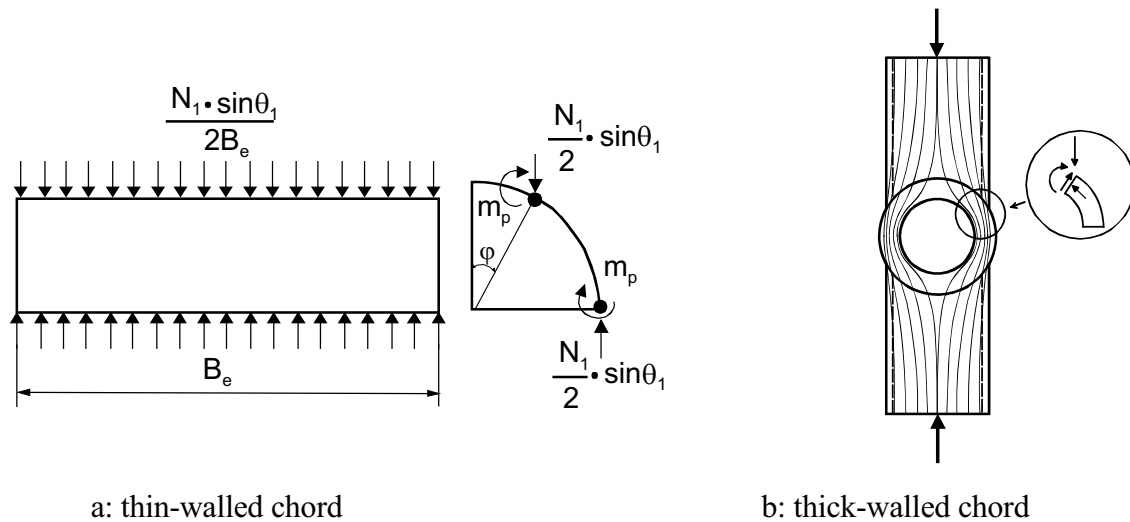


**Figure 6.** Ring model for thin- and thick-walled chords

In the investigations as summarised by Choo & Qian [25], the joint strength is defined based on a plastic limit load definition which agrees with Lu's 3% chord diameter limit for the joints with thinner chord sections. However, for joints with thick-walled chords the plastic limit load definition seems to give more consistent results. It was further observed that for X joints with a low inclined angle  $\theta$  in combination with a larger brace to chord diameter ratio  $\beta$ , chord shear, as shown in Figure 7 can reduce the load capacity, which is not covered in the current design recommendations.

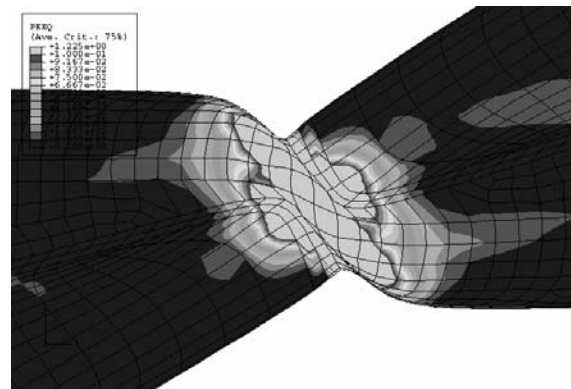


**Figure 7.** Interaction between chord plastification and chord shear in an X joint  
( $\theta = 30^\circ$ ,  $\beta = 1.0$  and  $2\gamma = 18$ )

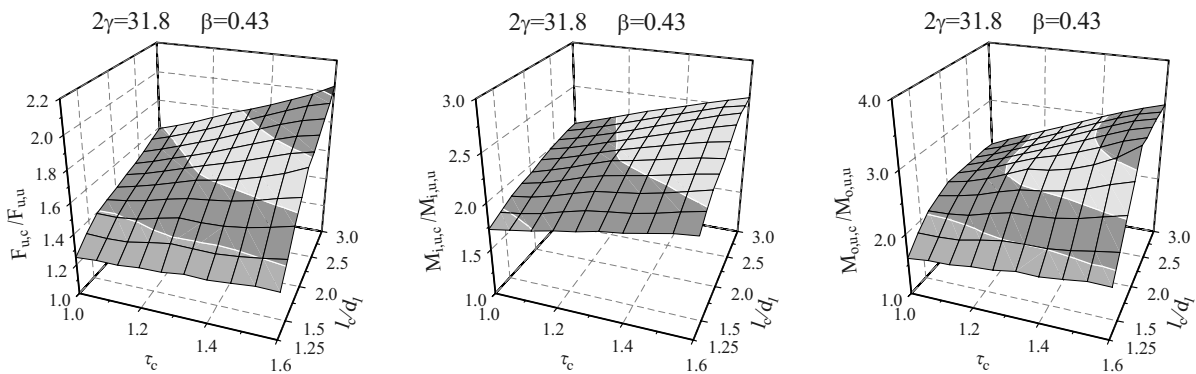
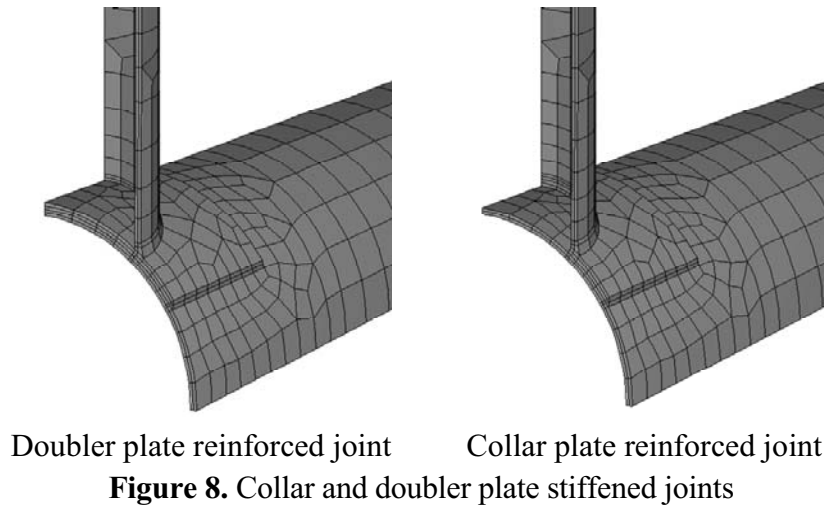
### ***Collar and doubler plate joints***

For the enhancement of the strength of joints with thin-walled chords, reinforcement by collar and doubler plates may be used, as highlighted by Choo *et al.* [34]. In case of collar plates, the brace is welded to the chord and the collar consisting of two or four parts is welded to the chord and the brace around the brace to chord connection, as shown in Figure 8. In case of doubler plates the doubler plate is welded to the chord and the brace is welded to the doubler plate.

These reinforced joints have been extensively investigated at the National University of Singapore under axial brace loading and under bending-in-plane moments, for example, as presented in [34-37]. In all the investigations it was shown that for collar and doubler plates with a thickness equal or larger than that of the chord, the strength could be enhanced by 30% upwards, depending on the



dimensions of the collar and doubler plates and geometrical parameters and the loading. As an example for joints with  $2\gamma=31.8$  and  $\beta=0.43$ , Figure 9 shows the ratio of the strength of the collar plate reinforced joint with respect to that of referenced un-reinforced joints, as a function of the relative plate-to-chord wall thickness ratio  $\tau_c (=t_c/t_0)$  and the relative plate length to brace diameter ratio  $l_c/d_1$ . The strengthening effect is further depending on the loading, i.e. compression, tension, bending in-plane or bending out-of-plane.



### ***Ring-stiffened joints***

Although in the past several experimental and numerical investigations have been carried out, more evidence is becoming available for the design of these joints with the recent and improved numerical methods [38,39].

## **STATIC DESIGN OF JOINTS WITH HOLLOW SECTION BRACES AND AN I-SECTION CHORD**

The design equations for overlap joints with an I-section chord will be modified in a similar way as for rectangular hollow section joints, see Table 1. This has not been investigated in tests but the behaviour is rather similar.

## MISCELLANEOUS

### *Static design of elliptical hollow section joints*

Nowadays elliptical hollow sections are used in various architectural projects because of their special appearance. However, limited evidence is available on the joint behaviour.

Currently, research is underway at the University of Liege [40] and the National University of Singapore [41]. These initial investigations, show that the ring model can be used for explaining the numerically determined strengths. Further, research is being carried out at Toronto University to define the class limitations for the sections.

### *Hollow section joints in high strength steel*

The revised IIW recommendations for hollow section joints will cover joints made of steels with design yield stresses up to 460 N/mm<sup>2</sup>. Previously the validity was limited to steels with design yield stresses up to 355 N/mm<sup>2</sup>. However, joints with higher yield stresses will have a lower ductility for redistribution (e.g. effective width and punching shear), a lower deformation capacity (e.g. thin-walled joints with a high  $\beta$  ratio) or in other cases a larger deformation under service load (thin walled joints with a low  $\beta$  ratio). Further, it was found by Kurobane [42], that the strength for circular hollow section K-joints is a function of the yield to ultimate stress ratio. The effect was found to be most pronounced for K-joints for which the following relation was given:

$$\left( \frac{f_y}{f_u} \right)^{-0.757} \quad (3)$$

Figure 10 shows the relative effect related to the yield stress ratio for S235. It is shown that compared to K-joints of steel S 235 the non-dimensional strength of circular hollow section K-joints of S 460 would drop by 17%.

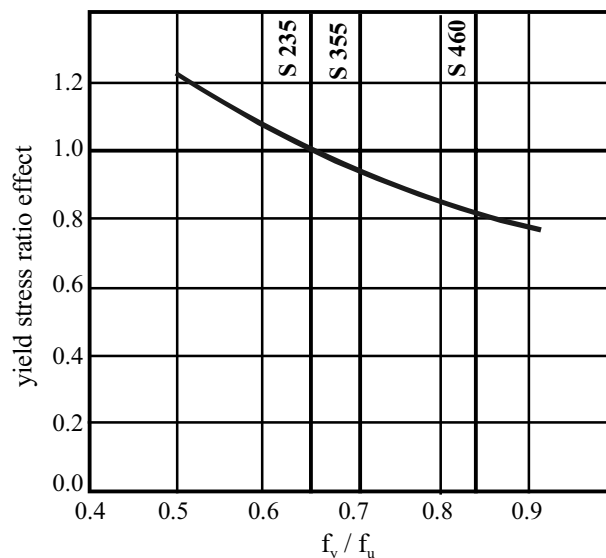


**Figure 10.** Influence yield to ultimate stress ratio for steel grades S 235, S 355 and S 460

Based on the ultimate strength only, without considering the ductility aspects and the larger deformation in Ref [43], it is proposed to limit the design yield stress to 0.8 times the ultimate stress, but even this does not fully compensate the lower non-dimensional strength.

Additional numerical calculations at Delft University of Technology [44] using the 3% of the chord width as ultimate deformation limit [45], showed that RHS K-joints made of S 460 had a 10 to 15% lower non-dimensional strength than comparable joints made from steel S 235, see Table 2.

**Table 2.** Non dimensional joint capacity related to the capacity for S 235

$2\gamma$	$\beta$					
	0.4		0.6		0.8	
	S 355	S 460	S 355	S 460	S 355	S 460
15	0.95	<b>0.90</b>	0.92	<b>0.84</b>	0.96*	**
25	0.95	<b>0.89</b>	0.95	<b>0.90</b>	0.96*	<b>0.92</b>
30	0.95	<b>0.90</b>	---	---	---	---
35	---	---	0.92	<b>0.85</b>	0.82*	<b>0.77*</b>

\* : Maximum capacity; others based on the 3% chord face indentation.

\*\* : Brace Buckling in compression.

The evaluation of the influence for the different steel grades on the static capacity of the joints is based on a factor R, which can be calculated by:

$$R = \frac{N_{ultimate, S...}}{N_{ultimate, S235}} \times \frac{f_y(S235)}{f_y(S...)} \quad (4)$$

Considering the larger deformations in joints of S460 in case the failure modes corresponding to chord face failure (RHS) or chord plastification (CHS) are governing, and the lower ductility in case of punching shear failure and brace effective width failure, it is proposed to adopt a general reduction factor of 0.9 and to limit the yield stress  $f_y$  to  $0.8f_u$  [44].

This avoids different corrections depending on the failure mode and this has been agreed by sub-commission IIW-XV-E for joints in steels with design yield stresses exceeding  $355 \text{ N/mm}^2$  up to  $460 \text{ N/mm}^2$ . This will result in a total joint capacity reduction of about 15%.

Furthermore, the b/t limitations given in the recommendations for the compression braces will be related to either class 1 or class 2 sections.

In Mang [46], it was shown that the strength of some tested K-joints made of S690 was only about 2/3 of the predicted joint strength using the joint strength equations developed for S235, thus care has to be taken to extrapolate the recommendations directly to joints of higher strength steel.

### ***Quality requirements for cold formed sections***

Since the available cold finished hollow sections on the market have different corner radii and different qualities, several investigations have been carried out during the last few years regarding checks for delivery requirements for cold-finished hollow sections [47]. Based on European research, e.g. recently at the University of Karlsruhe [48], it can be concluded that if welding is performed in or close to the corners, the corner radii have to meet the requirements given in Eurocode 3 [3], and in the IIW recommendations and recorded in Table 3. Furthermore, it is recommended to use fine-grained Al-killed steels. The modern steels are clean and have a low Carbon content. Si-killed steels may result in cracking after galvanizing.

In Europe the cold finished sections are delivered according to EN 10219-Part 2 (1998) [49] and up to 12 mm the average corner radii agree with those of table 3. However, a certain tolerance is allowed, which means that according to EN 10219 sections can be delivered with actual inner corner radii smaller than those in Table 3. In the research programme sections were also tested with small corner radii which satisfy the tolerances of EN 10219 but with actual corner radii smaller than those in Table 3. These sections are only allowed to be welded in the corners if these satisfy EN 10219 with the following additional material requirements:

- The maximum nominal wall- thickness is not exceeding 12.5 mm
- Aluminium killed steels with the quality grades J2H, K2H, MH, MLH, NH or NLH are used and
- the following maximum values are kept:  $C \leq 0.18\%$ ,  $P \leq 0.020\%$  and  $S \leq 0.012\%$

In other cases welding is only permitted at a distance of 5t from the corner or additional tests have to be performed to show that welding in the corners is permitted for that particular application. The requirements for steel S 460 are currently under discussion.

**Table 3.** Minimum inner corner radii for full aluminium ( $\geq 0.02\%$ ) killed cold finished hollow sections to allow welding in the corners

Steel grade	Wall thickness t (mm)	Minimum r/t (r = inner corner radius)	Remarks
<b>S235, S275, S355</b> (indicated by yield stresses in N/mm <sup>2</sup> )	<b>24</b>	<b>3.0</b>	The steels are indicated by yield stresses in N/mm <sup>2</sup>
	<b>12</b>	<b>2.0</b>	
	<b>10</b>	<b>1.5</b>	
	<b>6</b>	<b>1.0</b>	

No recommendation exists at present internationally for the determination of the required quality in relation to the service temperature, the welding condition, the loading, the static system, the thickness, the cold forming and the consequence of failure. According to the Dutch recommendations, NEN 6774 (2000) [50], the required quality for cold formed sections is generally one or two qualities higher than that required for hot-formed hollow sections. For example, if for a structural application in hot-formed hollow sections a Charpy value of 27 J at 20° is required, then for equivalent cold finished hollow sections this Charpy value is required at a temperature of 0° or -20°. Further work on this topic is being carried out at the University of Lappeenranta [51], where RHS K joints are tested at various temperatures between +20°C and -60°C. Based on this work it might be that proper selection criteria can be established.

## FATIGUE DESIGN OF HOLLOW SECTION JOINTS

### General

Based on the IIW-XV-E fatigue design recommendations for welded hollow section joints (IIW-XV-E, 1999) [6], CIDECT has published a design guide [52]. Since the publication, additional research is going on for thin-walled hollow section joints at the Monash University of Melbourne, and at the University of Karlsruhe. Further, stress concentration factors for bird beak connections are determined at the Delft University of Technology [53]. The connections with cast-steel nodes are under investigation at the Universities of Lausanne and Karlsruhe. During the last years, progress is also made in the development of 3D fracture mechanics models, for example at Nanyang Technological University in Singapore, the National University of Singapore and Delft University of Technology [54-56]. Currently, the hot spot stress method is reviewed to derive at a common procedure for hollow section joints and plate connections [57,58].

## GENERAL

At present still many investigations are going on and not all areas could be covered within the scope of this article. For example, many investigations just started in China, especially at the Tongji University, and it is expected that the coming years further improvements of the design rules may be expected.

In all areas the available information increases and many codes and recommendations become increasingly more voluminous and complicated with the probability of more errors. To the opinion of the authors, the information in codes should be limited to basic items and other relevant information should be given in background documents or design guides, for example, the CIDECT Design Guides and Packer & Henderson [59]. Furthermore, the recommendations should be consistent and as simple as possible. In the education, emphasis should be given to understanding by using simple models [60,61].

## ACKNOWLEDGEMENT

The authors wish to thank their colleagues in the IIW-XV-E committee and the CIDECT technical commission for their friendship and collaboration. Further, appreciation is extended to Dr.D.K.Liu, Dr.G.J.van der Vegte and Dr.X.D.Qian for providing the figures and doing final layout checks.

## REFERENCES

- [1] Wardenier, J. and Choo, Y.S., "Some developments in tubular joint research", Proceedings of the 4<sup>th</sup> International Conference on Advances in Steel Structures, Shanghai, China, Elsevier, 2005, Vol. 1, pp.31-40.
- [2] IIW-XV-E, International Institute of Welding Subcommittee XV-E, "Design recommendations for hollow section joints – Predominantly statically loaded", 2<sup>nd</sup> Edition, IIW. Doc. XV-701-89, International Institute of Welding, Paris, France, 1989.
- [3] CEN, Eurocode 3, "Design of steel structures, Part 1.8, Design of joints", Stage 49 Draft, Brussels, Belgium, November, 2003.
- [4] Kurobane, Y., Packer, J.A., Wardenier, J. and Yeomans, N., "Design guide for structural hollow section column connections", TUV-Verlag GmbH, Cologne, Germany, 2004.
- [5] Zhao, X-L., "Status of IIW static design recommendations for welded tubular joints", Proceedings of the 15<sup>th</sup> International Offshore and Polar Engineering Conference, Seoul, Korea, 2005, Vol. IV, pp.264-271.
- [6] IIW-XV-E, International Institute of Welding Subcommittee XV-E, "Recommended fatigue design procedure for welded hollow section joints, Part 1: Recommendations and Part 2: Commentary", IIW. Docs. XV-1035-99/XIII-1804-99, International Institute of Welding, Paris, France, 1999.
- [7] Packer, J.A., Wardenier, J., Kurobane, Y., Dutta, D. and Yeomans, N., "Design guide for rectangular hollow section (RHS) joints under predominantly static loading", TUV-Verlag GmbH, Cologne, Germany, 1992.
- [8] Liu, D.K. and Wardenier, J., "Multiplanar influence on the strength of RHS multiplanar gap KK-joints", Proceedings of the 9<sup>th</sup> International Symposium on Tubular Structures, Düsseldorf, Germany, Tubular Structures IX, A.A.Balkema Publishers, Lisse, The Netherlands, 2001, pp.203-212.

- [9] Liu, D.K. and Wardenier, J., "New chord stress functions for RHS gap K-joints", To be presented at the 11<sup>th</sup> International Symposium on Tubular Structures, Quebec City, Canada, 2006.
- [10] Wardenier, J., "Hollow section joints", Delft University Press, Delft, The Netherlands, 1982.
- [11] Chen, Y.Q., Liu, D.K. and Wardenier, J., "Design recommendations for RHS K-joints with 100% overlap", Proceedings of the 15<sup>th</sup> International Offshore and Polar Engineering Conference, Seoul, Korea, 2005, Vol. IV, pp.300-307.
- [12] Liu, D.K., Chen, Y.Q. and Wardenier, J., "Design recommendations for RHS K-joints with 50% overlap", Proceedings of the 15<sup>th</sup> International Offshore and Polar Engineering Conference, Seoul, Korea, 2005, Vol. IV, pp.308-315.
- [13] Veselcic, M., Herion, S. and Puthli, R.S., "Static behaviour of X, T and Y joints made of thin-walled RHS under brace axial load", Proceedings of the 9<sup>th</sup> International Symposium on Tubular Structures, Düsseldorf, Germany, Tubular Structures IX, A.A.Balkema Publishers, Lisse, The Netherlands, 2001, pp.155-164.
- [14] Rasmussen, J.R. and Young, B., "Tests on X- and K-joints in SHS stainless steel tubes", Journal of Structural Engineering, ASCE, 2001, 127(10), pp.1173-1182.
- [15] Kostas, N. and Packer, J.A., "Experimental examination of branch plate-to-RHS member connections", Proceedings of the 9<sup>th</sup> International Symposium on Tubular Structures, Düsseldorf, Germany, Tubular Structures IX, A.A.Balkema Publishers, Lisse, The Netherlands, 2001, pp. 135-144.
- [16] Karcher, D. and Puthli, R.S., "The static design of stiffened and unstiffened CHS L joints", Proceedings of the 9<sup>th</sup> International Symposium on Tubular Structures, Düsseldorf, Germany, Tubular Structures IX, A.A.Balkema Publishers, Lisse, The Netherlands, 2001, pp. 221-228.
- [17] Davies, G., Owen, J.S. and Kelly, R.B., "The effect of purlin loads on the capacity of overlapped bird beak K joints", Proceedings of the 9<sup>th</sup> International Symposium on Tubular Structures, Düsseldorf, Germany, Tubular Structures IX, A.A.Balkema Publishers, Lisse, The Netherlands, 2001, pp.229-238.
- [18] Willibald, S., Packer, J.A. and Puthli, R.S., "Experimental evaluation of bolted RHS flange-plate connection design models", Proceedings of the 9<sup>th</sup> International Symposium on Tubular Structures, Düsseldorf, Germany, Tubular Structures IX, A.A.Balkema Publishers, Lisse, The Netherlands, 2001, pp.127-134.
- [19] Jaurrieta, M.A., Alonso, A. and Chica, J.A., Eds., Proceedings of the 10<sup>th</sup> International Symposium on Tubular Structures, Madrid, Spain, Tubular Structures X, A.A.Balkema Publishers, Lisse, The Netherlands, 2003.
- [20] API, "Recommended practice for planning, designing and constructing offshore platforms RP-2A", American Petroleum Institute, USA, 1997.
- [21] ISO TC67/SC7/WG3/P3, "Draft code provisions for section E", Revision R6, International Organization for Standardization, 1997.
- [22] Dexter, E.M. and Lee, M.M.K., "Ultimate capacity of axially loaded K-joints in CHS", Proceedings of the 8<sup>th</sup> International Symposium on Tubular Structures, Singapore, Tubular Structures VIII, A.A.Balkema Publishers, Lisse, The Netherlands, 1998, pp.259-268.
- [23] Dier, A.F. and Lalani, M., "New code formulations for tubular joint static strength", Proceedings of the 8<sup>th</sup> International Symposium on Tubular Structures, Singapore, Tubular Structures VIII, A.A.Balkema Publishers, Lisse, The Netherlands, 1998, pp.107-116.
- [24] Yamada, Y., Morita, M., Makino, Y. and Wilmshurst, S.R., "A new ultimate capacity formula for unstiffened CHS T, TT, X, K and KK-joints under axial brace loads", Proceedings of the 8<sup>th</sup> International Symposium on Tubular Structures, Singapore, Tubular Structures XIII, A.A.Balkema Publishers, Lisse, The Netherlands, 1998, pp.213-222.

- [25] Choo, Y.S. and Qian, X.D., "Recent research on tubular joints with very thick-walled chords", Proceedings of the 15<sup>th</sup> International Offshore and Polar Engineering Conference, Seoul, Korea, 2005, Vol. IV, pp.272-278.
- [26] Van der Vegte, G.J., Makino, Y. and Wardenier, J., "The effect of chord pre-load on the static strength of uniplanar tubular K-joints", Proceedings of the 12<sup>th</sup> International Offshore and Polar Engineering Conference, Kitakyushu, Japan, 2002, Vol. IV, pp.1-10.
- [27] Van der Vegte, G.J., Liu, D.K., Makino, Y. and Wardenier, J., "New chord load functions for circular hollow section joints", Cidect report 5BK-4/03, Stevin report 6.03.1 (revised), Cidect, UK, 2003.
- [28] Pecknold, D.A., Ha, C.C. and Mohr, W.C., "Ultimate strength of DT tubular joints with chord preloads", Proceedings of the 19<sup>th</sup> International Conference on Offshore Mechanics and Arctic Engineering, New Orleans, USA, 2000.
- [29] Pecknold, D.A., Park, J.B. and Koppenhoefer, K.C., "Ultimate strength of gap K tubular joints with chord preloads", Proceedings of the 20<sup>th</sup> International Conference on Offshore Mechanics and Arctic Engineering, Rio de Janeiro, Brazil, 2001.
- [30] Van der Vegte, G.J., and Makino, Y., "Ultimate strength formulation for axially loaded CHS uniplanar T-joints", Proceedings of the 15<sup>th</sup> International Offshore and Polar Engineering Conference, Seoul, Korea, 2005, Vol. IV, pp.279-286.
- [31] Yura, J.A., "Ultimate capacity equations for tubular joints", OTC 3690, Houston, USA, 1980.
- [32] Wardenier, J., Kurobane, Y., Packer, J.A., Dutta, D. and Yeomans, N., "Design guide for circular hollow section (CHS) joints under predominantly static loading", TUV-Verlag GmbH, Cologne, Germany, 1991.
- [33] Choo, Y.S., "Recent development and innovation in tubular structures", Advances in Structural Engineering, 2005, 8(3), pp.217-230.
- [34] Choo, Y.S., Liang, J.X. and Van der Vegte, G.J., "An effective external reinforcement scheme for circular hollow section joints", Connections in Steel Structures V – Amsterdam, 2004, pp.423-432.
- [35] Choo, Y.S., Liang, J.X., Van der Vegte, G.J., and Liew, J.Y.R., "Static strength of doubler plate reinforced CHS X-joints loaded by in-plane moment", Journal of Constructional Steel Research, 2004, 60, pp.1725-1744.
- [36] Choo, Y.S., Liang, J.X., Van der Vegte, G.J., and Liew, J.Y.R., "Static strength of collar plate reinforced CHS X-joints loaded by in-plane moment", Journal of Constructional Steel Research, 2004, 60, pp.1745-1760.
- [37] Van der Vegte, G.J., Choo, Y.S., Liang, J.X., Zettlemoyer, N. and Liew, J.Y.R., "Static strength of T-joints reinforced with doubler or collar plates. Part II: Numerical simulations", Journal of Structural Engineering, ASCE, 2005, 131(1), pp.129-138.
- [38] Lee, M.M.K. and Llewelyn-Parry, A., "Strength estimation of offshore ring-stiffened DT joints", Proceedings of the 10<sup>th</sup> International Symposium on Tubular Structures, Madrid, Spain, Tubular Structures X, A.A.Balkema Publishers, Lisse, The Netherlands, 2003, pp.245-252.
- [39] Willibald, S., "The static design of ring-stiffened tubular T- and Y-joints", Proceedings of the 9<sup>th</sup> International Symposium on Tubular Structures, Düsseldorf, Germany, Tubular Structures IX, A.A.Balkema Publishers, Lisse, The Netherlands, 2001, pp.581-588.
- [40] Pietrapertosa, C. and Jaspart, J-P., "Study of the behaviour of welded joints composed of elliptical hollow sections", Proceedings of the 10<sup>th</sup> International Symposium on Tubular Structures, Madrid, Spain, Tubular Structures X, A.A.Balkema Publishers, Lisse, The Netherlands, 2003, pp.601-608.
- [41] Choo, Y.S., Liang, J.X. and Lim, L.V., "Static strength of elliptical hollow section X-joint under brace compression", Proceedings of the 10<sup>th</sup> International Symposium on Tubular

- Structures, Madrid, Spain, Tubular Structures X, A.A.Balkema Publishers, Lisse, The Netherlands, 2003, pp.253-258.
- [42] Kurobane, Y., "New developments and practices in tubular joint design", IIW Doc. XV-488-81 and XIII-1004-81, International Institute of Welding, Paris, France, 1981.
  - [43] Noordhoek, C. and Verheul, A., "Static strength of high strength steel tubular joints", ECSC Agreement 7210-MC/602-(F5.05d/93), 1996.
  - [44] Liu, D.K. and Wardenier, J., "Effect of the yield strength on the static strength of uniplanar K-joints in RHS", Doc. IIW-XVE-04-293, Delft University, Delft, The Netherlands, 2005.
  - [45] Lu, L.H., de Winkel, G.D., Yu, Y. and Wardenier, J., "Ultimate deformation limit for tubular joints", Proceedings of the 6<sup>th</sup> International Symposium on Tubular Structures, Melbourne, Australia, Tubular Structures VI, A.A.Balkema Publishers, Lisse, The Netherlands, 1994, pp.341-348.
  - [46] Mang, F., "Untersuchungen an Verbindungen von geschlossenen und offenen Profilen aus hochfesten Stählen", AIF – Nr. 3347, Universität Karlsruhe, Germany, 1978.
  - [47] Packer, J.A. and Henderson, J.E., "Hollow structural section connections and trusses – A design guide", Canadian Institute of Steel Construction, Toronto, Canada, 1997. (also available in Chinese)
  - [48] Puthli, R.S., Herion, S., Boellinghaus, Th. and Florian, W., "Welding in cold-formed areas of rectangular hollow sections", Cidect final report and addendum 1A-6/05, Cidect, UK, 2005.
  - [49] EN 10219-Part 2, "Cold formed structural hollow sections of non-alloy and fine grain structural steels – Part 2: Tolerances, dimensions and sectional properties", CEN, Brussels, Belgium, 1998.
  - [50] NEN 6774, "Eisen aan de staalkwaliteit voor constructiestaalsoorten in relatie tot het brosse breukgedrag voor overwegend statisch belaste constructies", NEN, Delft, The Netherlands, 2000.
  - [51] Björk, T., Marquis, G., Kemppainen, R. and Ilvonen, R., "The capacity of cold-formed rectangular hollow section K-gap joints", Proceedings of the 10<sup>th</sup> International Symposium on Tubular Structures, Madrid, Spain, Tubular Structures, X, A.A.Balkema Publishers, Lisse, The Netherlands, 2003, pp.227-234.
  - [52] Zhao, X-L., Herion, S., Packer, J.A., Puthli, R.S., Sedlacek, G., Wardenier, J., Weynand, K., Van Wingerde, A.M., and Yeomans, N.F., "Design guide for circular and rectangular hollow section welded joints under fatigue loading", Cidect design guide Nr. 8, TUV-Verlag GmbH, Cologne, Germany, 2000.
  - [53] Keizer, R., Romeijn, A., Wardenier, J. and Glijnis, P.C., "The fatigue behaviour of diamond bird beak T-joints", Proceedings of the 10<sup>th</sup> International Symposium on Tubular Structures, Madrid, Spain, Tubular Structures X, A.A.Balkema Publishers, Lisse, The Netherlands, 2003, pp. 303-310.
  - [54] Lie, S.T., Chiew, S.P., Lee, C.K. and Huang, Z.W., "Modelling through-thickness and surface cracks in tubular joints", Proceedings of the 9<sup>th</sup> International Symposium on Tubular Structures, Düsseldorf, Germany, Tubular Structures IX, A.A.Balkema Publishers, Lisse, The Netherlands, 2001, pp.285-290.
  - [55] Qian, X., Dodds, R.H. and Choo, Y.S., "Elastic-plastic crack driving force for tubular X-joints with mismatched welds", Engineering Structures, 2005, Vol. 27, Issue 9, pp.1419-1434.
  - [56] Oomens, M., Romeijn, A., Wardenier, J. and Dijkstra, O.D., "Development and validation of a 3D fracture mechanics model for thick-walled CHS T-joints", Proceedings of the 15<sup>th</sup> International Offshore and Polar Engineering Conference, Seoul, Korea, 2005, Vol. IV, pp.333-340.



- [57] Doerk, O., Fricke, W. and Weissenborn, C., “Comparison of different calculation methods for structural stresses at welded joints”, *International Journal of Fatigue*, 2003, 25(5), pp.359-369.
- [58] Marshall, P.W. and Wardenier, J., “Tubular vs non-tubular hot spot methods”, *Proceedings of the 15<sup>th</sup> International Offshore and Polar Engineering Conference*, Seoul, Korea, 2005 Vol. IV, pp.254-263.
- [59] Packer, J.A., “Whither tubular structures research?”, *Proceedings of the 10<sup>th</sup> International Symposium on Tubular Structures*, Madrid, Spain, Tubular Structures X, A.A.Balkema Publishers, Lisse, The Netherlands, 2003, pp.3-11.
- [60] Wardenier, J., “From a tubular morning mist to the tubular morning glow”, *Proceedings of the 9<sup>th</sup> International Symposium on Tubular Structures*, Düsseldorf, Germany, Tubular Structures IX, A.A.Balkema Publishers, Lisse, The Netherlands, 2001, pp.3-12.
- [61] Wardenier, J., “Hollow sections in structural applications”, *Bouwen met Staal*, Rotterdam, The Netherlands, 2002. (also available in Chinese and Spanish)

# RELIABILITY-BASED INTEGRATED DESIGN APPROACH FOR PLANAR STEEL FRAMES

Yu-Shu Liu\* and Guo-Qiang Li

*School of Civil Engineering, Tongji University, Shanghai, China*

*\*(Corresponding author: E-mail: yslu@mail.tongji.edu.cn)*

---

**ABSTRACT:** The current design method of steel structures is based on the member reliability and cannot assure the structural system reliability. To overcome the shortcoming of the current method, the integrated structural design approach, with consideration of system reliability for planar steel frames, is studied in this paper. The reliability-based integrated design approach (RID) directly checks the structural system limit states, based on structural nonlinear analysis, and the corresponding system reliability. In this paper, the reliability-based integrated design approach for planar steel frames is established on the basis of evaluating the ultimate load-carrying capacity and system reliability of planar steel frames. In the process of constructing the design formula, the target reliability index and importance factor are determined according to the current specification and the two common load combinations are considered. Design examples and comparisons demonstrate that RID provides a feasible way for structural engineers to improve the design quality of steel frame structures with certain and consistent system reliability levels.

**Keywords:** Reliability-based integrated design; Planar steel frames; Member reliability; System reliability; Target reliability index.

---

## 1. INTRODUCTION

As we all know, the system reliability of a structure is not only related to structural member reliability, but also influenced by the correlation between the members, the correlation between resistance and load, the configuration of the structure, the structural redundancy and ductility [1]. Actually, a building structure fulfills its function as an integrity, and a designer should aim at ensuring the reliability level of the structural system rather than the individual members. Therefore a structural design should be implemented based on integral structural analysis and reliability assessment [2]. However, the current limit state design for steel frames, e.g. AISC LRFD [3], is based on individual member checks, comprising the elastic integrated structural analysis for determining internal forces in the structural members and the capacity check of individual members. This approach leads to an ambiguous system reliability of the structure designed with only implementing member safety checks. The load and resistance factors design approach(LRFD), a probability-based limit state design approach, is just such a method. As an improvement, a structural design approach called preliminary integrated design(PID) [4] is constructed based on the frame analysis-frame check instead of the frame analysis-member check. Although it is a design approach oriented to system capacity limit states, PID cannot provide a check of the structural system reliability since the load and resistance factors in this approach are not obtained on the basis of the structural system reliability evaluation. However, the reliability-based integrated design approach(RID) proposed in this paper makes up the insufficiency of PID, which can ensure the structures designed to have the reliability index as close as possible to the target values.

## 2. APPROACH

### 2.1. Target Reliability Index

The target reliability index is the expected reliability index of structural design, it is an important factor in the reliability-based structural design. Theoretically, the value of target reliability index

should be established through optimal method according to the importance of structures, failure consequences, causes and modes of structures, and economic ability. Because of the deficiency of statistical information and considering the succession of the specifications, the target reliability index used in current codes is adopted by calibrating to the safety level implied by existing codes. Similar to AISC LRFD [3], GB50068-2001 [5] is also a probabilistic design code based on the limit states of structural components, and its target safety level, as shown in Table 1 ( $\beta$  denotes reliability index,  $P_f$  denotes failure probability), is taken to be the probabilities of structural failure implied by given codes which are judged to be acceptable in China. For the sake of simplification and conservative consideration, it is reasonable that the target reliability index used in RID can has a increase of 0.5 compared to the target reliability index employed in the limit state design approach based on individual members with ductile failure mode, because although the integrated failure of steel frames is ductile, its importance level is comparative to that of component failure of structures with brittle mode, so the target reliability index of the former is the same as the latter.

**Table 1.** Target reliability index employed in current specification and RID

Design method	Failure mode	Importance class of structures					
		Class 1		Class 2		Class 3	
		$\beta$	$P_f$	$\beta$	$P_f$	$\beta$	$P_f$
Current specification	Brittle failure	4.2	$1.3 \times 10^{-5}$	3.7	$1.1 \times 10^{-4}$	3.2	$6.9 \times 10^{-4}$
	Ductile failure	3.7	$1.1 \times 10^{-4}$	3.2	$6.9 \times 10^{-4}$	2.7	$3.5 \times 10^{-3}$
RID	Ductile failure	4.2	$1.3 \times 10^{-5}$	3.7	$1.1 \times 10^{-4}$	3.2	$6.9 \times 10^{-4}$

## 2.2. Load and Load Combination

Three types of loads need to be considered in the reliability-based integrated design of steel frames. They are dead load, live load and wind load. The statistic data of these loads are tabulated in Table 2. Two loading cases are investigated. One is vertical dead load with vertical live load and the other is vertical dead load with simultaneously vertical live load and horizontal wind load. In assessment of system reliability, dead load and live load are treated as random load in loading case 1 while only wind load is treated as random load in loading case 2.

**Table 2.** Statistic data of various loads

	Ratio of mean to normal value (K)	Coefficient of variance(COV)	Distribution type
Dead load	1.06	0.07	Normal
Live load	1.00	0.25	Gumbel
Wind load	0.999	0.193	Gumbel

## 2.3. Statistics of Structural Resistance

The randomness of structural resistance of steel frames is mainly relevant to the randomness of the sectional geometry, the randomness of material yielding strength and the randomness of calculation mode for determining structural resistance, the statistics of which are listed in Table 3 [6].

It is observed that the PDF curves of structural resistance of steel frames under the two loading cases fit lognormal distribution quite well [7]. Therefore, the structural integrated resistance of steel frames will be assumed to follow a lognormal distribution in the following calculation of load and resistance factors.

**Table 3.** Statistics of principal random variables influencing structural resistance

		Ratio of mean to normal value	Coefficient of variance
Geometrical parameters	Length or width thickness	1.000	0.0135
		1.000	0.0350
Yielding strength of steel	Q235	$t \leq 16\text{mm}$	1.070
		$16\text{mm} < t \leq 40\text{mm}$	1.074
		$40\text{mm} < t \leq 60\text{mm}$	1.118
		$60\text{mm} < t \leq 100\text{mm}$	1.087
	Q345	$t \leq 16\text{mm}$	1.040
		$16\text{mm} < t \leq 35\text{mm}$	1.025
		$35\text{mm} < t \leq 50\text{mm}$	1.125
		$50\text{mm} < t \leq 100\text{mm}$	1.184
Calculation mode for determining structural resistance	Vertical load	1.000	0.075
	Horizontal and vertical load	1.000	0.075

## 2.4. Practical Design Formula

Reliability-based integrated design method for steel portal frames is first introduced in [4]. The practical design formula of this method can be written as

$$R_n / \phi \geq \gamma_0 \cdot \sum \gamma_i \cdot S_{ni} \quad (1)$$

where  $R_n$  is the nominal value of structural resistance determined by nonlinear structural analysis,  $S_{ni}$  is a load effect,  $\phi$  and  $\gamma_i$  are the factors of structural resistance and load effect, which can be obtained by reliability analysis of structures,  $i$  stands for the number of load effects, and  $\gamma_0$  is the importance factor of structures. Though Eq.(1) is similar to that of traditional LRFD, they factually differ from each other because the factors of resistance and load in RID are based on ensuring reliability of structural system, rather than reliability of individual members as in LRFD.

### 2.4.1. Importance Factor

The value of importance factor  $\gamma_0$  used in conventional member-checked approach is taken as

1. for structure components whose importance class is class one or serviceable life is more than 100 years,  $\gamma_0$  should not be less than 1.1;
2. for structure components whose importance class is class two or serviceable life is 50 years,  $\gamma_0$  should not be less than 1.0;
3. for structure components whose importance class is class three or serviceable life is 5 years,  $\gamma_0$  should not be less than 0.9.

Since  $\gamma_0$  is only relevant to the importance of structures, the importance factor of structures employed in RID can take the same value as in LRFD, stated as above.

### 2.4.2. Load and Resistance Factors

The process of determining the load and resistance factors in the formula for RID is similar to that for traditional limit-state design, except that the factors of the former come from assessment of system reliability of structures whereas those of the latter from reliability calibration of individual members [2]. The flow chart for determining load and resistance factors for RID is given in

Figure 1 and the data used for this purpose are listed in Table 4, the values of resistance statistics in Table 4 are taken from the sampling of the structural resistance which is calculated by finite element program.

**Table 4.** Data used in calculation of load and resistance factors

(a) Q235						
Load case	Resistance factor	Load factor		Load ratio	Resistance statistics	
1	1.20	Dead load	Live load	Live load/ dead load	COV	$K_R^{(3)}$
		1.00-1.60 <sup>1)</sup>	1.40-3.00 <sup>1)</sup>	0.50-1.10 <sup>2)</sup>	0.110	1.035
2	1.20	Dead load+live load <sup>4)</sup>	Wind load	none	COV	$K_R^{(3)}$
		1.0	1.10-2.65 <sup>1)</sup>	none	0.108	1.065

(b) Q345						
Load case	Resistance factor	Load factor		Load ratio	Resistance statistics	
1	1.20	Dead load	Live load	Live load/ dead load	COV	$K_R^{(3)}$
		1.00-1.60 <sup>1)</sup>	1.40-3.00 <sup>1)</sup>	0.50-1.10 <sup>2)</sup>	0.110	1.046
2	1.20	Dead load+live load <sup>4)</sup>	Wind load	none	COV	$K_R^{(3)}$
		1.0	1.10-2.65 <sup>1)</sup>	none	0.121	1.103

1) Interval is equal to 0.05;

2) Interval is equal to 0.15;

3)  $K_R$  is the ratio of mean to normal value of structure resistance;

4) The summation of dead load and live load is treated as a constant load in load case 2.

For the convenience of practical application, the resistance factor,  $\phi$ , can be taken as a constant being equal to 1.2, and the optimal load factors can then be determined according to the target reliability with this strategy. Following the process of calculation shown in Figure 1, the load and resistance factors with a certain system reliability for reliability-based integrated design of steel frames can be determined. The relative errors between  $R_{Kij}$  and  $R_{Kj}^*$  indicated in Figure 1 under different load factors and different target reliability index is shown in Figure 2. The optimal load and resistance factors for RID aiming at definite target reliability levels are listed in Table 5.

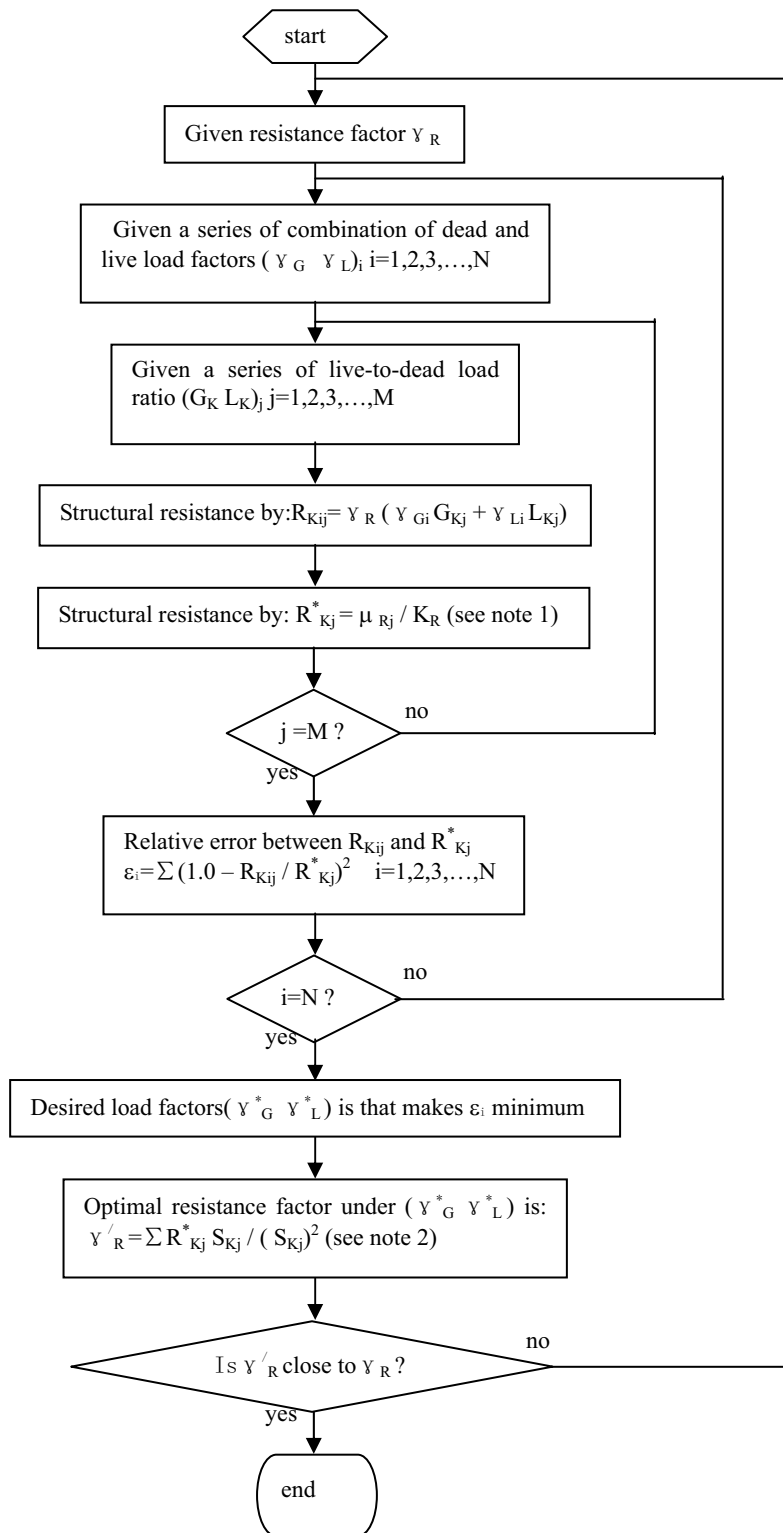
Since the final values of resistance factors are very close to the initial value 1.2, it is acceptable that uniform resistance factor for RID,  $\phi=1.2$ , can be employed in the practical application.

**Table 5.** Optimal load and resistance factors and their errors

(a) Q235						
$\beta_t$	Load case 1				Load case 2	
	$\gamma_G$	$\gamma_L$	$\gamma_R$	$\varepsilon$	$\gamma_W (\gamma_G + \gamma_L = 1.0)$	$\varepsilon$
2.7	1.10	1.60	1.1898	5.08398e-004	1.45	2.53647e-004
3.2	1.10	1.90	1.1969	7.09022e-005	1.70	1.46003e-005
3.7	1.10	2.25	1.2023	2.55264e-005	1.95	1.61455e-007
4.2	1.10	2.70	1.1927	2.21763e-004	2.25	9.66120e-006

(b) Q345						
$\beta_t$	Load case 1				Load case 2	
	$\gamma_G$	$\gamma_L$	$\gamma_R$	$\varepsilon$	$\gamma_W (\gamma_G + \gamma_L = 1.0)$	$\varepsilon$
2.7	1.10	1.55	1.1972	2.80723e-004	1.45	1.07029e-005
3.2	1.10	1.85	1.2025	1.02353e-004	1.65	8.15408e-005
3.7	1.10	2.20	1.2061	1.40213e-004	1.90	1.22249e-004
4.2	1.10	2.65	1.1948	1.13074e-004	2.20	5.76273e-005



note1.  $\mu_{Rj}$  is determined by First Order Second Moment(FOSM) method with the statistics listed in table 4;

note2.  $R_{Kj}$  is obtained by  $R_{Kj} = \gamma_G^* G_{Kj} + \gamma_L^* L_{Kj}$

**Figure 1.** Flow chart for calculation of load and resistance factors.

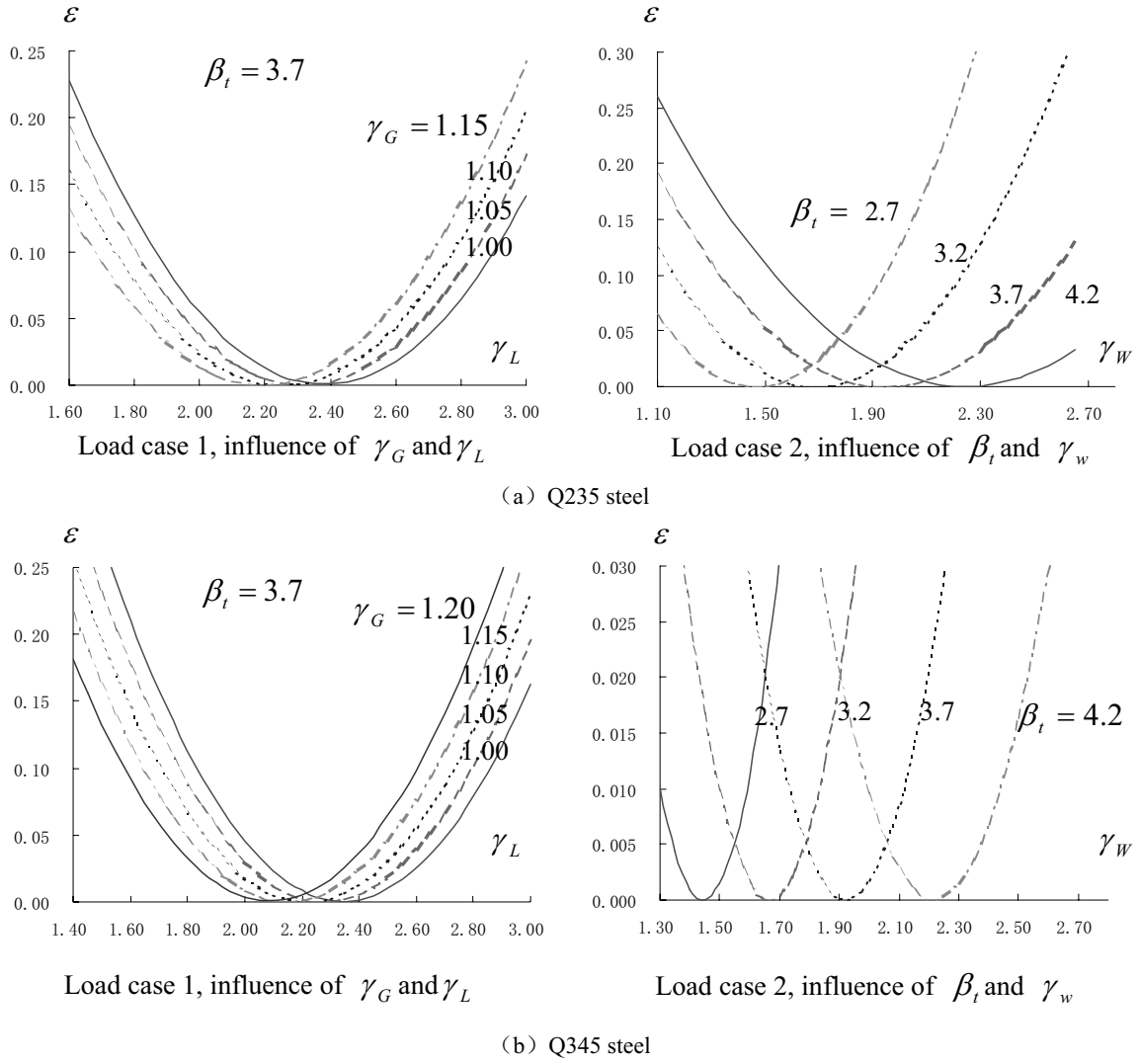


**Figure 2.** Relative error comparisons when calculating load and resistance factors

Then the expressions for design of steel frames under loading cases 1 and 2 with the target system reliability index being equals 3.7 can be obtained as

For Loading case 1, Q235 steel

$$R_n / 1.2 \geq 1.10 \cdot G_n + 2.25 \cdot L_n \quad (2a)$$

Q345 steel

$$R_n / 1.2 \geq 1.10 \cdot G_n + 2.20 \cdot L_n \quad (2b)$$

where  $R_n$  is the normal value of structure resistance under loading case 1, determined by nonlinear structural analysis;  $G_n$  and  $L_n$  represent the normal values of dead and live load effects.

For Loading case 2, Q235 steel

$$R_n / 1.2((G + L) = 1.00 \cdot (G_n + L_n)) \geq 1.95 \cdot W_n \quad (3a)$$

Q345 steel

$$R_n / 1.2((G + L) = 1.00 \cdot (G_n + L_n)) \geq 1.90 \cdot W_n \quad (3b)$$

where  $R_n$  is the normal value of structure resistance under loading case 2, determined by nonlinear structural analysis(in the process of calculation, the value of  $R_n$  is determined under constant dead load and live load);  $W_n$  represents the normal value of wind load.

## 2.5. Design steps

The design steps using RID are

1. determine the structural size, material type, and the values of nominal loads of the steel frame design for;
2. select a group of sectional dimensions for the frame and perform the integrated nonlinear frame analysis, by which the nominal resistances of the trial frame ( $R_n$  in the design formula) under two loading cases are obtained;
3. check the design formula with the nominal frame resistances and the nominal loads;
4. repeat steps 2 and 3 till the design equations are satisfactorily met.

## 3. APPLICATION

### 3.1. An Example

An asymmetric two-storey two-bay steel frame is shown in Figure 3 [8]. Using this example, we can compare different design methods such as RID, PID and LRFD. The loads in Figure 3 is the summation of normal values of dead load and live load and the ratio of dead to live load is 1.0. The statistics used for reliability analysis is listed in Table 6. The normal value of yielding strength of steel is 248MPa and the elastic modulus is 206GPa.

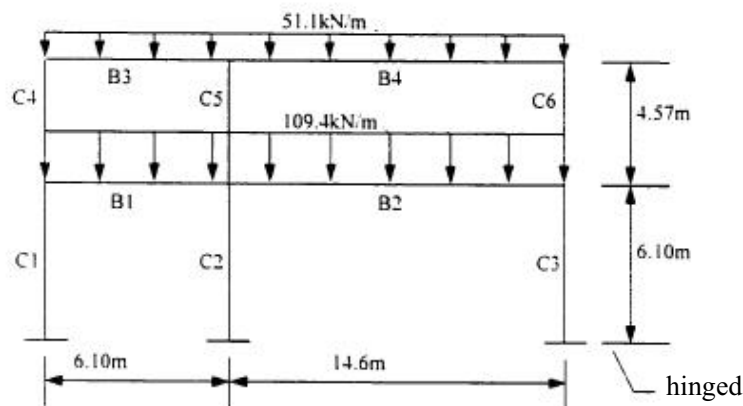


**Figure 3.** Dimensions and loads of a two-storey two-bay steel frame

**Table 6.** Statistics of loads and yielding strength of example frame [8]

Statistics	Ratio of mean to normal value	Coefficient of variance	distribution
Dead load	1.00	0.08	Normal
Live load	1.00	0.25	gumbel
Yielding strength	1.05	0.10	gumbel

The design steps of PID are similar with those of RID. However, the load and resistance factors employed in PID are taken from LRFD, as

for loading case 1

$$0.90 \cdot R_n \geq 1.20 \cdot G_n + 1.60 \cdot L_n \quad (4)$$



where  $R_n$  is the nominal value of the structural resistance against vertical loads determined by nonlinear integrated structural analysis, and  $G_n$  and  $L_n$  are respectively the nominal value of dead and live load effects, and

for loading case 2

$$0.90 \cdot R_n ((G + L) = 1.20 \cdot (G_n + L_n)) \geq 1.30 \cdot W_n \quad (5)$$

where  $R_n$  is the nominal value of the structural resistance against horizontal loads determined by nonlinear integrated structural analysis when the summation of dead load and live load is equal to 1.20 times of its nominal values, and  $W_n$  is the nominal value of wind load.

### 3.2. Design Results

The steel frame shown in Figure 3 is designed by various methods, including traditional LRFD, PID and RID. The sections of components and the steel consumption of the frame obtained by different design methods are given in Table 7. Since for this steel frame, the loading case 1 is the control loading case, then the reliability of loading case 2 is not considered.

The results of system reliability for the frame designed by various methods are listed in Table 8, where  $\beta$  and  $p_f$  are respectively the reliability index and failure probability.

The design results show that the system reliability index of the frame designed by LRFD is larger than the target reliability index, which is 3.7, but the system reliability of PID is lower than that level. While the reliability index of frame designed by RID is close to the expected reliability level and meets the requirement of structural integrated design. The steel consumption of the frame designed by RID is also reasonable, which is between the values obtained respectively by LRFD and PID.

**Table 7.** Comparison of component sections and steel consumption obtained by various methods

	Design method	LRFD	PID	RID
Components	C1	W12×19	W12×14	W12×16
	C2	W14×132	W14×99	W14×109
	C3	W14×109	W14×82	W14×99
	C4	W10×12	W10×12	W10×12
	C5	W14×109	W14×99	W14×109
	C6	W14×109	W14×99	W14×109
	B1	W27×84	W27×84	W27×84
	B2	W36×135	W30×108	W30×108
	B3	W18×40	W18×40	W18×40
	B4	W27×94	W27×84	W27×94
	Steel consumption (10 <sup>3</sup> kg)	9.59	8.51	9.12

**Table 8.** System reliability of the frame designed by LRFD, PID and RID

Design method	$\beta$	$P_f$
LRFD	4.4591	4.1148e-006
PID	3.2033	6.7923e-004
RID	3.8427	6.0856e-005

#### 4. CONCLUSIONS

The Reliability-based Integrated Design (RID) of planar steel frames is studied in this paper. The following conclusions can be drawn from above studies:

- 1). The system reliability index of steel frames designed by RID is larger than that designed by PID and lower than that designed by LRFD, while it is close to the expected reliability level and meets the requirement of structural integrated design.
- 2). Although it is also an integrated design method, PID cannot provide a check of the system reliability level since the load and resistance factors in its design expressions are coming directly from LRFD without consideration of system reliability. So the system reliability of a structure designed by PID cannot be guaranteed.
- 3). From the example concerning design of a steel frame, it can be seen that RID consumes less steel than LRFD. This novel design method can make up the insufficiency of conventional design method and facilitate the design procedure without requirement of member checks, while ensuring system reliability.

#### REFERENCES

- [1] Ellingwood, B.R., "Probability-based codified design: past accomplishments and future challenges", Structural Safety, 1994, 13, pp.159-176.
- [2] Li, J-H., "Probabilistic limit-state design for building structures", Beijing, Press of Chinese Construction Industry, 1990 (in Chinese).
- [3] AISC LRFD, "Manual of steel construction, load and resistance factor design", 2nd edition, Chicago (IL): American Institute of Steel Construction, 1994.
- [4] Li, J-J. and Li, G-Q, "Reliability-based integrated design of steel portal frames with tapered members", Structural Safety, 2004, 26, pp.221-239
- [5] GB 50068-2001, "The reliability design uniform standard for building structures", 2001 (in Chinese).
- [6] Zhang, X-P., "Reliability analysis and design for building structures", Beijing, Science Press, 2001 (in Chinese).
- [7] Liu, Y-S, "Research on theory of nonlinear analysis and integrated reliability design for planar steel frames", PhD dissertation, Tongji University, Shanghai, PR China, 2004 (in Chinese).
- [8] Zhou, W-X, "Reliability evaluations of reinforced concrete columns and steel frames", Ph.D dissertation, University of Western Ontario, 2000.

# ANALYTICAL AND EXPERIMENTAL INVESTIGATIONS OF BOLTED HAUNCHED BEAM-TO-COLUMN JOINTS WITH A VIEW OF SEISMIC DESIGN

A. Lachal\*, J.M. Aribert and G. Loho

*Institut National des Sciences Appliquées, Rennes, France*

*\*(Corresponding author: E-mail: Alain.Lachal@insa-rennes.fr)*

---

**ABSTRACT:** A possible solution to strengthen end-plate bolted composite joints is to extend the end-plate below the beam and to add a haunch in the corner with the column. This strengthening arrangement is studied in this paper from both theoretical and experimental approaches. Experimental results are analysed and compared with theoretical ones issued from analytical models essentially based on Eurocodes 3, 4 and 8 [1-6]. Results are interpreted in terms of rotational stiffness, moment resistance and rotation capacity. The contribution of haunches to strengthen a beam-to-column joint and to dissipate energy under cyclic loadings is quantified.

**Keywords:** Composite construction; Beam-to-column joint; End-plate bolted joint; Haunch; Seismic action.

---

## 1. INTRODUCTION

End-plate bolted beam-to-column joints are currently used in Europe in steel and composite constructions. In composite constructions, generally these joints appear semi-rigid and partial strength. The use of such joints in anti-seismic moment resisting frames is allowed now by the seismic code Eurocode 8 - Part 1 [5]. Nevertheless, recent studies have shown that such design should be limited to areas of low and medium seismicity; but in zone of high seismicity, the joints should be strengthened to become rigid and full-strength.

After Northridge earthquake, researches carried out on steel welded beam-to-column joints have shown that adding haunches provided a good solution to strengthen a joint and to obtain good seismic performances, SAC [7], Lee and Uang [8], NIST [9], Gross *et al.* [10], Yu *et al.* [11]. Main results of these researches were grouped in a State of the Art Report published by the Federal Emergency Management Agency, FEMA-355D [12], as well as recommendations, FEMA-351 [13], including a design procedure for welded haunch connections. More recently, a draft of Eurocode 8 - Part 3 [6] has proposed recommendations to strengthen beam-to-column steel and composite connections by adding haunches.

In the case of end-plate bolted composite connections, haunches located at the bottom side of the beam flanges seem more convenient for fabrication. Also it is suggested by Gross *et al.* [10] to adopt an haunch depth  $b \approx 0.33$  times the beam depth  $d_b$ , with an angle of the haunch  $\theta \approx 30^\circ$  to limit the haunch web slenderness. In the present study, we have opted for a simple predesign method adopting the haunch depth  $b$  equal to the steel beam depth  $d_b$  and the haunch length  $a$  equal to  $2b$ . These dimensions make easier the haunch fabrication cut out directly from the steel beam. In addition, such a predesign method allows to ensure a better balance between hogging and sagging moment resistances in a composite connection (Table 2).

Adopting such a strengthening strategy, 5 tests dealing with steel and composite joints equipped with haunched bolted end-plates, with two arrangements (T and cruciform as shown in Figures 1 and 2 respectively) has been fabricated and tested (group 1 in Table 1). A companion series of 5 similar tests, simply end-plate connected without haunch strengthening (Figures 3 and 4), has been fabricated simultaneously and then tested in order to clearly evaluate the haunch contribution (group 2 in Table 1).

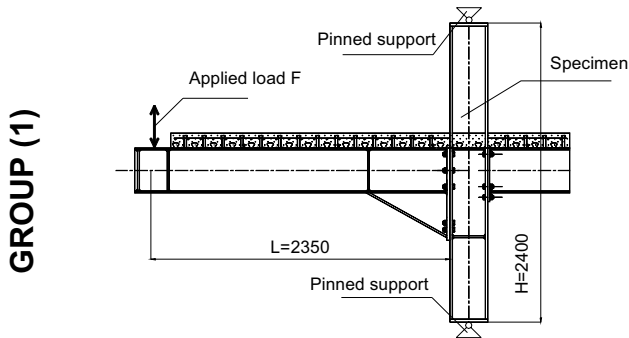


**Figure 1. T with an haunch**

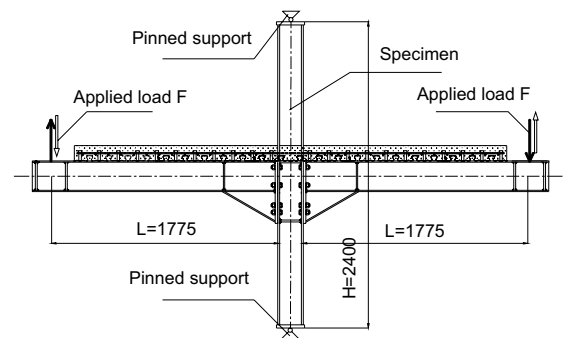


**Figure 2. Haunched joint**

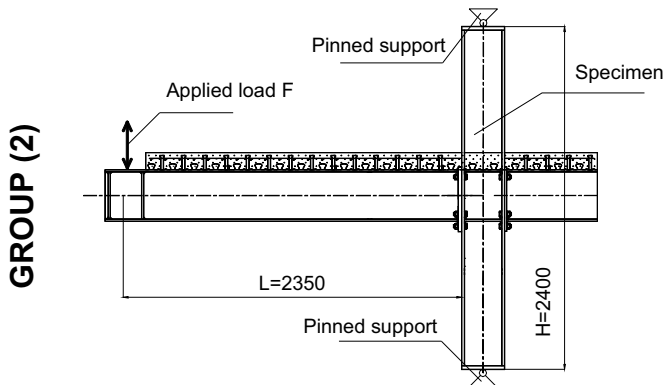


**Figure 3. T without haunch**

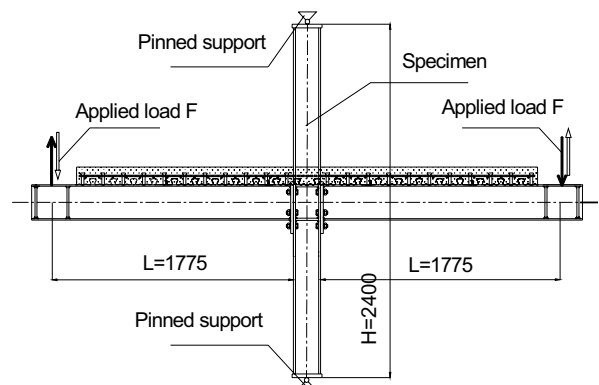


**Figure 4. Joint without haunch  
Cruciform arrangement  
(unsymmetrically loaded)**

**T arrangement**

An analytical approach mainly based on the works of Lee and Uang [8] and adopted recently in Eurocode 8 – Part 3 is firstly adapted to the static design of haunches in composite beam to steel column joints. In a second step the main characteristics of rotational stiffness and moment resistance of haunched end-plate bolted connections have been determined from Eurocodes 4 and 3 concepts (using measured material properties). Analytical results are compared to experimental ones in order to evaluate the good performances of these analytical models. The influence of the haunch on the joint design has been taken into account (with regard to shear connection, reinforcement, column web panel...). In addition the plastic energy dissipation mainly located outside the joint in the case of full-strength beam-to-column joints is evaluated experimentally and compared to the energy dissipation obtained in the case of partial-strength beam-to-column joints.

## 2. ANALYTICAL STATIC DESIGN MODELS

### 2.1. Haunch Static Design

#### 2.1.1. Determination of the bending moment and the vertical shear at the haunch tip

Previous studies, Yu *et al.* [11], have shown that the contribution of the haunch web to the stiffness in the haunch flange direction was minor (equal or less than 5%). So, a simplified model idealizing the haunch flange as an elastic strut has been developed. Considering the beam vertical shear,  $V_{Ed}^{\pm}$ , at the haunch tip, a parameter  $\beta^{\pm}$  is introduced to define the vertical reaction force  $\beta^{\pm} V_{Ed}^{\pm}$  transmitted to the steel beam at the haunch tip. This parameter  $\beta^{\pm}$  quantifies the force distribution within the haunch region.

The model was developed only for steel joints; in this study it is adapted to composite solutions of haunched joints, introducing composite beam characteristics and distinguishing moment values and neutral axis positions in sagging and hogging bending.

The static design of the haunch is based on the moment and vertical shear that develop at the tip of the haunch when a plastic hinge occurs in the beam. Following the step-by-step design procedure proposed by Yu *et al.* [11], a first step consists in the determination of maximum sagging and hogging bending moments  $M_{Ed}^{\pm}$  exerted by the composite beam, namely:

$$M_{Ed}^{\pm} = \alpha M_{pl,R}^{\pm} \quad (1)$$

$\alpha$  is a moment overstrength factor for which the adopted value of 1.1 seems reasonable in comparison with current codes (see 6.5.5 (3) in Eurocode 8 – Part 1).

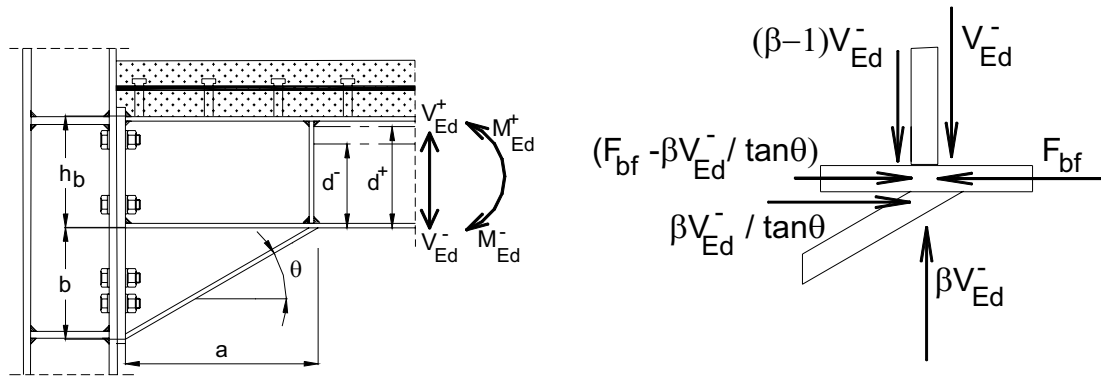


**Figure 5.** Simplified Model of Haunch Connection

In the experimental context of the present paper  $M_{pl,R}^{\pm}$  is determined using the mean measured values of the yield strength of structural steel  $f_y$ , of the concrete strength  $f_c$  and of reinforcement strength  $f_s$ . It should be noted that in actual design where the properties of the materials are defined generally by the nominal or characteristics values  $f_{yk}$ ,  $f_{ck}$  and  $f_{sk}$ , the strengths used to determine the design moment resistance  $M_{pl,Rd}^{\pm}$  would be obtained introducing material overstrength factors, in particular for the structural steel:  $f_{ye} = \gamma_{ov} f_y$  with  $\gamma_{ov} \approx 1.25$ . Also partial safety factors would be used for the materials taking into account the accidental nature of the seismic action (for instance:  $\gamma_a = 1.0$  for the structural steel;  $\gamma_s = 1.0$  for the reinforcing steel; and  $\gamma_c = 1.30$  for the concrete).

Considering the testing arrangement, the design vertical shear  $V_{Ed}^{\pm}$  is evaluated simply as follows:

$$V_{Ed}^{\pm} = M_{Ed}^{\pm} / L' \quad (2)$$

where :  $L' = L - a$  (see Figures 1 to 5)

In actual design,  $V_{Ed}^{\pm}$  would be given by:

$$|V_{Ed}^{\pm}| = \alpha \frac{M_{pl,Rd}^{+} + M_{pl,Rd}^{-}}{L''} + |V_{Ed,G}|$$

where

$L''$  would be the distance between the two plastic hinges occurring near the ends of the concerned beam span, and

$V_{Ed,G}$  would be the vertical shear at the plastic hinge location due to uniform and concentrated vertical loads acting within  $L''$ .

From the idealized model presented in Figure 5 of an elastic composite beam bearing on an elastic support represented by the haunch flange, the non-dimensional parameter  $\beta^\pm$  (in sagging (+) and hogging (-) bending respectively) may be evaluated considering the force equilibrium and the deformation compatibility at the haunch tip between the beam flange and the haunch flange.

So, in both sagging (+) and hogging (-) bendings,  $\beta^\pm$  is given by:

$$\beta^\pm = \frac{b}{a} \left( \frac{6L'd^\pm + 3ad^\pm + 3bL' + 2ab}{6(d^\pm)^2 + 6bd^\pm + 2b^2 + \frac{6I_{1,2}}{A_b^\pm} + \frac{6I_{1,2}}{A_{hf} \cos^3 \theta}} \right) \quad (3)$$

where:

$I_1$  and  $A_b^+$  are respectively the second moment of area under sagging bending and the associated cross-sectional area of the composite beam;

$I_2$  and  $A_b^-$  are respectively the second moment of area and the cross-sectional area of the composite beam, neglecting the concrete in tension but including reinforcement;

$A_{hf}$  is the area of the haunch flange;

$a$ ,  $b$  and  $\theta$  are the length, the depth and the angle of the haunch, defined in Figure 5;

$d^+$  ( $d^-$ ) is the distance from the plastic neutral axis under sagging bending (hogging bending) to the external face of the lower flange of the beam.

### 2.1.2. Design checking

Firstly, a global check should be satisfied which consists in having the sum of the moment resistances of the two columns above and below the joint greater than the sum of the moments transmitted by the two beams through the haunch that frame into the column. This condition has led to extend the supplementary web plates of the column sufficiently beyond the web panel (over 20 cm).

The strength and the stability of the haunch flange have to be checked using the following conditions:

$$\text{Strength: } A_{hf} \geq \frac{\beta^\pm V_{Ed}^\pm}{f_{y,hf} \sin \theta}; \quad (4)$$

$$\text{Stability: } \frac{c_{hf}}{t_{hf}} \leq 10 \sqrt{\frac{235}{f_{y,hf}}}, \text{ according to class 2 of Eurocode 3 - Part 1.1 [1]} \quad (5)$$

Likewise for the haunch web:

$$\text{Strength: } \tau_{hw}^\pm = \frac{aV_{Ed}^\pm}{2(1+\nu)I_{1,2}} \left[ \frac{L'}{2} - \frac{\beta^\pm}{\tan \theta} \left( \frac{d^\pm}{2} \right) + \frac{(1-\beta^\pm)a}{3} \right] \leq \frac{f_{y,hw}}{\sqrt{3}} \quad (6)$$

$$\text{Stability: } \frac{2a \sin \theta}{t_{hw}} \leq 38 \sqrt{\frac{235}{f_{y,hw}}} \quad (7)$$

(class 2 of Eurocode 3 for a web depth  $2a \sin \theta$  in compression)

$f_{y,hf}$  and  $f_{y,hw}$  are the mean yield strengths of the haunch flange and the haunch web respectively;

$c_{hf}$  and  $t_{hf}$  are the flange outstanding and the flange thickness of the haunch respectively;

$t_{hw}$  is the haunch web thickness.

Yielding and shear buckling of the web of the steel beam part above the haunch should be checked on the basis of the hereafter vertical shear:

$$V_{Ed,b}^{\pm} = (1 - \beta^{\pm}) V_{Ed}^{\pm} \quad (8)$$

noting that  $V_{Ed,b}^{\pm}$  is, in general, significantly less than  $V_{Ed}^{\pm}$ . It may be observed from (8) that the direction of the beam vertical shear  $V_{Ed,b}^{\pm}$  is opposite to that developed outside the haunch region when  $\beta^{\pm} > 1.0$  (which occurs most of the time)

The local resistance due to the concentrated load  $\beta^{\pm} V_{Ed}^{\pm} / \tan \theta$  where the haunch flange intersects the column flange should be checked and the column web should be stiffened if necessary; likewise the steel beam web at the haunch tip should possess sufficient strength to resist the concentrated load  $\beta^{\pm} V_{Ed}^{\pm}$ ; generally, it needs to be stiffened transversally.

Yielding in tension of the top flange of the steel beam part above the haunch and of the slab reinforcement under hogging bending should be checked appropriately. For instance, the tension stress in the steel flange is given by:

$$\sigma_{bft,Ed} = \frac{M_{Ed}^{-} + V_{Ed}^{-} (1 - \beta^{-}) a}{I_2} (h_b - d^{-}) - \frac{\beta^{-} V_{Ed}^{-} / \tan \theta}{I_2} \left[ (h_b - d^{-}) d^{-} - \frac{I_2}{A_b^{-}} \right] \quad (9)$$

A similar expression of (9) may be obtained for  $\sigma_{s,Ed}$  in the reinforcement. Conditions  $\sigma_{bft,Ed} = f_y$  and  $\sigma_{s,Ed} = f_{ys}$  lead to a minimum value  $\beta_{min}^{-}$  of  $\beta$ . If  $\beta$  is less than minimum value  $\beta_{min}^{-}$  the area of the haunch flange or the haunch geometry should be modified.

Also yielding of the lower flange of the steel beam and concrete strength in compression of the slab under sagging bending should be checked leading to satisfy other minimum value  $\beta_{min}^{+}$ .

Recommendations are made to use full penetration butt welds to connect the end of the beam and the haunch to the end-plate, the haunch to the lower flange of the beam and transverse stiffeners to the flanges of the beam and the column. According to Eurocode 8, full penetration butt welds are deemed to satisfy the overstrength criterion with regard to the adjacent structural steel.

Nevertheless if two-sides fillet welds were considered to connect webs of the beam and the haunch to the end-plate, also to connect the haunch web to the beam flange and the transverse stiffeners to the beam, the following requirement of Eurocode 8 should be met:

$$R_d \geq \alpha R_{ye};$$

where:

$R_d$  is the resistance of the two fillet welds;

$R_{ye}$  is the plastic resistance of the connected dissipative member based on the mean measured value of yield stress of material (adopting a value  $\gamma_{ov} R_{fy}$ , where  $\gamma_{ov}$  is the overstrength factor, in a design context).

## 2.2. Joint Static Design

The joint static design was based on the component method of Eurocode 3 – Part 1-8 [3] considering the joint as an assembly of simple components whose mechanical properties are clearly identified and able to characterize the whole behaviour of the joint generally expressed in terms of moment-rotation curve. A refined model for the general case of haunched composite beam-to-

column joint is shown in figure 6. All components are modelled physically by translational springs and are able to simulate the transmission of internal forces in the joint as tension, compression, bending or shear.

The particular case of haunched steel joints is very partially covered in clause 6.1.1 (2) of Eurocode3 Part 1-8.

It can be seen in Figure 6 that groups of springs may act in parallel or in series. The springs presented in this figure deal with the following components:

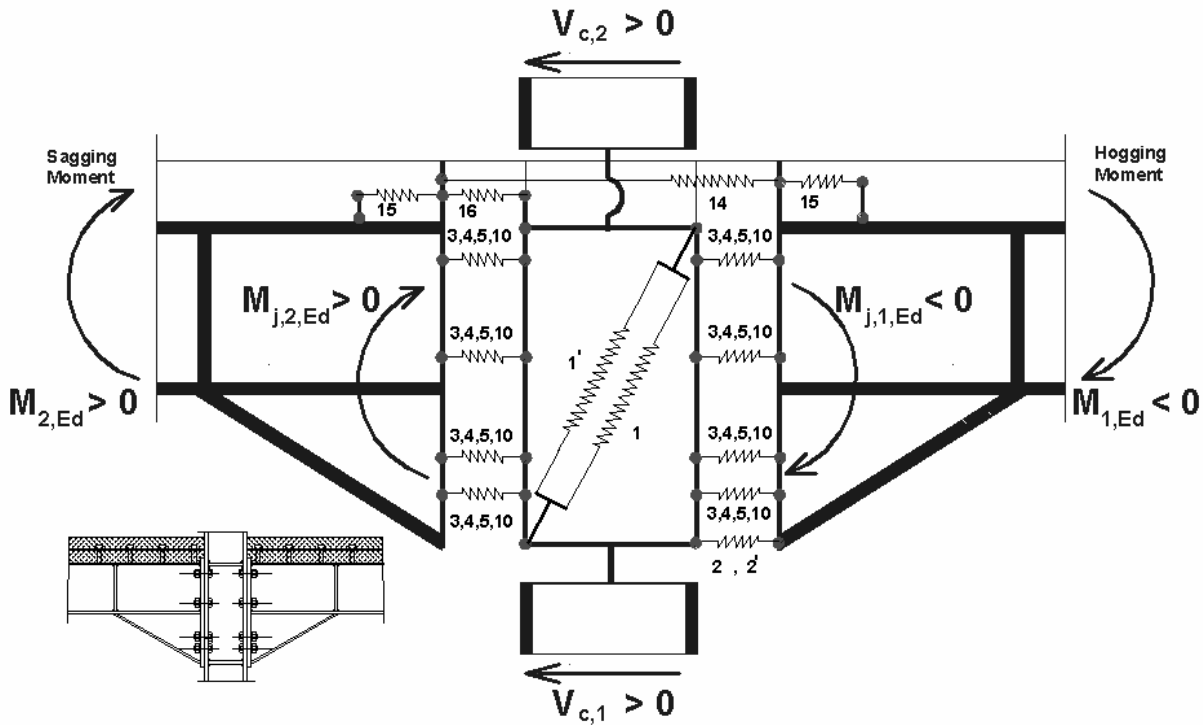


**Figure 6.** Component model for a composite beam-to-column haunched joint

Column web panel in shear (1); effect of concrete encasement on the stiffness and strength of the web panel (1');

Column web in transverse compression (2); effect of concrete encasement on the stiffness and strength of the column web (2');

Column web in tension (3);

Column flange in bending (4);

End-plate in bending (5);

Bolts in tension (10);

Longitudinal steel reinforcement in tension (14);

Shear connection (15);

Slab in compression facing the column (16).

In hogging bending, taking into account the position of a transverse stiffener just in front of the haunch flange, the centre of compression is assumed to be located at mid-thickness of the haunch flange. According to Eurocode 3 – Part 1-8 [3], the resistance moment in hogging bending  $M_{j,R}^{-(th)}$  may be determined from:

$$M_{j,R}^{-(th)} = F_{tr,s,R} \cdot h_{sr}^- + \sum_r F_{tr,R} \cdot h_r^- \quad (10)$$



where:

$F_{tr,R}$  is the effective design tension resistance of bolt-row  $r$ ;

$F_{tr,s,R}$  is the design tension resistance of a row  $r$  of the reinforcing bars included within the effective width of the concrete flange (adopting an effective width  $b_{eff}^- = (\ell_0 / 4) / (0.25 / 0.15)$  where  $\ell_0$  is the cantilever span and where 0.25/0.15 is an amplification factor for hogging bending zone in accordance with clause 5.4.1.2 in Eurocode 4.1.1 [4];

$h_{sr}^-$  and  $h_r^-$  are the distances from row  $r$  of reinforcing bars or bolts to the centre of compression,  $r$  is the number of a particular row.

The tension resistance  $F_{tr,R}$  of bolt-row  $r$  as an individual bolt-row should be taken as the smallest value of the tension resistance for an individual bolt-row of the following basic components: the column web in tension  $F_{t,wc,R}$ , the column flange in bending  $F_{t,fc,R}$ , the end-plate in bending  $F_{t,ep,R}$  and the beam web or the haunch web in tension  $F_{t,wb,R}$ .

Dealing with the bolt-rows closest to the centre of compression, a reduction of their tension resistances may be applied in such a way that:

$$F_{tr,s,R} + \sum_r F_{t,R} \leq \min(F_{c,wc,R}, F_{c,fb,R}, \frac{V_{wp,R}}{\beta}) \quad (11)$$

where:

$F_{c,wc,R}$  and  $F_{c,fb,R}$  are the resistance of the column web in compression and the resistance of the haunch flange in compression (and partially the web), respectively.

$V_{wp,Rd}$  is the plastic shear resistance of the column web panel (of appropriate slenderness) and

$\beta$  is a transformation parameter defined in clause 7.3.3 of Eurocode 3 Part 1-8:

$$\begin{aligned} \beta_1 &= \left| 1 - M_{j,2,Ed} / M_{j,1,Ed} \right| \leq 2 \\ \beta_2 &= \left| 1 - M_{j,1,Ed} / M_{j,2,Ed} \right| \leq 2 \end{aligned} \quad (12)$$

where:

$\beta_1$  is the value of the transformation parameter  $\beta$  for the right-hand side joint ;

$\beta_2$  is the value of the transformation parameter  $\beta$  for the left-hand side joint;

$M_{j,1,Ed}$  is the moment applied to the right joint at the load introduction cross section (figure 6);

$M_{j,2,Ed}$  is the moment applied to the left joint at the load introduction cross section (figure 6);

In the present study,  $\beta = 1$  for the T joint configuration and  $1.5 \leq \beta \leq 2.0$  for the cruciform one.

Provided that the axial force  $N_{Sd}$  in the connected member does not exceed 10% of the axial cross-sectional resistance  $N_{pl,Rd}$  of its cross-section, the initial rotational stiffness  $S_{i,ini}$  of a joint, for a moment  $M_{j,Sd}$  less than the moment resistance  $M_{j,Sd}$  of the joint, may be obtained from:

$$S_{j,ini}^{-(th)} = E_a (z_{eq}^-)^2 \left[ \frac{1}{k_1} + \frac{1}{k_2} + \frac{1}{k_{eq}^-} \right]^{-1} \quad (13)$$

$$k_{eq}^- = \frac{\sum_r k_{eff,r} h_r^-}{z_{eq}^-} \quad ; \quad z_{eq}^- = \frac{\sum_r k_{eff,r} (h_r^-)^2}{\sum_r k_{eff,r} h_r^-} \quad ; \quad k_{eff,r} = \left[ \sum_i \frac{1}{k_{i,r}} \right]^{-1} \quad (14)$$

where:

$E_a$  is the modulus of elasticity of steel;

$z_{eq}^-$  is the equivalent lever arm,

$k_1$  is the stiffness coefficient for the column web panel in shear,

$k_2$  is the stiffness coefficient for the column web in compression,

$k_{eq}^-$  is the equivalent stiffness coefficient related to the group of bolt-rows and longitudinal reinforcement in tension (the latter modified by the reduction factor  $k_{slip}$  due to the slip effect of the shear connection as given by clause (A5) in Eurocode 4 Part 1-1 [4];

$k_{eff,r}$  is the effective stiffness coefficient for layer  $r$ ; and

$k_{i,r}$  is the stiffness coefficient representing component  $i$  relative to layer  $r$ ;

$h_r^-$  is the distance between layer  $r$  and the centre of compression.

In sagging bending, assuming a centre of compression located at the mid-thickness of the concrete slab (only considering the thickness above the sheeting ribs), expressions similar to the above ones may be adopted, replacing  $F_{c,wc,R}$  and  $F_{c,fb,R}$  by the bearing resistance  $F_{c,R}$  between the slab and the column and introducing a specific stiffness coefficient  $k_c$  for the slab in compression. More details may be found in Ciutina [14].

$$M_{j,R}^{+(th)} = \sum_r F_{tr,R} \cdot h_r^+ \quad (15)$$

$$S_{j,ini}^{+(th)} = E(Z_{eq}^+)^2 \left[ \frac{1}{k_1} + \frac{1}{k_c} + \frac{1}{k_{eq}^+} \right]^{-1} \quad (16)$$

Under reversal bending moment, the total force due to the compression of the slab on one side plus the tension of the reinforcement on the other side should be transferred to the column using the resistances of two mechanisms Eurocode 8 - Part 1 (Annex C) [5]:

- a direct compression on the column flange:

$$F_{R1} = b_c d_{eff} (0.85 f_c) \quad (17)$$

where:

$b_c$  is the column flange width,

$d_{eff}$  is the thickness of the slab above the ribs of the profiled sheeting for composite slabs (and overall depth of the slab in case of solid slab);

- a compressed concrete struts inclined to  $45^\circ$  on the column sides:

$$F_{R2} = 0.7 h_c d_{eff} (0.85 f_c) \quad (18)$$

where  $h_c$  is the depth of the column steel section.

In addition the tension strut model requires a tension-tie cross-sectional area:

$$A_T \geq 0.5 \frac{F_{R2}}{f_{sk}} \quad (19)$$

over a width  $h_c$  and fully anchored. This area  $A_T$  is introduced on both sides of the column to account for reversal of bending moments

The resistance offered by the two mechanisms is given by:

$$F_{c,R} = F_{R1} + F_{R2} \quad (20)$$

It is to point out that the presence of haunch in a beam to column connection creates an enlarged panel zone. The distribution of internal forces in a such enlarged panel zone is different from that of

the single panel zone (without haunch). Lee and Uang [8] for welded beam-to-column joint and on the basis of results of finite element analysis and available full-scale test results have developed an analytical procedure to model the stiffness and strength of an enlarged panel zone. In the case of haunched end-plate bolted composite joints the problem is more complex and has not been investigated yet. In the next future one of the objectives of the authors of this paper is to develop a scientific background about this topic. For want of something better, a simplified checking may be used evaluating the panel shear as follows:

$$V_{wp,Ed} = \frac{M_{j2,Ed}}{Z_{eq}^+} - \frac{M_{j1,Ed}}{Z_{eq}^-} - \frac{V_{C2} - V_{C1}}{2} \leq 0.9 A_{vc} \frac{f_{y,cw}}{\sqrt{3}} \quad (21)$$

where

$V_{C1}$  and  $V_{C2}$  are the horizontal forces exerted by the column ends (Figure 6) and  $A_{vc}$  is the shear area of the column.

### 3. PRESENTATION OF THE EXPERIMENTAL INVESTIGATION

#### 3.1. Program of tests

Completing Figures 1 to 4, Table 1 presents the main characteristics of ten full-scale beam-to-column joints (major axis connections) tested at INSA of Rennes-France. All the specimens include bolted end plate connections, with upper and lower external rows of bolts in the case of steel joints and only lower external bolt row in the case of composite joints.

In Table 1, two main Groups of tests may be distinguished:

- Group 1 with full-strength joints with haunches;
- Group 2 with partial strength joints without haunches.

Each group comprises steel and composite joints with T and cruciform arrangements, monotonically or cyclically loaded.

For all the tests, as shown in Figures 1 to 4, transverse stiffeners have been welded to the column flanges in the web-panel. Except for test G13, all the bolts were tightened at their nominal preload. All the welds were made by the semi-automatic inert-gas arc method with full penetration butt welds, using E MAG 136 procedure and T46 4 MM2 H5 consumables, according to European norms (EN 287 and EN 288).

For all the composite specimens (except G18), common characteristics are a full shear connection with welded headed studs  $\Phi = 19$  mm ( $h = 80$  mm or  $100$  mm) and , a composite slab (cast on a steel sheeting COFRASTRA 40) whose cross-section of dimensions  $120 \times 1000$  mm is reinforced by 10 longitudinal rebars  $\Phi 10$  mm and by transverse rebars  $\Phi 10$  mm spaced each 10 cm, with 2 additional transverse rebars near the column flanges to ensure a strut-tie action according to (19).

Although the main objective of the present research is the effect of joint strengthening on the joint seismic performances by introducing haunches, other parameters are considered as the performance of the composite solution in comparison with the steel one (for that, steel reference tests have been performed prior each series of composite tests; i.e. G13, G16 and G19 in comparison with G15, G18 and G20 respectively. The contribution of the column web panel to the global performance of the joint is also analysed.

Table 1. Description of Specimens

Group	Test N°	Arrangement	<u>SPECIMEN</u> -Column -Column web stiffener -Beam	Type of loading	Supplementary web plates (thickness mm) (S235)	End plate Bolt
GROUP (1) FULL – STRENGTH JOINTS WITH HAUNCHES	G16 (steel)	<b>T</b>  (external joint)	HEB300 (S355) ( $f_y = 454 \text{ N/mm}^2$ )  web stiffeners IPE 360 (S235) ( $f_y = 278 \text{ N/mm}^2$ )	cyclic (ECCS)	NO	430×220×25 (S235) ( $f_y = 242 \text{ N/mm}^2$ ) HS10.9 Φ22mm
	G17			monotonic (hogging bending)		745×250×25 (S235) ( $f_y = 242 \text{ N/mm}^2$ ) HS10.9 Φ22mm
	G18			cyclic (ECCS)		
	G22	<b>Cruciform</b> (internal joint)	HEB200 (S355) ( $f_y = 350 \text{ N/mm}^2$ )  web stiffeners IPE 240 (S235) ( $f_y = 347 \text{ N/mm}^2$ )	cyclic (ECCS)	NO	510×160×20 (S235) ( $f_y = 320 \text{ N/mm}^2$ ) HS10.9 Φ20mm
	G23				YES (2×12)	
GROUP (2) PARTIAL – STRENGTH JOINTS	G13 (steel)	<b>T</b>  (external joint)	HEB300 (S355) ( $f_y = 454 \text{ N/mm}^2$ )  web stiffeners IPE 360 (S235) ( $f_y = 278 \text{ N/mm}^2$ )	cyclic (ECCS)	NO	500×200×15 (S235) HS10.9 Φ22mm
	G15					430×220×15 (S235) ( $f_y = 280 \text{ N/mm}^2$ ) HS10.9 Φ22mm
	G19 (steel)	<b>Cruciform</b>  (internal joint)	HEB200 (S355) ( $f_y = 413 \text{ N/mm}^2$ )  web stiffeners IPE 240 (S235) ( $f_y = 340 \text{ N/mm}^2$ )		NO	390×160×15 (S235) ( $f_y = 296 \text{ N/mm}^2$ ) HS10.9 Φ20mm
	G20				YES (2×6)	330×160×15 (S235) ( $f_y = 296 \text{ N/mm}^2$ ) HS10.9 Φ20mm
	G21				YES (2×10)	330×160×20 (S235) ( $f_y = 320 \text{ N/mm}^2$ ) HS10.9 Φ20mm

### 3.2. Test Setups

As presented in Figure 7 in the case of joints with a T arrangement the vertical load was applied at the end cross-section of the beam by means of an hydraulic servo controlled actuator.

In the case of joints with a cruciform arrangement two vertical loads were applied at each cantilever beam end on each side of the column (Figure 8) by two hydraulic servo controlled actuators acting out-of- phase for creating opposite directional loads. For all the tests the column was connected at its lower end to the platform by a fixed pinned support and at its upper end to a rigid braced frame by a moveable pinned support.

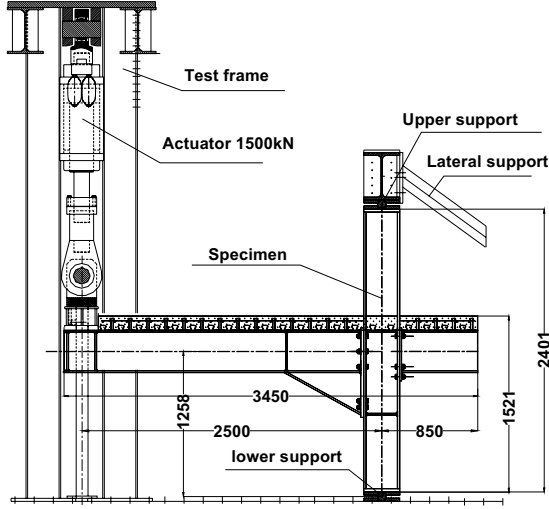


Figure 7. Test setup (T arrangement )

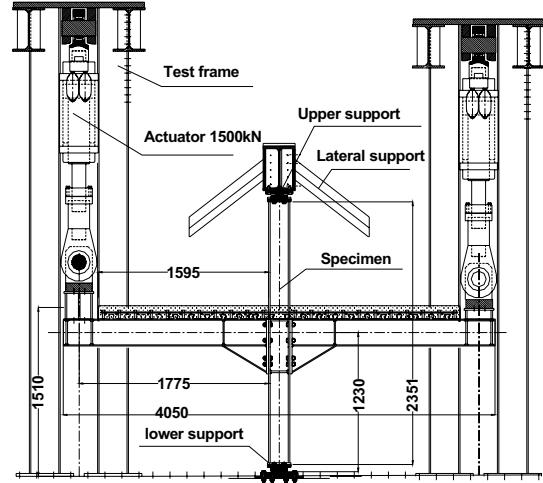


Figure 8. Test setup (Cruciform arrangement )

### 3.3. Loading Procedures

In the case of monotonic tests, increases in joint rotation were applied continuously up to failure of the joint. For cyclic tests, the ECCS procedure was followed [15] in order to simulate the seismic action. The implementation of this procedure requires the first determination of two conventional elastic limit rotations  $\Phi_y^-$  and  $\Phi_y^+$  associated with the corresponding elastic limit moments in hogging bending  $M_{j,y}^-$  and sagging bending  $M_{j,y}^+$  respectively.

As shown in Figure 9 the determination of such conventional elastic limit moments is obtained from the intersection between the initial tangent of slope  $S_{j,ini}$  to the monotonic curve and the particular tangent having a slope equal to  $S_{j,ini}/10$ . Due to the difficulty to determine practically the initial tangent to the monotonic curve, the authors propose to adopt a similar definition to the one given in Eurocode 3 [1-3]; then, the initial stiffness is defined as the slope of the secant line joining the origin and the point on the monotonic curve located at ordinate  $\frac{2}{3}M_{j,y}$ ; this construction requiring a short iterative procedure. Having no monotonic moment-rotation curves of reference for most of the tests presented in table 1, the skeleton curve enveloping the peaks of the first cyclic M- $\Phi$  curves have been used to determine the conventional characteristics  $\Phi_y^{+/-}$  useful to apply the ECCS procedure to the cyclic tests. So, the following simplified values have been adopted:

$$\Phi_y^- = \Phi_y^+ = \Phi_y = 2 \text{ mrad for external joints with a T configuration and;}$$

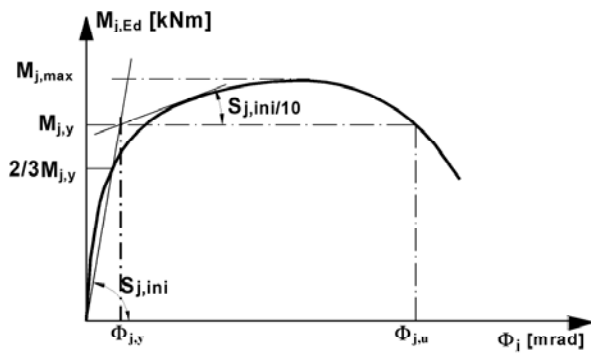
$$\Phi_y^- = \Phi_y^+ = \Phi_y = 4 \text{ mrad for internal joint with a cruciform configuration.}$$

Figure 10 shows the successive increases of rotation corresponding to the ECCS cyclic loading procedure:

$$4 \text{ cycles successively for the ranges } \pm \frac{\Phi_y}{4}, \pm \frac{\Phi_y}{2}, \pm \frac{3}{4}\Phi_y, \pm \Phi_y;$$

followed up to failure by series of 3 cycles each with a range  $\pm 2n\Phi_y$  where  $n = 1, 2, 3, \dots$

Figures 11 to 14 show the experimental arrangements used for the tests.



**Figure 9.**  $M-\Phi$  characteristic definitions

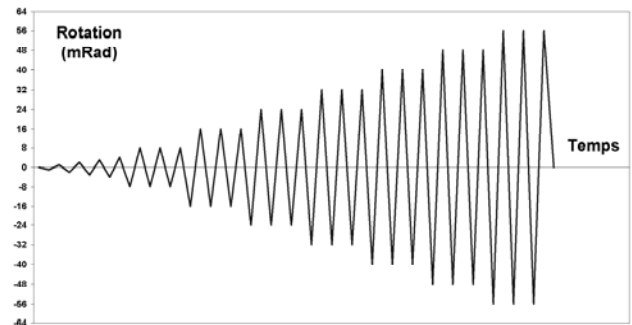


**Figure 10.** Load History

GROUP (1)

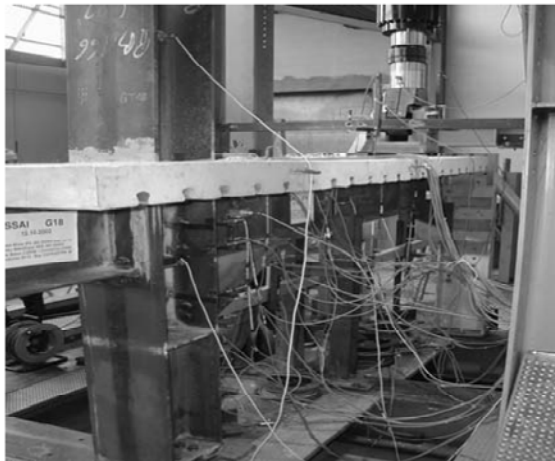


**Figure 11.** T with an haunch

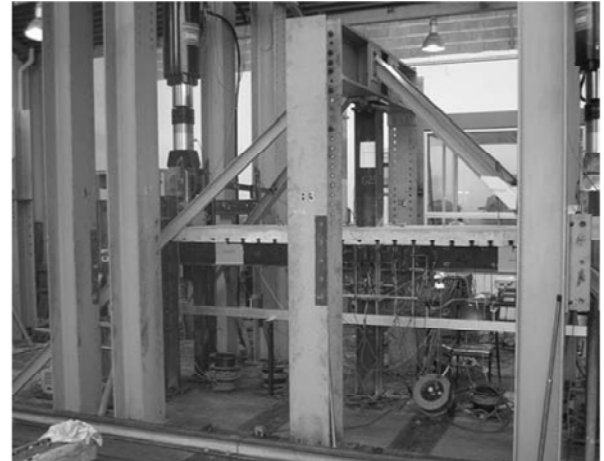


**Figure 12.** haunched joint

GROUP (2)

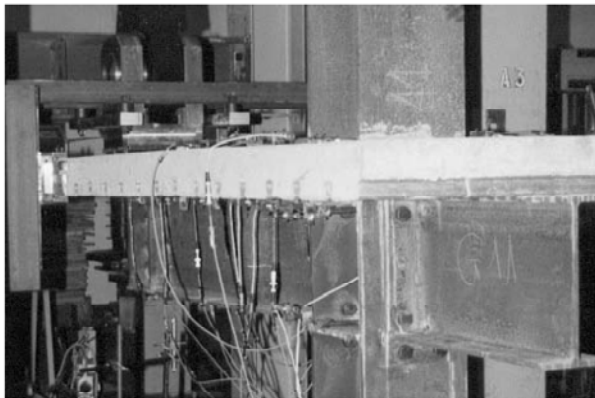


**Figure 13.** T without haunch



**Figure 14.** joint without haunch

**T arrangement**

**Cruciform arrangement  
(unsymmetrically loaded)**

### 3.4. Measuring Arrangement and Data Processing

The measurement system is shown in Figure 15 (Test G18) for a T arrangement and in Figure 16 (Test G23) for a cruciform arrangement. It comprises inclinometers for rotation measurements and transducers to measure deflection of the beams, slip between the composite slab and the steel flange in several locations along the beams, and displacements in significant zones of the joint:

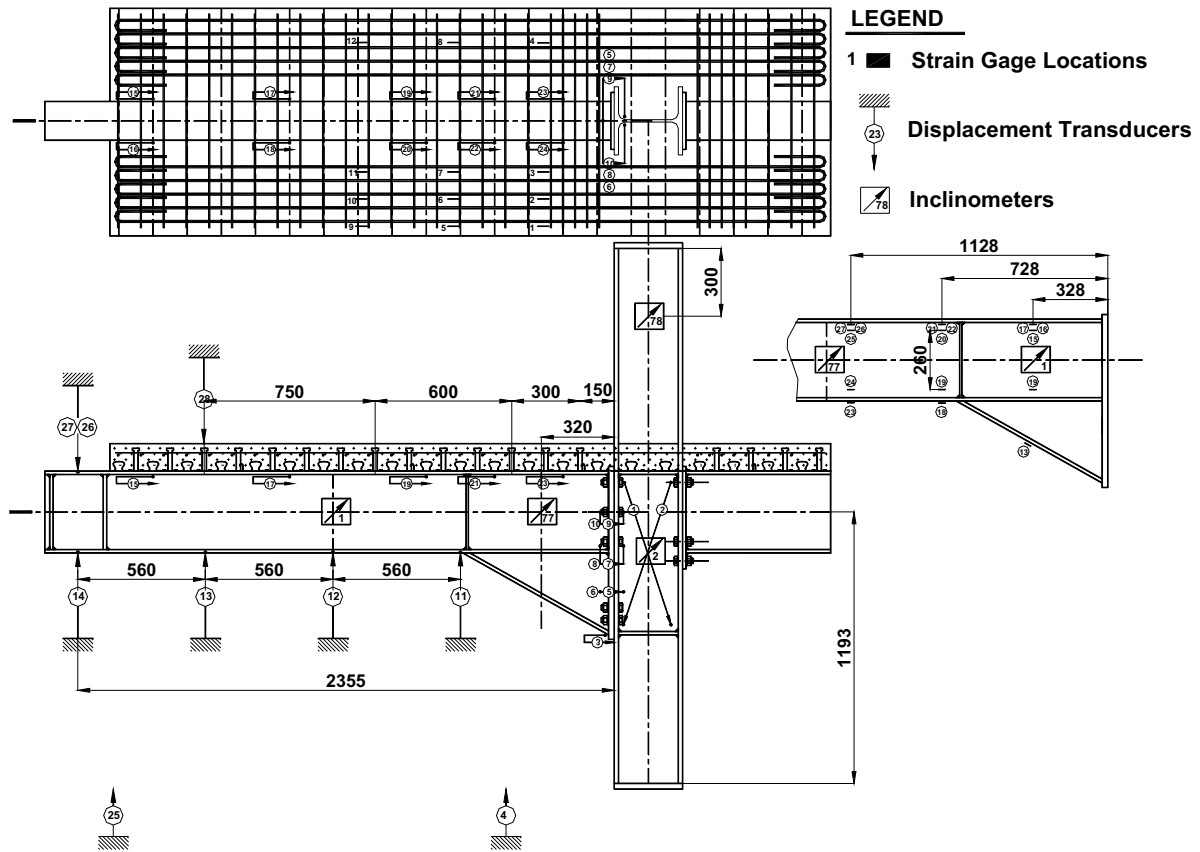


Figure 15. Measurement system used for T arrangement

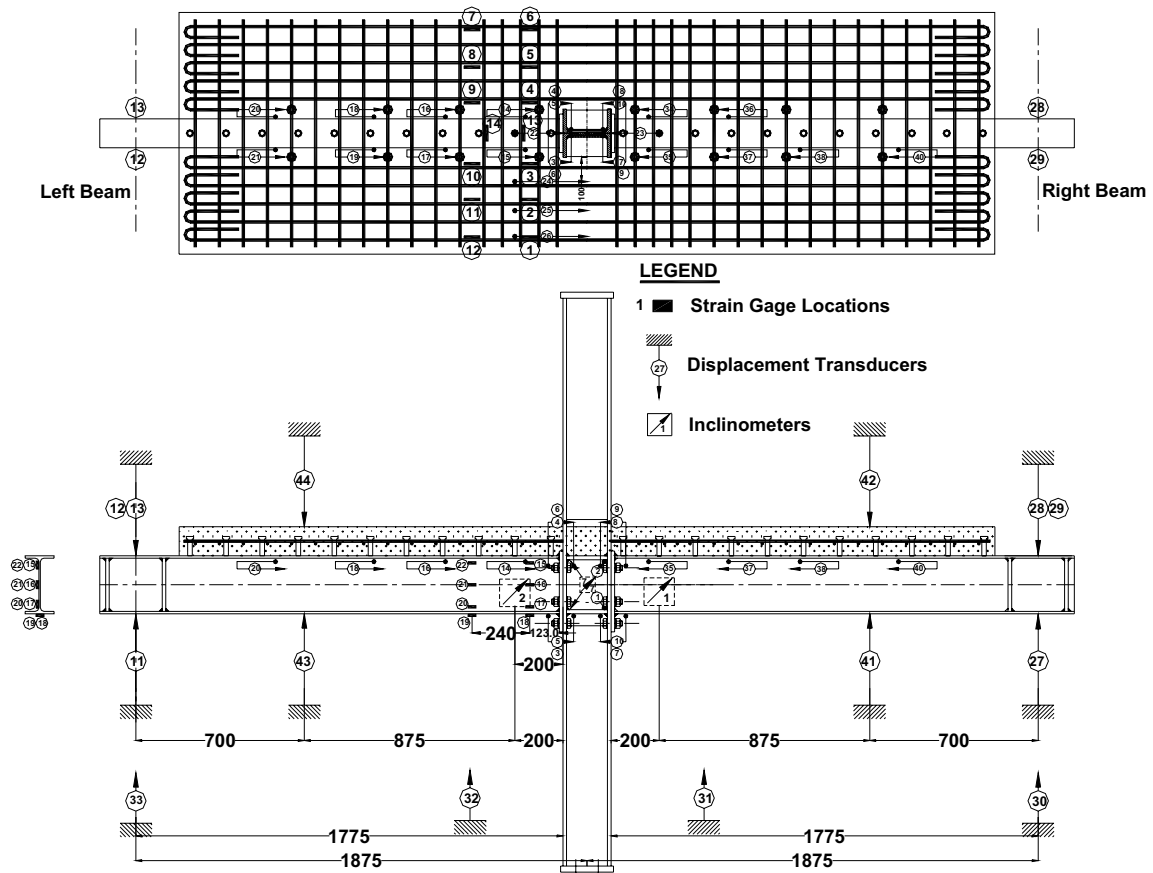


Figure 16. Measurement system used for Cruciform arrangement

elongation of bolts, flexural bending of end-plates and column flanges, shear deformation of the column web panel. Strain measurements are made for some tests by means of electric gauges bonded on longitudinal and transversal rebars near the column, in several beam cross-sections near the joint or inside the haunch.

To determine the moment-rotation curves presented later on the following definitions have been considered:

- the bending moment  $M_j$  applied to the joint is located at the column face, hence given by the product:

$$M_j = FL \text{ (kN.m)} \quad (21)$$

where  $L$  is the appropriate lever arm defined in Figures 1 to 4.

- the total joint rotation  $\Phi_j$ , including the connection rotation and the column web panel distortion, is deduced from the difference between the two inclinometers  $I_2$  (distinguishing  $I_{2L}$  on the left side and  $I_{2R}$  on the right side in the case of a cruciform joint) and  $I_1$ :

$$\Phi_j = I_2 - I_1 \text{ (mrad)} \quad (22)$$

For end-plate connections (without haunches) where the beam contribution to the joint rotation is low, inclinometer  $I_2$  has been located at a short distance from the column flange, equal to about the half depth of the steel beam. On the contrary, for end-plate connections with haunches, where the joint rotation is due essentially to the beam rotation with the formation of a plastic hinge near the end of the haunch, inclinometer  $I_2$  has been located at a distance from the end of the haunch, generally greater or at least equal to the depth of the steel beam. Inclinometer  $I_1$  gives the rotation due to the flexural bending of the column.

For joints with haunches, a supplementary inclinometer  $I_3$  is placed on the beam at mid-length of the haunch; allowing to distinguish the rotation due to the connection  $\Phi_{\text{connection}} = (I_3 - I_1)$  and the beam rotation  $\Phi_{\text{beam}} = (I_2 - I_3)$ .

A global evaluation of the column web panel distortion can be deduced from the algebraic elongations  $\Delta_1$  and  $\Delta_2$  of the two diagonal transducers 1 and 2 as follows:

$$\gamma = \sqrt{a^2 + b^2} (\Delta_1 - \Delta_2) / (2ab) \quad (23)$$

where  $a$  and  $b$  are the horizontal and vertical sizes of the web panel.

Other rotations of the connection part have been deduced from elongation measurements of bolt rows, in the longitudinal direction, located on the width of end-plates. These values have been compared to the ones directly measured.

## 4. EXPERIMENTAL RESULTS AND INTERPRETATION

### 4.1. Global Results For Rotational Stiffness, Moment Resistance And Rotational Capacity

All the experimental values collected in table 2 are defined at the load-introduction cross-section of the connection, i.e. the interface between end-plate and column flange. Elastic limit moments  $M_{j,y}^{(exp)+}$  in sagging bending and  $M_{j,y}^{(exp)-}$  in hogging bending, maximum bending moments  $M_{max}^{(exp)+/-}$ , initial rotational stiffnesses  $S_{j,ini}^{(exp)+/-}$  and global ultimate rotations  $\Phi_u^{(exp)+/-}$  (adding the joint and beam contributions) have been deduced from monotonic (test G17) or skeleton curves enveloping the peaks of cyclic  $M - \Phi$  curves; as a reminder the exact definitions adopted for these



characteristics were defined before (figure 9). Theoretical values of rotational stiffnesses  $S_{j,ini}^{(th)+/-}$  and moment resistances  $M_{j,R}^{(th)+/-}$  have been calculated from the above-mentioned formulae, using mean values of the material properties and geometrical characteristics measured on each specimen (safety factors for materials being considered equal to one).

**Table 2.** Theoretical (TH) and Experimental (EXP) Results

TEST N°	$\frac{S_{j,ini}^{(th)+}}{S_{j,ini}^{(th)-}}$ (kN.m/rad)	$\frac{S_{j,ini}^{(exp)+}}{S_{j,ini}^{(exp)-}}$ (kN.m/rad)	$\frac{M_{j,R}^{(th)+}}{M_{j,R}^{(th)-}}$ (kN.m)	$\frac{M_{j,y}^{(exp)+}}{M_{j,y}^{(exp)-}}$ (kN.m)	$\frac{M_{max}^{(exp)+}}{M_{max}^{(exp)-}}$ (kN.m)	$\frac{\Phi_u^{(exp)+}}{\Phi_u^{(exp)-}}$ (mrad)	failure mode
<b>GROUP (1)</b>							
<b>FULL – STRENGTH JOINTS WITH HAUNCHES</b>							
(cyclic) <b>G16</b> (steel)	179200/177300	120000/93500	598/608	483/484	620/560	60/51	yielding of the steel beam
(monotonic) <b>G17</b> (composite)	--/183700	--/126500	--/728	--/512	--/640	--/88	yielding of the composite beam
(cyclic) <b>G18</b> (composite)	207500/183700	132100/115900	696/728	541/494	740/670	40/35	yielding of the beam (limited by stud rupture)
(cyclic) <b>G22</b> (steel)	49900/53500	24900/22500	197/209	194/183	198/191	50/58	yielding of the steel beam
(cyclic) <b>G23</b> (composite)	87300/65900	150800/72300	306/308	290/245	345/255	54/45	yielding of the steel beam
<b>GROUP (2)</b>							
<b>PARTIAL – STRENGTH JOINTS WITHOUT HAUNCHES</b>							
(cyclic) <b>G13</b> (steel)	53600/53600	32400/32400	224/224	260/260	300/326	30/33	beam flange to end-plate weld rupture
(cyclic) <b>G15</b> (composite)	74600/38800	41100/53600	282/299	237/300	326/340	25/28	weld rupture under hogging bending
(cyclic) <b>G19</b> (steel)	16000/16000	8500/8500	74/74	94/72	125/105	70/70	beam flange to end-plate weld rupture
(cyclic) <b>G20</b> (composite)	35890/15830	50517/22837	150/150	162/101	237/150	48/58	beam flange to end-plate weld rupture
(cyclic) <b>G21</b> (composite)	44810/18940	55182/21983	172/157	194/126	235/159	25/31	beam flange to end-plate weld rupture

In general, for joints equipped with haunches, it is observed that theoretical values of stiffness and moment resistance are greater than the experimental ones (except the stiffness for test G23). The overstrength ratio between the theoretical moment resistance and the elastic limit moment (exerted by the haunched beam) ranges from 1.1 in sagging bending to 1.3 in hogging bending. These values appear sufficient compared to factor  $\alpha = 1.1$  already mentioned in relationship (1) to satisfy the principle of capacity design (leading to a main dissipation outside the joint). Consequently for tests of Group 1, the flexural yielding occurs systematically in the beam at the end of the haunch providing a rotation capacity generally greater than 35 mrad. As a reminder, this rotation capacity is required by Eurocode 8-1 (clause 6.6.4 (3)) in dissipative zones to consider frames in high ductility class (DCH) for which the behaviour factor  $q$  is equal to 6 at least.

A reduction in rotation capacity often appears for tests of group 2 (for T as well as cruciform joint arrangements) due to the premature rupture in low-cycle fatigue of welds connecting end-plate to the beams. It should be pointed out that some details of the joint may lead to a premature rupture of welds (for example, an increase of the thickness of end-plate and supplementary web plates between test G20 and test G21 produced a premature rupture of the weld connecting beam flanges to the end-plate, possibly explained by some lack of flexibility of the end-plates. Contrary to the

haunched joints, only the medium ductility class (DCM) seems acceptable for the partial-strength composite joints since the rotation capacity may be limited to 25 mrad (particularly in sagging bending).



**Figure 17.** Yielding rupture in the beam at the haunch toe



**Figure 18.** Yielding rupture in the beam at the haunch toe



**Figure 19.** End-plate deflection



**Figure 20.** Rupture of welds and fracture of beam web in heat affected zone (HAZ)

#### **T arrangement**

#### **Cruciform arrangement (unsymmetrical loaded)**

Whereas all failures of group 2 occurred by rupture of welds connecting beams to end-plates (Figures 19 and 20), failures of group 1 resulted from excessive flexural yielding of the steel section at the haunch tip (Figures 17 and 18). It is to underline that the haunch stiffening effect leads to a strong reduction of the deformations in the joint, these latter ones being transferred in the beam, and consequently to a limitation of risks of low-cycle fatigue in such components as welds, bolts and end-plates.

#### **4.2. Comments on the Moment-Rotation curves**

For test G20 of group 2 (without haunch) moment-rotation curves in Figures 21-1, 21-2 and 21-3 on the left side of the figure are related to the left side of the joint and show the respective contribution of the load introduction cross-section (connection) rotation  $\Phi_{li}$  (Figure 21-1) and the column web panel rotation  $\Phi_{wp}$  (Figure 21-2) to the global joint rotation  $\Phi_j$  (Figure 21-3). A similar comparison is made in Figures 22-1, 22-2 and 22-3 on the right side of the same test G20.

Considering the rotation ranges, the contribution of the connection rotation  $\Phi_{li}$  to the global joint rotation  $\Phi_j$  increases from 20% at the beginning of the test to 50% at the end before rupture of welds connecting beams to end-plates. The unsymmetrical behaviour observed in Figures 21 and 22 between left side and right sides of the joint is not only a consequence of the composite behaviour of the beams but also the plastic state initiated during the first cycles according to the sense of rotation.

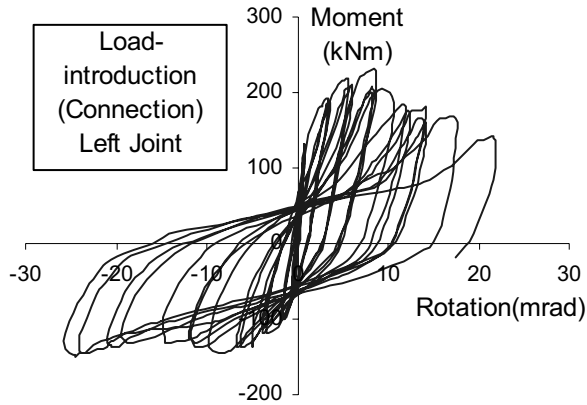


**Figure 21-1.**  $M_{j,2,Ed} - \Phi_{li}$  (Test G20)

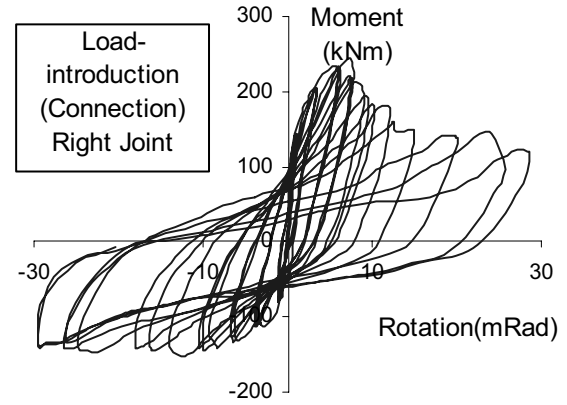


**Figure 22-1.**  $M_{j,1,Ed} - \Phi_{li}$  (Test G20)

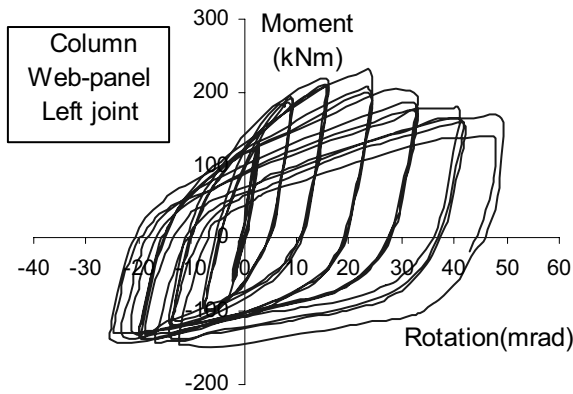


**Figure 21-2.**  $M_{j,2,Ed} - \Phi_{wp}$  (Test G20)

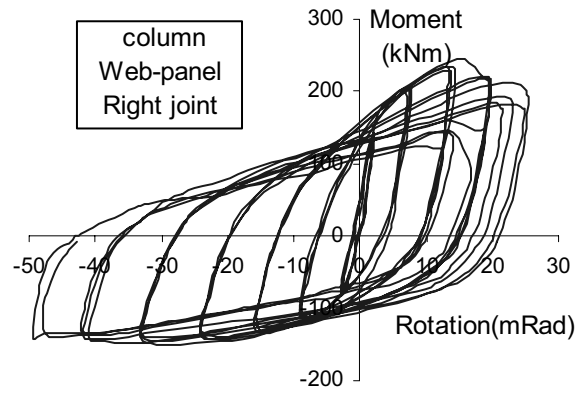


**Figure 22-2.**  $M_{j,1,Ed} - \Phi_{wp}$  (Test G20)

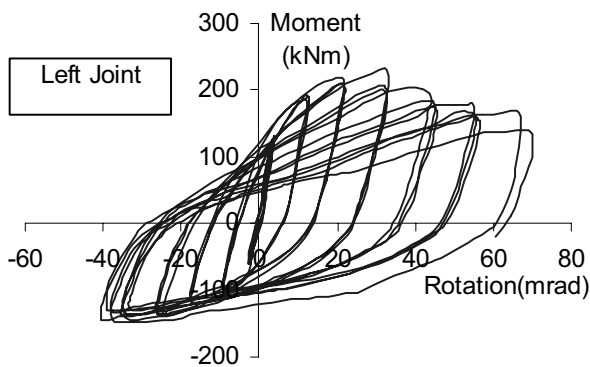


**Figure 21-3.**  $M_{j,2,Ed} - \Phi_j$  (Test G20)

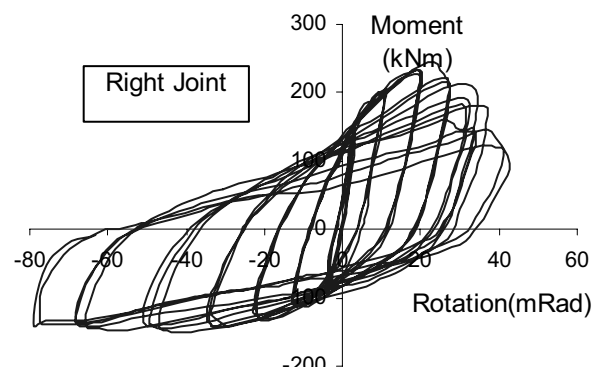


**Figure 22-3.**  $M_{j,1,Ed} - \Phi_j$  (Test G20)

For test G23 of group 1 (with haunch) moment-rotation curves of the connection, the column web panel, the joint and the beam (at the haunch tip) to the right side of the joint are presented in Figures 23-1, 23-2, 23-3 and 23-4 respectively. Considering the rotation ranges, the contribution of the connection rotation  $\Phi_{li}$  to the global joint rotation  $\Phi_j$  remains rather limited at the beginning of

the test in comparison to  $\Phi_{wp}$  and greater at the end of the test before beam failure to reach 45 % of the global joint rotation  $\Phi_j$  ; this latter remaining clearly lower (only 20%) than the beam rotation outside the haunch tip (as shown in Figure 23-4).

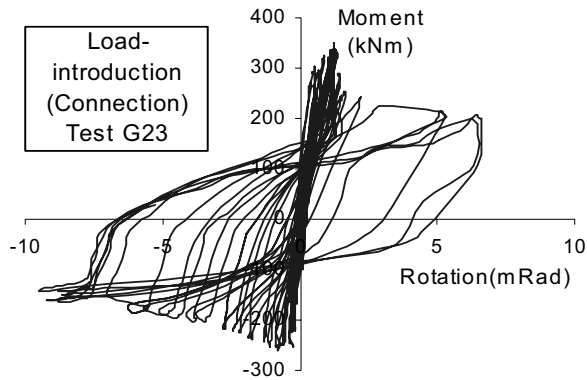


**Figure 23-1.**  $M_{j,2,Ed} - \Phi_{li}$  ( Right Joint)

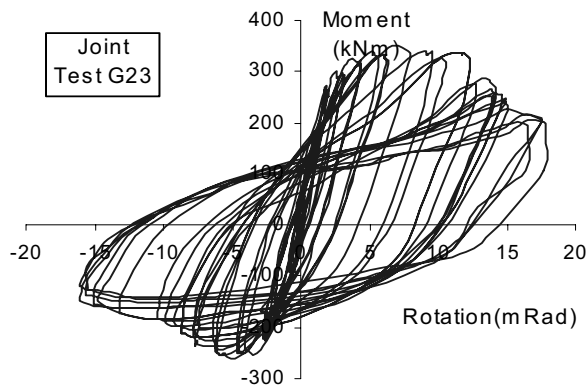


**Figure 23-2.**  $M_{j,2,Ed} - \Phi_{wp}$  ( Right Joint)

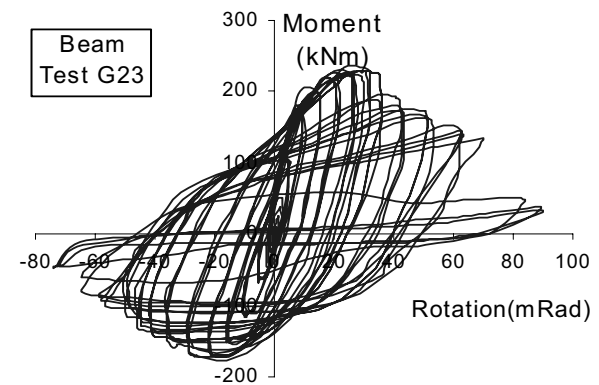


**Figure 23-3.**  $M_{j,2,Ed} - \Phi_j$  ( Right Joint)

**Figure 23-4.**  $M_{b,2,Ed} - \Phi_b$  ( Right Beam)

In figures 24-1 to 24-4 a comparison is made between the moment-rotation curves of the connection (Figure 24-1), the column web panel (Figure 24-2), the joint (Figure 24-3) and the beam (Figure 24-4) obtained for the monotonic test G17 and the corresponding cyclic test G18. For these tests, with a T arrangement, the same observations than the previous ones for tests G20 and G23 dealing with the relative contribution of the connection, the column web panel, the joint and the beam to the global rotation can be made.

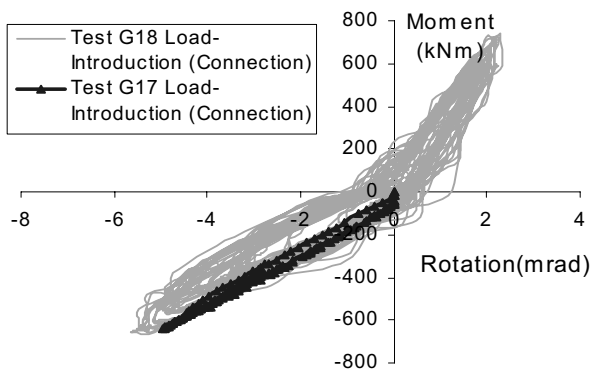


**Figure 24-1.**  $M_{j,Ed} - \Phi_{li}$

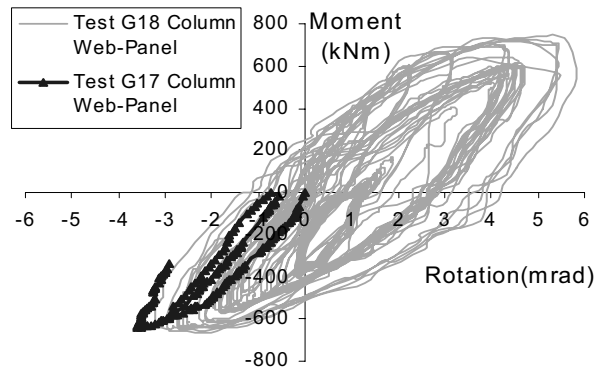


**Figure 24-2.**  $M_{j,Ed} - \Phi_{wp}$

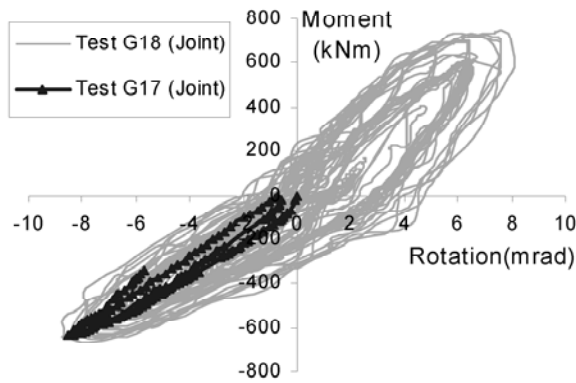


Figure 24-3.  $M_{j,Ed} - \Phi_j$

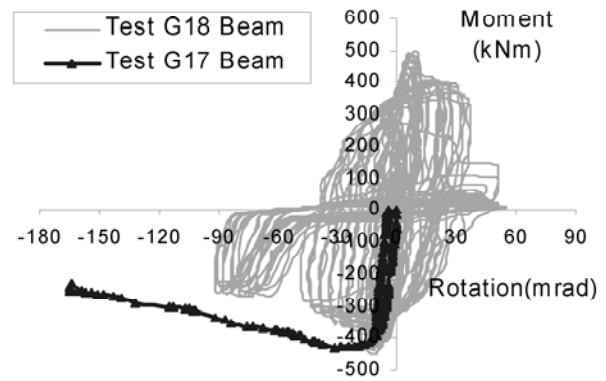


Figure 24-4.  $M_{b,Ed} - \Phi_b$

In addition, except for the beam rotation, it can be observed that the monotonic curves in hogging bending of the test G17 are enveloped by the cyclic curves of the test G18. The decrease of the beam cross-section moment resistance in hogging bending is mainly due to the yielding and the flange-web buckling of the beam cross-section near the haunch tip (Figure 25-1) which appears more pronounced in cyclic loading with the low-cycle fatigue effect than in monotonic loading. In sagging bending risks of flange buckling are excluded by the stiffening effect of the composite slab.

The stiffening effect of the composite slab is confirmed again in Figure 25-2 where skeleton curves enveloping the peaks of the cycles are compared between the two tests G23 and G22. In sagging bending the maximum moment of the composite test G23 appears 64% greater than the maximum moment of the steel companion test G22 ; in hogging bending the maximum moment of the composite test is only 32% greater than the corresponding steel one.

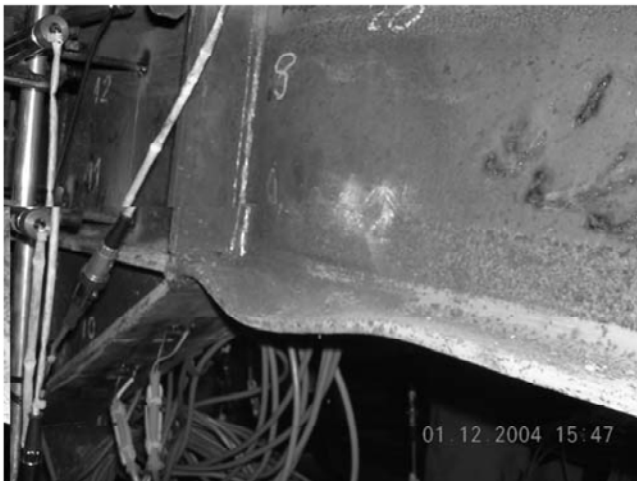


Figure 25-1. Buckling of beam web and beam bottom flange: haunch specimens

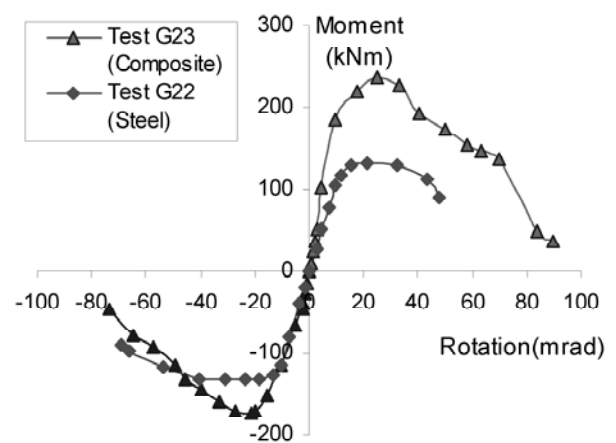
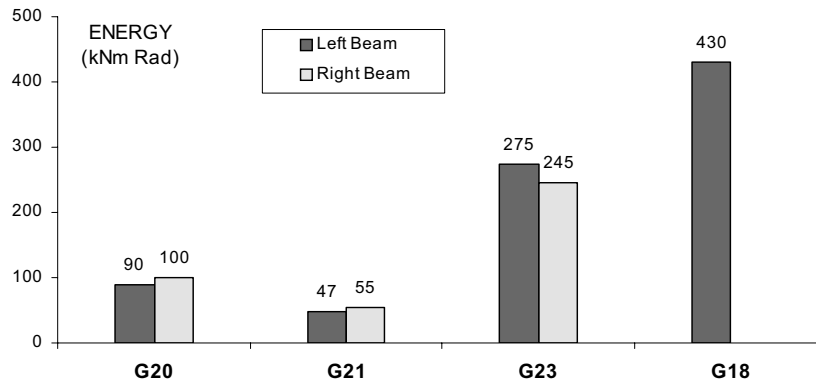


Figure 25-2. Moment-rotation envelopes: haunch specimens (right beam )

#### 4.3. Comparisons of Plastic Energy Dissipation Capacities

These results may be also interpreted in terms of cumulative plastic energy dissipation for all the cycles. As example, energy dissipation of bolted end plate joints (G20 and G21) is compared in Figure 26 to the dissipation of haunched bolted end-plate joints (G23 and G18); which appears 2.8 times greater for joints with haunches than for simple end-plate bolted joints.



**Figure 26.** Comparison of Energy dissipation capacities

In Figure 27, for haunched joints, the joint contribution is only 20% to 30% of the plastic beam energy dissipation (contrary to joints without haunches where the joint contribution is close to 100%). Contribution of the joint components to the plastic energy dissipation is illustrated in Figure 28 for test G20 (without haunch) where the contribution of the connection is about 20% for a web panel contribution of 80% to the total joint rotation.

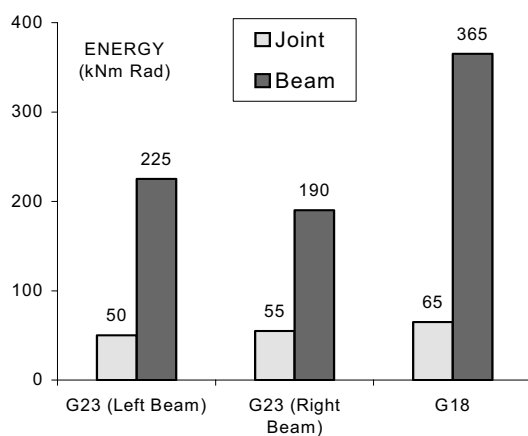


**Figure 27.** Comparison of plastic energy dissipation in beam and joint (haunch specimens)

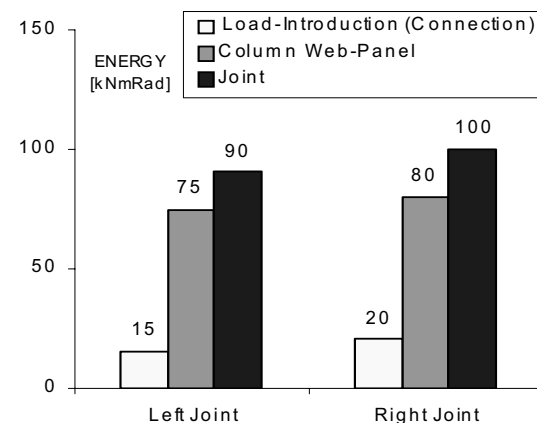


**Figure 28.** Comparison of plastic energy dissipation in the components of joint test (G20)

#### 4.4. Flexural Stress and Strain Distribution over the Depth of the Beams

Figure 29-1 for the test G23 in hogging bending and Figure 29-2 for the same test in sagging bending show the flexural strain distribution within the steelwork part of the depth of two beam cross sections located near the haunch tip, one in the haunch region at 328 mm from the flange column face and the other outside the haunch region at 528 mm from the flange column face.

In both cases, in hogging as well as in sagging bending a clear decrease of flexural strains appears in the lower part of the beam where the stiffening effect of the haunch acts. On the other end, in the upper part of the beam the strain reduction effect of the haunch remains negligible. For test G18 with a T joint configuration similar observations are made in Figures 30-1 and 30-2 in both hogging and sagging bending.

From tri-axial strain gauge measurements, load - shear strain curves from the mid-depth of the web of two beam cross sections located on each side of the stiffener above the haunch tip (Figure 31-1) may be compared in Figures 31-2 and 31-3. For a same load exerted by the actuator, it can be

observed that the shear strain in the haunch region is in opposite direction as compared with the corresponding shear strain outside the haunch region, the range of shear strain variation being more reduced in the haunch region than outside the haunch region.

This experimental result is a direct consequence of the effect of the vertical shear reaction transmitted by the haunch flange to the beam at the haunch tip. It confirms the hypotheses adopted previously in the haunch static design.

Flexural stress distributions within the depth of the steel beam in the haunch region at 328 mm from the flange column face are presented in Figures 32-1, 32-2, 32-3 and 32-4 for both tests G23 (cruciform internal joint) and G18 (T external joint). Test results are compared with two theoretical ones issued from the above proposed haunch design model on the one hand and from the simple beam theory on the other hand assuming the haunch region as a length of beam of variable cross-section. A better accordance appears between experimental results and the proposed model than the beam theory one, more particularly for test G18 where the depth beam (IPE360) is higher than for test G23 (IPE 240).

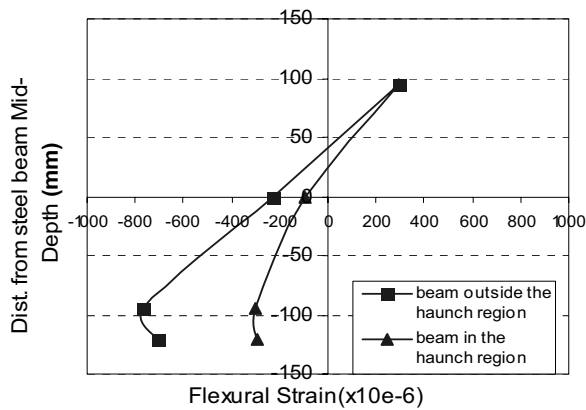


Figure 29-1. Hogging bending (Test G23)

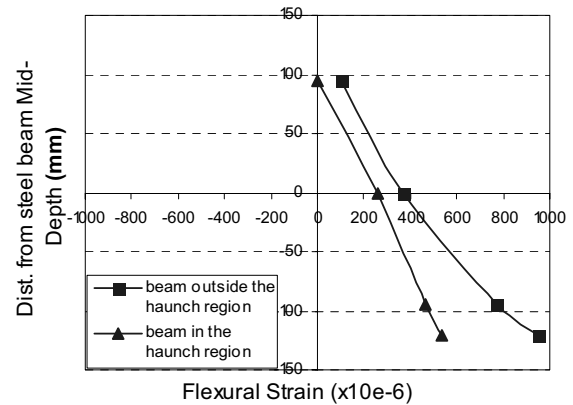


Figure 29-2. Sagging bending (Test G23)

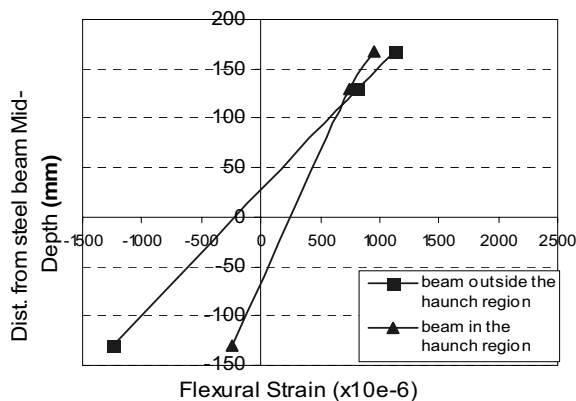


Figure 30-1. Hogging bending (Test G18)

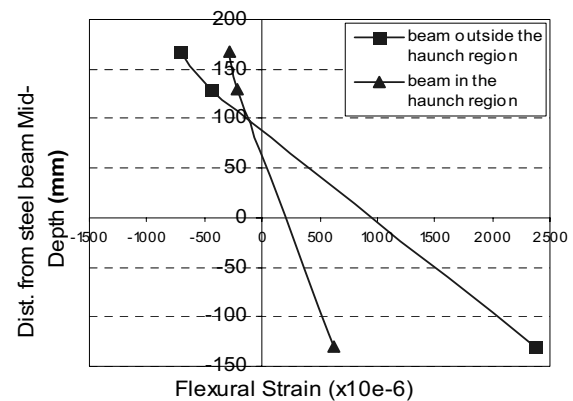


Figure 30-2. Sagging bending (Test G18)

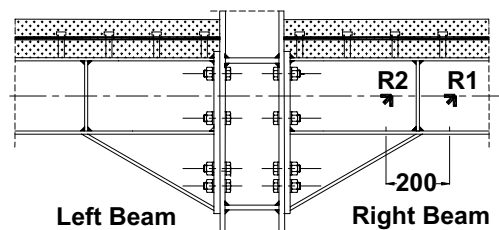
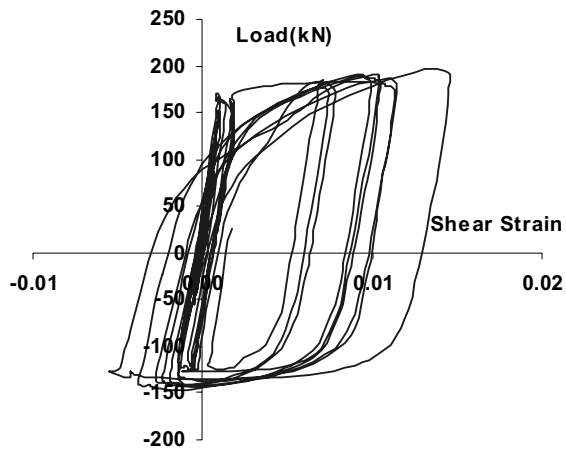
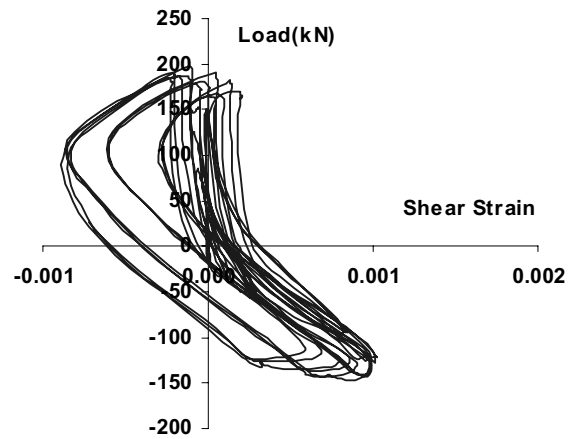


Figure 31-1. Location of rosette strain gauges



**Figure 31-2.** Shear strains of the beam web outside the haunch region R1



**Figure 31-3.** Shear strains of the beam web in the haunch region R2

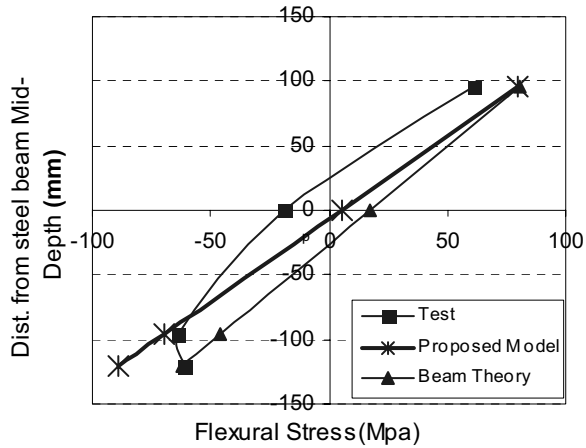


**Figure 32-1.** Hogging bending (Test G23)

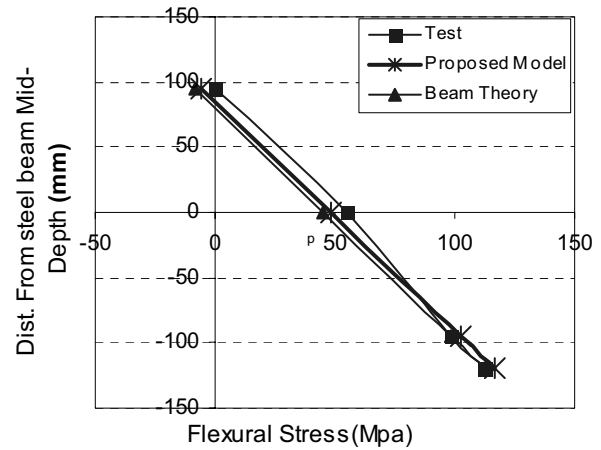


**Figure 32-2.** Sagging bending (Test G23)

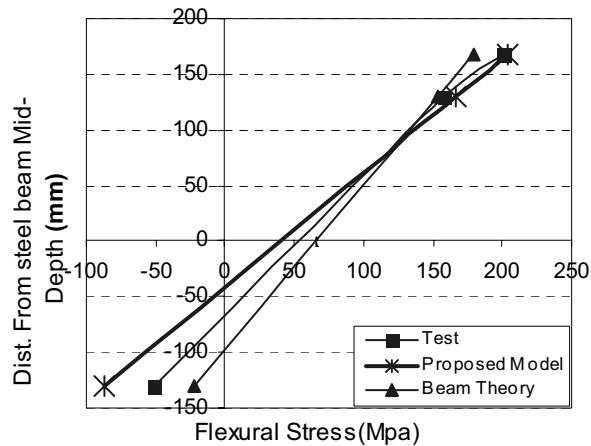


**Figure 32-3.** Hogging bending (Test G18)

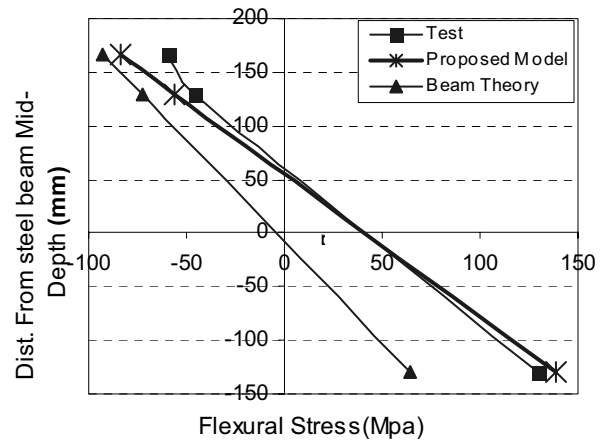


**Figure 32-4.** Sagging bending (Test G18)

## 5. CONCLUSIONS

Though haunched joints may be an expensive solution and their use limited to constructions with heavy loads in zones of high seismicity, the following conclusions may be drawn:



- Above results confirm, as well as for joints with a T arrangement than joints with a cruciform arrangement, that the use of haunch with a triangular shape cut out directly from a steel beam appears as a good solution to strengthen beam-to-column joints.
- Haunch solution improved significantly joint cyclic performances. Plastic energy dissipation may be twice greater at least and the rotation capacity can exceed 35mrad without risk of low-cycle fatigue rupture in the welds connecting beam flanges on the end-plates. A significant increase of rotational stiffness, moment resistance and rotation capacity was observed in comparison with similar beam-to-column composite joints without haunches.
- The stiffening effect of the composite slab prevents any risk of buckling in the upper beam flange leading under sagging cyclic bending to an increase of 60% of the maximum moment compared with a same steel joint. On the other hand, in hogging bending, the composite slab does not bring reinforcing effect on the lower beam flange and the increase of the maximal moment is only 30%.
- Experimental results are rather in good agreement with the simplified model developed by the authors which appears well adapted for the haunch static design in composite beam-to-column joints.
- It has been shown that Eurocodes 3 and 4 which do not give specific provisions about haunch strengthening, may offer a basic design guidance to suitably predict initial stiffnesses and moment resistances.

## ACKNOWLEDGEMENTS

The authors would like to thank the “French Ministry for Infrastructure, Transport, Spatial planning, Tourisme and the sea” through the DRAST (Research management) managed by Prof. André Colson for the financial support to the experimental part of this research.

## REFERENCES

- [1] Eurocode 3: Design of Steel Structures Part 1-1: General rules for buildings, European Committee for Standardization, CEN, 2003.
- [2] Eurocode 3: Design of Steel Structures Part 1-3: General rules – supplementary rules for cold-formed thin gauge members and sheeting, European Committee for Standardization, CEN, 2003.
- [3] Eurocode 3: Design of Steel Structures Part 1-8: Design of joints, European Committee for Standardization, CEN, 2003.
- [4] Eurocode 4: Design of composite steel and concrete structures Part 1-1: General rules and rules for buildings, European Committee for Standardization, CEN, 2003.
- [5] Eurocode 8: Design of structures for earthquake resistance Part 1: General rules, seismic actions and rules for buildings, European Committee for Standardization, CEN, 2003.
- [6] Eurocode 8: Design of structures for earthquake resistance Part 3: Strengthening and repair of buildings, European Committee for Standardization, CEN, 2003.
- [7] Rep. No. SAC-96-01, SAC Joint Venture, Sacramento, Calif., 1996.
- [8] Lee, C.H. and Uang, C.-M., “Analytical modeling of dual panel zone in haunch repaired SAC, “Technical report: Experimental investigations of beam-column subassemblies.” steel MRFs”, Journal of Structural Engineering, ASCE, 1997, 123(1), pp.20-29.

- [9] NIST, Modification of existing Welded Steel Moment Frame Connections for Seismic Resistance, Draft Report, National Institute for Standards and Testing, Gaithersburg, MD, 1998.
- [10] Gross, J.L., Engelhardt, M.D., Uang, C.M., Kasai, K. and Iwankiw, N.R., "Modification of Existing Welded Steel Moment Frame Connections for Seismic Resistance", AISC Design Guide Series 12, American Institute of Steel Construction, Chicago, Illinois, 1999.
- [11] Yu, Q.-S., Uang, C.-M. and Gross, J., "Seismic rehabilitation design of steel moment connection with welded haunch", Journal of Structural Engineering, ASCE, 2000, 126(1), pp.69-78.
- [12] FEMA- 355D, "State of the Art Report on Connection Performance". Ch 3, 2000.
- [13] FEMA- 351, "Recommended Seismic Evaluation and Upgrade Criteria for Existing Welded Moment-Frame Buildings", Ch 6, 2000.
- [14] Ciutina, A., Aribert, J.M. and Lachal, A., "Testing and numerical modelling of steel and composite bolted joints under seismic cyclic loads", French Journal of Steel Construction, 2004, n 1, pp.3-33.
- [15] ECCS, "Recommended Testing Procedures for Assessing the Behaviour of Structural Elements under Cyclic Loads", TC 1, TWG 1.3 – Seismic Design, 1986, n 45.

# THE CYCLIC BEHAVIORS OF BOX-SECTION STEEL BEAM-COLUMNS: EXPERIMENT AND NUMERICAL COMPARISON

Ming-zhou Su<sup>1,\*</sup>, Lin Shen<sup>2</sup>, Qiang Gu<sup>3</sup>

<sup>1</sup>*School of Civil Engineering, Xi'an University of Architecture & Technology, Xian, 710055, China*

*\*(Corresponding author: E-mail: sumingzhou@163.com)*

<sup>2</sup>*China Institute of Building Standard Design and Research, Beijing, 100044, China*

<sup>3</sup>*University of Science and Technology of Suzhou, Suzhou, 215011, China*

---

**ABSTRACT:** A series of tests were performed to evaluate the cyclic behaviors of box-section steel beam-columns under cyclic bending. The test was set up as a cantilever beam-column, loaded with cyclic transverse shear force at its free end, while the axial compression kept unchanged. Three sets of tests with various axial compression ratios were tested to find out their influencing on cyclic behaviors, which were 0.0, 0.4 and 0.6, respectively. In each set, there were five members with various width-to-thickness ratios of plates to consider their effects. The hysteretic curves and failure mechanisms of each member were given according the test results, and the main influencing factors, such as axial compression ratio of the member, width-to-thickness ratio of its plates, were analyzed. Then, the test results were compared with that of numerical analysis by the author. In general, there was a good agreement between two results, it revealed that the numerical analysis was reasonable and could be used in practice.

**Keywords:** Beam-column; Cyclic bending; Experiment; Numerical analysis; Hysteretic behavior; Box-section.

---

## 1. INTRODUCTION

High-rise building will not only undergo the gravity static loads, but also the dynamic horizontal actions, such as earthquake and wind action. In general, the latter becomes more important with the increase of building's height. In this case, the columns are subjected to large unchanged axial compression and varied bending moment. As the inflection point of columns generally lies near its mid-height, the problem can be simplified as a cantilever subjected to cyclic transverse shear at its free end, while the axial compression kept unchanged. For the facility of analysis, most researchers simplified the various action as a quasi-static manner, i.e., cyclic loading.

In the early 1969s, Kato [1] established the cyclic curve of beam-columns under cyclic bending. In his model, the relationship of moment-curvature was built based on monotonic loading, and the material was assumed to follow rigid plastic hardening, so the model was inaccurate and overestimated the bearing capacity of the member.

Toma and Chen [2] and Han and Chen [3] discussed the response of beam-columns under cyclic bending. Many simplifications were introduced in the analysis to get a closed-form solution, so only one or less cycle could be performed, the behavior of members could not be predict after several cycles.

Billio and Calado [4] carried out an experiment on beams under cyclic bending. The phenomenon of capacity deterioration of beams was found in case of local buckling occurred in their study. Furthermore, a simplified numerical model was established to consider the effect of local buckling and fracture on the capacity deterioration.

Macrae [5] performed an experiment on beam-columns under cyclic bending with constant or various axial compressions. The aim of the test was to investigate the influence of axial force on the behavior of beam-columns. It noted that the results on few tests were not reliable, and the limitation of axial force would not be relaxed before thorough analysis.

Watanabe [6] put forward a simplified model to study the cyclic behavior of beam-columns with square hollow section. In that model, the section was divided into many fibers, each fiber was assumed to follow uniaxial stress state, perfect elastic-to-plastic material was assumed, and the residual stress and initial geometric imperfection were not considered.

Hao [7] studied the cyclic behavior of beam-columns with H-shaped sections. The simplified plastic zone model was adopted in his numerical analysis, and the plastic damage accumulation was considered. But the critical factors in the model were based on experimental results and varied with each member, so it could not be used to predict the behavior of members untested.

Yamazaki and Minami [8] performed experiment and numerical analysis on box-section beam-columns under various axial force and cyclic bending. In their analysis, the plane section hypothesis was used, and the one-dimensional hysteretic model of Ohi *et al.* [9] was adopted. As a result, they found the transverse resistance of the member decreased dramatically with large axial compression, and the strength was between that of cyclic bending with constant maximum axial compression and that with minimum axial compression.

Miki and Nethercot [10] built up a multi-failure mechanism numerical model of beam-columns with varied cross-section. It found that two failure mechanisms would appear alternatively in one cycle, and the member would then lose its stability.

Gao *et al.* [11] performed a finite element analysis on the ultimate strength and ductility capacity correlation between centrally loaded and eccentrically loaded columns subjected to cyclic transverse load. Both geometrical and material nonlinearity was considered in the analysis, and a modified two-surface plasticity model is employed to model material nonlinearity. As a result, equations were proposed to evaluate the ultimate strength and ductility capacity of the eccentrically loaded columns from those of the centrally loaded columns.

To analysis the behavior of steel beam-columns under cyclic bending, the author [12,13] suggested a numerical method based on degenerated shell element, together with the updated Lagrange formulation and the mixed hardening material. As a result, the author gave suggestions about the limit of width-to-thickness ratio of plates and the bearing capacity of members.

In order to evaluate the hysteretic behavior of box-section steel beam-columns under cyclic bending, a series of tests was carried by the author. This paper contains a description of test specimens, set-up and instrumentation, procedure, and results. A comparison of the experimental and analytical results is also provided.

## 2. TEST SPECIMENS

A series of three group tests was conducted, corresponding with various axial compression ratios, which were 0.0, 0.4 and 0.6, respectively. Each of the three groups contained five members with various width-to-thickness ratios of their plates. These specimens were welded by hand-arc welds with E43 electrode rod, and the material of their plates is Q235B. The test was set up as a cantilever beam-column, loaded with cyclic transverse shear force at its free end, while the axial compression kept unchanged. The test was controlled by the transverse displacement at the free end. The configuration of specimens and loading scheme were described in Figure 1 and Table 1.

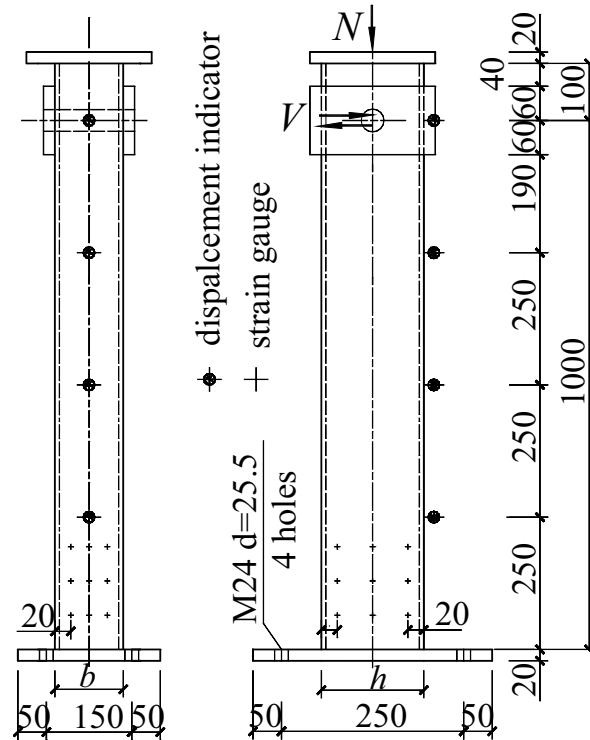
**Table 1.** Configuration of Specimens

Item	$h/t_w$	$b/t_f$	$h$ (mm)	$b$ (mm)	$t_f, t_w$ (mm)	$N/A_f f_y$	$\delta_y$ (mm)	Displacements (mm)		
								$\delta_1$	$\delta_2$	$\Delta$
S-1-0	23.0	19.0	92	76	4	0.0	9.81	10	20	10
S-2-0	33.3	23.5	133	94	4	0.0	6.79	7	10	10
S-3-0	33.5	29.0	134	116	4	0.0	6.74	7	10	10
S-4-0	43.3	29.0	173	116	4	0.0	5.22	5	10	10
S-5-0	43.5	36.0	174	144	4	0.0	5.19	5	10	5
S-1-4	23.8	19.0	95	76	4	0.4	5.70	6	10	10
S-2-4	33.3	23.5	133	94	4	0.4	4.07	4	5	5
S-3-4	33.5	29.0	134	116	4	0.4	4.04	4	5	5
S-4-4	43.3	29.0	173	116	4	0.4	3.15	3	5	5
S-5-4	43.5	36.0	174	144	4	0.4	3.14	3	5	5
S-1-6	23.0	19.0	92	76	4	0.6	3.96	4	5	2.5
S-2-6	33.5	23.5	134	94	4	0.6	2.72	3	5	2.5
S-3-6	33.5	29.0	134	116	4	0.6	2.72	3	5	2.5
S-4-6	44.0	29.0	176	116	4	0.6	2.08	2	5	2.5
S-5-6	43.5	36.0	174	144	4	0.6	2.11	2	5	2.5

Note: i.  $h$  and  $b$  are the height and the width of the cross-section, and  $t_w$  and  $t_f$  are the thickness of its web and flange, respectively.

ii.  $N/A_f f_y$  is the axial compression ratio.

iii.  $\delta_y$  is the transverse displacement when the extreme fiber at the fix end of the member yields.

**Figure 1.** Configuration of Specimens

### 3. TEST SET-UP AND TEST PROCEDURE

Test set-up was shown in Figure 2. The specimen (1) was fixed on the floor girder (2) through 4 high-strength bolts (3), the diameter of which are 24mm, with the material grade of 10.9S (the tensile ultimate strength of the material is  $1040\text{N/mm}^2$ , and the yield strength is  $940\text{N/mm}^2$ ). The tested member was subjected to transverse cyclic load applied through horizontal actuator (4), while a constant compressive load applied by vertical jack (5), which was free to move laterally in-plane on greased roller bearings (6). The jacks were fastened in the test rig (7). To prevent lateral-torsional buckling of the tested member, a lateral support (8) was provided.

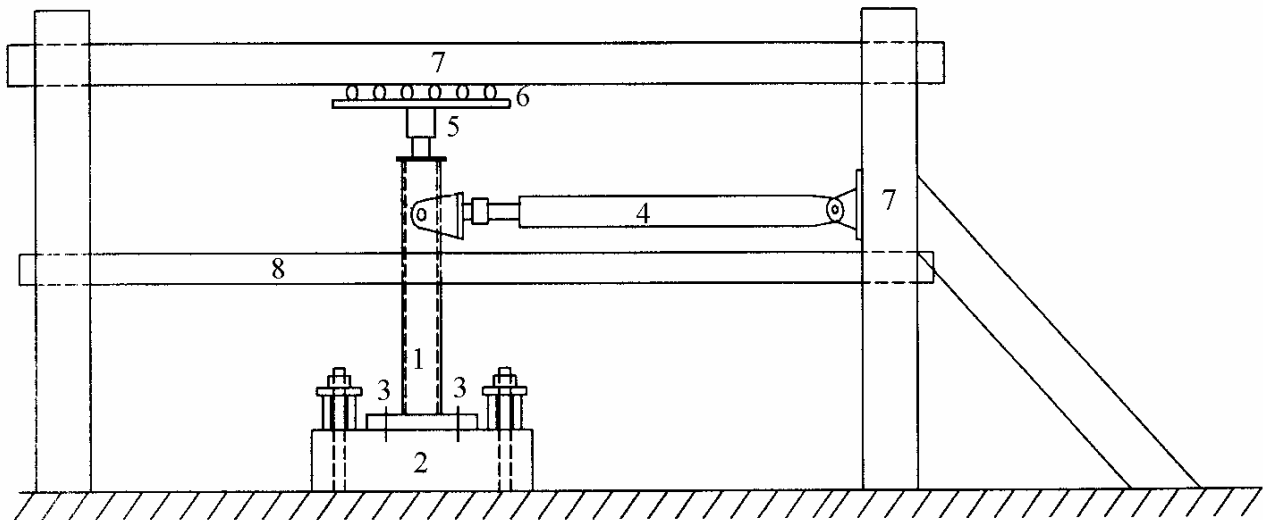


Figure 2. Test set-up

The following procedure was used to obtain accurate and reliable results of each specimen:

1. The specimen was set into position and connected to the floor girder.
2. Jacks were mounted, connected, and aligned in order to prevent eccentricity.
3. The axial compression was applied to the beam-column by vertical jack according to design.
4. The cyclic transverse displacements were applied according ECCS loading scheme. The displacement of first step was about  $\delta_1/2$  for one cycle as the member stayed in elastic state, and then displacement of  $\delta_1$  and  $\delta_2$  were applied for three cycles for some fibers of member yielded, after that an incremental displacement of  $\Delta$  was added to the former step for three cycles ( $\delta_1$ ,  $\delta_2$  and  $\Delta$  were shown in Table 1).
5. Test stopped when the specimen fractured or its bearing capacity dropped below 80% of the maximum.

### 4. TEST RESULTS AND DISCUSSION

#### 4.1. Results of Coupon Test

The coupon was designed according to the demand of Chinese National Standard *Metallic materials - Tensile testing at ambient temperature* (GB228-2002). Based on the testing results, the material Q235B used in the experiment had the following characteristic values: Yong's modulus  $E=2.05 \times 10^5 \text{MPa}$ , yield stress  $f_y=279 \text{MPa}$ , hardening modulus  $E_{st}=1.84\%E$ , hardening strain  $\varepsilon_{st}=1.1\%$ .

## 4.2. Test Results of Beam-Columns

### 4.2.1. Members without Axial Force ( $N/Af_y=0.0$ )

For members without axial force, the hysteretic curves were quite smooth and plump, the ductility factor was over 7.5, which revealed that the energy dissipation was very excellent. Figure 3 to Figure 7 gave the hysteretic curves of S-1-0 to S-5-0 respectively. In these figures, the vertical axis denotes the transverse shear at the free end of the member, while the horizontal one denotes the corresponding transverse displacement at the same point and the ductility factor of the member. Except that members S-2-0 and S-3-0 failed with welds fractured at the fix end due to lack of enough weld throat, all the others failed with plastic cracks of flanges near half of the section width away from the fix end, owing to low cycle fatigue. The cracks firstly developed in the intersect lines of flanges and webs, and then expanded with the increase of cyclic load, finally the section fractured. Before failure, the slop of hysteretic curve increased with the increase of displacement due to cracks closed, obviously in the member with large width-to-thickness ratios of plates, as shown in Figures 6 and 7. Fracture of S-5-0 was shown in Figure 8. The local buckling of all the five members just occurred before fracture and the buckling deformation was very small. The hysteretic behaviors of members without axial compression were listed in Table 2.

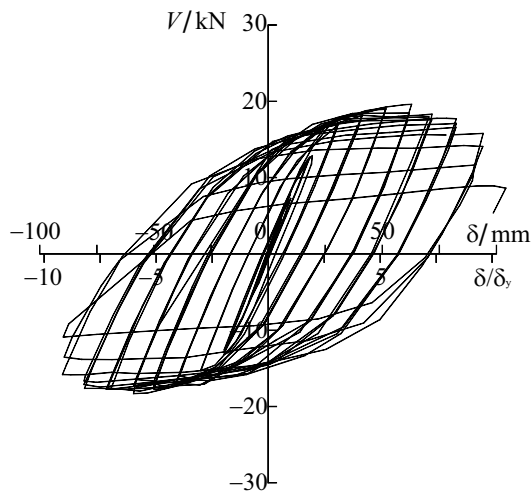


Figure 3. Hysteretic curve of S-1-0

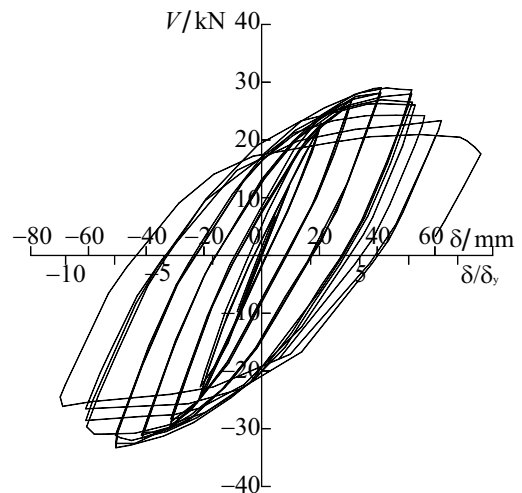


Figure 4. Hysteretic curve of S-2-0

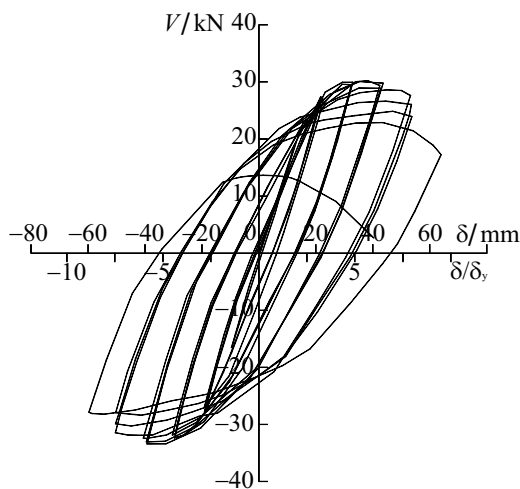


Figure 5. Hysteretic curve of S-3-0

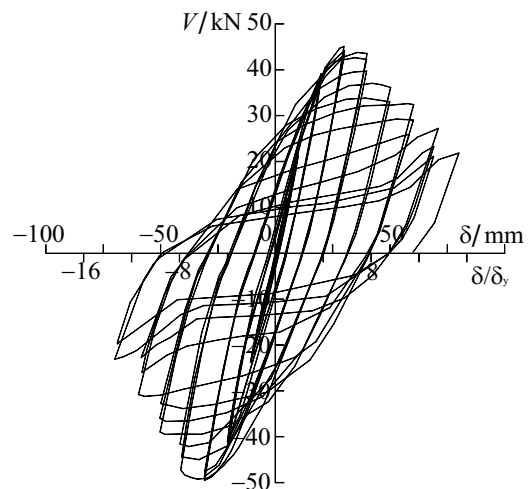
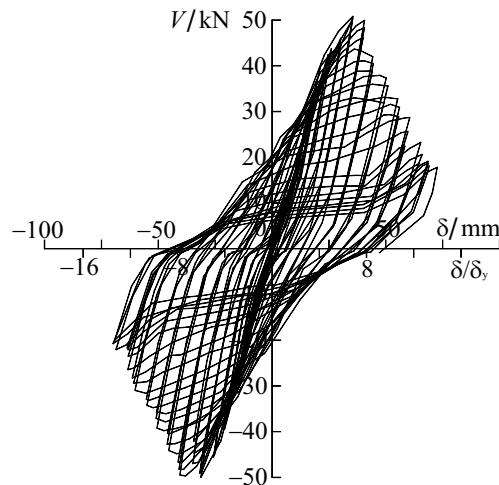


Figure 6. Hysteretic curve of S-4-0



**Figure 7.** Hysteretic curve of S-5-0



**Figure 8.** Fracture of member S-5-0

**Table 2.** The Hysteretic Behaviors of Members without Axial Force

Item	S-1-0	S-2-0	S-3-0	S-4-0	S-5-0
Rotation angle (%) <sup>a</sup>	9.0	6.0	5.0	5.0	5.0
Ductility factor <sup>b</sup>	9.5	9.0	7.5	8.0	8.3
Location of plastic hinge	0.53 <i>b</i>	0.53 <i>b</i>	0.47 <i>b</i>	0.52 <i>b</i>	0.38 <i>b</i>
Failure mode	Section fractured	Section cracked, but failure due to welds fractured at the fix end	Similar to S-2-0	Similar to S-1-0	Similar to S-1-0

Note: <sup>a</sup> Rotation angle is defined as total transverse displacement ( $\delta$ ) over the length of the member ( $l$ ).

<sup>b</sup> Ductility factor is termed as  $\delta$  over  $\delta_y$ .

#### 4.2.2. Members with axial compression ratio $N/Af_y=0.4$

The hysteretic curves of members S-1-4 to S-5-4 were shown in Figure 9 to Figure 13, respectively. It was shown in the figure that plates of members were susceptible to buckle locally as the existence of large axial compression, and the capacities of ductility and energy dissipation were seriously deteriorated owing to the local buckling. Even for the member S-1-4 with smallest plate width-to-thickness ratios, the ductility factor was only about 5. Local buckling developed in the section near the fix end with the increase of transverse shear, members failed owing to the cyclic local buckling, and no cracks were found in the section or in the welds of fix end. The members with small width-to-thickness ratios of plates failed due to dramatic decrease of bearing capacity, while ones with large width-to-thickness ratios failed due to severe local buckling. Local buckling of S-4-4 was shown in Figure 14, and hysteretic behaviors of these five members were described in Table 3. The failure mode in this Table referred to the dominant deformation of the member, Plastic referred to the failure mainly caused by plastic deformation; Local Buckling referred to the failure mainly caused by local buckling.

**Table 3.** The Hysteretic Behaviors of Members with Axial Compression Ratio  $N/Af_y = 0.4$

Item	S-1-4	S-2-4	S-3-4	S-4-4	S-5-4
Rotation angle (%)	3.0	2.0	2.0	1.3	1.0
Ductility factor	5.0	4.8	4.5	4.0	3.0
Location of local buckling	0.71 <i>b</i>	0.85 <i>b</i>	0.56 <i>b</i>	0.93 <i>b</i>	0.79 <i>b</i>
Failure mode	Plastic	Plastic, local Buckling	Plastic, local Buckling	Local buckling	Local buckling



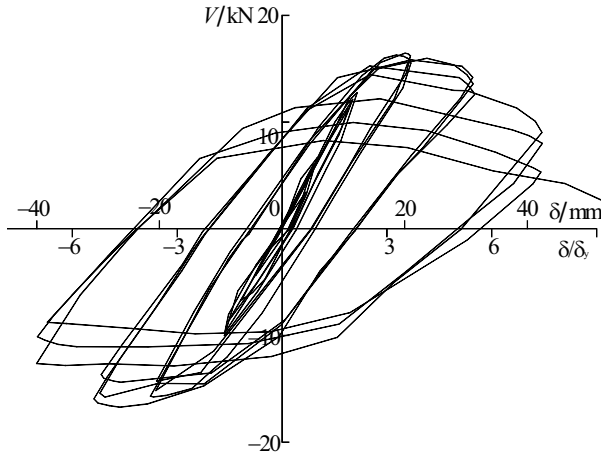


Figure 9. Hysteretic curve of S-1-4

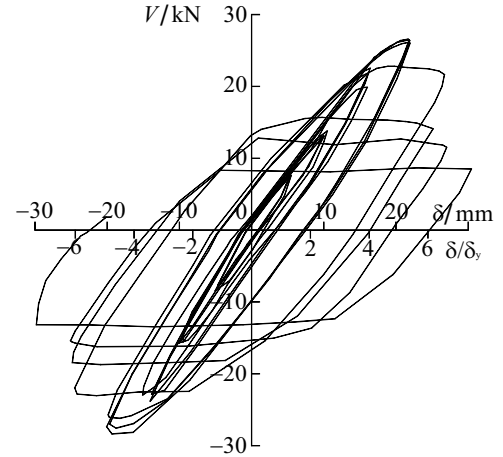


Figure 10. Hysteretic curve of S-2-4

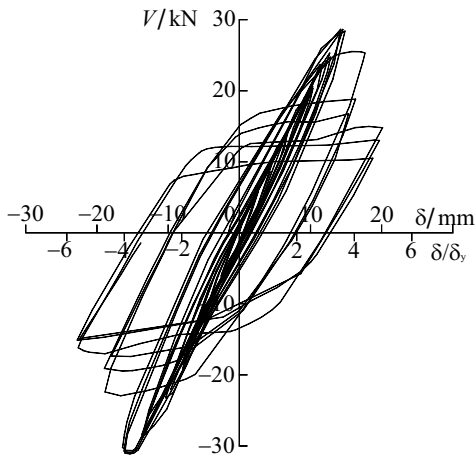


Figure 11. Hysteretic curve of S-3-4

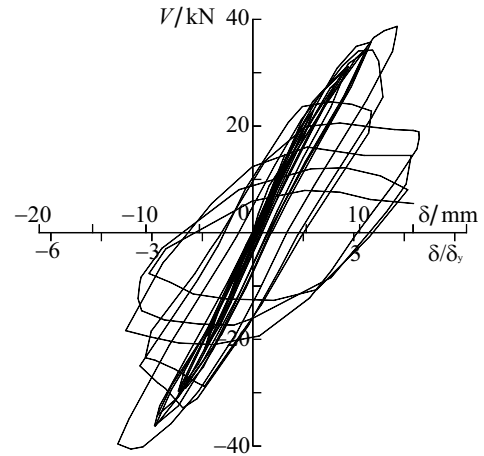


Figure 12. Hysteretic curve of S-4-4

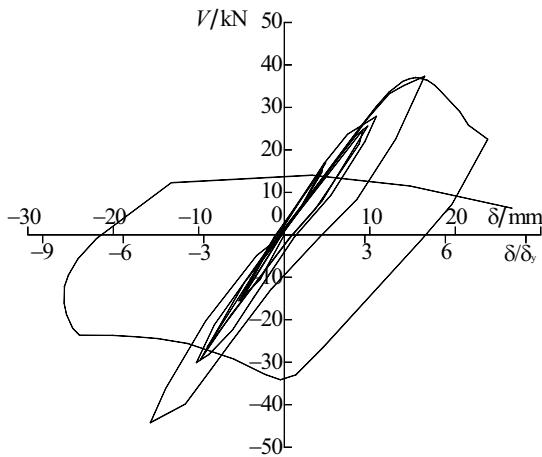


Figure 13. Hysteretic curve of S-5-4

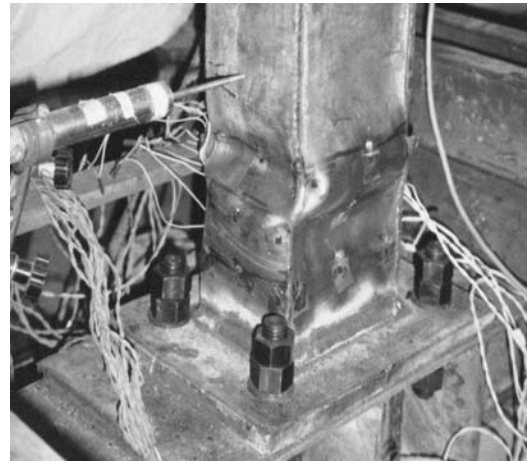
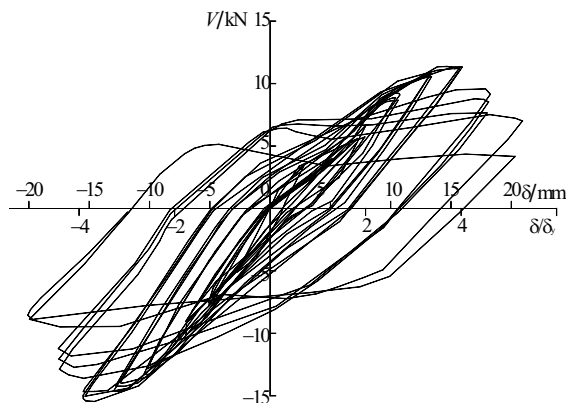


Figure 14. Local buckling of S-4-4

#### 4.2.3. Members with Axial Compression Ratio $N/Af_y=0.6$

The ductility and bearing capacity of members with  $N/Af_y=0.6$  deteriorated more seriously than those with  $N/Af_y=0.4$ . This phenomenon is mainly caused by severe local buckling of their plates due to the large axial compression ratio. These members failed mainly due to the local buckling.

As soon as the bearing capacity reached, the maximum load decreased quickly with the increase of transverse displacement, brittle failure might occur in the member with large plate width-to-thickness ratio, such as S-4-6 and S-5-6. The hysteretic curves of members with axial compression ratio  $N/Af_y = 0.6$  were shown in Figures 15 to 19. Except that S-1-6 underwent large plastic deformation, the other 4 members failed mainly due to local buckling. Figure 20 showed the local buckling of S-4-6 when failure occurred, which was similar to Figure 14. The hysteretic behaviors were listed in Table 4.



**Figure 15.** Hysteretic curve of S-1-6

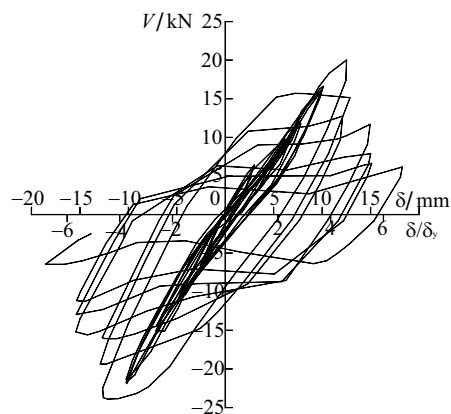


**Figure 16.** Hysteretic curve of S-2-6

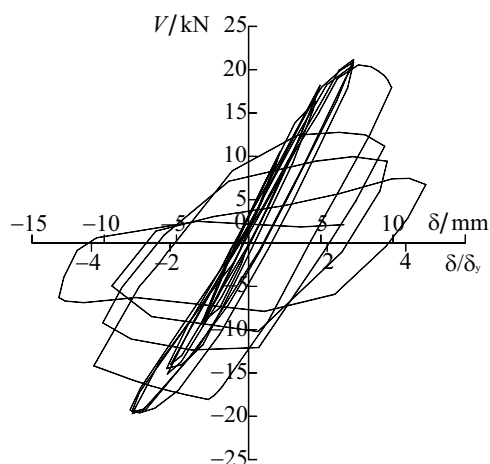


**Figure 17.** Hysteretic curve of S-3-6

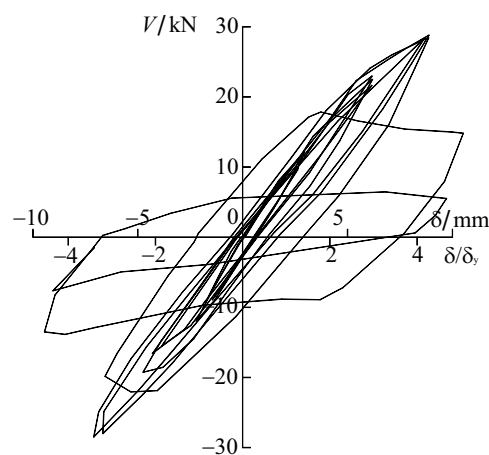


**Figure 18.** Hysteretic curve of S-4-6

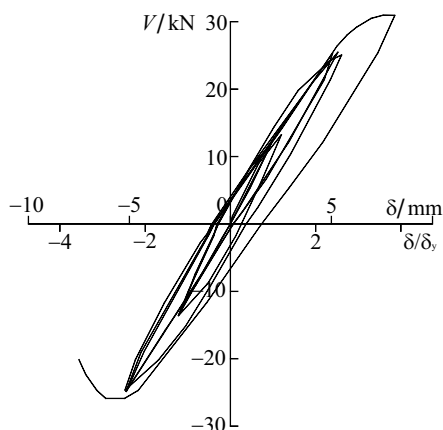


**Figure 19.** Hysteretic curve of S-5-6

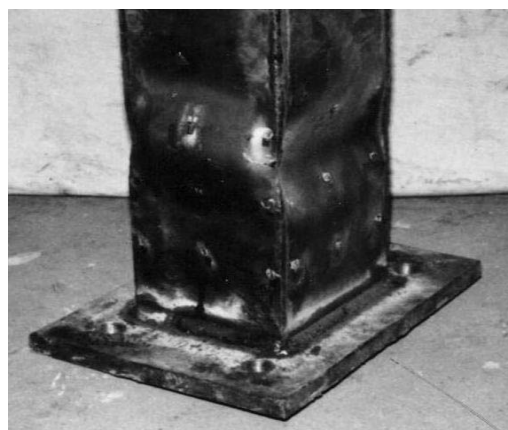


**Figure 20.** Local buckling of S-4-6

**Table 4.** The Hysteretic Behaviors of Specimens with Axial Compression Ratio  $N/Af_y = 0.6$ 

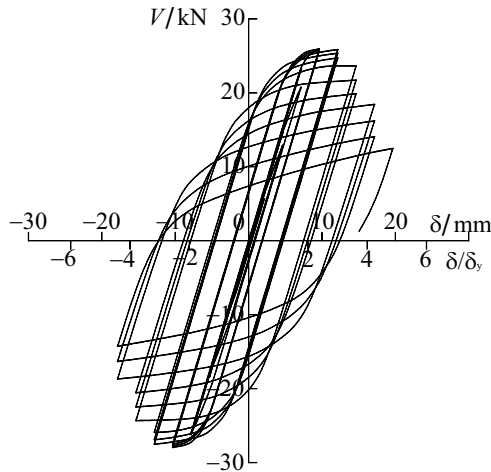
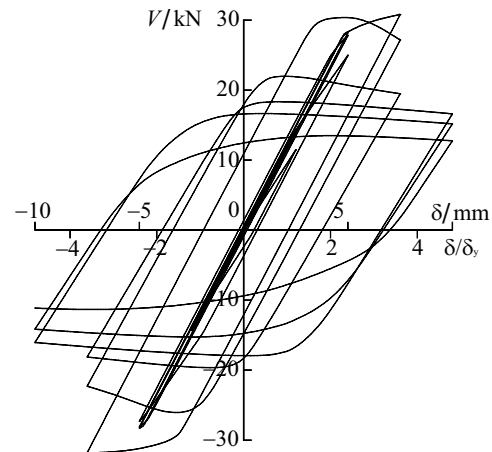
Item	S-1-6	S-2-6	S-3-6	S-4-6	S-5-6
Rotation angle (%)	1.8	1.3	0.75	0.75	0.5
Ductility factor	4.5	4.2	2.8	3.8	2.5
Location of local buckling	$0.98b$	$0.53b$	$0.56b$	$0.78b$	$1.30b$
Failure mode	Plastic	Plastic, local Buckling	Local buckling	Local buckling	Local buckling

## 5. THE COMPARISON OF EXPERIMENTAL AND NUMERICAL RESULTS

### 5.1. Comparisons of Hysteretic curves

A degenerated shell element with eight nodal points was used for implementing the formulation. Both material and geometric non-linearity were taken into account. The program had the following characteristics: 1) Degenerated shell element assumption is adopted, i.e., the normal of the mid-surface of shell keeps straight after deflection, but no longer keeps normal. 2) The virtual work equation is expressed in terms of updated Lagrange formulation. 3) The plastic flow theory is applied considering the Mises' yield function as a plastic potential. 4) The material is assumed to follow the mixed hardening law, which linearly combines isotropic and kinematic hardening. Details can be found in the reference [13].

Based on the numerical analysis, the calculated curves of S-3-4 and S-4-6 were shown in Figure 21 and Figure 22 respectively. By comparing of Figure 21 with Figure 11 and Figure 22 with Figure 18, it was shown that the bearing capacity, deterioration rate of maximum load and ductility

**Figure 21.** Numerical curve of S-3-4**Figure 22.** Numerical curve of S-4-6

factor of both curves were very close, so there was a good agreement between two results. However, there was an obvious difference in stiffness that the experimental one was lower than that of calculating, and the experimental curve was not as plumb as that of calculating. This was mainly due to the following reasons:

1. Only the welded residual stress along the longitudinal axial was considered in numerical analysis. As the thick end-plate was welded to the member, the distribution of residual stress in the end was very complex, it might have large influencing on the stiffness of the member, but it was very difficult to simulate and was not considered in the numerical analysis.

2. As the member was anchored to the floor beam by four high-strength bolts, the rotation of fix end could not be avoid, the bolts would loosen when many cycles repeated, this would decrease the stiffness of the member, and it was not considered in calculation.
3. Only initial deflection was considered in numerical analysis, the eccentricity of axial load was no to be taken into account, and this was unavoidable in experiment.

## 5.2. Verification of Interrelation of Bending Moment and Axial Compression

Eq. 1 gave the interrelation of non-dimensional bending moment and axial compression ( $M/M_P-N/N_P$ ), which was put forward by the author through numerical analysis [12]. The parameter  $a$  in Eq.1 could be taken as 1.10 for box-section steel beam-columns. The comparison of test data with Eq. 1 was given in Figure 23. The test data fully lay above the curve, so it was safety to use this equation. Eq. 2 could be used in practice according to Chinese Code for Design of Steel Structures GB50017-2003, in which plastic adoption  $\gamma_x$  (only part of plastic deformation considered) equal to  $1.05 \times a = 1.16$  might be adopted (1.05 is the original plastic adoption in this Code).

$$N/N_P + M/(a M_P) = 1 \quad (1)$$

$$\frac{N}{\phi_x A} + \frac{\beta_{mx} M}{\gamma_x W_x (1 - 0.8 N/N_{Ex})} \leq f \quad (2)$$

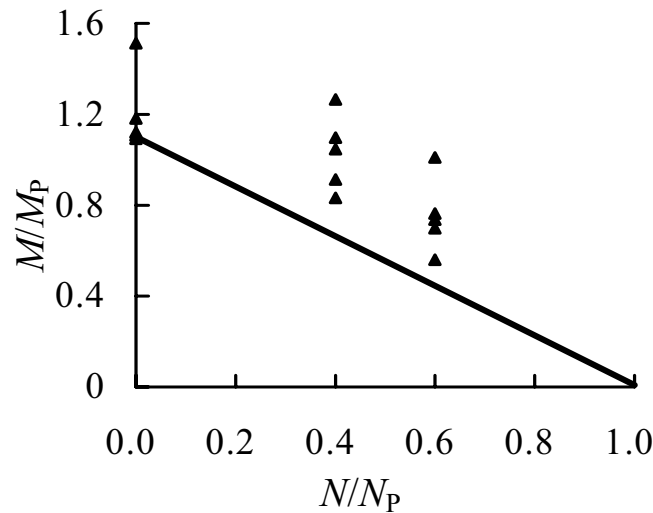


Figure 23. Interrelation of  $M/M_P-N/N_P$

## 6. CONCLUSIONS

This paper has described a series of tests of steel beam-columns with box-section under cyclic bending. Three axial compression ratios were taken into account to investigate its influence, which was 0.0, 0.3, and 0.6 respectively, and five width-to-thickness ratios of plates were considered. Then the test results were present and analyzed. At the last part of this paper, the experimental results were compared with the numerical ones. The following conclusions could be made from this paper:

1. Beam-columns under cyclic bending might fail in fatigue fracture when no axial force presented, otherwise they might fail in cyclic plastic deformation and/or local buckling based on their width-to-thickness ratios of their plates and on the axial compression carried.

2. The largest deformations generally located in the height of  $b/2 \sim b$  near the fix end according to test results.
3. By comparing the experimental and numerical results, the design formula was verified, and proved to be reasonable and could be used in practice.

## REFERENCES

- [1] Kato, B., "Inelastic bar subjected to thrust and cyclic bending", Journal of Structure Division, 1969, 95(1), pp.562-590.
- [2] Toma, S. and Chen, W.F., "Cyclic analysis of fix-ended steel beam-columns", Journal of Structure Division, ASCE, 1982, 108(6), pp.1385-1399.
- [3] Han, D.J. and Chen, W.F., "Buckling and cyclic inelastic analysis of steel tubular beam-columns", Engineering Structures, 1982, 5, pp.119-132.
- [4] Ballio, G. and Calado, L., "Steel bent sections under cyclic loads: experiments and numerical approaches", Costruzioni Metalliche, 1986, 1, pp.2-24.
- [5] Macrae, G.A., "Cyclic bending of steel I-shaped beam-columns", Proceeding of Pacific Structural Steel Conference, Brisbane, 1989.
- [6] Watanabe, E., "Modeling of hysteric behavior of thin-walled box members", Stability and Ductility of Steel Structures under Cyclic Loading. CRC press, 1992, pp.225-235.
- [7] Hao, J.P., "Test and theoretical study on the local buckling and low cycles fatigue of steel structures under cyclic loading", PhD. thesis, School of Civil Engineering, Xi'an University of Architecture & Technology, Xi'an, China, 1995 (in Chinese).
- [8] Yamazaki, S. and Minami, S., "Inelastic behavior of steel beam-columns subject to varying axial force and cyclic bending moment", Proceeding of the 5th International Colloquium on Stability and Ductility of Steel Structures, Nagoya, Japan, 1997, pp.561-568
- [9] Ohi, K., Chen, Y. and Takanashi, K., "An experimental study on inelastic behavior of H-shaped steel beam columns subject to varying axial and lateral load", Journal of Structure Engineering, Architecture Institute of Japan, 1996, 42B, pp.421-430.
- [10] Miki, T. and Nethercot, D.A., "Cyclic instability of beam-columns with variable cross-section due to combination of collapse mechanisms", Proceeding of the 5th International Colloquium on Stability and Ductility of Steel Structures, Nagoya, Japan, 1997, pp.569-576.
- [11] Gao, S.B., Usami, T. and Ge, H.B., "Eccentrically Loaded Steel Columns under Cyclic In-Plane Loading", Journal of Structural Engineering, ASCE, 2000, 126(8), pp.964-973.
- [12] Su, M.Z. and Gu, Q., "Study on Hysteretic Behavior of Box-section Steel Beam-columns under Cyclic Bending and on Limiting Ratio of Width-to-thickness of its Plates", Journal of Building Structures (in Chinese), 2000, 21(5), pp.41-47.
- [13] Su, M.Z., Gu, Q. and Guo, B., "Finite Element Analysis of Steel Members under Cyclic Loading", Finite Elements in Analysis and Design, 2002, 39(4), pp.43-54.

# STRUCTURAL PERFORMANCE OF COMPOSITE BASE COLUMN CONNECTIONS

L. Di Sarno<sup>1,\*</sup>, G. Fabbrocino<sup>2</sup> and M.R. Pecce<sup>1</sup>

<sup>1</sup> *Department of Engineering, University of Sannio, 82100, Benevento, Italy*

*\*(Corresponding author: E-mail: disarno@unina.it)*

<sup>2</sup> *Department S.A.V.A., University of Molise, 86100, Campobasso, Italy*

---

**ABSTRACT:** The present paper provides the results of a comprehensive experimental research program carried out on partially encased composite steel-concrete columns connected to the foundation block through traditional (bolted steel end plate) and an innovative system employing a socket type system. Experimental tests under monotonic loads show that the structural behaviour of the traditional connection is significantly influenced by the response of the anchorage bolts. The latter cause large fixed end rotations and exhibit limited energy dissipation. Conversely, innovative composite base column connections with socket systems possess adequate inelastic deformations and energy absorption. Furthermore, the use of socket-type connections is beneficial for the spreading of inelasticity at the base of the composite columns without damage localization on concrete and interface components. It can thus be argued that the innovative connection assessed in this study is a viable solution for applications in framed structures fulfilling capacity design requirements, e.g. structural systems in earthquake prone regions.

**Keywords:** Composite columns; Partially encased columns; Base column joint; Socket-type connection.

---

## INTRODUCTION

The composite lateral-resisting system has the desired characteristics of conventional structures, such as stiffness, strength and ductility, and fire resistance, and has been found to be very cost-effective for buildings [1-3]. Steel-composite columns are used extensively in modern medium-to-high rise buildings. Composite structural systems for buildings often include a steel moment resisting, consisting of steel beams (acting compositely with a metal deck reinforced slab) and encased composite columns, or braced frame with steel-concrete composite columns. Consequently, the lateral drifts under horizontal forces (wind and/or earthquakes) are lowered. Under severe earthquake loading concrete encasement cracks and reduces the flexural stiffness of composite beam-columns but the steel core acts as a back-up system in providing the shear strength and the ductility to prevent brittle collapse. Partial encased beam-columns with local buckling inhibitors have been found very efficient to prevent local buckling and enhance the global stability of the frame, thus reducing sensitivity to P- $\Delta$  effects [4]. Moreover, to achieve effective composite action, shear stresses should be transferred between the encased steel and reinforced concrete; hence, shear connectors may be placed along the column [5].

The assessment of structural response of composite steel and concrete columns is thus of paramount importance, especially in the earthquake design of framed systems [6,7]. The inelastic response of composite columns can be significantly affected by the beam-column, brace-to-beam, brace-to-column connections and column bases. A comprehensive review of the experimental tests carried on steel-concrete composite beam-columns (both encased and concrete-filled) can be found, for instance, in Cosenza and Pecce [8] and Shanmugam and Lakshmi [9]. It is noteworthy that, to date, analytical and experimental research focusing on the effects of the base connection layout on the performance of beam-columns, either partially or fully encased, is lacking [10]. Few results are available and were derived chiefly from steel structures; their applicability within the capacity-design framework should be further investigated [11,12]. The composite action, may, however, affect the failure modes thus endangering the inelastic performance of the member.

The present paper analyzes the inelastic response of composite joints at column-foundation joints. An innovative base column connection, employing a socket-type system, is discussed and its

response is compared to that of a traditional steel base plate connection. The latter was designed in compliance with the rules utilized for the composite frame tested at JRC Ispra laboratory [13,14]. Several tests under either monotonic or cyclic lateral loads and different levels of axial loads were performed. This work focuses on the response of composite columns under monotonic regime. In the following, the results of the tests on specimens with welded base steel plate (traditional) and socket-type joints are discussed. It is found that for the traditional connections, concentrations of inelastic demand occur in the anchorage bolts and relies chiefly on bond type mechanisms. Conversely, the socket-type system leads to large energy dissipation; plastic hinges form at column base and the strength capacity does not drop even at large lateral drifts (greater than 5-6%). As a consequence, socket-type foundations may be reliably utilized for steel and composite steel-concrete framed structures, especially in regions with moderate-to-high seismicity.

## EXPERIMENTAL PROGRAM AND TEST SET-UP

Recently, several research programs have prompted in Europe to investigate the inelastic response of steel and concrete composite buildings. The experimental projects were funded by the European Community, e.g. ECSC-7210-PR-250 (*Applicability of composite structures to sway frames*), ECOLEADER (*Cyclic and PsD testing of a 3D steel-concrete composite frame*) and/or National Ministry of Research, e.g. by MIUR in Italy, COFIN 2002 (*Advanced design and control of global performance of composite steel and concrete frames for earthquake resistant building*) and COFIN 2004 (*Composite steel and concrete earthquake-resistant frames: advanced dissipative joint systems, methods for damage assessment and seismic design guidelines*). The latter have involved eight Italian Universities. In particular, the working group of University of Sannio is assessing the inelastic static and dynamic (seismic) response of base column connections. In so doing, a number of partial encased column specimens, with different base joints, were tested in the laboratory of the Department of Structural Analysis & Design (DAPS, University of Naples, Italy). The sample specimens included monotonic and cyclic tests; different levels of axial loads were considered during the tests. In addition, pull-out tests were carried out to define the force-slip relationships of the hooked anchorage bolts. In this work the results of the monotonic tests are discussed in details. The experiments were carried out on two types of partially encased composite columns: HEB260 and HEB280. The specimens tested employed two types of layouts for the base column joints as per Figure 1: traditional (*bolted steel base plate*) and innovative (*socket-type*) joints. The former consist of tapered steel plates welded onto base plates and anchored to the foundation block through steel bolted bars (*see also [14]*). The latter is an alternative and innovative socket type joint in which the column is fixed to the foundation block utilizing a special concrete filler; such joint was developed and designed to benefit of composite action.

The first set of specimens (traditional base column connections) replicate the columns and base joints designed in compliance with the guidelines of European standards [5] and used for the full-scale composite frame tested in ISPRA [13]. Similarly, the socket-type foundation was designed in compliance with Eurocode 2 [15].

The lateral loads were applied at two different locations along the height of the column, namely 1.6 m (*traditional joint*) and 1.7 m (*socket type*) above the foundation block to account for the different location of the restraint. Traditional base plates are generally placed at floor level, conversely socket type solution enables to use pavings that cover the foundation block. The horizontal load (T), simulating the earthquake loading, was applied via a 500 kN-hydraulic jack; the test was under displacement control. As a consequence, the maximum flexural moments (M), located at the base connection, was increased until failure. The displacement controlled loading regime allowed the softening branch of the response (*capacity*) curve to be investigated. The

connection of the jack to the column is ensured by two steel plates 30mm thick bolted on two opposite faces of the column. The reaction wall for the horizontal load is a stiff tapered cantilever element bolted to a steel system; its layout is shown in Figure 2 along with the test set-up. The cantilever system is connected to the laboratory floor slab (strong floor) by means of large steel rebars crossing the slab and the steel elements. These rebars are loaded in tension to prestress the connection. The vertical load ( $N$ ) is applied by two hydraulic jacks connected with two bars at the hinges placed at the foundation level. The axial load  $N$  acts along the column centroid axis. The reaction system for  $N$  consists of a steel plate located under the foundation block and connected to the hinges. This layout ensures that the load remains along the member axis during the column deformation. The transversal beam, at the column top, employs large stiffeners where is connected to the jack. An adequate lateral restraint along four prestressing bars at the corners were used to prevent slip and rocking of the foundation block and to guarantee the transfer of the shear forces to the strong floor level. Further details of the reaction wall and the set-up of the tests can be found elsewhere [14].

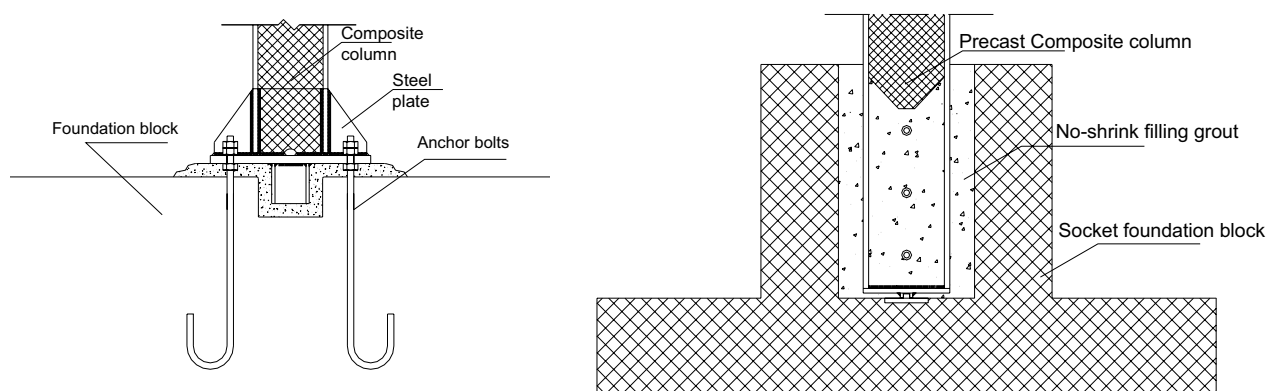


**Figure 1.** Layout of the sample base column connection: traditional (*left*) and socket-type (*right*).

## TEST SPECIMENS

The experimental program carried out at the laboratory of DAPS, in Naples, focuses on two sample partially encased composite steel and concrete columns: HEB260 and HEB280. The sample specimens tested were cantilever systems summarised as below (Table 1): partially encased columns with a steel HEB 260 member and traditional connection to foundation (stiffening plates and anchoring devices) and innovative socket-type system; HEB280 with socket-type foundation. The specimens were heavily instrumented to characterize reliably the concentration of inelastic demand at the base column. Figure 3 provides a close-up of the electrical displacement transducers (LVDTs) located at the base of the partially encased columns with either traditional or innovative joints.

The values of axial load ( $N$ ) used in the tests were equal to 170 kN and 330 kN. These values correspond to the minimum and maximum axial loads relative to the design load combinations of the full-scale composite framed building tested in the ELSA laboratory of JRC in Ispra [13]. The grade of the structural steel of the specimens was S235; the reinforcing bars grade was B450-C and the concrete was class C25/30. Actual values of the mechanical properties of steel and concrete were estimated from tensile (steel) and compression (concrete) tests. The values computed for the steel members and components are summarised in Table 2. Further details on the results of such tests can be found elsewhere [13]. The values of material overstrength ( $f_u/f_y$ ) relative to the element flange are on average higher than those in the webs. This result is in agreement with similar experimental data for steel members produced in Europe [16].



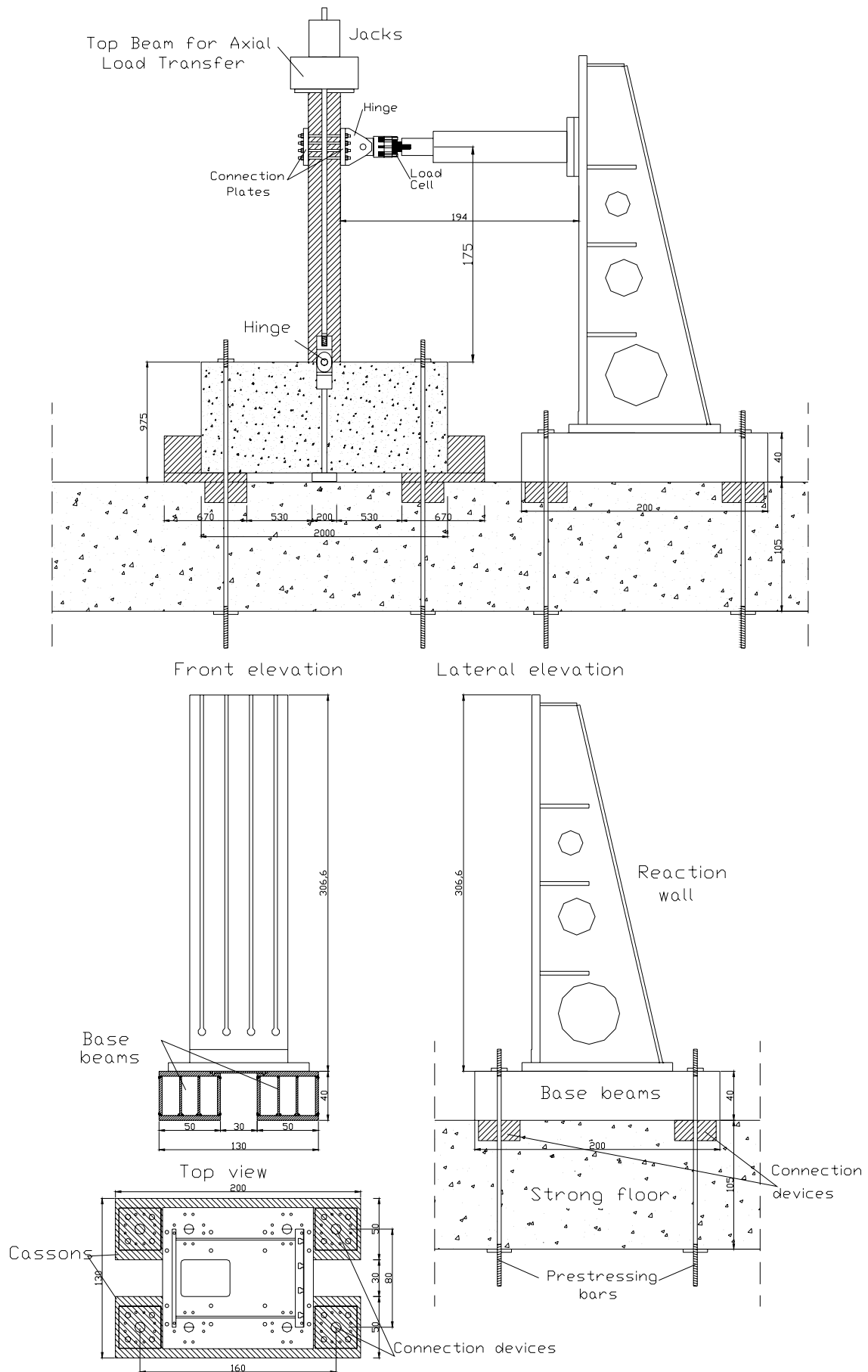


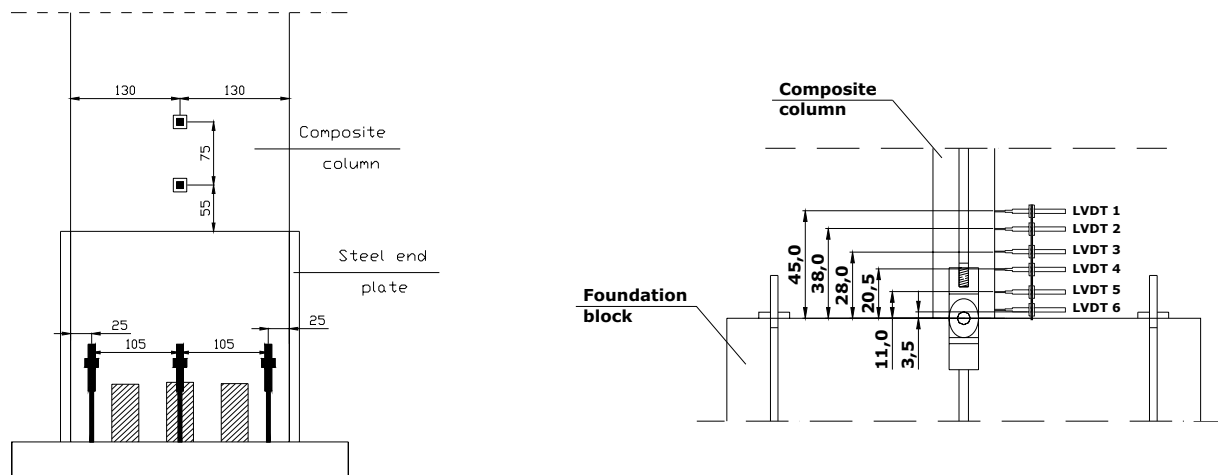
**Figure 2.** Layout of the test set-up (*top*) and reaction wall (*bottom*).

**Table 1.** Sample column specimens

Specimen	Axial load (kN)	Loading Type	Connection
HEB260	330	Monotonic	Traditional
HEB260	170	Monotonic	Traditional
HEB260	330	Monotonic	Socket

**Table 2.** Mechanical properties of the sample column specimens

Property	Beams				Columns			
	IPE240		IPE300		HEB260		HEB280	
	Web	Flange	Web	Flange	Web	Flange	Web	Flange
$f_y$ (MPa)	347	315	370	314	406	341	341	300
$f_u$ (MPa)	454	448	489	480	480	449	450	430
$f_u/f_y$	1.31	1.42	1.32	1.53	1.18	1.32	1.32	1.43
$\varepsilon_u$ (%)	32.6	31.0	35.6	30.7	31.8	35.7	34.5	37.1

**Figure 3.** Close-up of the electrical displacement transducers (LVDTs): traditional (*left*) and innovative (*right*) joint.

The details of the foundation system is displayed in Figure 1. The design of such foundation block was based on the ultimate limit state corresponding to the stress values and distribution at the column failure. The layout of the composite column specimen employing HEB 260 steel section and traditional base joint is displayed in Figure 4, while the specimen HEB260 with socket type connection is provided in Figure 5. The thicknesses of the base of the socket is equal to 300 mm, while the walls of the socket are 250 mm thick. The total height of the foundation is 1050 mm.

The values of the internal actions, i.e. axial load ( $N_{Sd,j}$ ), flexural moment ( $M_{Sd,j}$ ) and shear ( $V_{Sd,j}$ ) used for the design are  $N_{Sd,j}=308\text{kN}$ ,  $M_{Sd,j}=906\text{ kNm}$  and  $V_{Sd,j}=444\text{ kN}$ . These values were derived conservatively from the ultimate flexural capacity of the HEB 280. In fact, for such section, the ultimate bending moment, computed according to Eurocode 4 [17], is  $M_{Rd,col}=755\text{kNm}$ ; note that the design value  $M_{Sd,j}$  accounts for the overstrength ( $f_u/f_y=1.20$ ) at the base column connection.

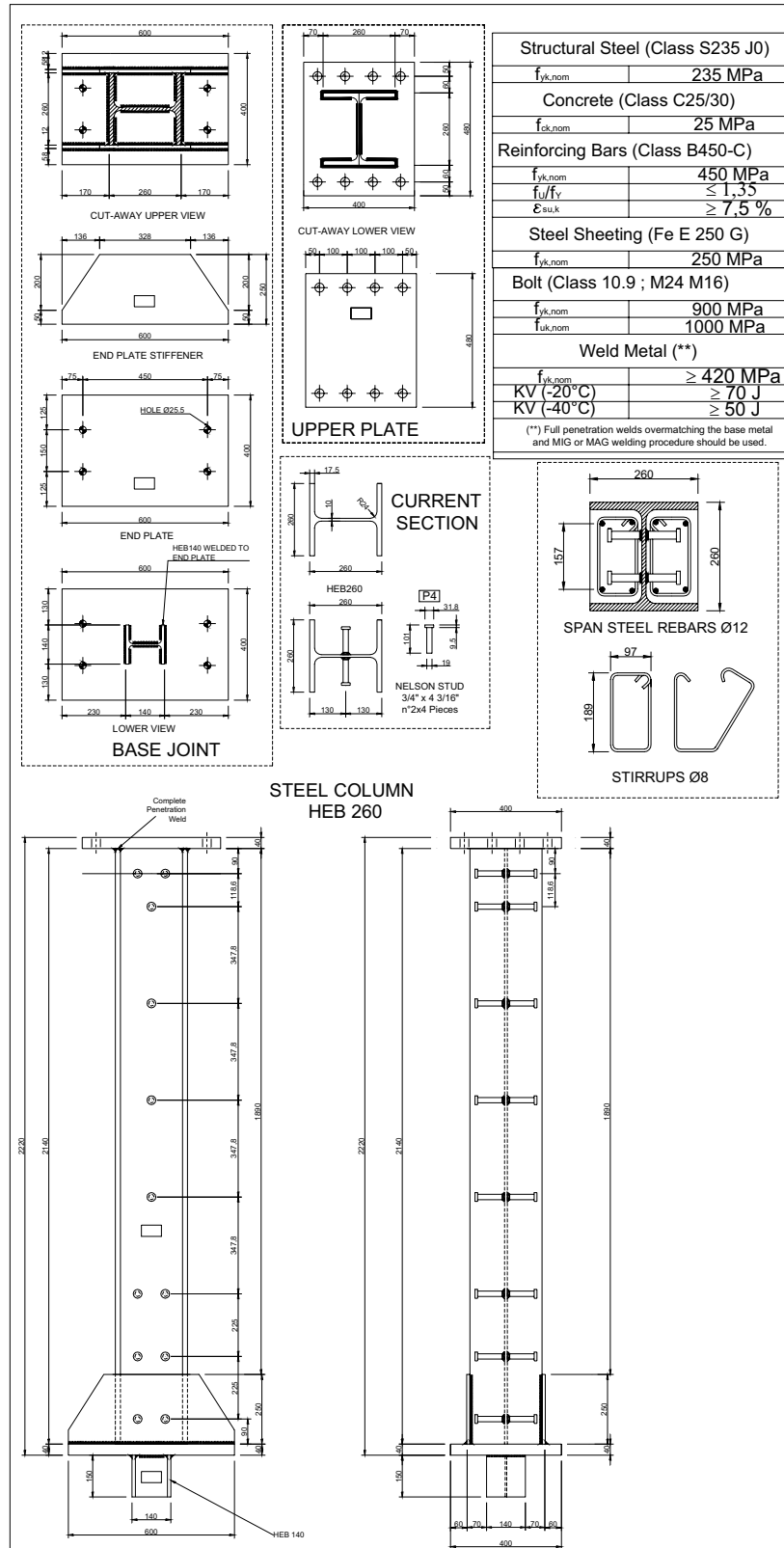


Figure 4. Traditional base column joint.

The value of the overstrength was derived by the provisions in Eurocode 3 [18]. The steel reinforcement used for the RC block of the traditional and socket type connections are displayed in Figures 6 and 7, respectively. It is worth mentioning that a solid foundation block is used to prevent an inelastic mechanism of the concrete component.

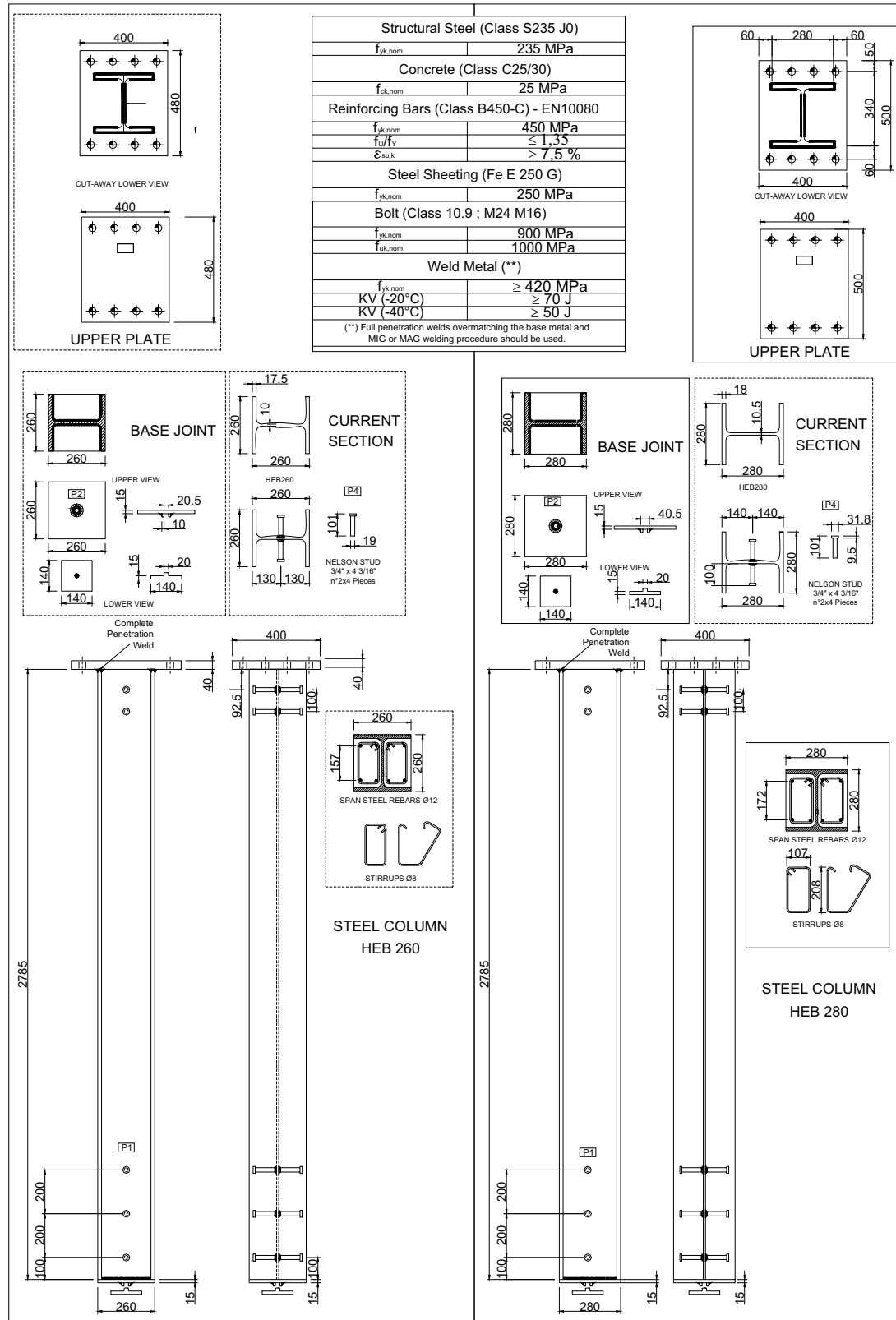
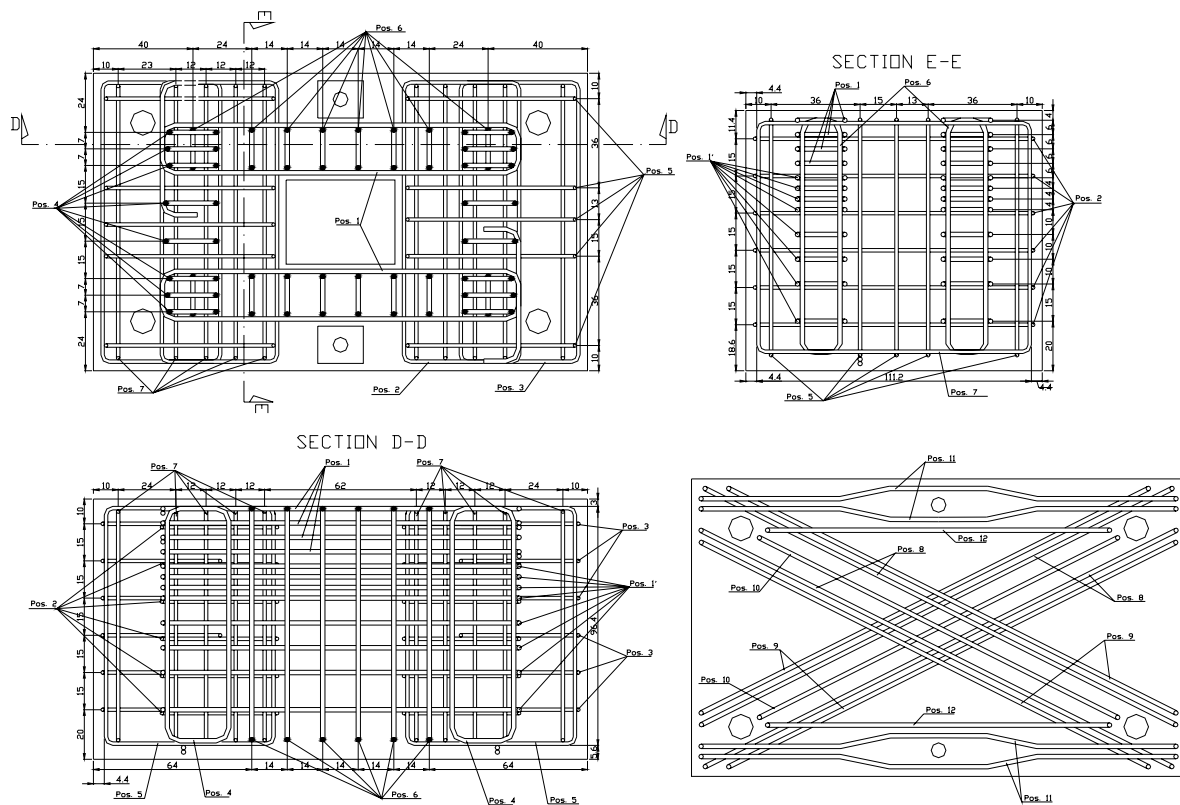
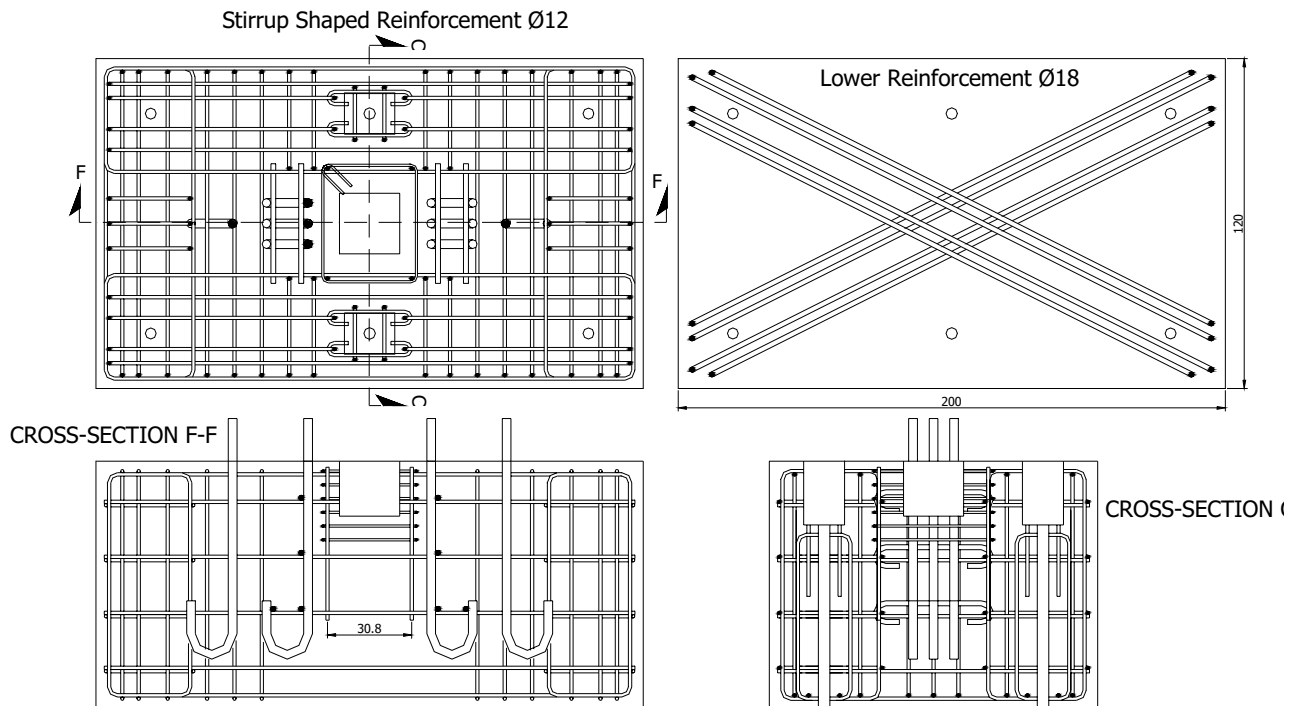


Figure 5. Socket-type base column joint.



**Figure 7.** Steel reinforcement used for the socket-type base column joint.

The results of the experimental tests carried out on composite columns employing innovative (socket-type) joints are discussed hereafter.

## TEST RESULTS

The test results of the partially encased composite columns were computed in terms of both local (moment-curvature  $M-\chi$  and moment-rotation  $M-\theta$ ) and global (lateral load-top displacement,  $F-\Delta$ ) response parameters. The capacity curves of the specimens HEB260 with axial load  $N=330\text{kN}$ , both traditional and innovative base connections, are provided in Figure 8. Such curves are expressed in terms of lateral force ( $F$ )-drift ( $d/H$ ), where  $H$  is the distance of the centreline of the hydraulic jack from the foundation and  $d$  the total horizontal displacement at the jack height. The forces corresponding to the onset of the plastic moment at the column base are also included in Figure 8. It is observed that the traditional connection layout exhibits higher lateral strength (600 kNm vs. 510 kNm) due to the steel stiffeners used at the base of the column and to overstrength for seismic design (*see also Fabbrocino et al., 2004*). Conversely, the ultimate deformation capacity of the socket type connection is about 50% higher than the counterpart traditional (about 0,0583 rad vs. 0,0875 rad); in both cases the requirement of 35 mrad given by Eurocode 8 [5] is fulfilled. This requirement is more stringent than the 3% drift, which is assumed as the onset of the ultimate limit state in steel and composite frames in the US practice, FEMA 356 [19].

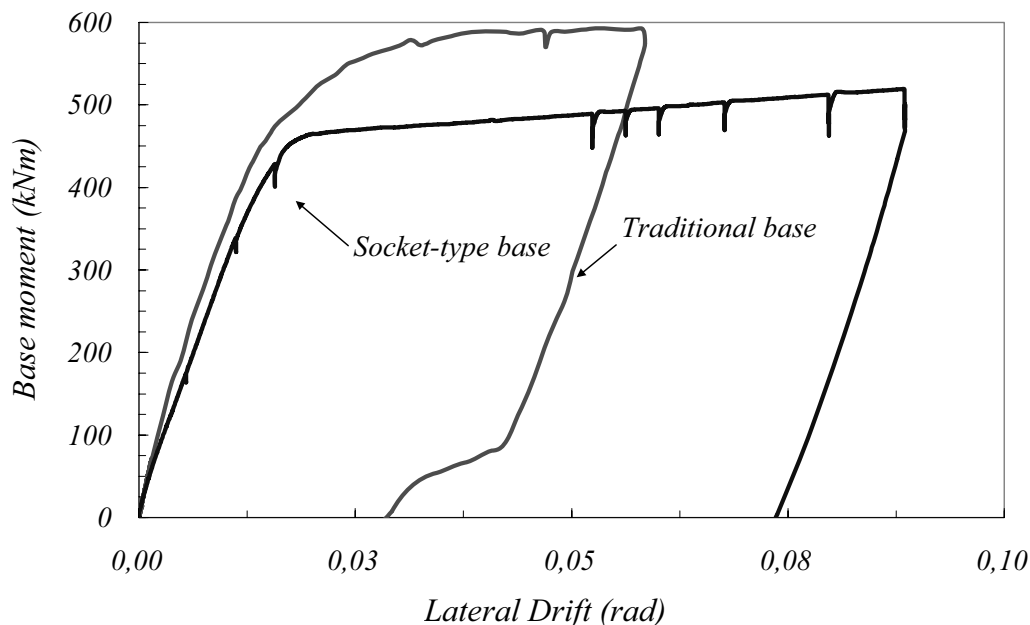


**Figure 8.** Capacity curves for the traditional and socket-type connections.

Furthermore the failure mode of the specimen with steel end plate is related to anchorage bolt fracture, while in the case of the socket type a very ductile mechanism is shown. At serviceability, the stiffness of the traditional connection is slightly higher than that of the socket connection. It can thus be argued that the experimental tests carried out both on traditional bolted steel end plate and innovative socket-type connections demonstrate that the former experience brittle failure modes. Rupture of anchorage bolts as per Figure 9 were observed under monotonic loads. The composite partially encased columns with traditional joint yield at about 310kN, which corresponds to a lateral drift of 26mm ( $d/h \sim 1.65\%$ ). The maximum force is equal, respectively, to 375kN for HEB260 with axial loads  $N=330\text{kN}$  and 340 kN for  $N=170\text{kN}$ . The lower value found in the second specimen (340kN) is related to the premature rupture of the base joint, probably caused by technological defects of the threaded bars [14]. In both specimens, i.e. with  $N=170\text{kN}$  and  $N=330\text{kN}$ , under monotonic regime, the column strength and energy dissipation do not exhibit significant loss for drift  $d/h \sim 5\text{-}6\%$ . The thick steel plate and the stiffeners used at the column base ensure that the end section of the column remains plane (rigid rotation). Under load reversal, the crushed concrete and the inelastic deformations in the steel components (anchorage), both at the

column base, endanger the global lateral stiffness of the composite column. Bond-related phenomena give rise to degrading effects, especially at large drifts, thus reducing significantly the energy dissipation capacity of the member. These results point out that traditional connections are not fully satisfactory, especially when relevance of reinforced concrete component increases, i.e. due to cross section dimensions. Conversely, innovative socket-type connections possess adequate ductility. Under monotonic load conditions, the test results show strain hardening of the base column equal to 1.32. This is due chiefly to the material over-strength of structural steel (see values of  $f_u/f_y$  of the member flange in Table 2). The contribution of the hardening of the longitudinal reinforcement bars is in fact very small (1.13 vs. 1.32). The tests carried out on the specimens employing the socket joint do not exhibit strength deterioration even at large lateral drifts, e.g.  $d/h > 0.04$ -0.05 radians. The formation of the plastic hinge occurs at the base column, as observed during the tests.



**Figure 9.** Close-up of the deformations of the specimen HEB260 with  $N=330\text{kN}$ .

Figure 9 shows the occurrence of inelastic deformations at the base column during the test on the HEB 260 with  $N=330\text{kN}$ ; the spreading of such inelasticity is also evident. At very large drifts, the flange plate of the column tends to bend outwards and the bond between the inner concrete and the exterior steel plate is broken as demonstrated by the close-up of the Figure 9, without any relevant effect on the global response. The tensile resistance of the concrete is exceeded and inclined (flexural) cracks initiate and propagate above the foundation block.

To shed light on the structural performance of the sample columns with either traditional or innovative socket-type member-to-foundation joint, the bending-axial load (M-N) interaction curves were computed for the specimens HEB 260 and HEB 280. These curves were estimated at two performance levels, namely yield and collapse, according to the provisions in Eurocode 4 [17]. The values of bending moments and axial loads at the ultimate stage of the monotonic tests are outlined in Tables 3 and 4 along with the values at yield and collapse. The computed values demonstrate that the failure mechanism is controlled in the case of traditional joint by the base column component. By contrast, for socket-type connections, the failure mode is controlled by the formation of the plastic hinges in the columns.

**Table 3.** Values of interaction curves for the test with HEB260 (N=170kN and N=330kN) and traditional joint at different performance state.

	Yield		Collapse		Test	
	M (kNm)	N (kN)	M (kNm)	N (kN)	M (kNm)	N (kN)
Section above stiffening plate	343	330	633	330	488	330
	339	170	628	170	433	170
Column base connection	440	330	550	330	596	330
	395	170	510	170	530	170

**Table 4.** Values of interaction curves for the test with HEB280 (N=330kN and N=520kN) and socket-type joint at different performance state (at column base connection).

Yield		Collapse		Test	
M (kNm)	N (kN)	M (kNm)	N (kN)	M (kNm)	N (kN)
390	330	740	330	608	330
420	520	750	520	762	520

The inelastic response of the critical region of the specimens with socket-type joints was monitored carefully through six electrical displacement transducers (LVDTs) located at the column base as displayed in Figure 3. These LVDTs record the lateral displacement of several points of the column flanges in order to define reliably the various inelastic phenomena, e.g. yielding, local buckling, fracture initiation, occurring at those locations during the tests. It is found that the section closer to the foundation block (LVDT #6) exhibits the typical response of reinforced concrete members. Conversely, the measurements derived from LVDT #5 and #6 show a typical structural steel nonlinear behaviour. Comparison between total cord rotation and the base column one derived from LVDT #6 measures enable to recognise that the higher is the drift, the higher is the contribution to the total drift given by the deformation of the socket type connection. Furthermore, due to the location of LVDT #1, 45.0cm far from the foundation, the socket type shows a yielding spreading that is nearly twice the width of the section (45.0cm vs. 52.0cm). As far as seismic design is concerned, the longer the spreading of inelasticity the higher the energy dissipation. By contrast, traditional connection systems, employing bolted steel end-plates [14] generate high concentrated inelastic demand on the anchorage bolts.

## CONCLUSIONS

Experimental tests carried out on composite steel and concrete columns were presented in this paper. Two layouts for the base column connections were assessed: the traditional system employing the bolted steel end plate and the innovative socket-type. The experimental results demonstrate that the socket system is beneficial for the spreading of inelasticity at the base of the composite columns. To assess the inelastic structural performance, the composite specimens were



subjected to monotonic loads at increasing lateral drifts (pushover experimental tests). It was found that the maximum drift of the socket type connection is nearly 50% higher than the traditional bolted steel end plate. Traditional base connections fail in a less ductile fashion because of the fracture of the anchorage bolts. Conversely, socket connections exhibit a ductile response due the formation of the plastic hinge at the base of the column, which extends over a length much higher than the cross section depth. As a result, socket-type joints can be reliably used for design of structures which may experience significant inelastic excursions. Further experimental tests and analytical simulations are being developed in order to assess the reliability and performance of the socket type connections under both monotonic, cyclic and earthquake loads.

## ACKNOWLEDGEMENTS

The present work was funded by the Italian Ministry of Research, through the grant PRIN02 (*Advanced design and control of global performance of composite steel and concrete frames for earthquake resistant building*); the financial support is gratefully acknowledged.

## REFERENCES

- [1] Ricles, J.M. and Paboojian, S.D., "Seismic performance of steel-encased composite columns", *Journal of Structural Engineering*, ASCE, 1994, 120(8), pp.2474-2494.
- [2] Broderick, B.M. and Elnashai, A.S., "Seismic response of composite frames-I. Response criteria and input motion", *Engineering Structures*, 1996, 18(9), pp.696-706.
- [3] Lee, T.K.L. and Pan, A.D.E., "Analysis of composite beam-columns under lateral cyclic loading", *Journal of Structural Engineering*, ASCE, 2001, 127(2), pp.186-193.
- [4] Elnashai, A.S. and Elghazouli, Y., "Performance of Composite Steel-Concrete Members Under Earthquake Loading, Part 2: Parametric Studies and Design Considerations", *Earthquake Engineering and Structural Dynamics*, 1993, 22(4), pp.347-368.
- [5] Eurocode 8, Design provisions for earthquake resistance of structures. Part 1.3: General rules. Specific rules for various materials and elements. European Committee for Standardization, Brussels, Belgium, 2004.
- [6] Fabbrocino, G., Manfredi, G., Cosenza, E. and Pecce, M.R., "Some remarks on deformation capacity of composite frames in seismic areas", *Proceeding of the 1<sup>st</sup> International Conference on Steel and Composite Structures*, ICSCS '01, Pusan, Korea, 2001.
- [7] Thermou, G.E., Elnashai, A.S., Plumier, A. and Doneux, C., "Seismic design and performance of composite frames", *Journal of Constructional Steel Research*, 2004, 60(1), pp.31-57.
- [8] Cosenza, E. and Pecce, M.R., "Le colonne composte acciaio-calcestruzzo: Analisi sperimentali, modelli di calcolo, indicazioni normative", *Costruzioni Metalliche*, 2001, 10(2), pp.49-60 (in *Italian*).
- [9] Shanmugam, N.E. and Lakshmi, B., "State of Art Report on Steel-Concrete Composite Columns", *Journal of Constructional Steel Research*, 2001, 57(10), pp.1041-1080.
- [10] Spacone, E. and El-Tawil, S., "Nonlinear analysis of steel-concrete composite structures: State of the art", *Journal of Structural Engineering*, ASCE, 2004, 130(2), pp.159-168.
- [11] Hajjar, J.F., "Composite Steel and Concrete Structural Systems for Seismic Engineering", *Journal of Constructional Steel Research*, 2002, 58(5-8), pp.702-723.
- [12] Mazzolani, F.M., "Steel and composite structures in European seismic areas: research, codification, design and applications", *Earthquake Spectra*, 2003, 19(2), pp.415-452.
- [13] Bursi, O.S., Caramelli, S., Fabbrocino, G., Molina, J., Salvatore, W. and Taucer, F., "3D Full-scale seismic testing of a steel-concrete composite building at ELSA", *Contr. No.*

- HPR-CT-1999-00059, European Community, 2004.
- [14] Fabbrocino, G., Pecce, M.R. and Di Sarno, L., “Inelastic Response of Steel and Concrete Columns”, Proceeding of The Fourth International Conference on Steel and Composite Structures, ICSCS '04, Seoul, Korea, 2004.
  - [15] Eurocode 2, Design of concrete structures. Part 1.1: General rules and rules for buildings. European Committee for Standardization, Brussels, Belgium, 2002.
  - [16] Byfield, M.P. and Nethercot, D.A., “Material and geometric properties of structural steel for use in design”, *The Structural Engineer, Journal of the Institution of Structural Engineers*, 1997, 75(21), pp.363-367.
  - [17] Eurocode 4. Design of composite steel and concrete structures. Part 1.1: General rules and rules for buildings. European Committee for Standardization, Brussels, Belgium, 2004.
  - [18] Eurocode 3. Design of steel structures. Part 1.1: General rules and rules for buildings. European Committee for Standardization, Brussels, Belgium, 2004.
  - [19] Federal Emergency Management Agency, “Prestandard and commentary for the seismic rehabilitation of buildings”, FEMA Report No.356., Washington D.C., USA, 2000.